

# UC San Diego

## UC San Diego Electronic Theses and Dissertations

### Title

Direct Access to Chemistry and Catalytic Behavior of the Zero-Valent MoL4 Fragment

### Permalink

<https://escholarship.org/uc/item/89d309jn>

### Author

Mandla, Kyle Andrew

### Publication Date

2018

Peer reviewed|Thesis/dissertation

UNIVERSITY OF CALIFORNIA SAN DIEGO

**Direct Access to Chemistry and Catalytic Behavior of the  
Zero-Valent MoL<sub>4</sub> Fragment**

A dissertation submitted in partial satisfaction of the requirements  
for the degree Doctor of Philosophy

in

Chemistry

by

Kyle Andrew Mandla

Committee in charge:

Professor Joshua S. Figueroa, Chair  
Professor Guy Bertrand  
Professor Joseph M. O'Connor  
Professor Jeffrey D. Rinehart  
Professor Dionicio Siegel

©

Kyle Andrew Mandla, 2018

All rights reserved.

The Dissertation of Kyle Mandla is approved, and it is acceptable in quality and form for publication on microfilm and electronically:

---

---

---

---

---

---

Chair

University of California San Diego

2018

## DEDICATION

Dedicated first to my mom, Janice R. Mandla Mattingly, for teaching us faith and love. Second to my dad, Dirk R. Mandla for teaching us resilience and strength. Third to Mark Mattingly for showing us how to bring all these things together as good and decent people. And finally, to my grandfather to for inspiring me to apply these lessons in chemistry.

## TABLE OF CONTENTS

Signature Page .....	iii
Dedication .....	iv
Table of Contents .....	v
List of Figures .....	vii
List of Schemes .....	xii
List of Tables .....	xiii
Acknowledgements .....	xiv
Vita .....	xxi
Abstract of the Dissertation .....	xxii
Chapter 1 Synthesis of Masked ML <sub>4</sub> Analogs to Mo(CO) <sub>4</sub> .....	1
1.1 Introduction .....	1
1.2 Synthesis of Group 6 Isocyanides .....	2
1.3 Application of <i>m</i> -Terphenyl Isocyanides in Mo-catalyzed Hydrostannation .....	6
1.4 The Pursuit and Synthesis of Masked Analogues to Mo(CO) <sub>4</sub> .....	12
1.5 Acknowledgements .....	18
1.6 References .....	18
Chapter 2 Regioselective Formation of ( <i>E</i> )-β-Vinylstannanes with a Topologically Controlled Molybdenum-Based Alkyne Hydrostannation Catalyst .....	24
2.1 Introduction .....	24
2.2 Results and Discussion .....	27
2.3 Synthetic Procedures, and Control Experiments .....	35
2.4 α/β-Vinylstannane Isomer Determinations and Assignments .....	42
2.5 Tabulated Characterization, Regioselectivity and Yield Data for Vinylstannanes .....	45
2.6 Determination of Kinetic Isotope Effect and Hammett Correlations .....	54
2.7 Crystallographic Structure Determinations .....	69
2.8 <sup>1</sup> H and <sup>13</sup> C-NMR Spectra of Isolated Vinylstannanes .....	72
2.9 Acknowledgements .....	89
2.10 References .....	89
Chapter 3 Photolytic Reductive Elimination of White Phosphorus from a Mononuclear <i>cyclo</i> -P <sub>4</sub> Complex: Bespoke P <sub>4</sub> Release Using Benign Stimulus .....	92

3.1	Introduction .....	92
3.2	Synthesis and photolytic reactivity of a mononuclear <i>cyclo</i> -P <sub>4</sub> complexes .....	94
3.3	Synthetic Procedures and Characterization Data .....	101
3.4	Analysis of Electronic Structure: UV-vis Spectroscopy, TD-DFT Analysis, and Structural Optimizations.....	108
3.5	Crystallographic Structure Determinations .....	115
3.6	Acknowledgements .....	118
3.7	References .....	118
Chapter 4 A <i>cyclo</i> -P <sub>4</sub> Analog of Mo(CO) <sub>3</sub> (η <sup>6</sup> -benzene).....		122
4.1	Introduction .....	122
4.2	Results and Discussion .....	124
4.3	Conclusions .....	132
4.4	Experimental .....	133
4.5	Crystal Structure Data .....	140
4.6	Acknowledgements .....	141
4.7	References .....	141
Chapter 5 The Electrochemistry of Molybdenum <i>cyclo</i> -P <sub>4</sub> Complexes and Isolation of the First Mononuclear <i>cyclo</i> -P <sub>4</sub> Radical.....		143
5.1	Introduction .....	143
5.2	Results and Discussion .....	145
5.3	Synthetic procedures, characterization data, and calculations .....	157
5.4	Details of DFT computational studies.....	161
5.5	Crystallographic determination of molecular structures .....	162
5.6	Acknowledgements .....	164
5.7	References .....	164
Chapter 6 Reactivity of <i>cyclo</i> -P <sub>4</sub> Opens New Routes to Phosphaallenes and <i>cyclo</i> -P <sub>3</sub> .....		166
6.1	Introduction .....	166
6.2	Results and discussion.....	168
6.3	Conclusions .....	188
6.4	Synthetic procedures, characterization data, and calculations .....	189
6.5	Details of DFT computational studies.....	192
6.6	Crystallographic determination of molecular structures .....	198
6.7	Acknowledgements .....	199
6.8	References .....	200

## LIST OF FIGURES

<b>Figure 1.1.</b> Molecular structure of Mo(CO) <sub>2</sub> (CNAr <sup>Dipp2</sup> ) <sub>2</sub> (OEt <sub>2</sub> ) <sub>2</sub> ( <b>13</b> ). Three-position disorder of Mo and equatorial ligands precluded accurate determination of bond distances and angles. ....	14
<b>Figure 1.2.</b> Molecular structure of DME-chelate <b>14</b> .....	15
<b>Figure 1.3.</b> Molecular structure of η <sup>3</sup> -styrene complex <b>15</b> .....	16
<b>Figure 1.4.</b> Top: Relative energy diagram of molecular orbitals in Mo(CO) <sub>4</sub> , Mo(CO) <sub>2</sub> (CNPh) <sub>2</sub> , and Mo(CNPh) <sub>4</sub> – determined by DFT (BP86, def2-TZVP, ZORA). Bottom: Assigned frontier molecular orbitals of Mo(CO) <sub>4</sub> ; <b>h1</b> and <b>h2</b> are hybrid orbitals. <sup>79</sup> .....	17
<b>Figure 2.1</b> <i>syn</i> Hydrostannation of diphenylacetylene with molybdenum precatalysts <b>1</b> and <b>3</b> ...	27
<b>Figure 2.2</b> Top: Proposed interconversion of molybdenum-based ( <i>E</i> )-β- and α-producing C-alkenyl intermediates through reversible β-H elimination/migratory insertion.....	32
<b>Figure 2.3.</b> Example showing α/β-assignments for an internal alkyne. ....	42
<b>Figure 2.4.</b> HSQC verifying regio-isomer assignments for α/β-tributylstannyl(vinyl)-cyclopentanol. ....	43
<b>Figure 2.5.</b> Example portion of <sup>1</sup> H NMR spectrum showing key J-coupling values and peak assignments for α- and β-vinyl protons. * denotes <sup>119/117</sup> Sn satellites.....	43
<b>Figure 2.6.</b> Example <sup>1</sup> H NMR spectrum, ( <i>E</i> )-β-tributyl(2,4,6-trimethylstyryl)stannane, showing coupling constants used to establish regio-stereochemical assignments .....	44
<b>Figure 2.7.</b> In addition to characteristic <i>J</i> -couplings for assignment of β-vinylstannanes, α-vinylstannanes are readily identifiable with very large Sn/H <sub>trans</sub> coupling constants ( <i>J</i> <sub>SnH,trans</sub> = 140 Hz), and smaller Sn/H <sub>cis</sub> coupling constants ( <i>J</i> <sub>SnH,cis</sub> = 64 Hz). ....	44
<b>Figure 2.8.</b> Hydrostannation of 1-phenyl-1-propyne gave ratios of vinyl <sup>H</sup> : vinyl <sup>D</sup> with linear dependence on the relative loading of HSnBu <sub>3</sub> /DSnBu <sub>3</sub> in the reaction mixture.....	54
<b>Figure 2.9.</b> Reference spectra showing crude <sup>1</sup> H NMR data for hydrostannation of 1-phenyl-1-propyne with 3 equiv. HSnBu <sub>3</sub> (1:0 HSnBu <sub>3</sub> /DSnBu <sub>3</sub> ). The sum of α- and β-vinyl integral values give [vinyl <sup>H</sup> ] <sub>0</sub> . Generation of H <sub>2</sub> ensues upon complete consumption of alkyne. ....	56
<b>Figure 2.10.</b> Experimental values [vinylH] / [vinylD] versus ratio of <i>m:n</i> HSnBu <sub>3</sub> /DSnBu <sub>3</sub> . Analysis by least squares linear regression gives KIE as the slope.....	57
<b>Figure 2.11</b> Plot of log(observed selectivity) (i.e. log(β/α)) vs. Hammett σ <sup>+</sup> parameter <sup>36</sup> <i>para</i> -substituted aryl alkynes in Table 1.....	58



<b>Figure 2.12.</b> Optimized $\beta$ -intermediates, $\text{Mo}(\text{CO})_2(\text{CNPh})_2(\eta^1\text{-RArCHCH})(\text{SnMe}_3)$ , R = NMe <sub>2</sub> , OEt, Me, H, NO <sub>2</sub> . Optimized coordinates of $\beta$ -H were modified and used as starting coordinates for all <i>p</i> -functionalized derivatives. ....	59
<b>Figure 2.13.</b> Optimization of <i>p</i> -NO <sub>2</sub> -vinyl complex with SnBu <sub>3</sub> gives an agostic complex analogous to the SnMe <sub>3</sub> complex $\beta$ -NO <sub>2</sub> . Selected bond distances (Å) .....	60
<b>Figure 2.14.</b> $\text{Mo}((\eta^2\text{-}H,C\text{-}(\text{H}_3\text{CCH}(\text{CH}_3))\text{-}\eta^1\text{-}N\text{-}N(\text{H})(i\text{-Pr}))(\text{CO})_2(\text{CNAr}^{\text{Dipp}2})_2$ ( <b>3</b> ). Selected bond lengths (Å) and angles (deg.) .....	70
<b>Figure 2.15.</b> <sup>1</sup> H and <sup>13</sup> C NMR of ( <i>E</i> )-tributyl(1,2-diphenylvinyl)stannane. ....	72
<b>Figure 2.16.</b> <sup>1</sup> H and <sup>13</sup> C NMR of ( <i>E</i> )- <i>N,N</i> -dimethyl-4-(2-(tributylstannyl)vinyl)aniline. ....	73
<b>Figure 2.17.</b> <sup>1</sup> H and <sup>13</sup> C NMR of ( <i>E</i> )-tributyl(1,3,5-trimethylphenyl)vinylstannane. ....	74
<b>Figure 2.18.</b> <sup>1</sup> H and <sup>13</sup> C NMR of ( <i>E</i> )-tributyl(4-ethoxystyryl)stannane .....	75
<b>Figure 2.19.</b> <sup>1</sup> H and <sup>13</sup> C NMR of ( <i>E</i> )-tributyl(4-methylstyryl)stannane. ....	76
<b>Figure 2.20.</b> <sup>1</sup> H and <sup>13</sup> C NMR of ( <i>E</i> )-tributyl(styryl)stannane. ....	77
<b>Figure 2.21.</b> <sup>1</sup> H and <sup>13</sup> C NMR of ( <i>E</i> )-tributyl(1-phenylprop-1-en-2-yl)stannane.....	78
<b>Figure 2.22.</b> <sup>1</sup> H and <sup>13</sup> C NMR of ( <i>E</i> )-tributyl(1-phenylbut-1-en-2-yl)stannane. ....	79
<b>Figure 2.23.</b> <sup>1</sup> H and <sup>13</sup> C NMR ( <i>E</i> )-tributyl(hex-1-en-1-yl)stannane. ....	80
<b>Figure 2.24.</b> <sup>1</sup> H and <sup>13</sup> C NMR of ( <i>E</i> )-tributyl(hex-2-en-2-yl)stannane.....	81
<b>Figure 2.25.</b> <sup>1</sup> H and <sup>13</sup> C NMR of ( <i>E</i> )-tributyl(2-cyclopropylvinyl)stannane.....	82
<b>Figure 2.26.</b> <sup>1</sup> H and <sup>13</sup> C NMR of <i>N</i> -( <i>E</i> )-(5-(tributylstannyl)pent-4-en-1-yl)phthalimide.....	83
<b>Figure 2.27.</b> <sup>1</sup> H and <sup>13</sup> C NMR of ( <i>E</i> )-1-(2-(tributylstannyl)vinyl)cyclopentan-1-ol. ....	84
<b>Figure 2.28.</b> <sup>1</sup> H and <sup>13</sup> C NMR of ( <i>E</i> )-1-(2-(tributylstannyl)vinyl)cyclooctan-1-ol. ....	85
<b>Figure 2.29.</b> <sup>1</sup> H and <sup>13</sup> C NMR of ( <i>E</i> )-3-methyl-1-(tributylstannyl)pent-1-en-3-ol.....	86
<b>Figure 2.30.</b> <sup>1</sup> H and <sup>13</sup> C NMR of mifepristone hydrostannation. ....	87
<b>Figure 2.31.</b> <sup>1</sup> H and <sup>13</sup> C NMR of tributyl(1-(4-nitrophenyl)vinyl)stannane. ....	88
<b>Figure 3.1.</b> Molecular structures of $\eta^4$ -( <i>cyclo</i> -P <sub>4</sub> ) complexes <b>2</b> (top) and <b>5</b> (bottom). ....	96
<b>Figure 3.2</b> Photolytic release and recapture of white phosphorus (P <sub>4</sub> ). ....	99

<b>Figure 3.3.</b> Major TD-DFT calculated excitations for model 5m corresponding to P <sub>4</sub> -releasing LMCTs.....	100
<b>Figure 3.4.</b> <sup>1</sup> H NMR (500.0 MHz, C <sub>6</sub> D <sub>6</sub> , 20 °C) spectrum of of <b>5</b> .....	103
<b>Figure 3.5.</b> <sup>31</sup> P{ <sup>1</sup> H} NMR (121.4 MHz, C <sub>6</sub> D <sub>6</sub> , 20 °C) spectrum of <b>2</b> .....	104
<b>Figure 3.6.</b> <sup>1</sup> H NMR (500.0 MHz, C <sub>6</sub> D <sub>6</sub> , 20 °C) spectrum of of <b>5</b> .....	105
<b>Figure 3.7.</b> <sup>31</sup> P{ <sup>1</sup> H} NMR (121.4 MHz, C <sub>6</sub> D <sub>6</sub> , 20 °C) spectrum of <b>5</b> and evaluation of homonuclear coupling: WinDNMR <sup>42</sup> simulated AA'BB' spectrum gives <i>J</i> AA' = 298 Hz, <i>J</i> BB' = 339 Hz, <i>J</i> AB = 278 Hz, <i>J</i> AB' = 1 Hz.....	106
<b>Figure 3.8.</b> VT <sup>31</sup> P-NMR (202.404 MHz, C <sub>6</sub> D <sub>6</sub> ) of <b>5</b> indicates hindered rotation of <i>cyclo</i> -P <sub>4</sub> is persistent up to 75 °C.....	107
<b>Figure 3.9.</b> <sup>31</sup> P NMR showing <b>5</b> prior to photolysis (top), after 20 min photolysis (middle), and thermal regeneration of <b>5</b> at 70 °C.....	108
<b>Figure 3.10.</b> Experimental UV-vis spectrum of <b>5</b> (left) and zoomed-in view of UV-vis with calculated vertical transitions represented by black bars (right).....	109
<b>Figure 3.11.</b> Optimized model complex (η <sup>4</sup> -P <sub>4</sub> )Mo(CO) <sub>2</sub> (CNPh) <sub>2</sub> ( <b>2M</b> ).....	111
<b>Figure 3.12.</b> Optimized model complex (η <sup>4</sup> -P <sub>4</sub> )MoI <sub>2</sub> (CO)(CNPh) <sub>2</sub> ( <b>5M</b> ).....	111
<b>Figure 3.13.</b> Molecular Orbitals Calculated for (η <sup>4</sup> -P <sub>4</sub> )Mo(CO) <sub>2</sub> (CNPh) <sub>2</sub> ( <b>2M</b> ).....	112
<b>Figure 3.14.</b> Molecular orbitals calculated for (η <sup>4</sup> -P <sub>4</sub> )MoI <sub>2</sub> (CO)(CNPh) <sub>2</sub> ( <b>5M</b> ).....	113
<b>Figure 3.15.</b> Molecular structure of (η <sup>4</sup> -P <sub>4</sub> )Mo(CO) <sub>2</sub> (CNAr <sup>Dipp2</sup> ) <sub>2</sub> ( <b>2</b> ). Selected bond distances (Å) and angles (deg).....	116
<b>Figure 3.16.</b> Molecular structure of (η <sup>4</sup> -P <sub>4</sub> )MoI <sub>2</sub> (CO)(CNAr <sup>Dipp2</sup> ) <sub>2</sub> ( <b>5</b> ). Selected bond distances (Å) and angles (deg).....	116
<b>Figure 3.17.</b> Molecular structure of MoI <sub>2</sub> (CO) <sub>2</sub> (CNAr <sup>Dipp2</sup> ) <sub>2</sub> (DME) ( <b>6</b> ).....	117
<b>Figure 4.1.</b> Molecular structure of [1] <sup>2-</sup> (K <sup>+</sup> and THF excluded for clarity).....	127
<b>Figure 4.2.</b> Polymeric structure of [1·K <sub>2</sub> ] and zoomed-in image showing cationic linkages...	128
<b>Figure 4.3.</b> Molecular structure of [(db18-C-6)·K][2·K].....	129
<b>Figure 4.4.</b> Filled d-orbitals of (η <sup>6</sup> -C <sub>6</sub> H <sub>6</sub> )Mo(CO) <sub>3</sub> (top) and [1] <sup>2-</sup> .....	131
<b>Figure 4.5.</b> Aromatic π-orbitals of Mo(CO) <sub>3</sub> (η <sup>6</sup> -benzene) and [1] <sup>2-</sup> .....	132

<b>Figure 4.6.</b> $^1\text{H}$ (300 MHz, $\text{C}_6\text{D}_6$ , top) and $^{31}\text{P}$ NMR (122 MHz, $\text{C}_6\text{D}_6$ , bottom) of [ <b>2</b> · <b>K</b> ]. ....	134
<b>Figure 4.7.</b> $^1\text{H}$ (300 MHz, $\text{C}_6\text{D}_6$ , top) and $^{31}\text{P}$ NMR (122 MHz, $\text{C}_6\text{D}_6$ , bottom) of $([(\text{db}18\text{-C-6})\cdot\text{K}][\text{2}\cdot\text{K}])$ .....	136
<b>Figure 4.8</b> MO correlation diagram of $(\eta^6\text{-C}_6\text{H}_6)\text{Mo}(\text{CO})_3$ and $(\eta^4\text{-P}_4)\text{Mo}(\text{CO})_2\text{-}(\text{CNAr}^{\text{Dipp}2})_2$ .....	137
<b>Figure 5.1.</b> CV of <i>cyclo</i> - $\text{P}_4$ complex <b>2</b> (0.3M $[\text{NBu}_4][\text{PF}_6]$ THF solution, $v = 100$ mV/s).....	146
<b>Figure 5.2.</b> DPV of <b>2</b> (1.0 mM complex, 0.3M $[\text{NBu}_4][\text{PF}_6]$ , THF solution).....	146
<b>Figure 5.3.</b> CV of <i>cyclo</i> - $\text{P}_4$ complex <b>1</b> (1.0 mM complex, 0.3M $[\text{NBu}_4][\text{PF}_6]$ , THF solution, scan rate 100 mV/s).....	148
<b>Figure 5.4.</b> Resolution of oxidative feature at -1.00 V by reversing sweep after the first cathodic event (1.0 mM complex <b>1</b> , 0.3M $[\text{NBu}_4][\text{PF}_6]$ , THF solution, scan rate 100 mV/s).....	148
<b>Figure 5.5.</b> Molecular structure of $(\eta^4\text{-P}_4)\text{MoI}(\text{CO})(\text{CNAr}^{\text{Dipp}2})_2$ ( <b>[5][CoCp<sub>2</sub>]</b> ).....	151
<b>Figure 5.6.</b> Cyclic voltammetry of <b>[5][CoCp<sub>2</sub>]</b> (1.0 mM complex, 0.3M $[\text{NBu}_4][\text{PF}_6]$ , THF solution, scan rate 100 mV/s).....	151
<b>Figure 5.7</b> Molecular structure of $(\eta^4\text{-P}_4)\text{MoI}(\text{CO})(\text{CNAr}^{\text{Dipp}2})_2(\text{TI})$ ( <b>[5·TI]</b> ).....	153
<b>Figure 5.8.</b> Molecular structure of $(\eta^4\text{-P}_4)\text{MoI}(\text{CO})(\text{CNAr}^{\text{Dipp}2})_2$ ( <b>6</b> ).....	154
<b>Figure 5.9.</b> EPR of <b>6</b> (10 mM complex in THF, 5K, 9.64 GHz) .....	155
<b>Figure 5.10.</b> DFT optimized (BP86, ZORA-def2-TZVP) structure of <b>6</b> showing SOMO (a) and spin-density-surface (b). .....	155
<b>Figure 5.11.</b> $^1\text{H}$ NMR (500 MHz, THF/ $d_8$ ) of $(\eta^4\text{-P}_4)\text{MoI}(\text{CO})(\text{CNAr}^{\text{Dipp}2})_2[\text{CoCp}_2]$ ( <b>[5][CoCp<sub>2</sub>]</b> ). Rapid ion exchange in THF enables resolution of coupling constants and the time-averaged cobaltocenium ( $^+\text{CoCp}_2$ ) chemical shift (br, 5.6 – 4.8 ppm). * $\text{C}_6\text{H}_6$ , **Si-grease .....	160
<b>Figure 5.12.</b> $^1\text{H}$ NMR (500 MHz, $\text{C}_6\text{D}_6$ ) of $(\eta^4\text{-P}_4)\text{MoI}(\text{CO})(\text{CNAr}^{\text{Dipp}2})_2(\text{TI})$ ( <b>[5·TI]</b> ), THF solvated crystals). *Si-grease present in the instrument probe. ....	160
<b>Figure 5.13.</b> $^1\text{H}$ NMR ( $\text{C}_6\text{D}_6$ , 300 MHz) of $(\eta^4\text{-P}_4)\text{MoI}(\text{CO})(\text{CNAr}^{\text{Dipp}2})_2$ ( <b>6</b> ).....	161
<b>Figure 5.14.</b> Optimized coordinates for model <i>cyclo</i> - $\text{P}_4$ radical complex <b>6M</b> . ....	161
<b>Figure 6.1.</b> Space-filling model of <b>2</b> . ....	167
<b>Figure 6.2.</b> Molecular structure of <b>[3]<sup>-</sup></b> . ....	169

<b>Figure 6.3.</b> Proton-decoupled spectrum of $[3]^-$ , $^{31}\text{P}\{^1\text{H}\}$ NMR (161.9 MHz, $\text{C}_6\text{D}_6$ ). $^{31}\text{P}$ NMR (161.9 MHz, $\text{C}_6\text{D}_6$ ) showing $^1\text{H}/^{31}\text{P}$ coupling of peak at 38 ppm ( $^1J_{\text{P-H}} = 412$ Hz).....	170
<b>Figure 6.4.</b> Proposed reaction mechanism for the formation of $[3]^-$ .....	170
<b>Figure 6.5.</b> Molecular structure of $[4]^-$ .....	171
<b>Figure 6.6.</b> Molecular structure of <b>5</b> .....	172
<b>Figure 6.7.</b> Molecular structure of $(\eta^3\text{-P}_3)\text{MoI}(\text{CO})_2(\text{CNAr}^{\text{Dipp}2})_2$ ( <b>6-P<sub>3</sub></b> ). Selected bond distances (Å) and angles (deg).....	174
<b>Figure 6.8.</b> Synthesis of <i>cyclo</i> -P <sub>3</sub> anion <b>7-P<sub>3</sub></b> <sup>-</sup> .....	175
<b>Figure 6.9.</b> Expanded view of <b>7-P<sub>3</sub></b> <sup>-</sup> showing trimeric structure with P···K <sup>+</sup> linkages (isopropyl groups excluded for clarity).....	175
<b>Figure 6.10.</b> Molecular structure of a <b>7-P<sub>3</sub></b> <sup>-</sup> monomeric unit.....	176
<b>Figure 6.11.</b> Occupied metal-based orbitals of the anionic <i>cyclo</i> -P <sub>3</sub> complex $[7\text{-P}_3]^-$ .....	179
<b>Figure 6.12.</b> Selected molecular orbitals. Mulliken designations are based on simplified C <sub>4v</sub> symmetric geometry.....	180
<b>Figure 6.13.</b> Geometry optimization of plausible intermediates in the elimination of PI from tetravalent <i>cyclo</i> -P <sub>4</sub> model complex $(\eta^4\text{-P}_4)\text{MoI}_2(\text{CO})(\text{CNPh})_2$ ( <b>1M</b> ).....	184
<b>Figure 6.14.</b> Proposed intermediate (in brackets), $^{31}\text{P}$ NMR (bottom), and WinDNMR simulated spectrum (top) of phosphorus species trapped by $\text{CNAr}^{\text{Dipp}2}$ . Coupling constants: JAA' = -15 Hz, JBB'=193 Hz, JAB = 403 Hz, JAB' = -184 Hz.....	186
<b>Figure 6.15.</b> $^{31}\text{P}$ NMR (121.5 MHz, $\text{CDCl}_3$ ) of triphosphazole salt <b>7</b> , $^1J_{\text{PP}} = 452$ Hz. ....	188
<b>Figure 6.16.</b> Optimized geometry of <i>cis,trans</i> - $\text{Mo}(\text{CO})_2(\text{CNAr}^{\text{Dipp}2})_2(\eta^3\text{-P}_3)$ ( $[7\text{-P}_3]^-$ ). ....	192
<b>Figure 6.17.</b> Optimized coordinates of $[3\text{M}]^-$ .....	192
<b>Figure 6.18.</b> Optimized coordinates of $[4\text{M}]^-$ .....	193

## LIST OF SCHEMES

<b>Scheme 1.1.</b> Stepwise decarbonylation of $\text{Mo}(\text{CO})_3(\text{CNAr}^{\text{Dipp}2})_2(\text{ACN})$ ( <b>1</b> ) with diiodine .....	3
<b>Scheme 1.2.</b> Synthesis of $\eta^6$ -arene complex <b>4-Mes2</b> .....	4
<b>Scheme 1.3.</b> Synthetic scheme demonstrating enhanced lability of electron-deficient arene in $\text{CNAr}^{\text{DArF}}$ .....	5
<b>Scheme 1.4.</b> Synthesis of divalent mono-carbonyl complexes. ....	8
<b>Scheme 1.5.</b> Thermolytic dissociation of $\text{Et}_2\text{O}$ . ....	9
<b>Scheme 1.6.</b> Synthesis of a bis- $\text{Et}_2\text{O}$ -masked source of $\text{ML}_4$ .....	14
<b>Scheme 1.7.</b> Synthesis of masked sources of the zero-valent, four-coordinate fragment $[\text{Mo}(\text{CO})_2(\text{CNAr}^{\text{Dipp}2})_2]$ . ....	15
<b>Scheme 2.1</b> Generalized reaction scheme for the production of vinylstannane regioisomers by metal-catalyzed syn-hydrostannation of terminal alkynes.....	25
<b>Scheme 2.2.</b> Hydrostannation of mifepristone with precatalyst <b>1</b> .....	32
<b>Scheme 3.1.</b> Synthesis of $\eta^4$ -( <i>cyclo</i> - $\text{P}_4$ ) complexes <b>2</b> and <b>5</b> .....	95
<b>Scheme 4.1.</b> Isolobal analogy of <i>n</i> -membered aromatic rings with Group 6 carbonyls. ....	123
<b>Scheme 4.2.</b> Synthetic pathway for synthesis of <i>cyclo</i> - $\text{P}_4$ dianions [ <b>2</b> · $\text{K}_2$ ] and [ <b>1</b> · $\text{K}_2$ ] (gives 2:1 ratio), and rectification of [ <b>1</b> · $\text{K}_2$ ] by thermolysis in presence of CO. ....	125
<b>Scheme 5.1.</b> Proposed mechanism for the formation of dianionic <i>cyclo</i> - $\text{P}_4$ complexes. ....	147
<b>Scheme 5.2.</b> Summary of electrochemical processes accessible to <b>1</b> (CV potentials vs $\text{Fc}^+/\text{Fc}$ in parenthesis) and chemical reagents utilized in synthetic routes. ....	149
<b>Scheme 5.3.</b> Synthesis of thallium adduct [ <b>5</b> · $\text{Tl}$ ].....	152
<b>Scheme 6.1</b> Nucleophilic addition reactions with <b>2</b> . ....	168
<b>Scheme 6.2.</b> P-atom extrusion pathways for synthesis of <b>6-P3</b> from di- and tetravalent <i>cyclo</i> - $\text{P}_4$ complexes, <b>1</b> and <b>2</b> , respectively. ....	182
<b>Scheme 6.3.</b> [P-I] group transfer with $\text{CNAr}^{\text{Dipp}2}$ and dppe. ....	187

## LIST OF TABLES

<b>Table 1.1.</b> Comparison of Mo bis-isocyanide catalysts in hydrostannation.....	10
<b>Table 2.1</b> Hydrostannation of aryl and alkyl alkynes using $\text{MoI}_2(\text{CO})_2(\text{CNAr}^{\text{Dipp}^2})_2$ ( <b>1</b> ).....	29
<b>Table 2.2.</b> Calculated structural parameters for $\beta$ -vinylstannane producing intermediates $\text{Mo}(\eta^1\text{-C-(C(H)=C(H)C}_6\text{H}_4\text{-p-X))}(\text{SnMe}_3)(\text{CNPh})_2(\text{CO})_2$ .....	60
<b>Table 2.3.</b> Crystallographic data collection and refinement information.....	71
<b>Table 3.1.</b> TD-DFT difference density plots (red = ground state, blue = excited state) and the corresponding orbital transitions.....	109
<b>Table 3.2.</b> Crystallographic Data Collection and Refinement Information.....	117
<b>Table 4.1.</b> X-Ray Crystallographic Data.....	140
<b>Table 5.1.</b> Selected bond parameters for <b>6</b> (XRD and DFT), [ <b>5</b> ][CoCp <sub>2</sub> ], and [ <b>5</b> • <b>TI</b> ].....	156
<b>Table 5.2.</b> Crystallographic Data Collection and Refinement Information.....	163
<b>Table 6.1.</b> Crystallographic Data Collection and Refinement Information.....	198

## ACKNOWLEDGEMENTS

The one most memorable piece of advice I got before coming to graduate school was from my supervisor at the time, Jordan Quinn; he said, “don’t do graduate school alone, it can’t be done.” Having never been one to learn life’s lessons the easy way, I can now add that one gains nothing by trying to do so. Not only has the involvement of many others made this endeavor possible, they have made it meaningful.

First and foremost, I want to thank Professor Joshua S. Figueroa. The “defining moment” for me as a graduate student happened before I even accepted the offer from UCSD. It was during recruitment weekend when I sat in Josh’s office as he presented a poster of the group’s work. Despite having no organometallics background, I was amazed by both the presentation and the presenter. I didn’t have to understand a lot of the chemistry to know that what he was doing was something that I wanted to be a part of. The elegance of Figueroa Chemistry is something that continues to inspire me in my work and beyond. Josh has this amazing ability to cut to the core of a problem and see things for what they are. And after almost five years of wandering in the dark trying to see things the way Josh does, Lo and Behold, the Key to Getting It Done was right where he said it would be. As an advisor and friend, Josh has truly given me something to aspire to.

Probably the best day in my first two years of grad school was when Joanne Chan and Myles Drance joined the group. The many hours of coffee-cart banter with Myles probably contributed as much to my intellectual development as all the coursework and experiments combined. I have been endlessly impressed by his ability to push through obstacles and make unbelievable discoveries. Joanne is probably tired of hearing that she “changed the group,” but she really did. It couldn’t have been easy coming into the testosterone wasteland we had going at the time, but if it wasn’t easy she never showed it. One of my personal favorite things about

Joanne, is that she is a great person to test ideas on, regarding science or otherwise. She has impeccable judgement and an inability to hide her disdain for bad ideas. If she gives you a side-smile and says nothing, you need to reassess your position.

I also want to thank the not quite fearless experimenters, who learned as I did that  $F_b = m_b a_b$ ,  $d_{PH} = (1/2)gt^2$ . Remarkable. Where would science be today without us? When Mike joined, I think I speak for everyone in saying I was shocked that someone with such a happy face would ever want to work with us. Amazingly, however, the guy knows how to produce and has already made some amazing discoveries. I'm also glad to know that the night shift shall live on for as long as Mike remains. Notwithstanding, when Mike is gone, I recommend throwing out that single-station. It's now inflicted two generations (Chuck and Mike) with affability. Our rep can't handle a third. Unlike Mike, Alejandra knew exactly what to do when she joined: say nothing, claim a desk, get in lab, get to work. She is torchbearer for the OGs – knowing how to push hard and get results. She also happens to be a great person. The lab will be in good hands with these two at the helm.

Of course, I owe a lot of thanks to the “older” guys, who are all somehow younger than me. Alex, what can I say? Stay wild. And remember, chairs are for sitting. No one can argue that Charles Mokhtarzazaldkdfalj isn't the best person to have ever graced the UCSD campus. Seeing this guy develop into an absolute beast of a chemist was probably one of the most inspiring things I encountered here. No Charlie has ever earned the title “Chuck” as hard as you have. Brandon Barnett was already a professor without the title when we arrived, so it was just an honor to have learned from his example in science and communication. Doug showed us what efficiency is supposed to look like. I've been trying to figure out his daily routing since I got here so I could eventually mimic his outcomes. Lastly, but no less importantly, I want to thank Treffly Ditri for



pushing the ball up the hill on Group 6. The entirety of this dissertation was derived from just one of his many molecules.

Regrettably, the night-shift has not been conducive to networking. Despite this fact, many great people within this department have gone out of their way to make this work what it is. First, I want to recognize Arnie Rheingold, Curtis Moore, and Milan Gembicky for all the work that has gone into building and maintaining one of the best X-ray facilities in the world. In speaking with graduate students at other universities, I realize what a rare and special opportunity it is to be given unabated access to such an amazing place even though it would be much easier not to. Doing so is a wonderful display of Arnie's commitment to our education. Of course, this is also true for Milan and Curtis who then suffer the consequences of our mistakes and misdeeds. The willingness of these guys to share their knowledge has been one of the most enriching aspects of graduate school for me and every other generation of students in the Figueroa group. It begins almost on Day 1 with Arnie's class, and is carried through to the end by Milan and Curtis in help with data collection and refinement.

Many others have also been giving of their time and resources to help myself and many others succeed. Professor Jeff Rinehart was an especially big encouragement early on in graduate school and helped me think about the big picture of academic study; it was also nice to see another face pass through the halls of Pacific Hall at 2 a.m. Professor Joe O'Conner provided my very first teachings about organometallics in what was one of the most important courses I took while at UCSD. I also appreciate Professor Guy Bertrand and Professor Dionicio Siegal for their thoughtful questions in my candidacy exam and at my defense. Thanks to Dr. Yongxuan Su for his help in fixing our GC-MS, and running many challenging samples through his ESI-MS. Professor Pomeroy and Jon Sauer were also extremely helpful in assisting us in very specialized

mass spectroscopy experiments. From outside of our department, but still in the UC family, I want to thank Professor Andy Borovik and Victoria Oswald of UC Irvine for help with collecting EPR data. Thanks to Jeremy Hilgar for being an all-around great person to talk to about science or otherwise. Jeremy was already more knowledgeable than most 5<sup>th</sup> year grads when he got to UCSD, so he was an excellent help understanding basic magnetometry and EPR data. I also want to send the strongest of thanks to Corey Weinstein for making the last four chapters of this dissertation possible with generous donation of sublimed P<sub>4</sub> – also Professor Bertrand for the material. Another huge thanks to Corey for sending me Sarah Barnhill’s beautiful template for this dissertation.

I want to thank the many lifelong friends I’ve made here. Anyone that knows me knows that I have trouble prioritizing anything that isn’t work related. So all of these people have been very understanding as I missed 95% of social activities so I could be in the lab. May-Linn Paulsen, in full knowledge of the extent of this deficit, used her network to help me find housing in the 9<sup>th</sup> hour as my leases expired. I want to thank Quint Frauman for being the most dependable person that I have ever met, and a genuinely great human being. Also, Greg Triefer for many great discussions, and getting me out to Big Bear for a much-needed snowboard trip. Thanks to Amit Pandey for explaining matrix math and group theory, and for all the ridiculous memes. Thanks Evan Horn for bringing the Eagle home to roost and life-saving victuals; I hope you survive the hurricane while in Mexico so I can set you straight for dissing my new whip. Thanks Posha for Chilladas and pirate stories. I also want to pour one out for Noah Mendelson, without whom I never would have gotten as far along as I have. Thanks to Ryan Holland to listening to hours of contemplation about hydrostannation and for his many intellectual contributions to this work. I

also want to thank Aaron for being a friend when Noah and Ryan left, even though I contribute nothing in conversations about football or basketball.

Before coming to graduate school, many people had a hand in my development both professionally and scientifically. First, I want to thank Dr. Steve DiBiase. It's seldom that one person can have such a profound impact on a young person (okay Alé, I realize I wasn't that young), but without Steve, I would have done an MBA as planned—definitely not a PhD. Having recently passed, he will be greatly missed as a source of wisdom and encouragement as I begin my career. Thanks to my other mentors at Elevance, Dr Jordan Quinn and Dr Paul Bertin for guiding me in my selection of UCSD, and amazing advice for succeeding as a graduate student. Also Prof. Nathan Gianneschi and Angela Blum (now Prof!) for guidance when I arrived at UCSD. Dr. Mike Donovan was a huge influence on my development as a scientist at AMCOL and can credited with teaching me the scientific method.

My experiences in research at Indiana University were incredibly important to my development as a scientist. Thanks first and foremost to Prof. Amar Flood for accepting me at a late-stage in undergraduate and taking the time to meet with me every week and help me progress into a competent chemist. Thanks to Dr. Kevin McDonald for teaching everything I know about chemical synthesis and teaching me to always weigh kinetics and thermodynamics when considering reaction outcomes. Thanks to Dr. Eddie Witlicki and Dr. Kumar Parimal for being the first people in my career to regard me as a colleague, and for letting me join you for walks and beers. Thanks also to Dr. Suraj Dixit for all your help finding a lab in undergraduate.

Over the last five years, I've relied heavily on the infinite supply of love and support from my family. So much so, that I am going to refer to my mom by her full name, Janice Renée Goff Mandla-Mattingly. I've watched in awe of what she is capable of, and in doing so, she's taught

me so much about love and faith (1 Corinth 13, Heb 11:1). Thanks to my dad, Dirk Mandla, for teaching me to treat all people with the respect and dignity they deserve (John 13:34-35), even if it seems like they don't (Rom 3:23). Thanks to Mark Mattingly for all the advice and being the example a guy needs growing up through his twenties and thirties (James 1:19, Titus 2:7). Thanks to my grandparents for helping me see the best in myself. Thanks to Uncle Brian and Aunt Mandy for being a huge source of encouragement and support when I needed it most. My brother and sisters have also been amazing in their support – I know that seeing me was at least 50% of the reason they came to sunny San Diego for frequent visits. Micah is still a legend, and the only guy I know to have gotten smarter after a massive blow to the head.

I also want to thank my Norwegian family, especially Anita and Jone (pronounced Yunuh), for being so gracious to me and my family in Norway. For me, graduate school swelled to encompass the whole continent of North America, but in Norway, especially when fishing with Jens (pronounced Yenz) and Jone – sweet relief. Finally, I want to thank the person who has been my number one source of love and support over the last five years, Hanna Khazri Ibrahimian. She's been my best friend and confidant despite so many obstacles, and a true blessing through all circumstances. I am honored to gain from her wisdom and experience, but most of all I am excited to spend my life with someone so full of joy.

To these and the many other people who have offered their support over the last years,  
Thank You.

**Chapters 1 and 2:** These chapters were adapted with permission from Mandla, K. A.; Moore, C. E.; Rheingold, A. L.; Figueroa, J. S. "Regioselective Formation of (*E*)- $\beta$ -Vinylstannanes with a Topologically Controlled Molybdenum-Based Alkyne Hydrostannation Catalyst,"

*Angewandte Chemie, International Edition*, **2018**, 57, 6853-6857. Copyright 2018 Wiley-VCH, Weinheim. The dissertation author is the first author of this paper.

**Chapter 3:** This chapter was adapted with permission from Mandla, K. A.; Moore, C. E.; Rheingold, A. L.; Figueroa, J. S. “Photolytic Reductive Elimination of White Phosphorus from a Mononuclear *cyclo*-P<sub>4</sub> Transition Metal Complex: Bespoke P<sub>4</sub> Release Using Benign Stimulus,” *Angewandte Chemie, International Edition*, **2018**, *Accepted*. Copyright 2018 Wiley-VCH, Weinheim. The dissertation author is the first author of this paper.

**Chapter 4:** This chapter was adapted with permission from Mandla, K. A.; Moore, C. E.; Rheingold, A. L.; Figueroa, J. S. “A *cyclo*-P<sub>4</sub> Analog of Mo(CO)<sub>3</sub>( $\eta^6$ -benzene),” *In Preparation*. The dissertation author is the first author of this paper.

**Chapter 5:** This chapter was adapted with permission from Mandla, K. A.; Neville, M.; Moore, C. E.; Gembicky, M.; Rheingold, A. L.; Figueroa, J. S. “The Electrochemistry of Molybdenum *cyclo*-P<sub>4</sub> Complexes and Isolation of the First Mononuclear *cyclo*-P<sub>4</sub> Radical,” *In Preparation*. The dissertation author is the first author of this paper.

**Chapter 6:** This chapter was adapted with permission from Mandla, K. A.; Moore, C. E.; Gembicky, M.; Rheingold, A. L.; Figueroa, J. S. “*cyclo*-P<sub>4</sub> as a Stoichiometrically Precise Source of P-I,” *In Preparation*. The dissertation author is the first author of this paper.

## VITA

2018 Ph.D. in Chemistry, University of California San Diego

2015 M.S. in Chemistry, University of California San Diego

2010 B.S. in Chemistry with Honors, Indiana University

## PUBLICATIONS AND PATENTS

Mandla, K. A.; Moore, C. E.; Rheingold, A. L.; Figueroa, J. S. “Photolytic Reductive Elimination of White Phosphorus from a Mononuclear *cyclo*-P<sub>4</sub> Complex: Bespoke P<sub>4</sub> Release Using Benign Stimulus”, *Angewandte Chemie, International Edition*, **2018**, *Accepted*.

Mandla, K. A.; Moore, C. E.; Rheingold, A. L.; Figueroa, J. S. “Regioselective Formation of (*E*)- $\beta$ -Vinylstannanes with a Topologically Controlled Molybdenum-Based Alkyne Hydrostannation Catalyst” [VIP, COVER], *Angew. Chem. Int. Ed.* **2018**, *57*, 6853-6857.

Brekan, J.; Quinn, J.; Mandla, K.; Littich, R. “Branched Diesters for Use as a Base Stock and in Lubricant Applications,” Pat. No. US10059903B2/WO2015134251A1. March 2014.

R. Arnold, K. Mandla, et. al. “Overcoming Matrix Effects in a Complex Sample: Analysis of Multiple Elements in Multivitamins by Atomic Absorption Spectroscopy,” *Journal of Chemical Education*, **2011**, *88*, 484-487.

## IN PREPARATION

Mandla, K. A.; Moore, C. E.; Rheingold, A. L.; Figueroa, J. S. “A *cyclo*-P<sub>4</sub> Analog of Mo(CO)<sub>3</sub>( $\eta^6$ -benzene).”

Mandla, K. A.; Moore, C. E.; Gembicky, M.; Rheingold, A. L.; Figueroa, J. S. “The Electrochemistry of Molybdenum *cyclo*-P<sub>4</sub> Complexes and Isolation of the First Mononuclear *cyclo*-P<sub>4</sub> Radical,”

Mandla, K. A.; Moore, C. E.; Gembicky, M.; Rheingold, A. L.; Figueroa, J. S. “*cyclo*-P<sub>4</sub> as a Stoichiometrically Precise Source of P-I.”

ABSTRACT OF THE DISSERTATION

**Direct Access to Chemistry and Catalytic Behavior of  
the Zero-Valent  $\text{MoL}_4$  Fragment**

by

Kyle Andrew Mandla

Doctor of Philosophy in Chemistry

University of California San Diego, 2018

Professor Joshua S. Figueroa, Chair

This dissertation describes investigations in the reactivity of mixed carbonyl-isocyanide complexes of molybdenum. A primary challenge in isolating functional surrogates of low-coordinate, zero-valent Group 6 carbonyls, e.g.  $\text{M}(\text{CO})_2$ ,  $\text{M}(\text{CO})_3$ ,  $\text{M}(\text{CO})_4$  has been the tendency of these compounds form intramolecular  $\eta^6$ -arene interactions with the flanking rings of supporting ligands. In this work, a screening of catalysts for hydrostannation provided insight into stabilization of four-coordinate, zero-valent metal centers. Accordingly, reduction of

$\text{MoI}_2(\text{CO})_2(\text{CNAr}^{\text{Dipp}2})_2$  with two equivalents of  $\text{HSnBu}_3$  in the presence of weakly coordinating Lewis bases (e.g. diisopropyl amine  $[\text{HN}^i\text{Pr}_2]$ ,  $\text{Et}_2\text{O}$ ) provided access to masked sources of  $\text{ML}_4$ . The unprecedented reactivity and  $\beta$ -(*E*)-regioselectivity of  $\text{MoI}_2(\text{CO})_2(\text{CNAr}^{\text{Dipp}2})_2$  in hydrostannation of alkynes are discussed in Chapter 2. Chapter 3 describes the use of  $\text{MoI}_2(\text{CO})_2(\text{CNAr}^{\text{Dipp}2})_2$  and the CH-agostic complex,  $\text{Mo}(\kappa^2\text{-N,CH})\text{-HNiPr}_2(\text{CO})_2(\text{CNAr}^{\text{Dipp}2})_2$  in the activation of elemental phosphorus ( $\text{P}_4$ ). The tetravalent product,  $(\eta^4\text{-P}_4)\text{MoI}_2(\text{CO})(\text{CNAr}^{\text{Dipp}2})_2$  was found to undergo photolytic reductive elimination of white phosphorus. In Chapter 4, the synthesis of two dianionic *cyclo*- $\text{P}_4$  complexes is discussed. Investigations with these compounds revealed *cyclo*- $\text{P}_4$  ligand to be isolobal to benzene in Fischer's classic half-sandwich complex  $\text{Mo}(\text{CO})_3(\eta^6\text{-C}_6\text{H}_6)$ . Chapter 5 further explores the redox chemistry of *cyclo*- $\text{P}_4$  complexes by cyclic voltammetry. Chapter 6 describes the functionalization of *cyclo*- $\text{P}_4$ , including the stoichiometric release of [P-I] by treatment of  $(\eta^4\text{-P}_4)\text{Mo}(\text{CO})_2(\text{CNAr}^{\text{Dipp}2})_2$  upon treatment with 1 equiv  $\text{I}_2$ .



# Chapter 1

## Synthesis of Masked $ML_4$ Analogs to $Mo(CO)_4$

### 1.1 Introduction

The ability of transition metal complexes to affect activation of chemical bonds (e.g. [E-H], [E-X], [E-E]; E = C, Si, Sn, P, N)<sup>1-10</sup> is a primary driving force motivating continued exploration within the field of synthetic inorganic chemistry.<sup>11</sup> The incorporation of elementary bond-breaking and bond-making steps into catalytic processes have brought far reaching advancements in chemical syntheses<sup>12,13</sup> relevant to food production,<sup>14</sup> pharmaceuticals,<sup>15,16</sup> and materials.<sup>17</sup> To affect bond activation, an essential precondition of the transition metal complex is the availability of substrate-accessible coordination sites.<sup>18</sup> Indeed, the accessibility and stability of coordinatively unsaturated intermediates are key elements in the design and performance of a catalyst.<sup>19</sup> These specifications are especially challenging to address where highly activating, low-valent metal centers are required. Well suited for this purpose, however, are the binary metal carbonyls,  $M(CO)_n$ . Accordingly, CO-ligand dissociation by exposure to light or heat provides access to low-coordinate intermediates thermodynamically stabilized by the  $\pi$ -acidic ligand field.<sup>18,20</sup> It is unsurprising, therefore, that binary metal carbonyls remain state-of-the-art catalysts for a number of industrial scale processes.

Among the most versatile metal carbonyls utilized in organic synthesis is  $Mo(CO)_6$ .<sup>21</sup> Investigations have demonstrated the capability of  $Mo(CO)_6$  as a catalyst in alkyne metathesis,<sup>22-26</sup> Pauson-Khand reactions,<sup>27-32</sup> alkyne cyclotrimerization,<sup>33,34</sup> cyclo-isomerizations of epoxyalkynes to furans,<sup>35-38</sup> catalytic oxidation of dialkyl furans,<sup>39</sup> reduction of N-O bonds.<sup>40-45</sup> and hydrosilylation.<sup>46</sup> Indeed, the diverse reactivity of  $Mo(CO)_6$  provides a glimpse into the rich chemistry available to the coordinatively unsaturated fragments –  $[Mo(CO)_4]$ ,  $[Mo(CO)_3]$ , and

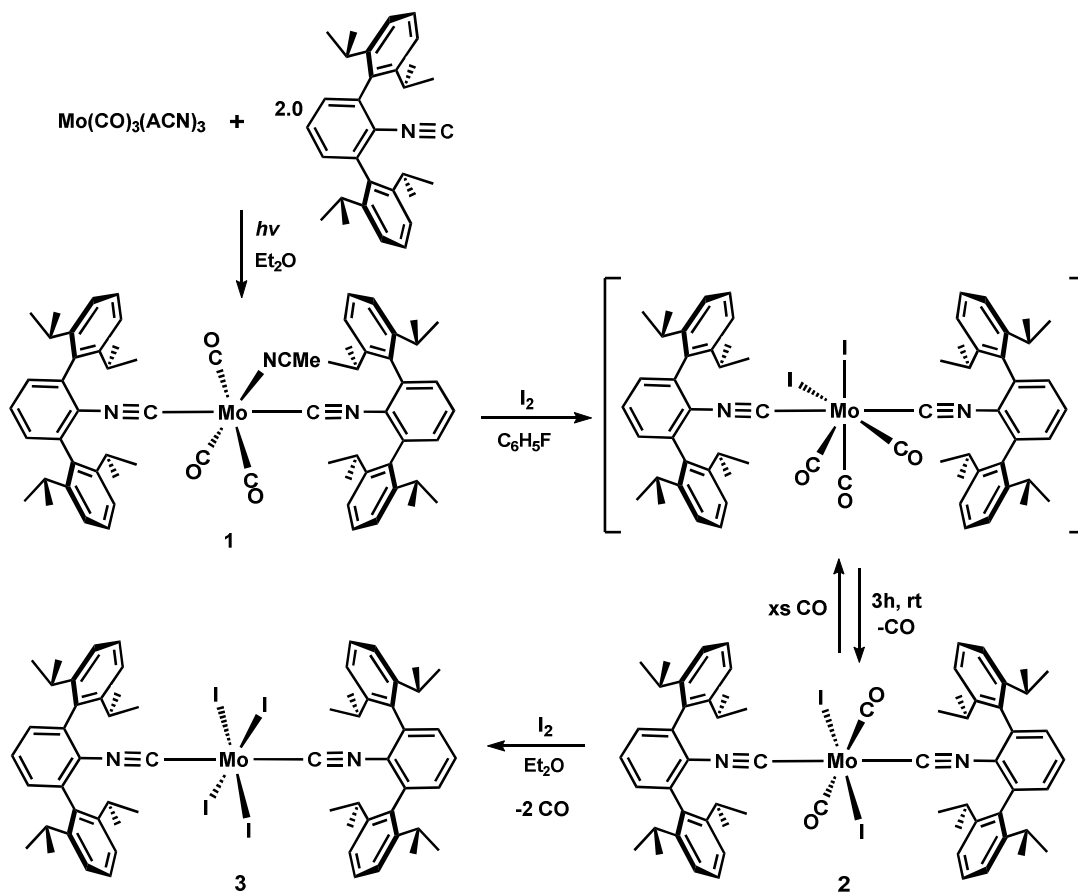
[Mo(CO)<sub>2</sub>] – which are undoubtedly involved in the aforementioned catalytic processes. Paradoxically, however, the highly activating, electron rich metal centers that render these complexes so interesting have also restricted direct observation to gas-phase matrix isolation studies. The systematic analysis of reactivity patterns for these species has thus been prevented.

Over the past decade, a major focus of our research group has been the synthesis of isolable structural mimics to coordinatively unsaturated metal carbonyls. Recognizing that an isolobal analogy exists between CO and isocyanide ligands, our group has developed a library of sterically encumbering, *m*-terphenyl isocyanide ligands which, upon coordination, retain a  $\pi$ -acidic coordination environment while also providing enhanced kinetic stabilization of the low-coordinate metal center compared to their carbonyl congeners. Importantly, *m*-terphenyl isocyanides have proven to be effective in isolating homoleptic isocyanide analogs to Co(CO)<sub>4</sub>,<sup>47</sup> Ni(CO)<sub>3</sub>,<sup>48,49</sup> Pd(CO)<sub>2</sub>.<sup>50</sup> Disappointingly, however, attempts to extend these strategies to more electron-deficient, Group 6 transition metals were met by challenges not encountered in the late transition metal systems.<sup>51–53</sup>

## 1.2 Synthesis of Group 6 Isocyanides

It was initially hoped that reduction of commercially available Group 6 metal halides in the presence of CNAr<sup>Dipp2</sup> (Ar<sup>Dipp2</sup> = 2,6-(2,6-(*i*-Pr)<sub>2</sub>C<sub>6</sub>H<sub>3</sub>)<sub>2</sub>C<sub>6</sub>H<sub>3</sub>) would provide a direct route to low-coordinate, zero-valent [M(CNAr<sup>Dipp2</sup>)<sub>n</sub>] (n < 6) complexes.<sup>53</sup> While these methods have been successful in preparation of homoleptic M(CNR)<sub>6</sub> complexes,<sup>54,55</sup> reduction experiments with *m*-terphenyl isocyanides led to intractable mixtures. Furthermore, attempts to generate high-valent precursors from typical starting materials MoCl<sub>3</sub>(THF)<sub>3</sub> or MoCl<sub>4</sub>(NCMe)<sub>2</sub> failed to give productive isocyanide binding. To address these synthetic limitations, Colton's classic oxidative

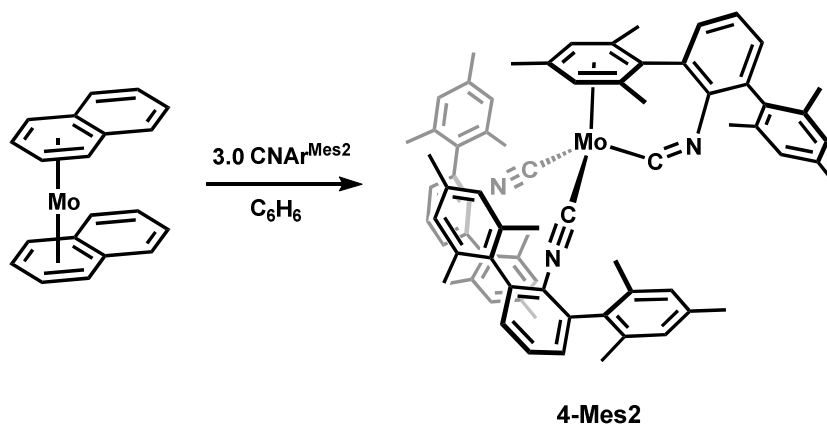
decarbonylation strategy<sup>56–62</sup> was used in conjunction with the mixed carbonyl isocyanide *trans*- $M(\text{CNAr}^{\text{Dipp}2})_2(\text{CO})_3(\text{CNAr}^{\text{Dipp}2})_2(\text{ACN})$  ( $M = \text{Mo}, \text{W}$ ) to generate isocyanide-substituted metal-halide precursors (Scheme 1.1). Accordingly, stepwise oxidation of  $\text{Mo}(\text{CNAr}^{\text{Dipp}2})_2(\text{CO})_3(\text{CNAr}^{\text{Dipp}2})_2(\text{ACN})$ <sup>51</sup> with one and two equivalents of  $\text{I}_2$  readily afforded di- and tetra-valent decarbonylation products **2** and **3**. Notably, divalent dicarbonyl complex **2** provides an exceedingly rare example of a paramagnetic Group 6 complex with the general formula  $\text{MX}_2(\text{CO})_2\text{L}_2$ .<sup>59,60</sup> In the absence of encumbering ligands, the related tetracarbonyl species,  $[\text{MX}_2(\text{CO})_4]$  ( $M = \text{Mo}, \text{W}; \text{X} = \text{Cl}, \text{Br}, \text{I}$ ), form bridging-halide dimers to



**Scheme 1.1.** Stepwise decarbonylation of **1** with diiodine.<sup>52</sup>

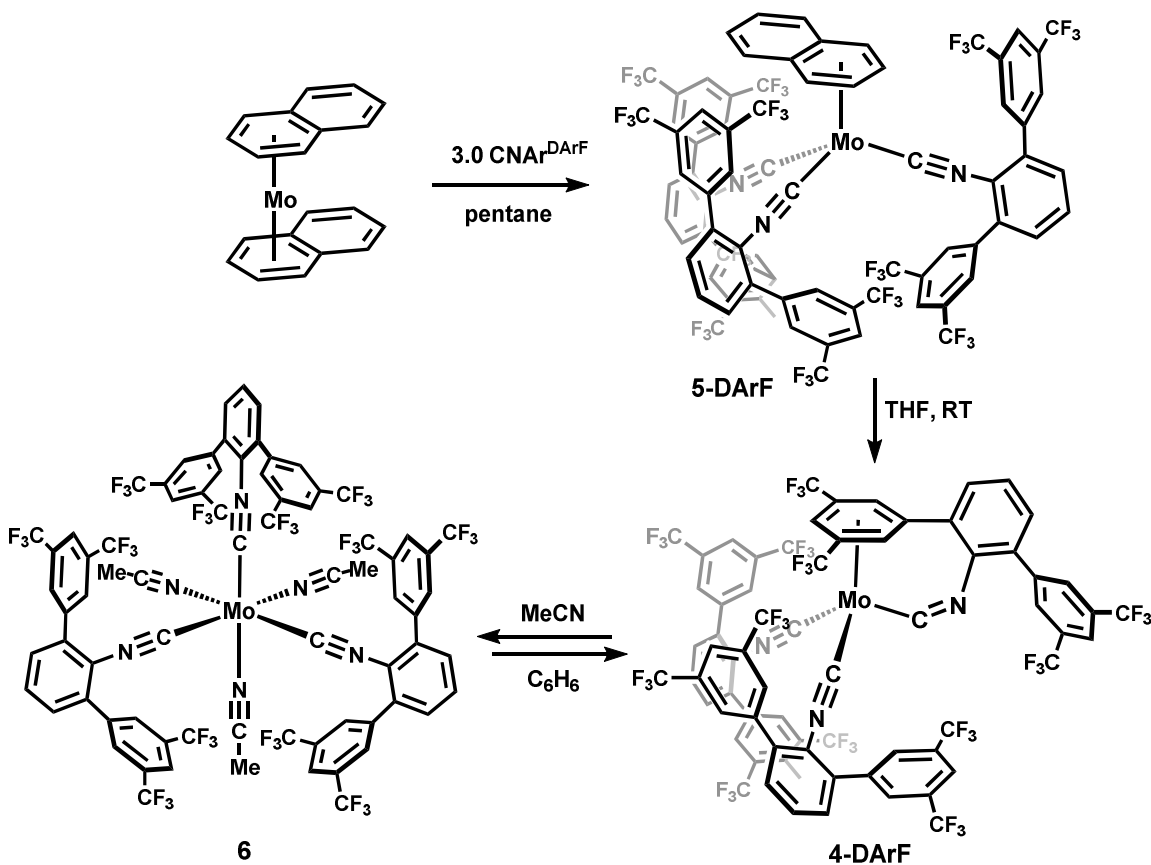
give 7-coordinate 18-electron metal-centers.<sup>56,61,63,64</sup> Isolation of **2** as a mononuclear, 16-electron complex thus serves as testament to the ability of the trans-disposed CNAr<sup>Dipp</sup><sub>2</sub> ligands to support low-coordination numbers. Despite having a mixed carbonyl-isocyanide coordination environment, the triplet ground state of **2** reflects a preservation of the electronic structure expected for the theoretical mononuclear MoX<sub>2</sub>(CO)<sub>4</sub> complexes.<sup>65</sup> In contrast, decreased  $\pi$ -acceptance in the related MX<sub>2</sub>(CO)<sub>2</sub>L<sub>2</sub> complexes<sup>66</sup> where L = PR<sub>3</sub> results in a pronounced O<sub>h</sub>  $\rightarrow$  C<sub>2v</sub> distortion to give a larger HOMO-LUMO gap and spin pairing.<sup>65</sup>

Attempts to access the corresponding zero-valent, 4-coordinate mixed carbonyl-isocyanide by reduction of **2** in these early works resulted in intractable mixtures.<sup>52</sup> Interestingly, however, Na/Hg reduction of **3** resulted in  $\eta^6$ -coordination of benzene solvent, and one equivalent of dinitrogen to give ( $\eta^6$ -C<sub>6</sub>H<sub>6</sub>)Mo(CNAr<sup>Dipp</sup><sub>2</sub>)<sub>2</sub>(N<sub>2</sub>). The occupation of four coordination sites by exogenous ligands, C<sub>6</sub>H<sub>6</sub> and N<sub>2</sub>, suggest that coordinatively unsaturated intermediates are adequately stabilized, albeit on short time scales, such that degradation of the [MoL<sub>2</sub>] unit is prevented. Unfortunately, however, the coordination of exogenous benzene in this system foreshadowed a major obstacle to obtaining molecular sources of zero-valent, coordinatively unsaturated Mo-complexes.<sup>52</sup>



**Scheme 1.2.** Synthesis of  $\eta^6$ -arene complex **4-Mes2**.<sup>53</sup>

A major challenge in accessing coordinatively unsaturated Group 6 complexes has been the tendency of the desired low-coordinate Mo-species to attain 18-electron configuration through robust intramolecular  $\eta^6$ -arene interactions with a flanking ring of the *m*-terphenyl group (Scheme 1.2). Accordingly, attempts to access three- and four-coordinate complexes by treatment of the zero-valent bis-naphthalene complex  $\text{Mo}(\eta^6\text{-C}_{10}\text{H}_8)_2$  with  $\text{CNAr}^{\text{Mes}2}$  ( $\text{Ar}^{\text{Mes}2} = 2,6\text{-}(2,4,6\text{-Me}_3\text{C}_6\text{H}_2)_2\text{C}_6\text{H}_3$ ) or  $\text{CNAr}^{\text{Dipp}2}$  resulted in formation of the “ $\eta^6$ -arene-capped” structure  $\text{Mo}(\eta^6\text{-}(\text{Mes})\text{-}\kappa^1\text{-C-CNAr}^{\text{R}})(\text{CNAr}^{\text{R}2})_2$  (i.e. **4-Mes2**, Scheme 1.2). Efforts to prevent arene-capping by using the more sterically encumbering *m*-terphenyl isocyanide  $\text{CNAr}^{\text{Dipp}2}$  were unsuccessful, resulting in formation of the analogous complex, **4-Dipp2** [ $\text{Mo}(\eta^6\text{-}(\text{Dipp})\text{-}\kappa^1\text{-C-CNAr}^{\text{Dipp}})(\text{CNAr}^{\text{Dipp}2})_2$ ].



**Scheme 1.3.** Synthetic scheme demonstrating enhanced lability of electron-deficient arene in  $\text{CNAr}^{\text{DArF}}$ .<sup>53</sup>

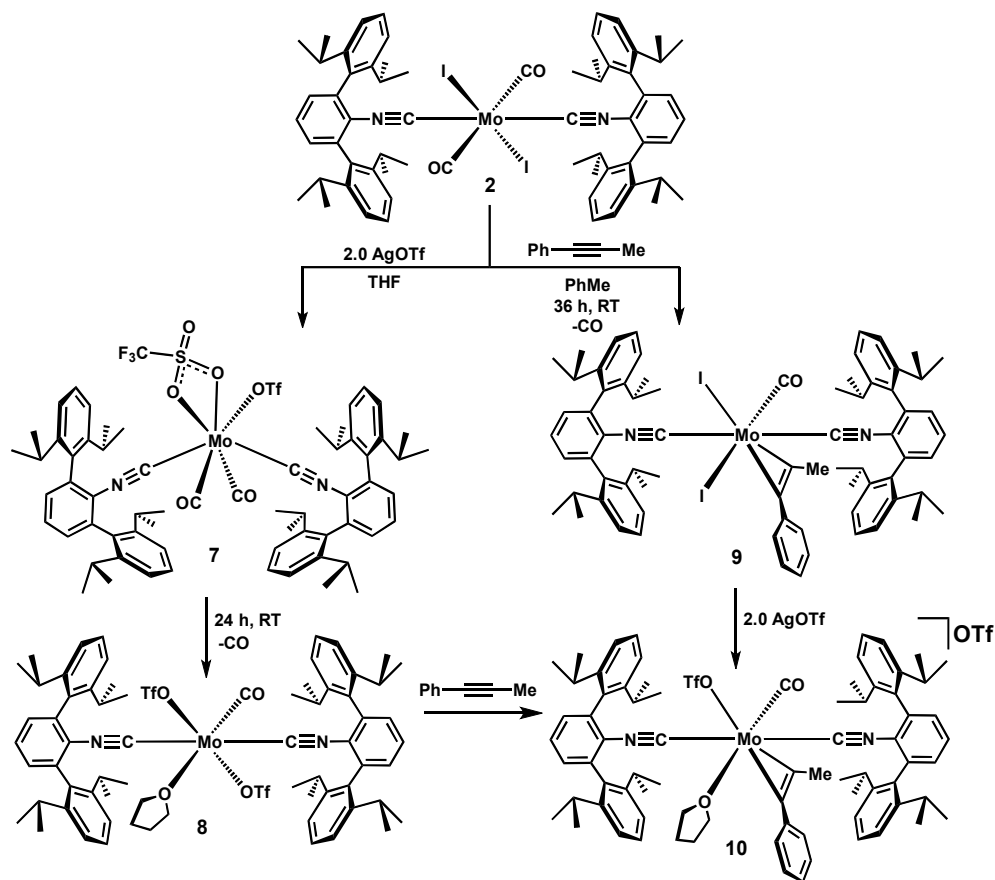
To address these challenges, *m*-terphenyl isocyanides bearing more electron deficient flanking arenes were investigated. Interestingly, the reduced electron-donating ability of 2,6-dichloro-arene in  $\text{CNAr}^{\text{Clips}}$  ( $\text{Ar}^{\text{Clips}} = 2,6-(2,6\text{-Cl}_2\text{C}_6\text{H}_3)_2(4\text{-}t\text{-Bu})\text{C}_6\text{H}_2$ ) resisted intramolecular  $\eta^6$ -arene-capping to give the mono-naphthalene complex  $\text{Mo}(\eta^6\text{-C}_{10}\text{H}_8)(\text{CNAr}^{\text{Clips}})_3$  (**5-Clips**). Unfortunately, decomposition pathways involving Ph-Cl bond activation prevented access to low-coordinate, zero-valent species. To address the problem of C-X bond activation while retaining electron deficiency in the flanking arene rings, another ligand,  $\text{CNAr}^{\text{DArF}}$  ( $\text{Ar}^{\text{DArF}} = 2,6-(3,5\text{-}(\text{CF}_3)_2\text{C}_6\text{H}_3)_2\text{C}_6\text{H}_3$ ) was developed. Similar to  $\text{CNAr}^{\text{Clips}}$ , the electron deficient flanking rings of  $\text{CNAr}^{\text{DArF}}$  were slow to displace the second naphthalene ligand, thus giving the intermediate mono-naphthalene structure **5-DArF** (Scheme 1.3. Synthetic scheme demonstrating enhanced lability of electron-deficient arene in  $\text{CNAr}^{\text{DArF}}$ ). Although  $\eta^6$ -arene-capped structure **4-DArF** was generated in THF, enhanced lability of the arene-interaction enabled displacement upon dissolution in more strongly-coordinating solvents, as was demonstrated by the reversible formation of **6** in acetonitrile. Lability of the  $\eta^6$ -arene interaction suggests that **4-DArF** may serve as suitable source of the  $\text{ML}_3$  fragment in cases where moderately  $\sigma$ -donating substrates are present in high concentration.<sup>53</sup> However, spontaneous reversal of this process upon dissolution of **6** in  $\text{C}_6\text{H}_6$  suggest the thermodynamic favorability of intramolecular  $\eta^6$ -arene interactions remain limiting. Despite significant progress, these findings indicated that new strategies would have to be implemented in order to fully harness the reactivity of coordinatively unsaturated Mo.

### 1.3 Application of *m*-Terphenyl Isocyanides in Mo-catalyzed Hydrostannation

With an extensive survey of synthetic methodology for preparation of Group 6 isocyanides at our disposal,<sup>51-53</sup> recent investigations have sought to exploit the well-defined, sterically

encumbered coordination environments for use in catalysis.<sup>67</sup> Previously, Kazmaier and co-workers showed that inclusion of *tert*-butyl isocyanide ligands in the complex  $\text{Mo}(\text{CO})_3(\text{CN}^t\text{Bu})_3$  (**MoBI<sub>3</sub>**) provided greatly enhanced turn-over-numbers and regioselectivity as a catalyst in hydrostannation of alkynes compared to  $\text{Mo}(\text{CO})_6$ .<sup>68–71</sup> Interestingly, however,  $\alpha$ -regioselectivity in this system was restricted to alkynes bearing electron-withdrawing substituents in the propargyl position. Motivated by these reports, we hypothesized that inclusion of  $\text{CNAr}^{\text{Dipp}^2}$  ligands would further constrain coordination geometries of active catalytic intermediates to give enhanced regioselectivities. As is described in detail in Chapter 2,  $\text{MoI}_2(\text{CO})_2(\text{CNAr}^{\text{Dipp}^2})_2$  (**2**) was found to be the first highly selective catalyst for preparation of  $\beta$ -(*E*)-vinylstannanes.<sup>67</sup> The investigations disclosed in this section describe work undertaken toward the optimization and elucidation of active catalytic intermediates in hydrostannation. Reactivity studies showed dissociation of CO to be a general feature of most chemical reactions involving **2**. To our surprise, however, mono-decarbonylated products prepared in these studies [e.g.  $\text{MoI}_2(\text{CO})(\text{CNAr}^{\text{Dipp}^2})(\eta^2\text{-PhC}\equiv\text{CMe})$  (**9**),  $\text{MoI}_2(\text{CO})(\text{CNAr}^{\text{Dipp}^2})(\text{OEt}_2)$  (**11**)] were found to be inactive in hydrostannation. Importantly, a systematic analysis of bis-isocyanide complexes revealed the zero-valent, four-coordinate fragment  $[\text{Mo}(\text{CO})_2(\text{CNAr}^{\text{Dipp}^2})_2]$  to be critical for efficient catalysis. These findings paved the way for synthesis of masked- $\text{ML}_4$  complexes.

### 1.3.1 Survey of $\text{MoI}_2(\text{CO})_2(\text{CNAr}^{\text{Dipp}})_2$ (**2**) reactivity – synthesis of mono-carbonyl bis-isocyanide complexes



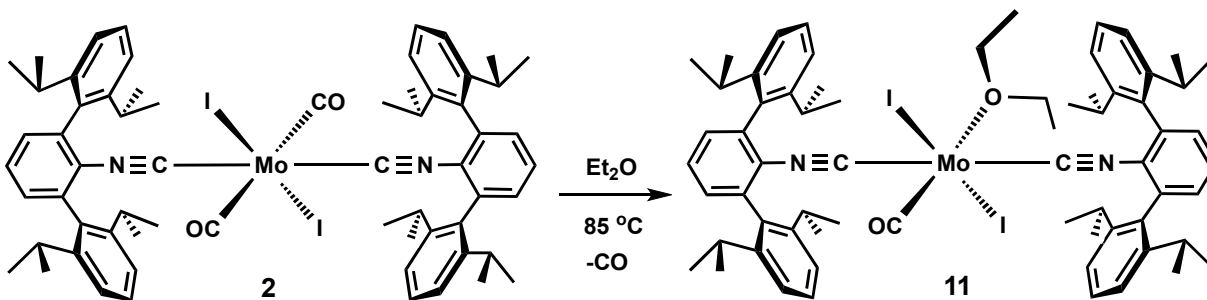
**Scheme 1.4.** Synthesis of divalent mono-carbonyl complexes.

A preliminary assessment of reactivity with **2** showed CO ligand dissociation to be a common feature of that compound's reactivity (Scheme 1.4 & 1.5). As shown in Scheme 1.4, **2** readily exchanges both I ligands by salt-metathesis with  $\text{AgOTf}$  to give the 18-electron  $\kappa^2\text{-O,O-OTf}$  complex, **7**. Interestingly, after 24 h stirring at RT, dissociation of 1 equiv CO affords the paramagnetic 16-electron THF-complex, **8**. Notably in the structure of **8**,  $\kappa^1$ -coordination mode of both triflate ligands likely reflects increased electron-density at the metal center due to exchange of  $\pi$ -acidic CO for a purely  $\sigma$ -donating THF ligand. Interestingly, treatment of **8** with 1 equiv 1-phenyl-1-propyne reveals triflate to be more labile than THF, thus giving the alkyne-substituted



triflate salt, **10**. The synthesis of **10** from **8** is convergent with the salt-metathesis product obtained by treatment of diiodide-alkyne complex **9** with 2 equiv AgOTf.

The lability of CO in **2** is especially evident in the solvolysis with diethyl ether – stirring of an Et<sub>2</sub>O solution of **2** at 85 °C for 3 h resulted in exchange of CO to give the paramagnetic diethyl ether complex, **11**. Although diethyl etherate complexes are well known for high-valent Group 6 complexes,<sup>72–74</sup> it is notable that **11** is, to the best of our knowledge, the first such example among neutral, mononuclear Mo<sup>II</sup>-species. Interestingly, facile dissociation of Et<sub>2</sub>O from **11** renders that species a viable source of the 14-electron fragment [MoI<sub>2</sub>(CO)(CNAr<sup>Dipp</sup>)<sub>2</sub>]. Demonstrating this fact is the reactivity of **11** toward the hindered alkyne 1-phenyl-1-propyne (PhC≡CMe). Whereas **2** undergoes slow exchange of CO for PhC≡CMe over the course of 36 h at RT (**Scheme 1.4**. Synthesis of divalent mono-carbonyl complexes.), **9** is generated nearly instantaneously upon treatment of **11** with the alkyne as indicated by a sudden darkening of solution to black and confirmation by <sup>1</sup>H NMR.



**Scheme 1.5.** Thermolytic dissociation of Et<sub>2</sub>O.

### 1.3.2 Assessment of bis-Isocyanide complexes as catalysts for alkyne hydrostannation

An initial screening of previously reported<sup>51,52</sup> bis-CNAr<sup>Dipp</sup> complexes in hydrostannation of PhC≡CMe revealed divalent-dicarbonyl complex **2** (Table 1.1, entry 3) to be

significantly more reactive than available zero-valent catalysts,  $\text{Mo}(\text{CO})_4(\text{CNAr}^{\text{Dipp}2})_2$  (entry 1) and  $\text{Mo}(\text{CO})_3(\text{CNAr}^{\text{Dipp}2})_2(\text{ACN})$  (**1**, entry 2). Initially, the enhanced reactivity of **2** appeared to reflect the possibility of a  $\text{Mo}^{\text{II}}/\text{Mo}^{\text{IV}}$  redox pair in catalysis. Inconsistent with this notion, however, were the identical outcomes observed in catalysis with diiodide **2** and bis-triflate **7** (entries 3 and 4). Noting that the regioselectivity in hydrostannation is sensitive to subtle variation in ligand topology (see entry 5 for catalytic activity of  $\text{CNAr}^{\text{Tripp}2}$  [ $\text{Ar}^{\text{Tripp}2} = 2,6-(2,4,6\text{-}(\text{iPr})_3\text{C}_6\text{H}_2)_2(\text{C}_6\text{H}_3)$ ] analog of **2**),<sup>5,75</sup> it can be surmised that all X-ligands were cleared from the coordination sphere of **2** and **7** in the activation steps preceding entry into the catalytic cycle.

**Table 1.1.** Comparison of Mo bis-isocyanide catalysts in hydrostannation.

Entry	Catalyst	Metal Oxidation state	X-type Ligand	# of L-type ligands	NMR Yield t = 30 min. (%) <sup>[a]</sup>	Selectivity ( $\beta : \alpha$ ) <sup>[b]</sup>
1	$\text{Mo}(\text{CO})_4(\text{CNAr}^{\text{Dipp}2})_2$	0	None	6	<5	n.d.
2	$\text{Mo}(\text{CO})_3(\text{CNAr}^{\text{Dipp}2})_2(\text{ACN})$ ( <b>1</b> )	0	None	5	16	91 : 9
3	$\text{MoI}_2(\text{CO})_2(\text{CNAr}^{\text{Dipp}2})_2$ ( <b>2</b> )	II	$\text{I}^-$	4	<b>100</b>	91 : 9
4	$\text{Mo}(\text{OTf})(\kappa^2\text{-O, O-OTf})(\text{CO})_2(\text{CNAr}^{\text{Dipp}2})_2$ ( <b>7</b> )	II	$\text{-OTf}$	4	<b>100</b>	91 : 9
5	$\text{MoI}_2(\text{CO})_2(\text{CNAr}^{\text{Tripp}2})_2$	II	$\text{I}^-$	4	<b>100</b>	84 : 16
6	$\text{Mo}(\text{OTf})_2(\text{CO})(\text{CNAr}^{\text{Dipp}2})_2(\text{THF})$ ( <b>8</b> )	II	$\text{-OTf}$	3	6	91 : 9 <sup>[c]</sup>
7	$\text{MoI}_2(\text{CO})(\text{CNAr}^{\text{Dipp}2})_2(\eta^2\text{-PhC}\equiv\text{CMe})$ ( <b>9</b> )	II	$\text{I}^-$	3	<5	n.d.
8	$[\text{Mo}(\text{OTf})(\text{CO})(\text{CNAr}^{\text{Dipp}2})_2(\eta^2\text{-PhC}\equiv\text{CMe})(\text{THF})]\text{OTf}$ ( <b>10</b> )	II	$\text{-OTf}$	3	8	91 : 9 <sup>[c]</sup>
9	$\text{MoI}_2(\text{CO})(\text{CNAr}^{\text{Dipp}2})_2(\text{OEt}_2)$ ( <b>11</b> )	II	$\text{I}^-$	3	<5	n.d.

[a] Reaction conditions: 1-Phenyl-1-propyne (0.170 mmol, 1.00 equiv), and  $\text{HSnBu}_3$  (1.05 equiv) were added to a thawing  $\text{C}_6\text{D}_6$  solution (1 mL) of the catalyst catalyst (0.0034 mmol, 2.0 mol%). The reaction mixture was allowed to react 30 min at room temperature.

[b] Selectivity determined by  $^1\text{H}$  NMR of crude reaction mixture.

[c] Reaction was allowed to proceed for 3 h before determination of selectivity by  $^1\text{H}$  NMR.

Indeed, the absence of X-ligands in the active species strongly suggested activation of **2** and **7** is achieved by two-electron reduction *in situ* with HSnBu<sub>3</sub>.<sup>76</sup> This postulate is further supported by the identical selectivity between **2** and the zero-valent acetonitrile complex, **1**. It is thus likely that disparate reactivity leading to slow turnovers with **1** was the presence of an additional CO ligand. Notwithstanding, the observed 16% conversion of alkyne to vinylstannane products (entry 2) indicates that the active catalytic species is accessible by dissociation of one or more CO ligands.

To further explore the relationship of the ancillary ligand field to catalyst reactivity, divalent mono-carbonyl species were evaluated (entries 6-9, Table 1.1). Noting that dissociation of CO from **2** is a general feature of that compound's reactivity (Schemes 1.4 & 1.5), it seemed likely that ligand dissociation would similarly occur in the activation steps with **2**. Furthermore, it is well known that alkynes can donate all four  $\pi$ -electrons in bonding interactions with a transition metals,<sup>77,78</sup> so it is reasonable that a 12-electron [ML<sub>3</sub>] fragment could interact with alkyne and HSnBu<sub>3</sub> to give [ML<sub>3</sub>( $\eta^2$ -PhC $\equiv$ CMe)(H)(SnBu<sub>3</sub>)] as an 18-electron catalytic intermediate. To our surprise, however, mono-carbonyl complexes showed only trace conversion to vinylstannanes after 30 min (entries 6-9). Evidently, the loss of carbonyl from **2** results in an almost complete shutdown in catalysis.

Remarkably, in cases where yields were high enough to determine  $\alpha/\beta$ -(E) ratio (entries 6 & 8), the selectivities remained identical to that of **2**. In fact, all CNAr<sup>Dipp2</sup> complexes which were competent in catalysis gave identical selectivity (entries 2-4, 6 & 8). Important to note, the relationship between selectivity and catalyst topology is apparent when comparing the results in Table 1.1 with previously reported methodologies— $\beta$ -(E)-selectivity had not exceeded 60% with PhC $\equiv$ CMe.<sup>6,76</sup> It is evident, therefore, that the active catalytic intermediates are *precisely* defined and independent of the CNAr<sup>Dipp2</sup>/CO ratio present in the parent complex. Slow catalysis with the

mono-carbonyl complexes (entries 6-9) thus arises because one CO ligand must be gained by a metal-center (by ligand redistribution) before entering the catalytic cycle. By contrast, the reaction profile of **1** reflects the slow activation of that catalyst by dissociation of one CO ligand. Indeed, these investigations pointed to the critical importance of the  $[\text{Mo}(\text{CO})_2(\text{CNR})_2]$  fragment in catalysis. In line with our group's broader research interests, we were intrigued by the possibility that **2** could serve as a direct source of zero-valent  $[\text{MoL}_4]$ .

## 1.4 The Pursuit and Synthesis of Masked Analogues to $\text{Mo}(\text{CO})_4$

Having established the critical importance of the  $[\text{Mo}(\text{CO})_2(\text{CNAr}^{\text{Dipp}2})_2]$  fragment for efficient catalysis of hydrostannation as described in Section 1.3, synthetic investigations were undertaken to confirm speculations of *in situ* reduction by  $\text{HSnBu}_3$ . Chapter 2 describes the earliest confirmation of a zero-valent active species by trapping of the reactive intermediate, generated by treatment of **2** with 2 equiv  $\text{HSnBu}_3$ , with diisopropyl amine ( $\text{HN}^i\text{Pr}_2$ ) to give an unusual  $\text{Mo}^0$  amine  $\kappa^1\text{-N}/\eta^2\text{-H,C}$  chelate, **12**. Importantly, the reactivity and selectivity in reactions catalyzed by **12** were found to be indistinguishable from those catalyzed by **2**, providing rapid conversion of alkynes to the corresponding vinylstannanes. The finding thus supported our earlier assessment that  $[\text{Mo}(\text{CO})_2(\text{CNAr}^{\text{Dipp}2})_2]$  is the catalytic-element which remains unchanged throughout the catalytic cycle. Although **12** is a suitable source of  $[\text{Mo}(\text{CO})_2(\text{CNAr}^{\text{Dipp}2})_2]$  for hydrostannation, the release of a moderately basic substrate,  $\text{HN}^i\text{Pr}_2$ , could affect the outcome of experiments seeking to probe the reactivity of the four-coordinate core. To address this problem, a series of weakly coordinating ligands have been evaluated as  $\text{ML}_4$  masking agents.

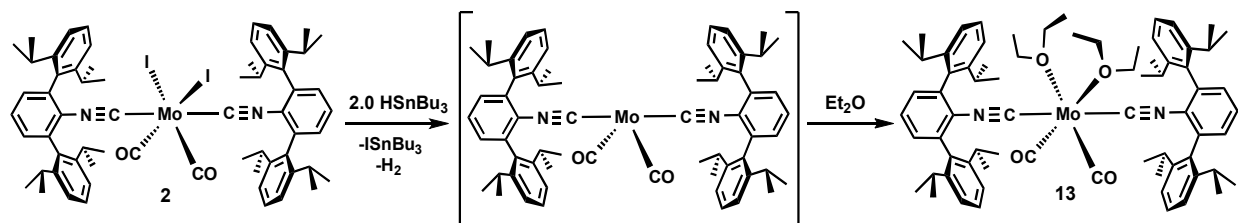
### 1.4.1 Synthesis of masked $\text{MoL}_4$ complexes

Over the course of 30 min, a stirred  $\text{Et}_2\text{O}$  suspension of **2** containing 2 equiv  $\text{HSnBu}_3$  changed from light red to deep purple. The resulting solution was concentrated and washed with

cold pentane to remove tributyltin iodide ( $\text{ISnBu}_3$ ) generated as a by-product of the reduction. The brownish purple solid was in 3:1 pentane/ $\text{Et}_2\text{O}$  and crystallized at  $-40\text{ }^\circ\text{C}$  to give large purple crystals of  $\text{Mo}(\text{CO})_2(\text{CNAr}^{\text{Dipp}^2})_2(\text{OEt}_2)_2$  (**13**) in 64% yield. Interestingly, cis-arrangement of the two  $\text{Et}_2\text{O}$  ligands, as confirmed by X-ray crystallography (Figure 1.1), is consistent with theoretical and spectroscopic investigations proposing cis-divacant geometry in  $\text{Mo}(\text{CO})_4$ .<sup>79,80</sup> In contrast to the agostic amine-chelate (**12**), the bis-etherate mask of **13** provides an inert leaving group, thus ensuring reactivity of **13** will accurately mimic that of the unmasked  $\text{ML}_4$  species. Furthermore, the rapid, irreversible formation of **12** by treatment of **13** with 1 equiv  $\text{HNiPr}_2$  indicates that **13** is a superior surrogate to  $\text{Mo}(\text{CO})_4$ .

Although **13** can be stored for up to one week at  $-40\text{ }^\circ\text{C}$  in the presence of excess  $\text{Et}_2\text{O}$ , the enhanced reactivity of this complex does limit reliability over longer durations. To address this problem, DME was used as a chelating mask in **14** as shown in **Scheme 1.7** and Figure 1.1. Importantly, the chelate-effect and decreased volatility of DME allowed for storage of **14** at  $-40\text{ }^\circ\text{C}$  for durations exceeding two months. Interestingly, treatment of **13** with 1 equiv styrene (Scheme 1.6) afforded the unusual  $\eta^3$ -styrene complex **15**. Although  $\eta^4$ -coordination of vinyl-arenes is relatively common,<sup>81,82</sup>  $\eta^3$ -coordination had been only been reported in multinuclear systems wherein the vinyl-arene bridges two metal centers.<sup>83</sup> Interestingly, one such intermediate was implicated in the hydrogenative C-atom abstraction from styrene to generate a mono-carbide Ni-cluster and toluene.<sup>82</sup> Although further investigation regarding the reactivity of **15** are still under way, it is interesting to note that this complex was found to be the most stable among the masked- $\text{ML}_4$  species shown in **Scheme 1.7**, showing no sign of degradation after three weeks at room-temperature under  $\text{N}_2$ -atmosphere. Importantly, screening of complexes **12-15** as catalysts (2 mol%) in the hydrostannation of  $\text{PhC}\equiv\text{CMe}$  (under conditions identical to those used in Section

1.3.2, Table 1.1) revealed all four of the zero-valent complexes to be suitable source of ML<sub>4</sub>; all gave the same selectivity as divalent dicarbonyl **2** (91:9 β/α), with complete conversion to the vinylstannane in under 30 min.



**Scheme 1.6.** Synthesis of a bis-Et<sub>2</sub>O-masked source of ML<sub>4</sub>, **13**.

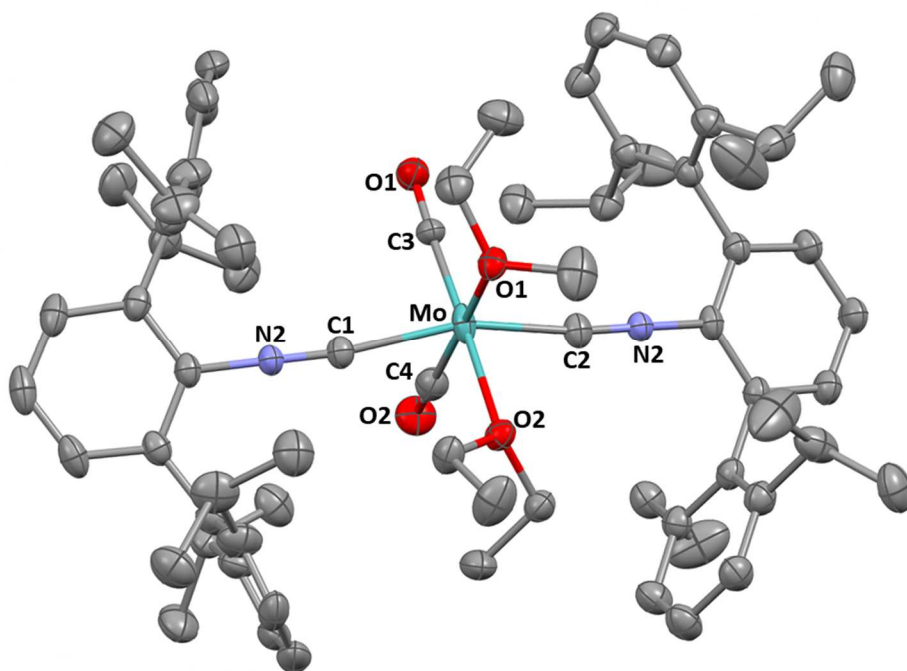
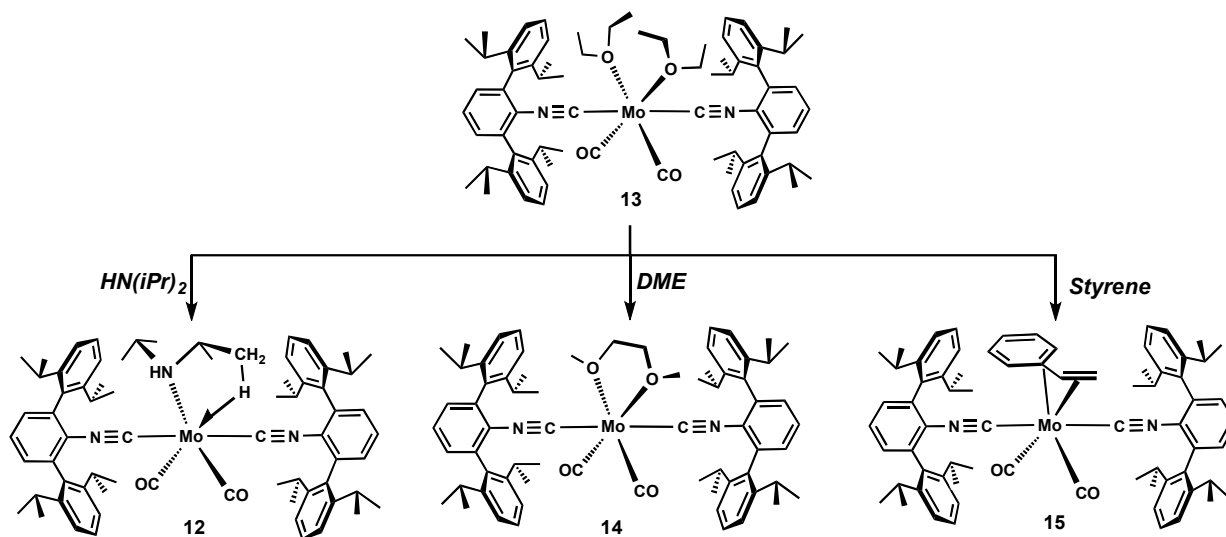


**Figure 1.1.** Molecular structure of Mo(CO)<sub>2</sub>(CNAr<sup>Dipp2</sup>)<sub>2</sub>(OEt<sub>2</sub>)<sub>2</sub> (**13**). Three-position disorder of Mo and equatorial ligands precluded accurate determination of bond distances and angles.



**Scheme 1.7.** Synthesis of masked sources of the zero-valent, four-coordinate fragment  $[\text{Mo}(\text{CO})_2(\text{CNAr}^{\text{Dipp}2})_2]$ .

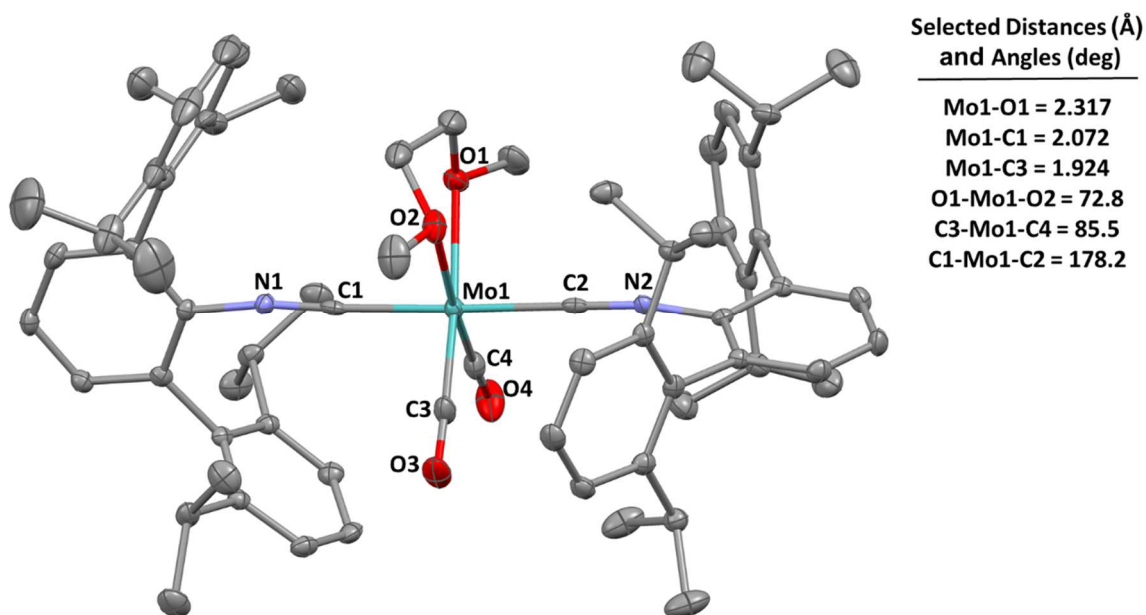


**Figure 1.2.** Molecular structure of DME-chelate 14.

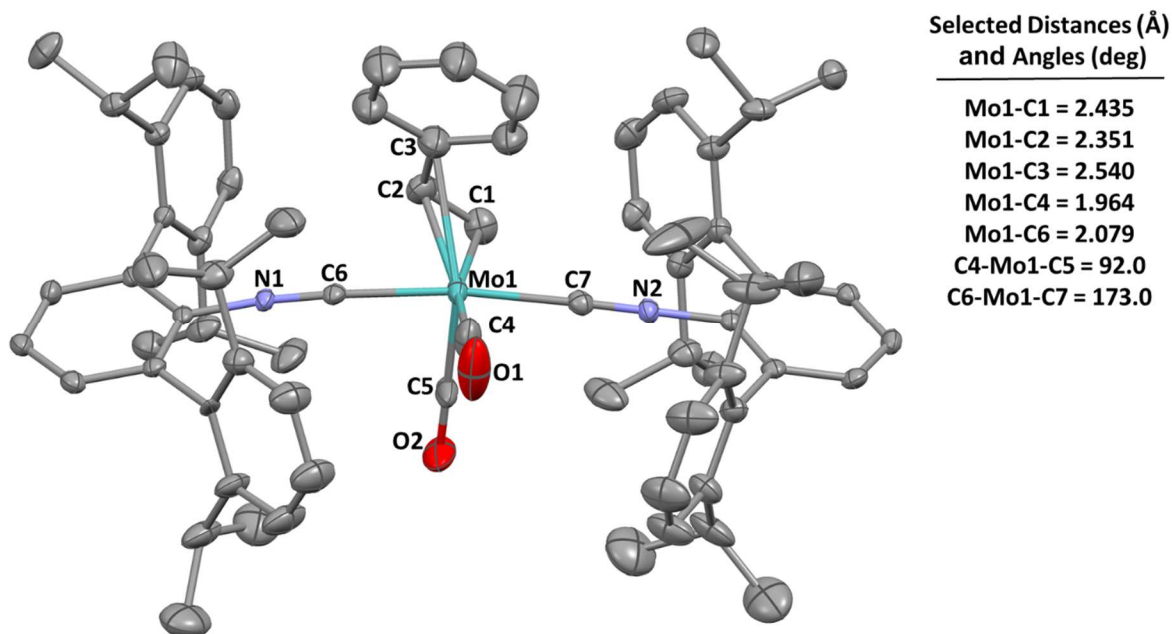


**Figure 1.3.** Molecular structure of  $\eta^3$ -styrene complex **15**.

#### 1.4.2 Electronic structure of four-coordinate molybdenum

An important aspect regarding the reactivity of the  $d^6$ -four-coordinate fragment  $[\text{Mo}(\text{CO})_2(\text{CNAr}^{\text{Dipp}2})_2]$  is the preferential coordination of weak Lewis bases (e.g. bis- $\text{Et}_2\text{O}$ -coordination in **13**) as opposed to dinitrogen. In direct contrast to this are the classic tetrakis-phosphine-bis- $\text{N}_2$  complexes, e.g. *trans*- $\text{Mo}(\text{N}_2)_2(\text{dppe})_2$ ,<sup>84,85</sup> whose strong preference for coordination with  $\pi$ -acids (even poor ones, i.e.  $\text{N}_2$ ) is evidenced by their stability in THF.<sup>86,87</sup> The fact that THF does not disrupt  $\text{N}_2$ -coordination sharply distinguishes the behavior of  $[\text{Mo}(\text{PR}_3)_4]$  from the  $\pi$ -acidic coordination environment of  $[\text{Mo}(\text{CO})_2(\text{CNAr}^{\text{Dipp}2})_2]$  in this work.

Encouraged that reactivity of reactivity profile of  $[\text{Mo}(\text{CO})_2(\text{CNAr}^{\text{Dipp}2})_2]$  seemed to be in line with what would be expected for the binary carbonyl  $\text{Mo}(\text{CO})_4$ , we sought to more firmly establish the electronic structure relationship between these species. It has been well-established that isocyanides are stronger  $\sigma$ -donors, and weaker  $\pi$ -acids than  $\text{CO}$ .<sup>88,89</sup> It is unsurprising therefore, that the HOMO-LUMO energy difference for  $\text{Mo}(\text{CO})_4$  and  $\text{Mo}(\text{CO})_2(\text{CNPh})_2$



compares even more favorably than  $\text{Mo}(\text{CO})_4$  does with the homoleptic isocyanide model  $\text{Mo}(\text{CNPh})_4$ . In the following chapters, investigations probing the activation chemistry of masked- $[\text{Mo}(\text{CO})_2(\text{CNAr}^{\text{Dipp}2})_2]$  will thus provide insight more broadly into the capabilities of a classic molecule which has only been observed in the gas phase, cis-divacant  $\text{Mo}(\text{CO})_4$ .

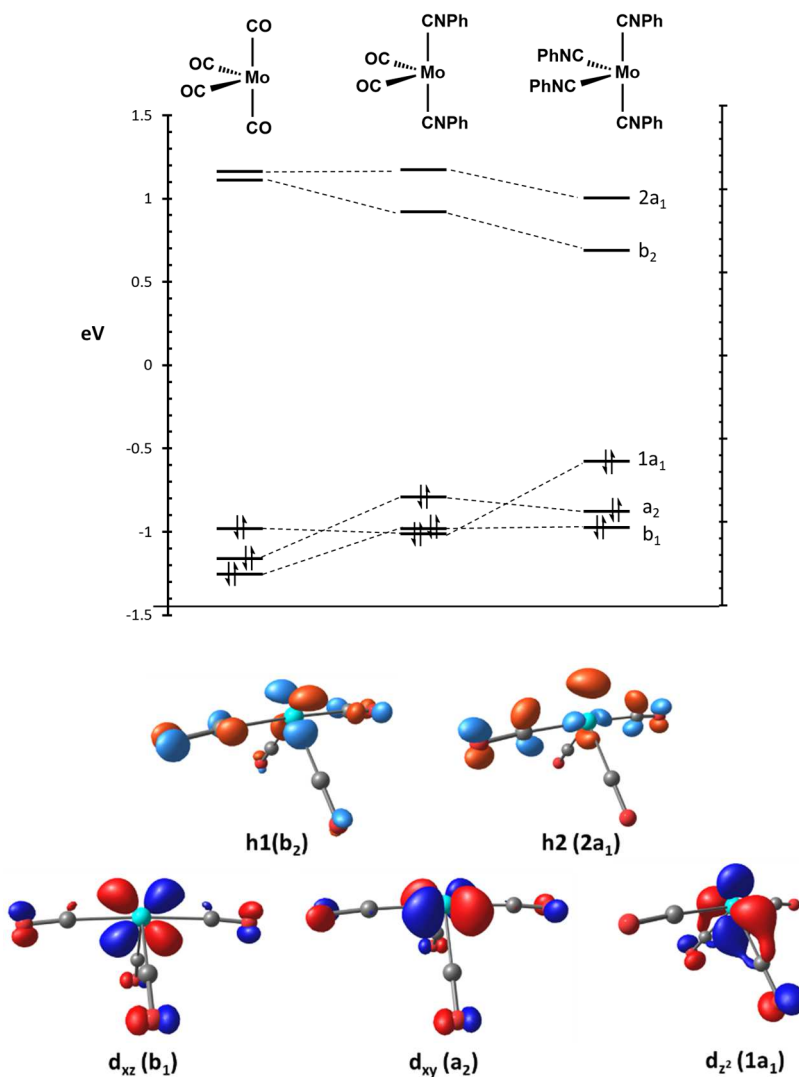


**Figure 1.4.** Top: Relative energy diagram of molecular orbitals in  $\text{Mo}(\text{CO})_4$ ,  $\text{Mo}(\text{CO})_2(\text{CNPh})_2$ , and  $\text{Mo}(\text{CNPh})_4$  – determined by DFT (BP86, def2-TZVP, ZORA). Bottom: Assigned frontier molecular orbitals of  $\text{Mo}(\text{CO})_4$ ; **h1** and **h2** are hybrid orbitals.<sup>79</sup>

## 1.5 Acknowledgements

Parts of this chapter were adapted with permission from Mandla, K. A.; Moore, C. E.; Rheingold, A. L.; Figueroa, J. S. “Regioselective Formation of (*E*)- $\beta$ -Vinylstannanes with a Topologically Controlled Molybdenum-Based Alkyne Hydrostannation Catalyst”, *Angewandte Chemie, International Edition*, **2018**, *57*, 6853-6857. Copyright 2018 Wiley-VCH, Weinheim. The dissertation author is the first author of this paper.

## 1.6 References

- (1) Bergman, R. *Nature* **2007**, *446*, 391–393.
- (2) Burger, B. J.; Thompson, M. E.; Cotter, W. D.; Bercaw, J. E. *J. Am. Chem. Soc.* **1990**, *112* (4), 1566–1577.
- (3) Marciniak, B.; Maciejewski, H.; Pietraszuk, C.; Pawluć, P. Marciniak, B., Matison, J., Eds.; Springer, 2008.
- (4) Hofmann, R.; Vlatković, M.; Wiesbrock, F. *Polymers (Basel)*. **2017**, *9* (12), 534.
- (5) Trost, B. M.; Ball, Z. T. *Synthesis (Stuttg)*. **2005**, *2005* (6), 853–887.
- (6) Smith, N. D.; Mancuso, J.; Lautens, M. *Chem. Rev.* **2000**, *100* (8), 3257–3282.
- (7) Cossairt, B.; Cummins, C. *Angew. Chemie Int. Ed.* **2010**, *49* (9), 1595–1598.
- (8) Cherry, J. P. F.; Johnson, A. R.; Baraldo, L. M.; Tsai, Y. C.; Cummins, C. C.; Kryatov, S. V.; Rybak-Akimova, E. V.; Capps, K. B.; Hoff, C. D.; Haar, C. M.; et al. *J. Am. Chem. Soc.* **2001**, *123* (30), 7271–7286.
- (9) Caporali, M.; Gonsalvi, L.; Rossin, A.; Peruzzini, M. *Chem. Rev.* **2010**, *110* (7), 4178–4235.
- (10) Müller, T. E.; Hultsch, K. C.; Yus, M.; Foubelo, F.; Tada, M. *Chem. Rev.* **2008**, *108* (9), 3795–3892.
- (11) Crabtree, R. H. 5th ed.; John Wiley & Sons, Inc.: Hoboken, New Jersey, 2009.
- (12) Schlosser, M. Wiley, 2004.
- (13) Corey, E. J.; Cheng, X. 1st ed.; John Wiley & Sons, Inc.: New York, 1995.

- (14) Smil, V. MIT Press, 2004.
- (15) Magano, J.; Dunetz, J. R. *Chem. Rev.* **2011**, *111* (3), 2177–2250.
- (16) Allardyce, C. S.; Dorcier, A.; Scolaro, C.; Dyson, P. J. *Appl. Organomet. Chem.* **2005**, *19* (1), 1–10.
- (17) Buriak, J. M. *Chem. Rev.* **2002**, *102* (5), 1271–1308.
- (18) Kochi, J. K. Academic Press, 1978.
- (19) Puddephatt, R. J.; Manojlovic-Muir, L.; Muir, K. W. *Polyhedron* **1990**, *9* (23), 2767–2802.
- (20) Wrighton, M. S.; Ginley, D. S.; Schroeder, M. A.; Morse, D. L. *Pure Appl. Chem.* **1975**, *41* (4), 671–697.
- (21) Marradi, M. *Synlett* **2005**, *2005* (7), 1195–1196.
- (22) Mortreux, A.; Blanchard, M. *J. Chem. Soc., Chem. Commun.* **1974**, No. 19, 786–787.
- (23) Kaneta, N.; Hirai, T.; Mori, M. *Chem. Lett.* **1995**, *24* (8), 627–628.
- (24) Baruah, J. B. *ChemInform* **2008**, *39* (24).
- (25) Brizius, G.; Bunz, U. H. F. *Org. Lett.* **2002**, *4* (17), 2829–2831.
- (26) Villemin, D.; Héroux, M.; Blot, V. *Tetrahedron Lett.* **2001**, *42* (22), 3701–3703.
- (27) Jeong, N.; Lee, S. J.; Lee, B. Y.; Chung, Y. K. *Tetrahedron Lett.* **1993**, *34* (25), 4027–4030.
- (28) Adrio, J.; Rivero, M. R.; Carretero, J. C. *Org. Lett.* **2005**, *7* (3), 431–434.
- (29) Brummond, K. M.; Kerekes, A. D.; Wan, H. *J. Org. Chem.* **2002**, *67* (15), 5156–5163.
- (30) Brummond, K. M.; Mitasev, B. *Org. Lett.* **2004**, *6* (13), 2245–2248.
- (31) Shen, Q.; Hammond, G. B. *J. Am. Chem. Soc.* **2002**, *124* (23), 6534–6535.
- (32) Cao, H.; Ornum, S. G. Van; Deschamps, J.; Flippen-Anderson, J.; Laib, F.; Cook, J. M. *J. Am. Chem. Soc.* **2005**, *127* (3), 933–943.
- (33) Ardizzoia, G. A.; Brenna, S.; LaMonica, G.; Maspero, A.; Masciocchi, N. *J. Organomet. Chem.* **2002**, *649* (2), 173–180.
- (34) Czeluśniak, I.; Kociecka, P.; Szymańska-Buzar, T. *J. Organomet. Chem.* **2012**, *716*, 70–78.

- (35) McDonald, F. E.; Schultz, C. C. *J. Am. Chem. Soc.* **1994**, *116* (20), 9363–9364.
- (36) Bernard, A. M.; Cocco, M. T.; Onnis, V.; Piras, P. P. *Synthesis (Stuttg.)*. **1997**, *1997* (01), 41–43.
- (37) Bernard, A. M.; Cocco, M. T.; Onnis, V.; Piras, P. P. *Synthesis (Stuttg.)*. **1998**, *1998* (03), 256–258.
- (38) Shimizu, I.; Khien, K. M.; Nagatomo, M.; Nakajima, T.; Yamamoto, A. *Chem. Lett.* **1997**, *26* (9), 851–852.
- (39) Massa, A.; Acocella, M. R.; Rosa, M. De; Soriente, A.; Villano, R.; Scettri, A. *Tetrahedron Lett.* **2003**, *44* (4), 835–837.
- (40) Nitta, M.; Kobayashi, T. *J. Chem. Soc. Perkin Trans. 1* **1985**, 1401.
- (41) Donati, D.; Ferrini, S.; Fusi, S.; Ponticelli, F. *J. Heterocycl. Chem.* **2004**, *41* (5), 761–766.
- (42) Baraldi, P. G.; Barco, A.; Benetti, S.; Manfredini, S.; Simoni, D. *Synthesis (Stuttg.)*. **1987**, *1987* (03), 276–278.
- (43) Tranmer, G. K.; Tam, W. *Org. Lett.* **2002**, *4* (23), 4101–4104.
- (44) Cicchi, S.; Goti, A.; Brandi, A.; Guarna, A.; De Sarlo, F. *Tetrahedron Lett.* **1990**, *31* (23), 3351–3354.
- (45) Zimmer, R.; Reissig, H. U. *J. Org. Chem.* **1992**, *57* (1), 339–347.
- (46) Asako, S.; Ishikawa, S.; Takai, K. *ACS Catal.* **2016**, 3387–3395.
- (47) Margulieux, G. W.; Weidemann, N.; Lacy, D. C.; Moore, C. E.; Rheingold, A. L.; Figueroa, J. S. *J. Am. Chem. Soc.* **2010**, *132* (14), 5033+.
- (48) Fox, B. J.; Millard, M. D.; DiPasquale, A. G.; Rheingold, A. L.; Figueroa, J. S. *Angew. Chemie - Int. Ed.* **2009**, *48* (19), 3473–3477.
- (49) Emerich, B. M.; Moore, C. E.; Fox, B. J.; Rheingold, A. L.; Figueroa, J. S. *Organometallics* **2011**, *30* (9), 2598–2608.
- (50) Labios, L. A.; Millard, M. D.; Rheingold, A. L.; Figueroa, J. S. *J. Am. Chem. Soc.* **2009**, *131* (32), 11318–11319.
- (51) Ditri, T. B.; Fox, B. J.; Moore, C. E.; Rheingold, A. L.; Figueroa, J. S. *Inorg. Chem.* **2009**, *48* (17), 8362–8375.

- (52) Ditri, T. B.; Moore, C. E.; Rheingold, A. L.; Figueroa, J. S.; Ditri, B.; Moore, C. E.; Rheingold, A. L.; Figueroa, J. S. *Inorg. Chem.* **2011**, *50* (20), 10448–10459.
- (53) Ditri, T. B.; Carpenter, A. E.; Ripatti, D. S.; Moore, C. E.; Rheingold, A. L.; Figueroa, J. S. *Inorg. Chem.* **2013**, *52* (22), 13216–13229.
- (54) Chiu, K. W.; Howard, C. G.; Wilkinson, G.; Galas, A. M. R.; Hursthouse, M. B. *Polyhedron* **1982**, *1* (11–12), 803–808.
- (55) Mann, K. R.; Cimolino, M.; Geoffroy, G. L.; Hammond, G. S.; Orio, A. A.; Albertin, G.; Gray, H. B. *Inorganica Chim. Acta* **1976**, *16*, 97–101.
- (56) Colton, R.; Tomkins, I. B. *Aust. J. Chem.* **1966**, *19* (7), 1143.
- (57) Colton, R.; Tomkins, I. B. *Aust. J. Chem.* **1966**, *19* (8), 1519.
- (58) Anker, M. W.; Colton, R.; Tomkins, I. B. *Aust. J. Chem.* **1967**, *20* (1), 9.
- (59) Colton, R.; Rix, C. J. *Aust. J. Chem.* **1968**, *21* (5), 1155.
- (60) Bowden, J. A.; Colton, R. *Aust. J. Chem.* **1968**, *21* (11), 2657.
- (61) Colton, R.; Rix, C. J. *Aust. J. Chem.* **1969**, *22* (2), 305.
- (62) Drew, M. G. B.; Tomkins, I. B.; Colton, R. *Aust. J. Chem.* **1970**, *23* (12), 2517.
- (63) Colton, R. *Coord. Chem. Rev.* **1971**, *6* (2–3), 269–284.
- (64) Cotton, F. A.; Poli, R. *J. Am. Chem. Soc.* **1986**, *108* (18), 5628–5629.
- (65) Kubacek, P.; Hoffmann, R. *J. Am. Chem. Soc.* **1981**, *103* (15), 4320–4332.
- (66) Herrick, R. S.; George, M. S.; Duff, R. R.; D'Aulnois, F. H.; Jarret, R. M.; Hubbard, J. L. *Inorg. Chem.* **1991**, *30* (19), 3711–3718.
- (67) Mandla, K. A.; Moore, C. E.; Rheingold, A. L.; Figueroa, J. S. *Angew. Chemie Int. Ed.* **2018**, *57* (23), 6853–6857.
- (68) Kazmaier, U.; Schauss, D.; Pohlman, M. *Org. Lett.* **1999**, *1* (7), 1017–1019.
- (69) Kazmaier, U.; Pohlman, M.; Schauß, D. *European J. Org. Chem.* **2000**, *2000* (15), 2761–2766.
- (70) Wesquet, A. 25emO. O.; Kazmaier, U. *Adv. Synth. Catal.* **2009**, *351* (9), 1395–1404.

- (71) Braune, S.; Kazmaier, U. *J. Organomet. Chem.* **2002**, *641* (1–2), 26–29.
- (72) Tsang, W. C. P.; Jamieson, J. Y.; Aeilts, S. L.; Hultzs, K. C.; Schrock, R. R.; Hoveyda, A. H. *Organometallics* **2004**, *23* (9), 1997–2007.
- (73) MacAdams, L. A.; Buffone, G. P.; Incarvito, C. D.; Rheingold, A. L.; Theopold, K. H. *J. Am. Chem. Soc.* **2005**, *127* (4), 1082–1083.
- (74) Sarkar, S.; McGowan, K. P.; Kuppuswamy, S.; Ghiviriga, I.; Abboud, K. A.; Veige, A. S. *J. Am. Chem. Soc.* **2012**, *134* (10), 4509–4512.
- (75) Hamze, A.; Veau, D.; Provot, O.; Brion, J. D.; Alami, M. *J. Org. Chem.* **2009**, *74* (3), 1337–1340.
- (76) Zhang, H. X.; Guibe, F.; Balavoine, G. *J. Org. Chem.* **1990**, *55* (6), 1857–1867.
- (77) Winston, P. B.; Burgmayer, S. J. N.; Tonker, T. L.; Templeton, J. L. *Organometallics* **1986**, No. 26, 1707–1715.
- (78) Templeton, J. In *Advances in Organometallic Chemistry, vol 29*; Stone, F., West, R., Eds.; Academic Press: London, 1989; pp 1–93.
- (79) Elian, M.; Hoffmann, R. *Inorg. Chem.* **1975**, *14* (5), 1058–1076.
- (80) Perutz, R. N.; Turner, J. J. *J. Am. Chem. Soc.* **1975**, *4800*, 4800–4804.
- (81) Brookhart, M.; Chandler, W. A.; Pfister, A. C.; Santini, C. C.; White, P. S. *Organometallics* **1992**, *11* (3), 1263–1274.
- (82) Arce, A. J.; Karam, A.; De Sanctis, Y.; Machado, R.; Capparelli, M. V.; Manzur, J. *Inorganica Chim. Acta* **1997**, *254* (1), 119–130.
- (83) Johnson, B. F. G.; Lewis, J.; Lunniss, J.; Braga, D.; Grepioni, F. *J. Organomet. Chem.* **1991**, *412* (1–2), 195–201.
- (84) Tominari, K.; Uchida, Y.; Misono, A.; Hi, M.; Comm, C.; Scheidegger, H. A.; Armor, J. N.; Taube, H.; Amer Chein SOL, J.; P Kane-Maguire, L. A.; et al. 1969.
- (85) Chatt, J.; Dilworth, J. R.; Richards, R. L. *Chem. Rev.* **1978**, *78* (6), 589–625.
- (86) Anderson, S. N.; Richards, R. L. *J. Chem. Soc. Dalton Trans.* **1986**, 245–252.
- (87) Carmona, E.; Marín, J. M.; Poveda, M. L.; Atwood, J. L.; Rogers, R. D.; Wilkinson, G. *Angew. Chemie Int. Ed. English* **1982**, *21* (6), 441–442.

- (88) Carpenter, A. E.; Mokhtarzadeh, C. C.; Ripatti, D. S.; Havrylyuk, I.; Kamezawa, R.; Moore, C. E.; Rheingold, A. L.; Figueroa, J. S. *Inorg. Chem.* **2015**, *54* (6), 2936–2944.
- (89) Barybin, M. V.; Young, V. G.; Ellis, J. E. *J. Am. Chem. Soc.* **2000**, *122* (19), 4678–4691.

## Chapter 2

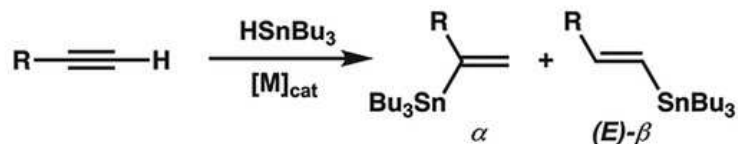
# Regioselective Formation of (*E*)- $\beta$ -Vinylstannanes with a Topologically Controlled Molybdenum-Based Alkyne Hydrostannation Catalyst

### 2.1 Introduction

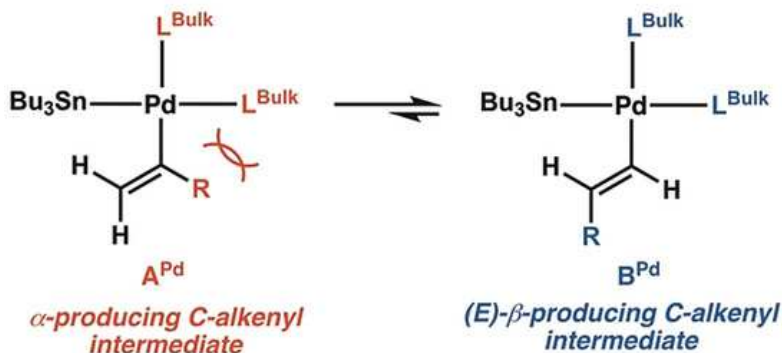
Vinylstannanes are well recognized as versatile synthetic precursors for C–C bond-forming reactions.<sup>1,2</sup> Accordingly, transition-metal-catalyzed alkyne hydrostannation has been extensively investigated as an efficient, atom-economic route to vinylstannanes.<sup>3</sup> However, despite substantial progress in the development of alkyne hydrostannation catalysts, precise control over the hydrometalation regioselectivity continues to be an important challenge. Several catalysts have now been reported that reliably provide  $\alpha$ -vinylstannane products by catalyst-controlled hydrometalation (Scheme 2.1, top).<sup>3–11</sup> In contrast, catalysts that deliver (*E*)- $\beta$ -vinylstannanes by regioselective *syn* Sn–H addition have been particularly difficult to develop for alkyne substrates that lack steric or electronic directing groups (Scheme 2.1, top).<sup>4,12–16</sup> Indeed, the only systems known to provide reasonable regioselectivities for (*E*)- $\beta$ -vinylstannanes are highly encumbered palladium/phosphine catalysts that operate through a formal Pd<sup>0</sup>/Pd<sup>II</sup> cycle.<sup>3,4,12,14,15</sup> However, the regioselectivity achieved with these systems is not general over a wide scope of substituted alkynes,<sup>4,15</sup> and the systems lack the predictability associated with the most regioselective catalysts for the production of  $\alpha$ -vinylstannanes.



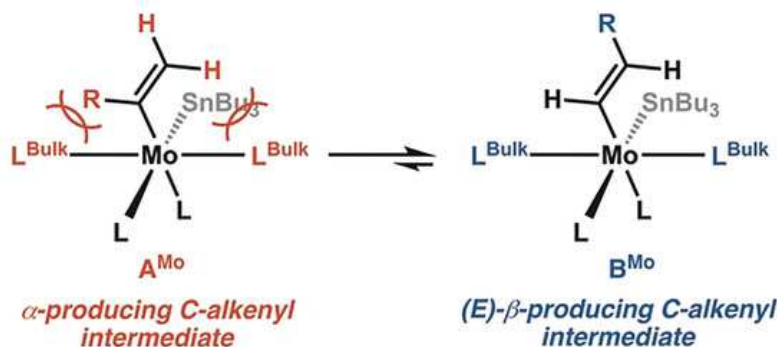
**Regiochemical Outcomes for Metal-Catalyzed Syn-Hydrostannation of Alkynes**



**Previous – Pd-Catalyzed  $\beta$ -(E)-Selective Hydrostannation with Encumbering Ligands: Square-Planar Intermediates**



**This Work – Enhancement of  $(E)$ - $\beta$ -Regioselectivity with an Octahedral, Mo-Based Hydrostannation Catalyst**



**Scheme 2.1** *Top*: Generalized reaction scheme for the production of vinylstannane regioisomers by metal-catalyzed syn-hydrostannation of terminal alkynes. *Middle*: The key square-planar C-alkenyl intermediates proposed to be responsible for regioselectivity in palladium-catalyzed alkyne hydrostannation. *Bottom*: Conceptual framework for enhanced  $(E)$ - $\beta$ -regioselectivity by application of additional steric pressures in a six-coordinate molybdenum-based alkyne hydrostannation catalyst system.  $L^{\text{Bulk}}$  = encumbering ligand.

A commonality among the Pd catalysts that show selectivity for  $(E)$ - $\beta$ -vinylstannanes is the formation of a square-planar *cis*-[Pd(C-alkenyl)(SnR<sub>3</sub>)L<sub>2</sub>] intermediate during the hydrometalation process (Scheme 2.1, middle). The square-planar coordination geometry of this intermediate positions ancillary ligands both *cis* and *trans* to the key C-alkenyl fragment that is

generated upon initial hydride transfer to the alkyne substrate. It has been argued that when these catalyst systems are sufficiently encumbered, the regioselectivity for (*E*)- $\beta$ -vinylstannanes originates from steric hindrance between the *cis*-ancillary ligand and the  $\alpha$ -vinylstannane-producing *C*-alkenyl unit (Intermediate **A**<sup>Pd</sup>; Scheme 2.1).<sup>15</sup> These unfavorable interactions encourage the formation of the (*E*)- $\beta$ -vinylstannane-producing *C*-alkenyl intermediate, where steric interference from the *cis*-ancillary ligand is minimized (**B**<sup>Pd</sup>; Scheme 2.1). Based on this postulate, we reasoned that a modified catalyst architecture, where two encumbering ligands are positioned *cis* to the *C*-alkenyl unit, could further destabilize the formation of  $\alpha$ -vinylstannane-producing intermediates and lead to increased regioselectivity for the formation of (*E*)- $\beta$ -vinylstannanes by *syn* hydrometalation. Accordingly, we sought to develop an encumbered alkyne hydrostannation system where an overall octahedral metal coordination geometry is conserved throughout the hydrometalation process. Such a modification would allow for two additional axial ligands to exert mutually *cis* steric pressure on a *C*-alkenyl unit in a manner not achievable with systems that generate square-planar intermediates (Scheme 2.1, bottom).<sup>3,4,12,14,15</sup>

Previously, we reported the six-coordinate complex MoI<sub>2</sub>(CO)<sub>2</sub>(CNAr<sup>Dipp2</sup>)<sub>2</sub> (**1**; Ar<sup>Dipp2</sup>=2,6-(2,6-(*i*-Pr)<sub>2</sub>C<sub>6</sub>H<sub>3</sub>)<sub>2</sub>C<sub>6</sub>H<sub>3</sub>; Figure 2.1),<sup>17</sup> which features two sterically encumbering *m*-terphenyl isocyanide ligands in a *trans* orientation.<sup>18–20</sup> Notably, diiodide **1** is related to the six-coordinate *cis*-Mo(*C*-alkenyl)(SnR<sub>3</sub>)L<sub>4</sub> intermediates proposed by Kazmaier and co-workers for alkyne hydrostannation with the zero-valent tris-isocyanide tricarbonyl catalyst precursor Mo(CN-*t*-Bu)<sub>3</sub>(CO)<sub>3</sub>.<sup>6,21–25</sup> Indeed, Mo(CN-*t*-Bu)<sub>3</sub>(CO)<sub>3</sub> possesses relatively unencumbered ligands, and correspondingly, its use as an alkyne hydrostannation pre-catalyst results in excellent regioselectivity for  $\alpha$ -vinylstannanes.<sup>6,21–25</sup> Herein, we show that the more sterically encumbered complex **1** also serves as a highly efficient alkyne hydrostannation catalyst precursor. However,

owing to its increased steric profile, **1** catalyzes the regioselective formation of (*E*)- $\beta$ -vinylstannanes for a wide range of terminal and unsymmetrically substituted internal alkynes without the need for sterically biased substrates. Pre-catalyst **1** can be readily activated under mild conditions to a well-defined and stabilized 14 e<sup>-</sup> zero-valent active species, in which the rigid and encumbering *trans* topology of the *m*-terphenyl isocyanide ligands is maintained. In addition, we show that this ligand orientation is responsible for the high regioselectivity for (*E*)- $\beta$ -vinylstannanes, which can be further modulated by substrate-dependent electronic perturbation of key intermediates during hydrometalation.

## 2.2 Results and Discussion

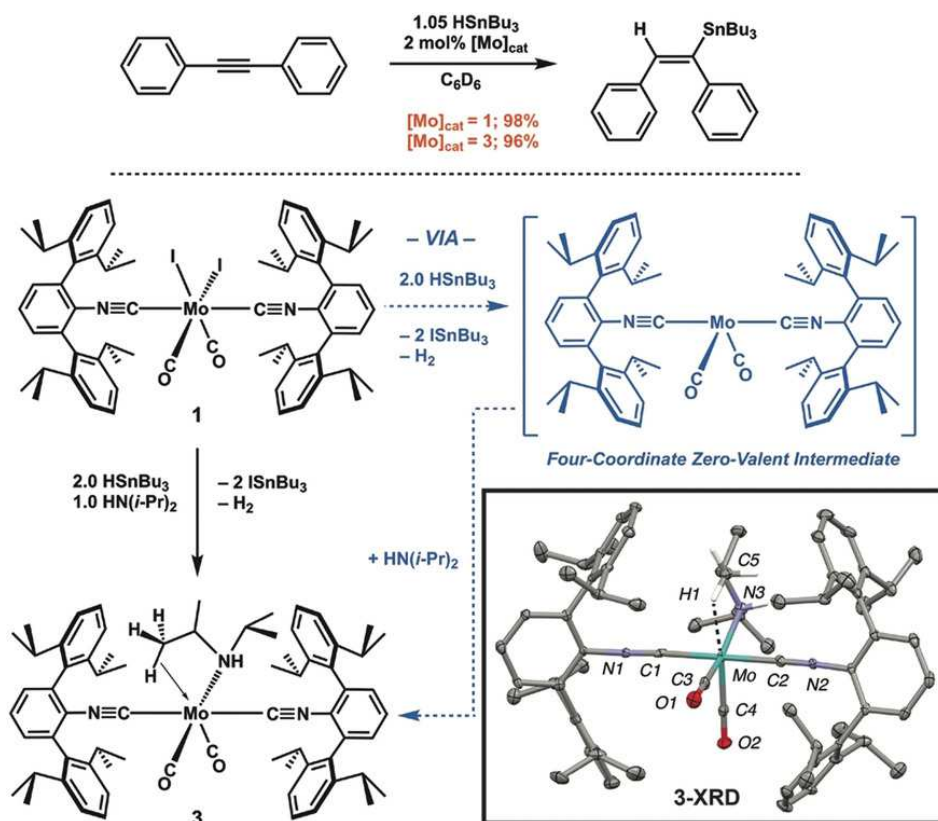


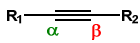
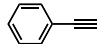
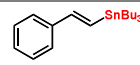
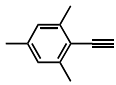
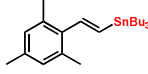
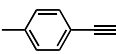
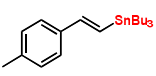
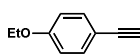
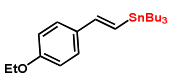
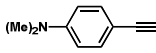
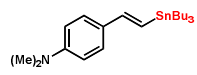
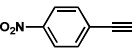
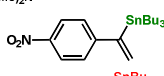
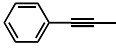
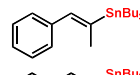
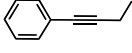
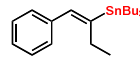
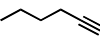
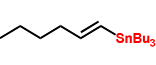
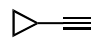
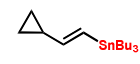
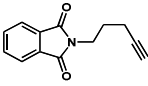
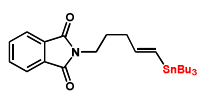
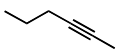
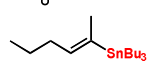
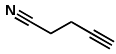
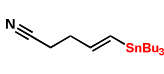
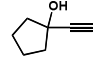
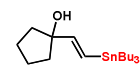
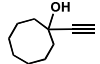
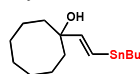
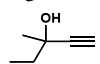
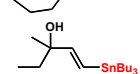
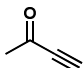
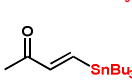
**Figure 2.1** Top: *syn* Hydrostannylation of diphenylacetylene with molybdenum pre-catalysts **1** and **3**. Bottom: Synthesis, proposed formation, and molecular structure of the zero-valent amine/C,H agostic complex **3** from divalent diiodide **1**. Selected bond lengths [Å] and angles [°] for **3**: Mo–H1 2.126(5), Mo–C5 2.806(2), Mo–N3 2.327(3); Mo–H1–C5 125.11(30).

In an initial screen of **1** for catalytic hydrostannation, diphenylacetylene was chosen as a test substrate. Upon using 2 mol % of **1** and 1.05 equiv of HSnBu<sub>3</sub>, the *syn* hydrostannation product (*E*)-tributyl(1,2-diphenylvinyl)stannane was isolated in 98 % yield after 20 min of reaction at room temperature in C<sub>6</sub>D<sub>6</sub> solution (Figure 2.2, top). Notably, the efficiency of this reaction at room temperature indicates that diiodide **1** is rapidly converted into a catalytically active species. Indeed, treatment of diiodide **1** with 2.0 equiv of HSnBu<sub>3</sub> in the absence of alkyne substrate rapidly generates the Mo<sup>0</sup> tetracarbonyl complex Mo(CO)<sub>4</sub>(CNAr<sup>Dipp2</sup>)<sub>2</sub> (**2**)<sup>18</sup> through an apparent reduction/ligand redistribution process, along with H<sub>2</sub> and I<sub>2</sub>SnBu<sub>3</sub>, as determined by <sup>1</sup>H NMR spectroscopy and GCMS. Hydride-for-halide exchange has been observed previously in reactions between HSnBu<sub>3</sub> and metal halide complexes and likely proceeds by a radical-chain mechanism.<sup>26,27</sup> Accordingly, for this system, we propose that a double H/I exchange process produces an intermediate Mo<sup>0</sup> ML<sub>4</sub> species that is active for alkyne hydrostannation, but redistributes when substrate is not present (Figure 2.2).

Most notably, when diiodide **1** is treated with stoichiometric HSnBu<sub>3</sub> in the presence of diisopropylamine (HN(*i*-Pr)<sub>2</sub>), the Mo<sup>0</sup> amine/C–H-agostic complex **3** can be isolated in approximately 80 % yield (Figure 2.2). Structural characterization of complex **3** reveals the *trans* orientation of the CNAr<sup>Dipp2</sup> ligands, which is similar to that found in diiodide **1**, while an HN(*i*-Pr)<sub>2</sub> ligand is bound through an unusual κ<sup>1</sup>-N/η<sup>2</sup>-H,C chelate (Figure 2.2). The isolation of complex **3** strongly suggests that the four-coordinate zero-valent species [Mo(CO)<sub>2</sub>(CNAr<sup>Mes2</sup>)<sub>2</sub>], which is analogous to the intermediate proposed for hydrostannation by Mo(CN-*t*-Bu)<sub>3</sub>(CO)<sub>3</sub>,<sup>21</sup> is likely produced in this reaction sequence and is sufficiently reactive to be trapped with a weakly coordinating substrate such as HN(*i*-Pr)<sub>2</sub>. Consistent with this notion, **3** is also highly active for diphenylacetylene hydrostannation, producing the corresponding vinylstannane in 96 % yield

upon isolation under the same reaction conditions as those employed for diiodide **1** (Figure 2.2, top).

**Table 2.1** Hydrostannation of aryl and alkyl alkynes using MoI<sub>2</sub>(CO)<sub>2</sub>(CNAr<sup>Dipp</sup>)<sub>2</sub> (**1**).

Entry	R <sub>1</sub> -  -R <sub>2</sub>	Major Product	(E)-β/α <sup>[b]</sup>	Yield <sup>[c]</sup> [%]
1			87:13	95
2			98:2	97
3			91:9	92
4			98:2	94
5			99:1	93
8			45:55	86
9			92:8	94
11			80:20	96
12			91:9	92
13			91:9	93
14			92:8	94
15			89:11	94
16			61:39	84
17			90:10	92
18			97:3	97
19			83:17	92
20			78:22	95

[a] Reaction conditions: alkyne (0.170 mmol, 1.00 equiv), **1** (2.0 mol%), HSnBu<sub>3</sub> (1.05 equiv), C<sub>6</sub>D<sub>6</sub> (1.0 mL), room temperature, 30 min.

[b] Selectivity determined by <sup>1</sup>H NMR analysis of the reaction mixture. [c] Isolated as a mixture of the α and β-(E) isomers.

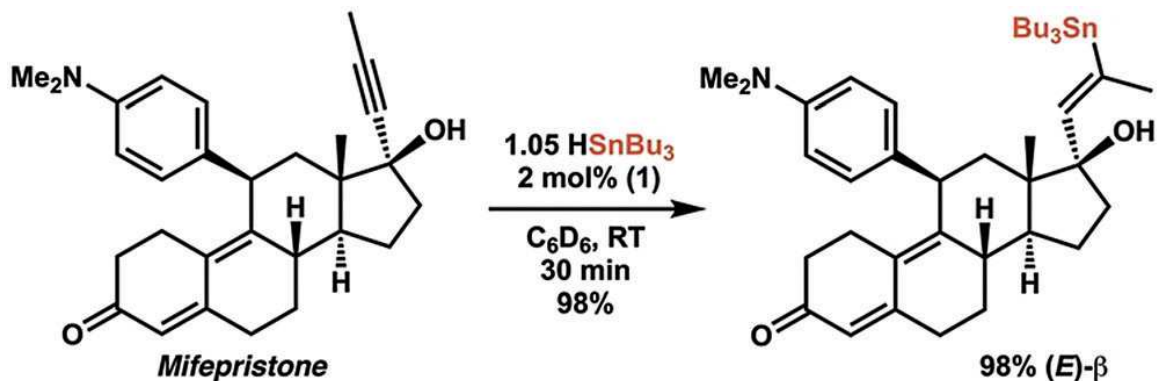
All runs showed complete conversion into vinylstannanes in crude reaction mixtures.

Whereas complex **3** yields an active system for catalysis, the operational simplicity of the *in situ* activation of diiodide **1** with only a slight excess  $\text{HSnBu}_3$  rendered it our preferred precursor for additional hydrostannation studies. Accordingly, at 2.0 mol % loading, complex **1** is effective for the hydrostannation of a range of terminal and internal alkynes into (*E*)- $\beta$ -vinylstannanes with exceptional regioselectivity. In addition, catalytic hydrostannation mediated by **1** proceeds efficiently at room temperature with only 1.05 equiv of  $\text{HSnBu}_3$  per alkyne substrate and without the need for additives or radical scavengers (Table 2.1).<sup>6,24</sup> For example, under these conditions, **1** converts phenylacetylene into the corresponding (*E*)- $\beta$ -vinylstannane with 13:87  $\alpha$ /(*E*)- $\beta$  regioselectivity after 20 min in  $\text{C}_6\text{D}_6$  solution (entry 1). The (*Z*)- $\beta$ -vinylstannane isomer, which is known to form in some metal-catalyzed hydrostannation processes,<sup>4</sup> is not produced in this reaction. Notably, this level of  $\alpha$ /(*E*)- $\beta$  regioselectivity for phenylacetylene hydrostannation is markedly superior to that of the well-utilized catalyst precursor  $\text{PdCl}_2(\text{PPh}_3)_2$  ( $\alpha$ /(*E*)- $\beta$ =46:54 for the same substrates).<sup>4,5</sup> Complex **1** also outperforms the more encumbered catalyst system  $\text{Pd}_2(\text{dba})_3/[\text{HPCy}_3]\text{BF}_4/\text{NEt}(i\text{-Pr})_2$ , which has previously yielded the greatest level of  $\alpha$ /(*E*)- $\beta$  regioselectivity for phenylacetylene hydrostannation ( $\alpha$ /(*E*)- $\beta$ =19:81).<sup>15</sup>

Other terminal aryl alkynes can also be converted with high regioselectivity. As shown in Table 2.1, complex **1** transforms sterically demanding (entry 2) and electron-rich (entries 3-5) terminal aryl alkynes into (*E*)- $\beta$ -vinylstannanes with regioselectivities greater than 98%. Similarly, unsymmetrically substituted internal aryl alkyl alkynes can be converted into vinylstannanes with a high degree of preferential placement of the  $[\text{SnBu}_3]$  unit proximal to the alkyl group (i.e., formal  $\alpha$ -H addition; entries 7 and 8).<sup>13</sup> These results indicate that the catalytic intermediates generated by complex **1** likely impose strong steric control over alkyne orientation during hydrostannation. However, it is critical to note that the presence of strongly electron-withdrawing substituents, such

as in the case of para-nitrophenylacetylene, significantly degrades the regioselectivity displayed by the system (entry 6). In fact, for this substrate, the  $\alpha$ -vinylstannane is marginally favored. Remarkably, aliphatic alkynes also undergo hydrostannation to (*E*)- $\beta$ -vinylstannanes with high regioselectivity in the presence of complex **1** (entries 9-13). Of these latter examples, the conversion of 2-hexyne into the corresponding (*E*)- $\beta$ -vinylstannane with 9:91  $\alpha$ /(*E*)- $\beta$  regioselectivity is particularly noteworthy (entry 12), as this result indicates that the molecular topology accessible from **1** can finely discriminate between methyl and propyl groups on opposing ends of an unsymmetrically substituted dialkyl alkyne. However, when electron-withdrawing substituents were present, as in the case of 4-cyano-1-butyne (entry 13), the regioselectivity of the hydrostannation process was again diminished. This observation illustrates that the electronic properties of the alkyne substrate can alter the regioselectivity governed by the inherent topological features of the catalyst system. It is also important to note that sterically biased propargyl alcohols can be converted into (*E*)- $\beta$ -vinylstannanes with high regioselectivity (entries 14-16), as has been reported previously for other hydrostannation catalysts.<sup>4</sup> Accordingly, the scope of the regioselective alkyne hydrostannation to (*E*)- $\beta$ -vinylstannanes using complex **1** is expanded, rather than compromised, relative to other catalyst systems. To this end, it is noteworthy that **1** produces the (*E*)- $\beta$ -vinylstannane isomer of mifepristone (Scheme 2.2) with 2:98  $\alpha$ /(*E*)- $\beta$  regioselectivity and in 98% yield, thereby demonstrating that a fair degree of molecular complexity can be accommodated by the system without loss of selectivity or activity. Catalysis can be scaled without significant loss of selectivity or activity as well. This was demonstrated by the hydrostannation of 1.0 g of the internal alkyne 1-phenyl-1-propyne, which proceeded in 90% yield and 91% regioselectivity for the (*E*)- $\beta$ -vinylstannane isomer at room temperature in 2 hours. Nevertheless, the use of 3-butyne-2-one resulted in a non-negligible degradation of regioselectivity (entry 17),

further illustrating that electron-withdrawing groups predictably alter the regiochemical outcome of hydrostannation in this system.<sup>28</sup>



**Scheme 2.2.** Hydrostannation of mifepristone with precatalyst 1.

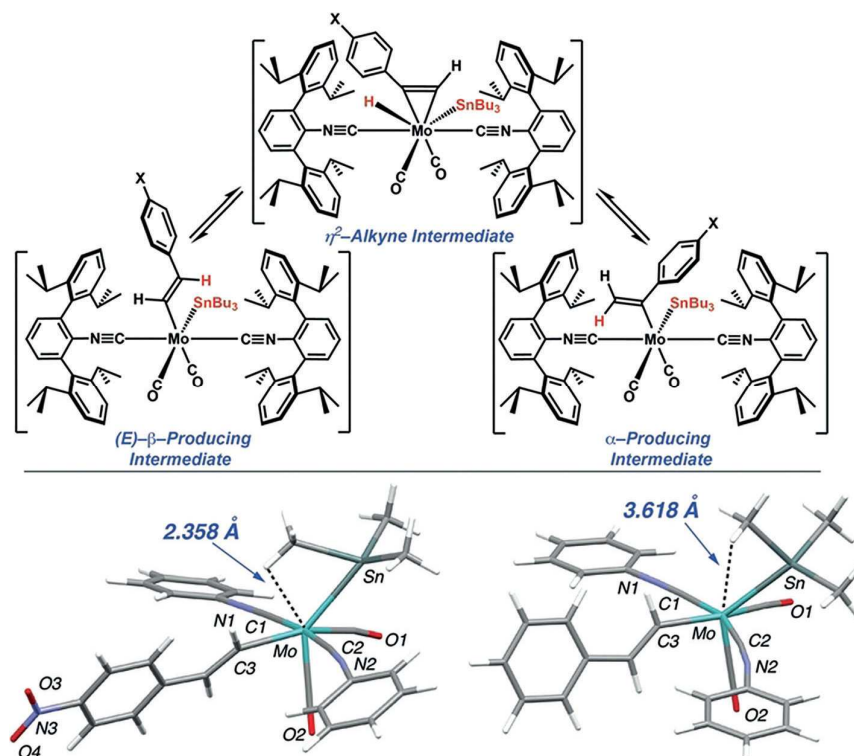


**Figure 2.2** Top: Proposed interconversion of molybdenum-based (*E*)- $\beta$ - and  $\alpha$ -producing *C*-alkenyl intermediates through reversible b-H elimination/migratory insertion. Bottom: DFT-calculated structures for (*E*)- $\beta$ -producing, aryl-substituted molybdenum-based *C*-alkenyl intermediates for X = NO<sub>2</sub> (left) and H (right), with the closest Mo $\cdots$ H contacts between the SnMe<sub>3</sub> group indicated.



A preliminary assessment of the hydrostannation mechanism by both experimental and computational studies suggests that the encumbering steric profile of the  $\text{CNAr}^{\text{Dipp}2}$  ligands is primarily responsible for the regiochemical preference of hydrostannation in post-insertion steps. However, the electronic properties of the alkyne substrates also exert an important influence over the properties of certain intermediates along the hydrostannation pathway. Hydrostannation of phenylpropyne using complex1 and a 1:1 mixture of  $\text{HSnBu}_3/\text{DSnBu}_3$  (3:1  $[\text{Sn}]_{\text{tot}}/[\text{alkyne}]$ ) resulted in an intermolecular H/D kinetic isotope effect of 1.11(7), thereby indicating that neither Sn–H bond cleavage nor C–H bond formation, through either migratory insertion or reductive elimination, are the rate limiting aspects of catalysis in this system.<sup>29,30</sup> Importantly, a plot of the  $\log(\alpha/(E)\text{-}\beta)$  vinylstannane isomeric ratio versus the Hammett  $\sigma$  parameter (see Section 1.5.2, Figure 2.11) for the para-substituted terminal aryl alkynes listed in Table 2.1 reveals a distinct positive correlation between selectivity for the (*E*)- $\beta$ -vinylstannane isomer and the electron-releasing capacity of the para substituent. We believe that these observations reflect the fact that the electronic properties of the alkyne substrate affect the stability of post-insertion intermediates, which are ultimately responsible for dictating the regiochemical outcome of the hydrostannation process prior to rate-limiting Sn–C bond-forming reductive elimination.

It has been well established that Chalk–Harrod-type hydrometalation processes are governed by the interconversion of *C*-alkenyl metal intermediates through reversible hydride migratory insertion/ $\beta$ -H elimination (Figure 2.2).<sup>28–30</sup> In addition, in our studies on Group 6 metal complexes featuring two  $\text{CNAr}^{\text{Dipp}2}$  ligands, we had previously shown that the steric encumbrance of these isocyanides enforces a mutually trans orientation through multiple redox transformations of the metal center.<sup>18,19</sup> We believe that to relieve steric pressure, this constrained, trans isocyanide environment around the metal center shifts the equilibrium between the two *C*-alkenyl insertion

products to the configuration favoring production of the (*E*)- $\beta$ -vinylstannane isomer (Figure 2.2). This argument is analogous to that made for regioselective (*E*)- $\beta$ -vinylstannane formation using palladium and encumbering phosphine ligands,<sup>15</sup> with the added feature that two *cis*-oriented ligands provide steric pressure in this six-coordinate Mo system.

Notably, DFT calculations on the truncated *C*-alkenyl intermediates [Mo( $\kappa^1$ -*C*-(C(H)=C(H)C<sub>6</sub>H<sub>4</sub>-*p*-X))(SnMe<sub>3</sub>)(CNPh)<sub>2</sub>(CO)<sub>2</sub>], which would give rise to (*E*)- $\beta$ -vinylstannanes after C-Sn bond-forming reductive elimination, optimize to stable minima and have unremarkable structural features for X=H, Me, OMe, and NMe<sub>2</sub> (Figure 2.2 and Section 2.5.3, Figure 2.12). However, for X = NO<sub>2</sub>, the calculations reveal a pronounced *H,C*-agostic interaction between the Mo center and a methyl group of the trimethylstannyl unit (Figure 2.2). This result indicates that the Lewis acidity of the Mo center is augmented when electron-withdrawing substituents are present on the (*E*)- $\beta$ -producing *C*-alkenyl intermediate. Inclusion of the full SnBu<sub>3</sub> ligand in the calculations also results in a stable minimum featuring an agostic interaction between an  $\alpha$ -methylene group and the Mo center (*see* Section 2.5.3, Figure 2.13). We therefore tentatively propose that this increase in metal Lewis acidity may produce a favorable pathway for  $\beta$ -hydride elimination/alkyne reinsertion to the  $\alpha$ -vinylstannane-producing *C*-alkenyl intermediate,<sup>31</sup> despite the steric preference of the catalyst. Lending credence to this notion is the finding that hydrostannation of *para*-nitrophenylacetylene with Mo(CN-*t*-Bu)<sub>3</sub>(CO)<sub>3</sub> produces the  $\alpha$ -vinylstannane with >98% regioselectivity (*see* Section 1.2.7), thereby indicating that in the absence of encumbering ligands, the electronic profile of the alkyne dominates the regiochemical outcome. While we are further evaluating the validity of this mechanistic proposal, the combined observations suggest that regioselective production of (*E*)- $\beta$ -vinylstannanes by complex **1** is driven by steric factors but can be predictably modulated by adjusting the electronic properties of the

alkyne substrate or a reduction in the steric profile of the Mo catalyst. Nevertheless, we anticipate that this catalytic alkyne hydrostannation system may be particularly useful in applications where (*E*)- $\beta$ -vinylstannanes are desired and strongly electron-withdrawing substituents are not in close proximity to either end of the alkyne substrate.

## 2.3 Synthetic Procedures, and Control Experiments

### 2.3.1 General Considerations.

All manipulations were carried out under an atmosphere of dry dinitrogen using standard Schlenk and glovebox techniques. Solvents were dried and deoxygenated according to standard procedures.<sup>32</sup> Unless otherwise stated, reagent-grade starting materials were purchased from commercial sources and used as received or purified by standard methods. The *m*-terphenyl isocyanide,<sup>18</sup>  $\text{CNAr}^{\text{Dipp}2}$ , and the complexes  $\text{MoI}_2(\text{CO})_2(\text{CNAr}^{\text{Dipp}2})_2$  (**MoI<sub>2</sub><sup>Dipp2</sup>**),  $\text{Mo}(\text{CO})_3(\text{CNAr}^{\text{Dipp}2})_2(\text{ACN})$  (**Mo<sup>Dipp2</sup>**),<sup>17</sup> and  $\text{Mo}(\text{CO})_3(\text{tBuNC})_3$  (**Mo<sup>tBu</sup>**)<sup>33</sup> were prepared according to published procedures. Benzene-*d*<sub>6</sub> (Cambridge Isotope Laboratories) was distilled from NaK/benzophenone and stored over 4 Å molecular sieves for 2 d prior to use. All glassware was dried at 180 °C for 8 h. SiO<sub>2</sub> used in chromatography was dried in an open container at 180 °C for 2 d. Solution <sup>1</sup>H and <sup>13</sup>C{<sup>1</sup>H} NMR spectra were recorded on Varian Mercury 400 spectrometers, a Varian X-Sens 500 spectrometer, or a JEOL ECA-500 spectrometer. <sup>1</sup>H and <sup>13</sup>C{<sup>1</sup>H} chemical shifts are reported in ppm relative to SiMe<sub>4</sub> (<sup>1</sup>H and <sup>13</sup>C  $\delta$  = 0.0 ppm) with reference to residual solvent resonances of 7.16 ppm (<sup>1</sup>H) and 128.06 ppm (<sup>13</sup>C) for benzene-*d*<sub>6</sub>.<sup>34</sup> FTIR spectra were recorded on a Thermo-Nicolet iS10 FTIR spectrometer. Samples were prepared as C<sub>6</sub>D<sub>6</sub> solutions injected into a ThermoFisher solution cell equipped with KBr windows. For solution FTIR spectra, solvent peaks were digitally subtracted from all spectra by comparison

with an authentic spectrum obtained immediately prior to the sample. The following abbreviations were used for the intensities and characteristics of important IR absorption bands: vs = very strong, s = strong, m = medium, w = weak, vw = very weak; b = broad, vb = very broad, sh = shoulder. High-resolution mass spectrometry (HRMS) was performed using an Agilent 6230 ESI-TOFMS instrument running in positive ion mode.

**Note:** HSnBu<sub>3</sub> was obtained from commercial sources and comes with 0.5% 2,6-bis(1,1-dimethylethyl)-4-methylphenol as stabilizer. The reagent was used as received, and was stored under inert atmosphere at -40 °C. Slow decomposition to Sn<sub>2</sub>Bu<sub>3</sub> and H<sub>2</sub> occurs over time at room temperature. The purity of HSnBu<sub>3</sub> was verified upon arrival from the manufacturer by NMR. In several instances, the material was received with a non-negligible amount of the decomposition product, Sn<sub>2</sub>Bu<sub>6</sub>. While partially decomposed reagent was avoided in this work, it is worth noting that Sn<sub>2</sub>Bu<sub>6</sub> is inert to the reaction conditions, and can generally be removed from product by chromatography.

### 2.3.2 Synthesis of Mo( $\eta^2$ -*H,C*-(H<sub>3</sub>CCH(CH<sub>3</sub>))-*k1-N-N(H)(i-Pr)*)(CO)<sub>2</sub>(CNAr<sup>Dipp2</sup>)<sub>2</sub> (3).

To a thawing toluene (15 mL) solution of diisopropyl amine (37  $\mu$ L, 0.263 mmol, 1.1 equiv.) and MoI<sub>2</sub>(CO)<sub>2</sub>(CNAr<sup>Dipp2</sup>)<sub>2</sub> (0.300 g, 0.239 mmol, 1.0 equiv) was added HSnBu<sub>3</sub> (142  $\mu$ L, 0.527 mmol, 2.1 equiv.). The reaction mixture was allowed to warm to room temperature and stirred for a total of 40 minutes. The solvent was removed in vacuo and the resulting red residue was suspended in n-pentane (ca. 4 mL), stirred for 10 minutes and the slurry then frozen. The thawing suspension was filtered, washed with thawing n-pentane, and dried in vacuo to give 3 as a dark- S-3 red solid (0.207 g, 0.188 mmol, 78.6% yield). Crystals suitable for X-ray diffraction were obtained from a concentrated n-pentane solution stored at -40 °C. 1 H NMR (500 MHz, C<sub>6</sub>D<sub>6</sub>, 20 °C):  $\delta$  = 7.29 (t, J = 7.7 Hz, 4H, *p*-Dipp), 7.18 (d, J = 7.7 Hz, 8H, *m*-Dipp), 6.96 (d, J =

7.5 Hz, 4H, *m*-Ph), 6.87 – 6.83 (m, 2H, *p*-Ph), 2.82 (sept, *J* = 6.8 Hz, 8H, ArCH(CH<sub>3</sub>)<sub>2</sub>), 2.26 – 2.15 (m, 2H, NCH<sub>2</sub>(CH<sub>3</sub>)<sub>2</sub>), 1.37 (d, *J* = 6.8 Hz, 24H, CH(CH<sub>3</sub>)<sub>2</sub>), 1.08 (d, *J* = 6.8 Hz, 24H, CH(CH<sub>3</sub>)<sub>2</sub>), 0.66 (d, *J* = 6.1 Hz, 6H, NCH<sub>2</sub>(CH<sub>3</sub>)), –0.23 (d, *J* = 6.1 Hz, 6H, η<sup>2</sup>-*C,H*-NCH<sub>2</sub>(CH<sub>3</sub>)) ppm. <sup>13</sup>C{<sup>1</sup>H} NMR (126 MHz, C<sub>6</sub>D<sub>6</sub>, 20 °C): δ = 227.5 (CO), 183.6 (CN), 146.7, 138.2, 136.2, 130.1, 129.7, 129.1, 125.3, 123.3, 49.9, 31.3, 24.9, 24.3, 23.5 ppm. FTIR (C<sub>6</sub>D<sub>6</sub>, KBr windows): ν(CN) = 2052(s), 1949(vs) cm<sup>-1</sup> ; ν(CO) = 1863(s), 1817(s) cm<sup>-1</sup> , also 2961, 2927, 2870, 1578, 1464, 1413, 1384, 1363, 756 cm<sup>-1</sup> . Anal. Calcd. for C<sub>70</sub>H<sub>89</sub>MoN<sub>3</sub>O<sub>2</sub>: C 76.4, H 8.15, N 3.82. Found: C 75.92, H 7.81, N 3.70.

### 2.3.3 Synthetic Procedure for MoI<sub>2</sub>(CO)<sub>2</sub>(CNAr<sup>Dipp</sup>)<sub>2</sub> (1) Catalyzed Hydrostannation.

Under N<sub>2</sub>-atmosphere, an NMR tube charged with a C<sub>6</sub>D<sub>6</sub> solution of 1 (0.0047 g, 0.004 mmol, 2 mol %, 1 mL) was frozen in N<sub>2(l)</sub>-cooled cold well. The frozen reaction mixture was layered with the alkyne substrate (0.170 mmol) and HSnBu<sub>3</sub> (0.050 g, 0.179 mmol, 53 μL, 1.05 equiv). The mixture was then allowed to thaw and the tube was shaken. Analysis by <sup>1</sup>H NMR spectroscopy indicated rapid conversion to products (< 20 min). The regio-isomeric ratio (α:β) was determined using the crude sample when it was determined that all alkyne starting material had been consumed. The reaction was then concentrated in vacuo and was flash-chromatographed over Florisil (100-200 mesh) with cold *n*-pentane (–78 °C) eluent (note: polar vinylstannanes, e.g. propargyl alcohols, were eluted with a cold (–78 °C) Et<sub>2</sub>O/*n*-pentane solution (1:30)). The resulting solution was concentrated to give an oil ranging from colorless to light yellow. In some cases, proteo-destannation of vinylstannanes on Florisil resulted in small amounts of alkene byproduct (typically <2%). Yields ranged between 84% and 97% (Table 2.1).

**Note:** HSnBu<sub>3</sub> was obtained from commercial sources and comes with 0.5% 2,6-bis(1,1-dimethylethyl)-4-methylphenol as stabilizer. The reagent was used as received and was stored under inert atmosphere at -40 °C. Slow decomposition to Sn<sub>2</sub>Bu<sub>3</sub> and H<sub>2</sub> occurs over time at room temperature. The purity of HSnBu<sub>3</sub> was verified upon arrival from the manufacturer by NMR. In several instances, the material was received with a non-negligible amount of the decomposition product, Sn<sub>2</sub>Bu<sub>6</sub>. While partially decomposed reagent was avoided in this work, it is worth noting that Sn<sub>2</sub>Bu<sub>6</sub> is inert to the reaction conditions and can generally be removed from product by chromatography.

#### 2.3.4 Large-Scale Hydrostannation of 1-Phenyl-1-Propyne.

To a thawing benzene solution of MoI<sub>2</sub>(CO)<sub>2</sub>(CNAr<sup>Dipp2</sup>)<sub>2</sub> (**1**; 0.108 g, 1.0 mol%, 0.0861 mmol, 15 mL) was added thawing HSnBu<sub>3</sub> (2.56 g, 1.02 equiv, 8.80 mmol), followed by thawing 1-phenyl-1-propyne (1.00 g, 1.0 equiv, 8.61 mmol). The reaction mixture was stirred for 2 h at room temperature then concentrated to a viscous oil. The oil was purified by flash chromatography with Florisil (*n*-pentane eluent) to give a yellow liquid consisting of a mixture of (*E*)-β- and (*E*)-α-vinylstannane regioisomers (3.16 g, 7.76 mmol, 90% yield, (*E*)-β:(*E*)-α = 91:9). The purity of the resulting yellow liquid was confirmed by <sup>1</sup>H NMR spectroscopy.

#### 2.3.5 Hydrostannation with Low Catalyst Loading.

Reactions with 0.1 mol% **1** (0.001 equiv.) were carried out under conditions described as described in *section 2.2.3* with phenyl acetylene, and phenyl propyne. Reaction mixture was stirred for 24 h, at which point 100% conversion was achieved.

### 2.3.6 Hydrostannation Catalyzed by $\text{Mo}(\text{CO})_3(\text{CNAr}^{\text{Dipp}2})_2(\text{ACN})$ .

Reactions catalyzed by  $\text{Mo}(\text{CO})_3(\text{CNAr}^{\text{Dipp}2})_2(\text{ACN})$  under conditions described in the general procedure showed identical selectivities to **1** with 1-phenyl-1-propyne, phenyl acetylene, and 1-hexyne, but required extended reaction times (>24 h). Reactions were accelerated at elevated temperatures (60 °C) to give complete conversion of the acetylenic substrates to vinylstannanes in 12-18 h.

Identical selectivities and decreased reaction rates of  $\text{Mo}(\text{CO})_3(\text{CNAr}^{\text{Dipp}2})_2(\text{ACN})$  compared to the divalent precatalyst **1** suggest identical coordination environments in the catalytically active species generated upon activation. The longer reaction times required for the zero-valent catalyst,  $\text{Mo}(\text{CO})_3(\text{CNAr}^{\text{Dipp}2})_2(\text{ACN})$ , therefore, are thought to originate in the activation steps.  $\text{Mo}(\text{CO})_3(\text{CNAr}^{\text{Dipp}2})_2(\text{ACN})$  is activated upon loss of CO, whereas **1** is activated by reduction with two equivalents of  $\text{HSnBu}_3$ .

### 2.3.7 Hydrostannation Catalyzed by $\text{Mo}(\text{CO})_3(\text{CN}^{\text{tBu}})_3$ .

Under  $\text{N}_2$ -atmosphere, an NMR tube was charged with a  $\text{C}_6\text{D}_6$  (0.5 mL) solution of  $\text{Mo}(\text{CO})_3(\text{CN}^{\text{tBu}})_3$  (0.04 equiv), hydroquinone (0.1 equiv) alkyne (0.1 mmol, 1 equiv.) and  $\text{HSnBu}_3$  (0.25 mmol, 2.5 equiv).<sup>6</sup> The reaction mixture was heated for 6 h until the alkyne substrate was fully consumed. The ratio  $\alpha:\beta$  was determined for the crude reaction mixture.

*Note:* Reactions catalyzed by  $\text{Mo}(\text{CO})_3(\text{CN}^{\text{tBu}})_3$  did not benefit, in terms of rate or selectivity, from low-temperature addition of substrates. Rate of  $\text{HSnBu}_3$  decomposition to  $\text{Sn}_2\text{Bu}_6$  and  $\text{H}_2$  is similar to rate of hydrostannation, thus excess tin-reagent is required.

### 2.3.8 Control Experiments Probing for Background Radical Hydrostannation and Reversible C-Sn Bond Cleavage

#### Uncatalyzed reactions at room temperature:

Under N<sub>2</sub>-atmosphere, an NMR tube charged with diphenyl acetylene (0.1 mmol), HSnBu<sub>3</sub> (53 μL, 0.105 mmol), and C<sub>6</sub>D<sub>6</sub> (0.5 mL). After stirring 24 h at r.t., no conversion to vinylstannanes was observed. This procedure was repeated with 1-hexyne and phenyl acetylene which gave the same result.

#### Control experiments probing radical-type hydrostannation in the presence of MoI<sub>2</sub>(CO)<sub>2</sub>(CNAr<sup>Dipp</sup>)<sub>2</sub> (1):

**A – Pre-activation of MoI<sub>2</sub>(CO)<sub>2</sub>(CNAr<sup>Dipp</sup>)<sub>2</sub> (1) with HSnBu<sub>3</sub> followed by treatment with TEMPO:** To a frozen C<sub>6</sub>D<sub>6</sub> (0.4 mL) solution of **1** (0.005 g, 0.0047 mmol; 2 mol%) was added HSnBu<sub>3</sub> (0.050 g, 0.179 mmol, 53 μL, 1.05 equiv). To the thawing catalyst solution was added a C<sub>6</sub>D<sub>6</sub> (0.1 mL) solution of TEMPO (0.007 g; 0.04 mmol; 22 mol%). Upon complete mixing, the reaction mixture was immediately frozen and phenyl propyne (0.020 g, 0.17 mmol) was added. Catalysis was not inhibited and complete conversion to the vinylstannane was observed. This indicates that radical species that are intercepted by TEMPO do not significantly contribute to the generation of vinylstannane product.

**B – Pre-activation of MoI<sub>2</sub>(CO)<sub>2</sub>(CNAr<sup>Dipp</sup>)<sub>2</sub> (1) with HSnBu<sub>3</sub> Followed by Treatment with Hydroquinone.** To a frozen THF-*d*<sub>8</sub> (0.4 mL) solution of **1** (0.005 g, 0.0047 mmol; 2 mol%) was added HSnBu<sub>3</sub> (0.050 g, 0.179 mmol, 53 μL, 1.05 equiv). To the thawing catalyst solution was added a THF-*d*<sub>8</sub> (0.1 mL) solution of hydroquinone (0.002 g; 0.018 mmol; 10 mol%). Upon complete mixing, the reaction mixture was immediately frozen and phenyl propyne (0.020 g, 0.17



mmol) was added. Catalysis was not inhibited and complete conversion to the vinylstannane was observed. This indicates that radical species that are intercepted by hydroquinone do not significantly contribute to the generation of vinylstannane product.

**C – Pre-treatment of  $\text{MoI}_2(\text{CO})_2(\text{CNAr}^{\text{Dipp}2})_2$  (**1**) with TEMPO.** To a frozen  $\text{C}_6\text{D}_6$  (0.5 mL) solution of **1** (2 mol%, 0.02 equiv) and TEMPO (0.24 equiv) was added 1-phenyl-1-propyne ( $\mu\text{L}$ , 0.17 mmol) and  $\text{HSnBu}_3$  (49.5 mg, 53  $\mu\text{L}$ , 1.05 equiv). The resulting complex was not active in hydrostannation, and only starting material persisted in solution. This result indicates that TEMPO deactivates **1** when  $\text{HSnBu}_3$  is not present and that hydrostannation does not occur.

### 2.3.9 Irreversibility of Reductive Elimination.

Tributyl(styryl)stannane was prepared as a 68:32 mixture of  $\alpha/\beta$ -(*E*) regioisomers by hydrostannation of phenyl acetylene with  $\text{Mo}(\text{CO})_3(\text{tBuNC})_3$  according to the procedure in Section 1.2.3. The catalyst was removed from the reaction mixture by flash chromatography ( $\text{SiO}_2$ ) with pentane eluent. The resulting mixture of vinylstannanes (0.053 g, 0.14 mmol) was concentrated under vacuum and taken up in 100  $\mu\text{L}$   $\text{C}_6\text{D}_6$  and frozen in the cold-well of a glove box ( $\text{N}_2(l)$ ). The thawing vinylstannanes solution was added to a frozen  $\text{C}_6\text{D}_6$  (400  $\mu\text{L}$ ) solution of  $\text{MoI}_2(\text{CO})_2(\text{CNAr}^{\text{Dipp}2})_2$  (**1**; 0.0085 g, 5 mol%). To ensure catalyst activation,  $\text{HSnBu}_3$  (0.0392 g, 36.3  $\mu\text{L}$ , 0.14 mmol) was added to the frozen mixture, and the solution was allowed to thaw at room-temperature. After stirring 24 h, NMR showed no change in the ratio of regioisomers ( $\alpha/\beta$ ). Since hydrostannation of phenyl acetylene with  $\text{MoI}_2(\text{CO})_2(\text{CNAr}^{\text{Dipp}2})_2$  is known to give a 12:88  $\alpha/\beta$  ratio (see below), this result indicates tributyl(styryl)stannane cannot re-enter the catalytic cycle under standard reaction conditions and that the final reductive elimination is irreversible.

## 2.4 $\alpha/\beta$ -Vinylstannane Isomer Determinations and Assignments

Alkynyl carbon atoms of the parent alkyne were assigned  $\alpha$  and  $\beta$ , with the highest priority alkynyl C-atom being denoted as the  $\alpha$ -position. The resulting vinylstannanes are termed  $\alpha$ - or  $\beta$ -stannanes, according to the position occupied by the  $\text{SnBu}_3$  fragment (Figure 2.3). Regioselectivity is reported as ratio of isomers ( $\alpha:\beta$ ) as determined in the crude reaction mixtures by integration of vinylic proton signals in the NMR.

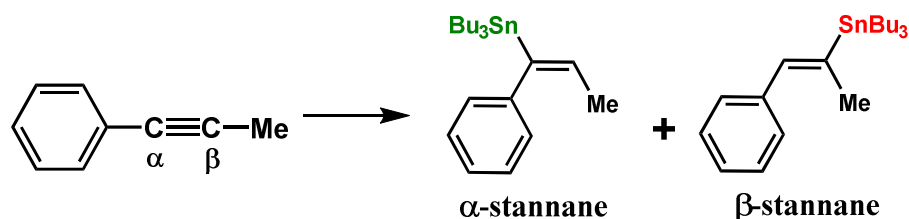


**Figure 2.3.** Example showing  $\alpha/\beta$ -assignments for an internal alkyne.

Vinylic signals were assigned to  $\alpha$  or  $\beta$ -isomers by HSQC, HMBC, and  $J$ -coupling constants as determined by  $^1\text{H}$  NMR spectroscopy. HSQC readily distinguished the two vinylstannane isomers;  $\alpha$ -stannanes showed coupling of one vinyl carbon to two vinyl protons, ( $E$ )- $\beta$ -vinylstannanes showed two vinyl carbons, each coupled to one vinyl proton (Figure 2.4).  $J$ -coupling of *trans*-vicinal protons in terminal ( $E$ )- $\beta$ -vinylstannanes provide diagnostic 18-20 Hz coupling, while  $\alpha$ -vinylstannanes show small germinal coupling of terminal protons (ca. 1.6-2 Hz).  $^{119/117}\text{Sn}/^1\text{H}$  coupling provide unambiguous assignment of vinyl  $^1\text{H}$  chemical shifts;  $J_{\text{SnH},\text{cis}}$  is typically 60-80 Hz, while  $J_{\text{SnH},\text{trans}}$  is much larger at 120-150 Hz (Figure 2.5-7).

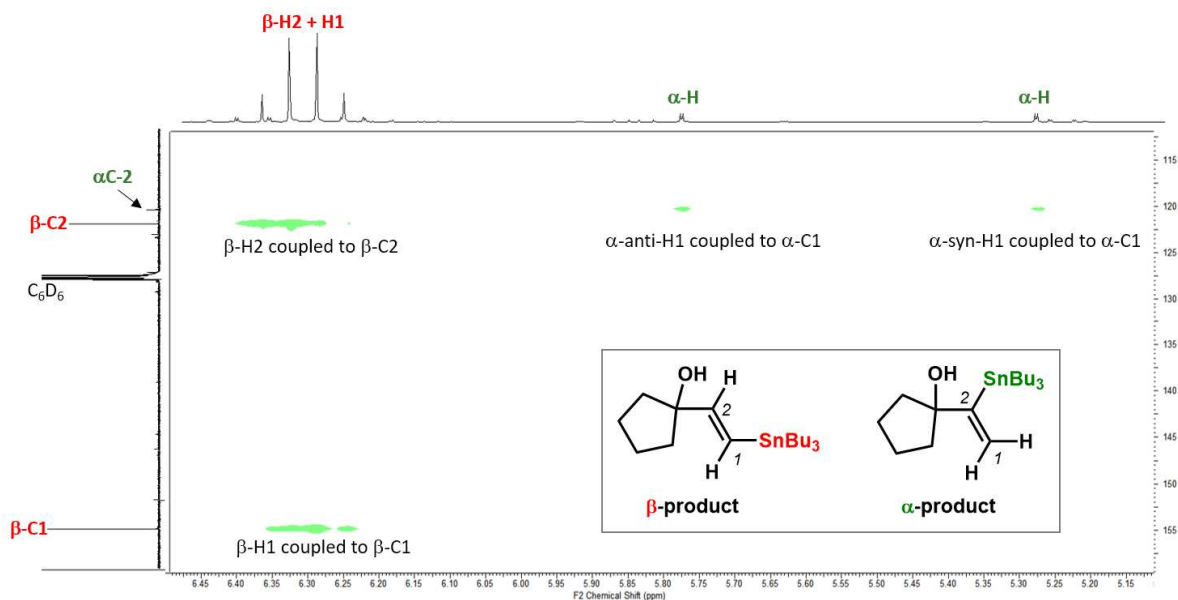


**Figure 2.4.** HSQC verifying regio-isomer assignments for  $\alpha/\beta$ -tributylstannyl(vinyl)-cyclopentanol.

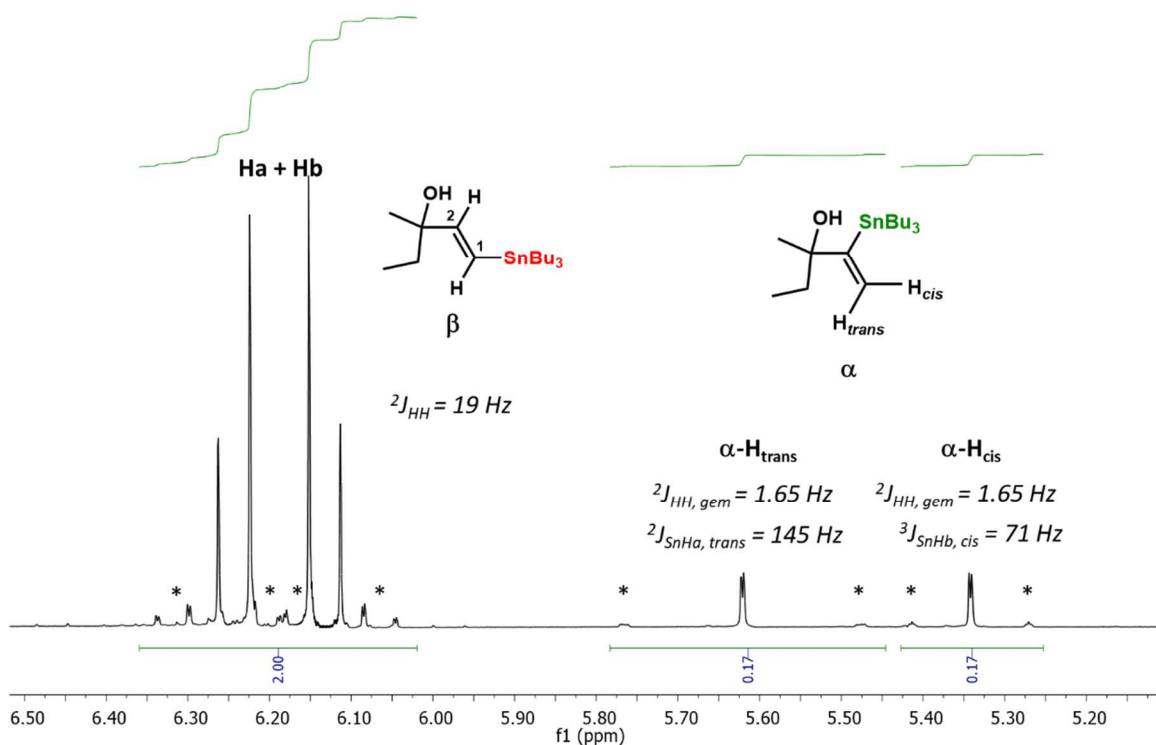


**Figure 2.5.** Example portion of  $^1\text{H}$  NMR spectrum showing key J-coupling values and peak assignments for  $\alpha$ - and  $\beta$ -vinyl protons. \* denotes  $^{119/117}\text{Sn}$  satellites.

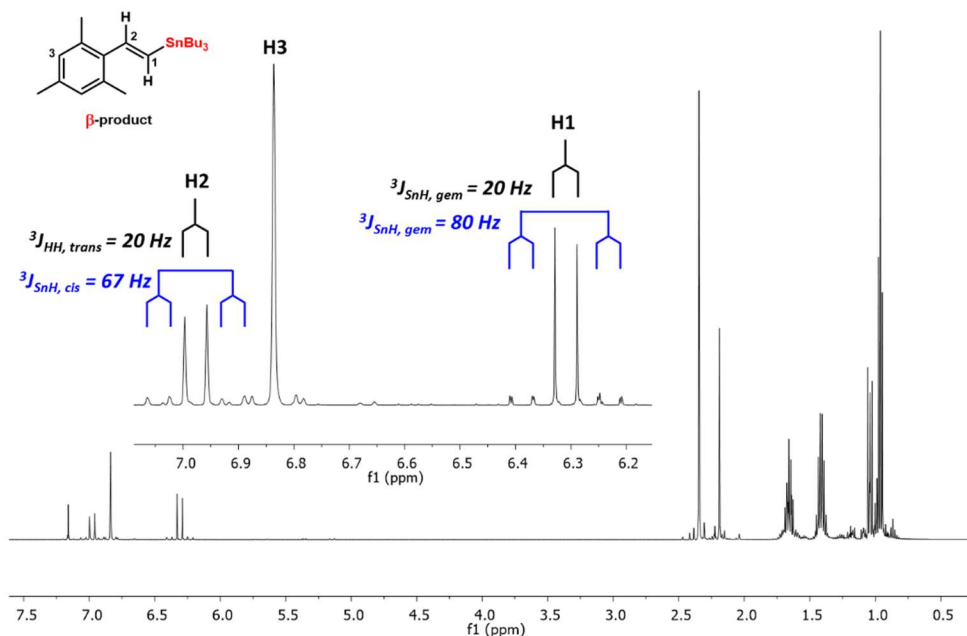


**Figure 2.6.** Example  $^1\text{H}$  NMR spectrum, (*E*)- $\beta$ -tributyl(2,4,6-trimethylstyryl)stannane, showing coupling constants used to establish regio-stereochemical assignments. Large coupling constant of the vicinal protons ( $^3J = 20$  Hz) unambiguously confirms the (*E*)- $\beta$  assignment of the product.

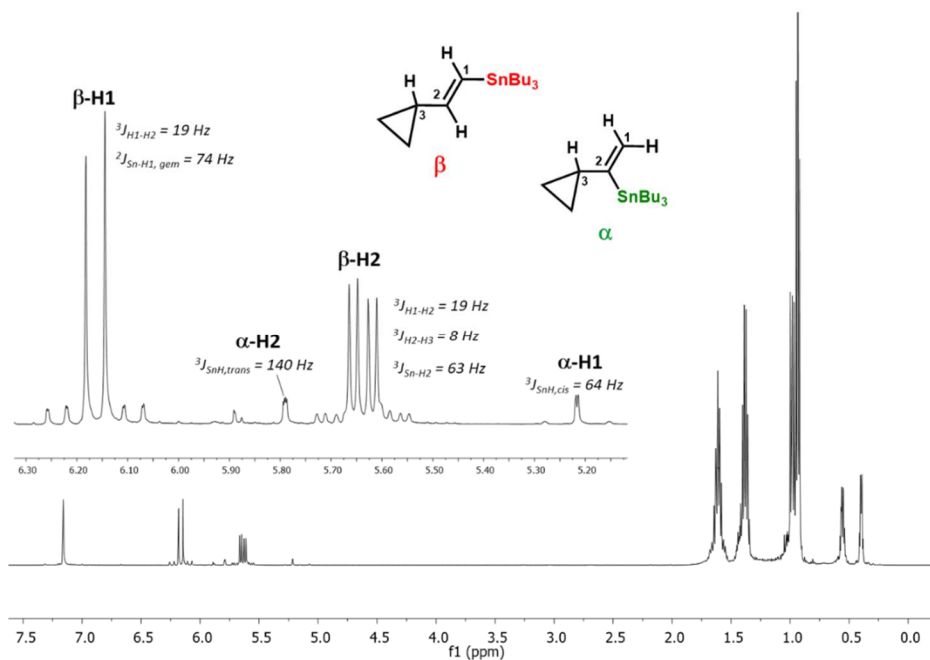
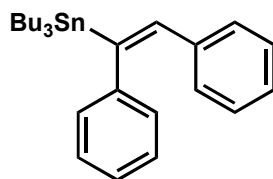
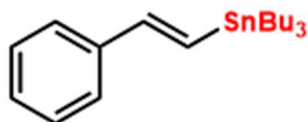


**Figure 2.7.** In addition to characteristic  $J$ -couplings for assignment of  $\beta$ -vinylstannanes,  $\alpha$ -vinylstannanes are readily identifiable with very large Sn/H<sub>trans</sub> coupling constants ( $J_{\text{SnH,trans}} = 140$  Hz), and smaller Sn/H<sub>cis</sub> coupling constants ( $J_{\text{SnH,cis}} = 64$  Hz).

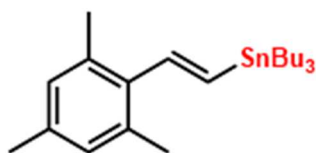
## 2.5 Tabulated Characterization, Regioselectivity and Yield Data for Vinylstannanes



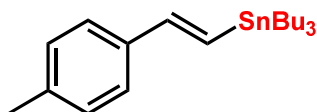
**(E)-tributyl(1,2-diphenylvinyl)stannane.** Colorless oil (92.9 mg, 99%).  $^1\text{H}$  NMR (500 MHz,  $\text{C}_6\text{D}_6$ , 20 °C):  $\delta$  = 7.22 (d,  $J$  = 7.6 Hz, 2H), 7.17 (m, 4H), 7.04 – 6.96 (m, 3H), 6.96 – 6.85 (m, 2H), 1.70 – 1.52 (m, 6H), 1.45 – 1.33 (m, 6H), 1.15 – 1.00 (m, 6H), 0.94 (t,  $J$  = 7.3 Hz, 9H) ppm.  $^{13}\text{C}\{^1\text{H}\}$  NMR (126 MHz,  $\text{C}_6\text{D}_6$ , 20 °C):  $\delta$  = 150.0, 146.2, 139.2, 138.0, 129.8, 129.8, 129.7, 129.2, 128.4, 127.2, 126.8, 125.6, 29.5, 27.8, 14.0, 10.5 ppm.  $^{119}\text{Sn}$  NMR (187 MHz,  $\text{C}_6\text{D}_6$ , 20 °C):  $\delta$  = -33.53 ppm. Anal. Calcd for  $\text{C}_{26}\text{H}_{38}\text{Sn}$ : C 66.54, H 8.16. Found: C 65.4, H 8.26.



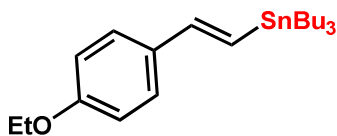
**Entry 1: (E)-tributyl(styryl)stannane.** Colorless oil, (253 mg, 95%,  $\beta$ : $\alpha$  = 87:13 NMR).  $^1\text{H}$  NMR (500 MHz,  $\text{C}_6\text{D}_6$ , 20 °C):  $\delta$  = 7.39 (d,  $J$  = 7.7 Hz, 2H), 7.16 (m, 3H), 7.1 (d,  $J$  = 19.5 Hz, 1H), 6.98 (d,  $J$  = 19.5 Hz, 1H), 1.63 (m, 6H), 1.40 (m, 6H), 1.04 (m, 6H), 0.94 (m, 6H) ppm;  $\alpha$ -isomer:  $\delta$  = 6.14 (d,  $J$  = 2.4,  $J_{\text{SnH}}$  = 129.7 Hz, 1H), 5.52 (d,  $J$  = 2.4,  $J_{\text{SnH}}$  = 71.0 Hz, 1H) ppm.  $^{13}\text{C}\{^1\text{H}\}$  NMR (126 MHz,  $\text{C}_6\text{D}_6$ , 20 °C):  $\delta$  = 147.1, 139.3, 129.1, 128.9, 128.0, 126.5, 29.6, 27.8, 14.0, 9.9 ppm. Anal. Calcd for  $\text{C}_{20}\text{H}_{34}\text{Sn}$ : C 61.09, H 8.72. Found: C 58.28, H 8.59.



**Entry 2: (*E*)-tributyl(2,4,6-trimethylstyryl)stannane.** Colorless oil (92 mg, 97%,  $\beta:\alpha = 99:1$ ).  $^1\text{H}$  NMR (500 MHz,  $\text{C}_6\text{D}_6$ , 20 °C):  $\delta$  6.98 (d,  $^2J_{\text{HH}} = 20$ ,  $^3J_{\text{SnH},\text{cis}} = 67$  Hz, 1H), 6.84 (s, 2H) 6.31 (d,  $^2J_{\text{HH}} = 20$ ,  $^2J_{\text{SnH},\text{gem}} = 80$  Hz, 1H) 2.34 (s, 6H), 2.19, (s, 3H), 1.66 (pent,  $J = 7.8$  Hz, 6H), 1.41 (sext,  $J = 7.45$  Hz, 6H), 1.04 (t, 8.02 Hz, 6H), 0.96 (t,  $J = 7.45$  Hz, 9H) ppm.  $^{13}\text{C}\{^1\text{H}\}$  NMR: (126 MHz,  $\text{C}_6\text{D}_6$ , 20 °C):  $\delta = 146.3, 137.9, 135.9, 135.1, 133.9, 129.1, 27.73, 27.75, 21.14, 21.09, 14.1, 9.98$  ppm. Anal. Calcd for  $\text{C}_{23}\text{H}_{40}\text{Sn}$ : C 63.47; H 9.26. Found: C 63.38, H 9.61.

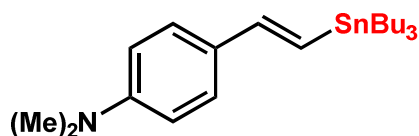


**Entry 3: (*E*)-tributyl(4-methylstyryl)stannane.** Colorless oil, (82 mg, 92%,  $\beta:\alpha = 91:9$  NMR).  $^1\text{H}$  NMR (500 MHz,  $\text{C}_6\text{D}_6$ , 20 °C):  $\delta = 7.35$  (d,  $J = 7.8$  Hz, 2H), 7.10 (d,  $J = 20$ , 1H), 6.99 (d,  $J = 7.8$  Hz, 2H), 6.96 (d,  $J = 20$  Hz, 1H), 2.11 (s, 3H), 1.64 (m, 6 H), 1.40 (m, 6H) 1.05 (m, 6H), 1.20 (m, 9H) ppm;  $\alpha$ -isomer:  $\delta = 6.20$  (d,  $J = 2.4$ ,  $J_{\text{SnH}} = 131.6$  Hz, 1H), 5.52 (d,  $J = 2.4$ ,  $J_{\text{SnH}} = 62.4$  Hz, 1H) ppm.  $^{13}\text{C}\{^1\text{H}\}$  NMR (126 MHz,  $\text{C}_6\text{D}_6$ , 20 °C):  $\delta 147.0, 137.6, 136.8, 129.6, 126.5, 29.7, 29.5, 27.81, 27.8, 21.2, 14.0, 14.0, 9.9$  ppm. Anal. Calcd for  $\text{C}_{21}\text{H}_{36}\text{Sn}$ : C 61.94, H 8.91. Found: C 61.76, H 8.91.

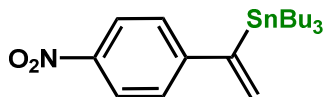


**Entry 4: (*E*)-tributyl(4-ethoxystyryl)stannane.** Light yellow oil, (70 mg, 94%,  $\beta:\alpha = 98:2$  NMR).  $^1\text{H}$  NMR (400 MHz,  $\text{C}_6\text{D}_6$ , 20 °C):  $\delta = 7.37$  (d,  $J = 8.8$  Hz, 2H), 7.10 (d,  $J = 19.4$  Hz, 1H), 6.86 (d,  $J = 19.4$  Hz, 1H), 6.81 (d,  $J = 8.8$  Hz, 2H), 3.57 (q,  $J = 7.0$  Hz, 2H), 1.76 – 1.32 (m,

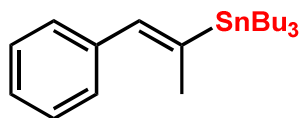
15H), 1.09 (m, 6H), 0.95 (m, 9H) ppm;  $\alpha$ -isomer:  $\delta$  = 6.18 (d,  $J$  = 2.6,  $J_{\text{SnH}}$  = 132.1 Hz, 1H), 5.5 (d,  $J$  = 2.6,  $J_{\text{SnH}}$  = 68.0, 1H) ppm.  $^{13}\text{C}\{^1\text{H}\}$  NMR (126 MHz,  $\text{C}_6\text{D}_6$ , 20 °C):  $\delta$  = 159.4, 146.6, 132.2, 127.8, 125.6, 114.8, 63.2, 31.2, 29.7, 27.8, 14.0, 9.9 ppm.  $^{119}\text{Sn}$  NMR (187 MHz,  $\text{C}_6\text{D}_6$ , 20 °C):  $\delta$  = -42.3 ppm. HRMS (HR-APCI-TOFMS, pos. ion,  $\text{CH}_2\text{Cl}_2$ )  $m/z$  calcd for  $[\text{C}_{22}\text{H}_{39}\text{SnO}]^+$  (M+H) $^+$  439.2021. Found 439.2025.



**Entry 5: (E)-N,N-dimethyl-4-(2-(tributylstannyl)vinyl)aniline.** Colorless oil (108 mg, 93%,  $\beta$ : $\alpha$  = 99:1 NMR). Note: This vinylstannane reacts with magnesium silicate (Florisil<sup>®</sup>) – purification was achieved by flash chromatography over  $\text{SiO}_2$  with a thawing 94:1:5 mixture of pentane,  $\text{Et}_2\text{O}$ , and triethylamine, as eluent.  $^1\text{H}$  NMR (500 MHz,  $\text{C}_6\text{D}_6$ , 20 °C):  $\delta$  = 7.46 (d,  $J$  = 9.05 Hz, 2H), 7.15 (d,  $J$  = 19.3,  $J_{\text{SnH}}$  = 66.8 Hz, 1H), 6.84 (d,  $J$  = 19.3,  $J_{\text{Sn-H}}$  = 71.5 Hz, 1H), 6.56 (d,  $J$  = 8.8 Hz, 2H), 2.50 (s, 6H), 1.67 (pent, 7.6 Hz, 6 H), 1.42 (sxt,  $J$  = 7.5 Hz, 6H), 1.07 (t, 7.8 Hz, 6H), 0.95 (t,  $J$  = 7.3 Hz, 9H) ppm;  $\alpha$ -isomer:  $\delta$  = 6.28 (d,  $J$  = 2.45 Hz,  $J_{\text{SnH}}$  = 137.1 Hz, 1H), 5.48 (d,  $J$  = 2.45,  $J_{\text{SnH}}$  = 63.84 Hz, 1H) ppm.  $^{13}\text{C}\{^1\text{H}\}$  NMR (101 MHz,  $\text{C}_6\text{D}_6$ , 20 °C):  $\delta$  = 150.6, 147.3, 128.5, 127.6, 122.6, 112.7, 40.1, 29.7, 27.8, 14.0, 10.0 ppm.  $^{119}\text{Sn}$  (187 MHz,  $\text{C}_6\text{D}_6$ , 20 °C):  $\delta$  = -47.0 ppm. FTIR ( $\text{C}_6\text{D}_6$ ,  $\text{cm}^{-1}$ ):  $\tilde{\nu}$  = 3086.6, 2957, 2927, 2871, 2851, 2811, 1609, 1588, 1519, 1424, 1376, 1355, 1291, 1229, 1175, 1131, 1071, 986, 948, 828, 776, 662, 597. HRMS (ESI-TOF, pos. ion; benzene)  $m/z$  calcd for  $[\text{C}_{22}\text{H}_{40}\text{NSn}]^+$  (M+H) $^+$  438.2181. Found 438.2175.

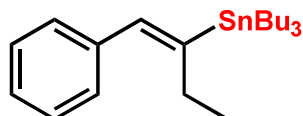


**Entry 6: Tributyl(1-(4-nitrophenyl)vinyl)stannane.** Catalyzed by  $\text{MoI}_2(\text{CO})_2(\text{CNAr}^{\text{Dipp}^2})_2$ : NMR yield 99%,  $\beta:\alpha = 45:55$ . Catalyzed by  $\text{Mo}(\text{CO})_3(\text{CN}^{\text{tBu}})_3$ : Colorless oil, 30 mg, 82%,  $\beta:\alpha = 2:98$ .  $^1\text{H}$  NMR (500 MHz,  $\text{C}_6\text{D}_6$ , 20 °C), major  $\alpha$ -isomer:  $\delta = 7.87$  (d,  $^3J = 8.5$  Hz, 2H), 6.90 (d,  $^3J = 8.5$  Hz, 2H, ), 5.87 (d,  $^3J_{\text{HH,gem}} = 2.2$  Hz,  $^3J_{\text{SnH,trans}} = 120$  Hz, 1H), 5.45 (d,  $^3J_{\text{HH,gem}} = 2.2$  Hz,  $^3J_{\text{SnH,cis}} = 58$  Hz, 1H), 1.59 – 1.39 (m, 6H), 1.36 – 1.24 (m, 6H), 0.98 – 0.94 (m, 6H), 0.88 (t,  $J = 7.3$  Hz, 9H) ppm; minor  $\beta$ -isomer:  $\delta = 6.97$  (d,  $^3J_{\text{HH,trans}} = 19.6$  Hz, 1H), 6.82 (d,  $^3J_{\text{HH,trans}} = 19.6$  Hz, 1H) ppm.  $^{13}\text{C}\{^1\text{H}\}$  NMR (126 MHz,  $\text{C}_6\text{D}_6$ , 20 °C):  $\delta = 153.7, 153.3, 129.7, 126.9, 124.0, 29.4, 27.7, 13.9, 10.6$  ppm.

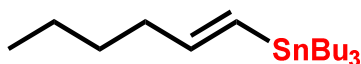


**Entry 7: (E)-tributyl(1-phenylprop-1-en-2-yl)stannane.** Colorless oil, (114 mg, 94%,  $\beta:\alpha = 92:8$ ).  $^1\text{H}$  NMR (500 MHz,  $\text{C}_6\text{D}_6$ , 20 °C):  $\delta = 7.32$  (d,  $J = 7.3$  Hz, 2H), 7.20 (t, 7.6 Hz, 2H), 7.08 (m,  $J = 7.3$  Hz, 1H), 6.85 (d,  $J = 1.5$  Hz,  $J_{\text{SnH}} = 71.6$  Hz, 1H), 2.17 (d,  $J = 1.7$  Hz,  $J_{\text{SnH}} = 47.4$  Hz, 3H), 1.64 (m, 6H), 1.40 (m, 6H), 1.04 (t,  $J = 8.07$  Hz), 0.95 (t,  $J = 7.33$  Hz, 9H) ppm;  $\alpha$ -isomer:  $\delta = 6.0$  (vinyl, q,  $J = 6.5$  Hz,  $J_{\text{Sn-H}} = 66.0$  Hz, 1H) ppm.  $^{13}\text{C}\{^1\text{H}\}$  NMR (126 MHz,  $\text{C}_6\text{D}_6$ ):  $\delta = 143.6, 140.0, 138.6, 129.4, 128.5, 126.7, 29.7, 27.9, 21.4, 14.0, 9.6$  ppm.  $^{119}\text{Sn}$  (187 MHz,  $\text{C}_6\text{D}_6$ ):  $\delta = -36.03$  ppm. Anal. Calcd for  $\text{C}_{21}\text{H}_{36}\text{Sn}$ : C 61.94, H 8.91. Found: C 61.76, H 9.19.

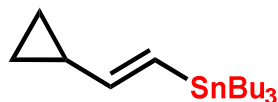




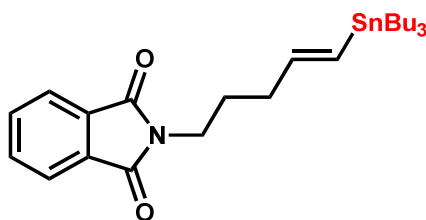
**Entry 8: (*E*)-tributyl(1-phenylbut-1-en-2-yl)stannane.** Colorless oil, (89 mg, 96%,  $\beta$ : $\alpha$  = 80:20).  $^1\text{H}$  NMR (500 MHz,  $\text{C}_6\text{D}_6$ , 20 °C):  $\delta$  = 7.30 (d,  $J$  = 7.3 Hz, 2H), 7.20 (t,  $J$  = 7.5 Hz, 2H), 7.12 – 7.01 (m, 1H), 6.85 (vinyl-H, s,  $J_{\text{Sn-H}}$  = 71.9 Hz, 1H), 2.62 (methylene-H, q,  $J$  = 7.3 Hz,  $J_{\text{SnH}}$  = 60.7 Hz), 1.66 (m, 6H), 1.41 (m, 6H), 1.06 (m, 6H), 0.96 (t,  $J$  = 7.3 Hz, 9H), 0.91 (t,  $J$  = 7.3 Hz, 3H) ppm;  $\alpha$ -Isomer:  $\delta$  = 5.94 (vinyl-H, t,  $J$  = 7.0 Hz,  $J_{\text{Sn-H}}$  = 66.3 Hz, 1H), 2.13 (methylene-H, m, 2H) ppm.  $^{13}\text{C}\{^1\text{H}\}$  NMR (126 MHz,  $\text{C}_6\text{D}_6$ , 20 °C):  $\delta$  = 153.7, 153.3, 147.4, 145.8, 144.5, 144.0, 138.1, 136.4, 126.9, 124.0, 29.6, 29.4, 29.4, 27.8, 27.6, 27.6, 14.0, 13.9, 11.2, 10.6, 9.9 ppm.  $^{119}\text{Sn}$  (187 MHz,  $\text{C}_6\text{D}_6$ , 20 °C):  $\delta$  = -36.1 ppm. Anal. Calcd for  $\text{C}_{22}\text{H}_{38}\text{Sn}$ : C 62.73, H 9.09. Found: C 64.12, H 8.05.



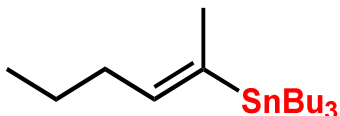
**Entry 9: (*E*)-tributyl(hex-1-en-1-yl)stannane.** Colorless oil, (72 mg, 94%,  $\beta$ : $\alpha$  = 91:9).  $^1\text{H}$  NMR (500 MHz,  $\text{C}_6\text{D}_6$ , 20 °C):  $\delta$  = 6.21 – 5.98 (m, 2H), 2.18 (dt,  $J$  = 7.0, 5.19 Hz, 2H), 1.62 (m 6H), 1.39 (sext, m, 6H), 1.03 - 0.91 (m, 15H) ppm; *minor*  $\alpha$ -isomer:  $\delta$  = 5.86 (dt,  $J_{\text{gem}}$  = 2.7 Hz,  $^4J$  = 1.2 Hz,  $J_{\text{SnH}}$  = 142 Hz), 5.32 (m,  $J_{\text{SnH}}$  = 65 Hz, 1H), 2.38 (t,  $J$  = 7.8, 2H) ppm.  $^{13}\text{C}\{^1\text{H}\}$  NMR (126 MHz,  $\text{C}_6\text{D}_6$ , 20 °C):  $\delta$  = 150.2, 127.3, 38.2, 31.2, 29.7, 27.8, 22.6, 14.24, 14.1, 9.8 ppm. Anal. Calcd for  $\text{C}_{18}\text{H}_{38}\text{Sn}$ : C 57.93, H 10.26. Found: C 55.43, H 10.15.



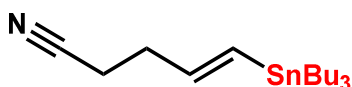
**Entry 10: (*E*)-tributyl(2-cyclopropylvinyl)stannane.** Colorless oil, (78 mg, 93%,  $\beta$ : $\alpha$  = 91:9).  $^1\text{H}$  NMR (500 MHz,  $\text{C}_6\text{D}_6$ , 20  $^\circ\text{C}$ ):  $\delta$  6.13 (d,  $^3J_{\text{HH},\text{trans}} = 18.8$  Hz,  $^2J_{\text{SnH}} = 74$  Hz 1H), 5.62 (dd,  $^3J_{\text{HH},\text{trans}} = 18.8$ , 8.3 Hz,  $^3J_{\text{SnH}} = 63$  Hz, 1H), 1.70 - 1.75 (m, 6H), 1.46 - 1.29 (m, 7H), 1.02 - 0.84 (m, 15 H), 0.55 (m, 2H), 0.39 (m, 2H) ppm; *minor  $\alpha$ -isomer*:  $\delta$  = 5.79 (dd,  $J = 2.4$  Hz,  $J_{\text{SnH}} = 136.6$  Hz, 1H), 5.22 (d,  $J = 2.4$  Hz,  $J_{\text{HSn}} = 63.3$  Hz, 1H) ppm.  $^{13}\text{C}\{^1\text{H}\}$  NMR (126 MHz,  $\text{C}_6\text{D}_6$ , 20  $^\circ\text{C}$ ):  $\delta$  = 152.9, 123.5, 29.3, 29.2, 27.4, 18.4, 13.6, 9.4, 7.0 ppm.  $^{119}\text{Sn}$  NMR (187 MHz,  $\text{C}_6\text{D}_6$ , 20  $^\circ\text{C}$ ):  $\delta$  = -47.9 ppm. Anal. Calcd for  $\text{C}_{17}\text{H}_{34}\text{Sn}$ : C 57.17, H 9.60. Found: C 55.76, H 9.53.



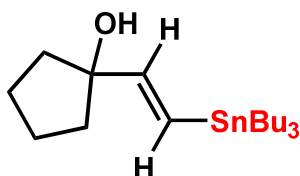
**Entry 11: *N*-(*E*)-5-(tributylstannyl)pent-4-en-1-ylphthalimide.** Colorless oil, (82 mg, 94%,  $\beta$ : $\alpha$  = 92:8).  $^1\text{H}$  NMR (500 MHz,  $\text{C}_6\text{D}_6$ , 20  $^\circ\text{C}$ ):  $\delta$  = 7.45 (dd,  $J = 5.4$ , 3.0 Hz, 2H), 6.90 (dd,  $J = 5.4$ , 3.0 Hz, 2H), 6.16 - 5.95 (m, 2H), 3.61 - 3.48 (m, 1H), 2.15 - 2.02 (m, 1H), 1.77 - 1.68 (m, 1H), 1.68 - 1.49 (m, 4H), 1.38 (sxt,  $J = 7.45$  Hz, 4H), 1.06 - 0.78 (m, 9H) ppm; *minor  $\alpha$ -isomer*:  $\delta$  = 5.8 (dt,  $J_{\text{gem}} = 2.5$  Hz,  $4J = 1.1$  Hz,  $J_{\text{SnH}} = 140$  Hz), 5.26 (dt,  $J_{\text{gem}} = 2.5$  Hz,  $^4J = 1.1$  Hz,  $J_{\text{SnH}} = 64$  Hz), 2.28 (t,  $J = 7.7$  Hz,  $J_{\text{SnH}} = 45$  Hz, 2H) ppm.  $^{13}\text{C}\{^1\text{H}\}$  NMR (126 MHz,  $\text{C}_6\text{D}_6$ , 20  $^\circ\text{C}$ ):  $\delta$  167.93, 148.42, 133.40, 132.70, 128.45, 122.91, 37.63, 35.35, 29.63, 28.02, 27.79, 14.06, 9.73 ppm.  $^{119}\text{Sn}$  (187 MHz,  $\text{C}_6\text{D}_6$ , 20  $^\circ\text{C}$ ):  $\delta$  -49.6 ppm.



**Entry 12: (*E*)-tributyl(hex-2-en-2-yl)stannane.** Colorless oil, (72 mg, 94%,  $\beta:\alpha = 89:11$ ).  $^1\text{H}$  NMR (500 MHz,  $\text{C}_6\text{D}_6$ , 20 °C):  $\delta = 5.69$  (td,  $J = 6.8, 1.8$  Hz,  $J_{\text{Sn-H}} = 67.6$  Hz, 1H), 2.09 (q,  $J = 6.9$  Hz, 2H), 1.94 – 1.83 (m,  $J_{\text{SnH}} = 47.5$  Hz, 3H), 1.66-1.47 (m, 6 H), 1.43-1.25 (q, 8H), 1.03-0.98 (m, 6H), 0.97-0.86 (m, 12H) ppm; *minor  $\alpha$ -isomer*:  $\delta = 2.37$  (t,  $J = 7.6$  Hz,  $^3J_{\text{SnH}} = 60.5$  Hz, 2H) ppm.  $^{13}\text{C}\{^1\text{H}\}$  NMR (126 MHz,  $\text{C}_6\text{D}_6$ , 20 °C):  $\delta = 141.7, 137.9, 30.6, 29.7, 27.9, 23.2, 19.4, 14.0, 14.0, 9.50$  ppm.  $^{119}\text{Sn}$  (187 MHz,  $\text{C}_6\text{D}_6$ , 20 °C):  $\delta = -41.06$  ppm. Anal. Calcd for  $\text{C}_{18}\text{H}_{38}\text{Sn}$ : C 57.93, H 10.26. Found: C 58.55, H 10.76.

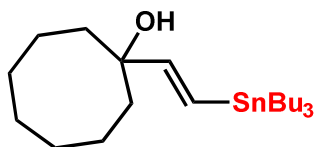


**Entry 13: (*E*)-5-(tributylstannyl)pent-4-enitrile.** NMR yield >99%,  $\beta:\alpha = 39:61$ .  $^1\text{H}$  NMR (500 MHz,  $\text{C}_6\text{D}_6$ , 20 °C):  $\delta = 5.96$  (d,  $J = 18.7, J_{\text{Sn-H}} = 38.5$  Hz, 1H), 5.76 (dt,  $J = 19.1, 6.2$  Hz, 1H), 1.90 (m, 2H), 1.73 – 1.29 (m, 18H), 0.94 (m, 9H) ppm;  $\alpha$ -isomer:  $\delta = 5.65$ , (s,  $J_{\text{Sn-H}} = 68.6$ , 1H), 5.21 (s,  $J_{\text{Sn-H}} = 31.2$  Hz, 1H), 2.15 (t,  $J = 7.33$  Hz,  $J_{\text{Sn-H}} = 22.4$  Hz, 2H) ppm.  $^{119/117}\text{Sn}$  NMR (187 MHz,  $\text{C}_6\text{D}_6$ , 20 °C):  $\delta = -48.4$  ppm.

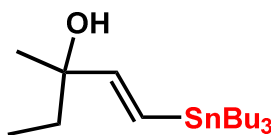


**Entry 14: (*E*)-1-(2-(tributylstannyl)vinyl)cyclopentan-1-ol.** Colorless oil, (93 mg, 92%,  $\beta:\alpha = 90:10$ ).  $^1\text{H}$  NMR (500 MHz,  $\text{C}_6\text{D}_6$ , 20 °C):  $\delta = 6.35, 6.31$  (ABq,  $J_{\text{AB}} = 19.8$  Hz, 2H), 1.87

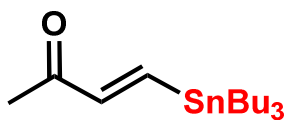
(m, 2 H), 1.77 – 1.50 (m, 12H) 1.38 (m, 6H), 1.02 – 0.9 (m, 15H) ppm.  $^{13}\text{C}\{^1\text{H}\}$  NMR (126 MHz,  $\text{C}_6\text{D}_6$ , 20 °C):  $\delta$  = 155.3, 122.3, 83.5, 40.9, 29.6, 27.7, 24.3, 14.0, 9.8 ppm. FTIR (film,  $\text{cm}^{-1}$ ):  $\tilde{\nu}$  = 3429, 3350, 2957, 2925, 2872, 2854, 2815, 1599, 1464, 1377, 1070, 1029, 992, 691, 597  $\text{cm}^{-1}$ . HRMS (ESI-TOF, neg. ion;  $\text{CH}_2\text{Cl}_2$ )  $m/z$  calcd for  $[\text{C}_{19}\text{H}_{37}\text{OSn}]^-$  (M–H) $^-$  401.1875; found 401.1881.



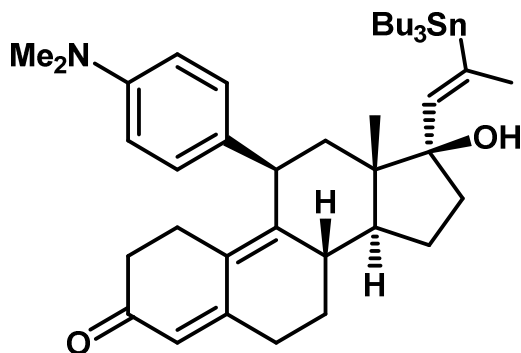
**Entry 15: (E)-1-(2-(tributylstannyl)vinyl)cyclooctan-1-ol.** Colorless oil, (87 mg, 91%,  $\beta:\alpha = 97:3$ ).  $^1\text{H}$  NMR (400 MHz,  $\text{C}_6\text{D}_6$ , 20 °C):  $\delta$  = 6.27 (ABq,  $J_{AB} = 19.5$  Hz, 1H), 1.85 – 1.72 (m, 4H), 1.71 – 1.18 (m, 26H), 0.95 – 0.76 (m, 9H); *minor  $\alpha$ -isomer*:  $\delta$  = 5.62 (s,  $J_{\text{SnH}} = 147.0$  Hz, 1H), 5.29 (s,  $J_{\text{SnH}} = 73.9$  Hz, 1H) ppm.  $^{13}\text{C}\{^1\text{H}\}$  NMR (126 MHz,  $\text{C}_6\text{D}_6$ , 20 °C):  $\delta$  = 157.0, 122.2, 76.2, 36.8, 29.6, 28.7, 27.7, 25.0, 22.5, 14.0, 9.8 ppm;  $^{119}\text{Sn}$  (187 MHz,  $\text{C}_6\text{D}_6$ , 20 °C):  $\delta$  = -44.4 ppm.



**Entry 16: (E)-3-methyl-1-(tributylstannyl)pent-1-en-3-ol.** Colorless oil, (72 mg, 92%,  $\beta:\alpha = 83:17$ ).  $^1\text{H}$  NMR (500 MHz,  $\text{C}_6\text{D}_6$ , 20 °C):  $\delta$  ppm 6.19 (ABq,  $J_{AB} = 19.6$  Hz,  $J_{\text{SnH},gem} = 72$  Hz,  $J_{\text{SnH},cis} = 66$  Hz, 2H), 1.77-1.31 (m, 18H), 1.183 (s, 3H), 0.99-0.86 (m, 12H);  $\alpha$ -stannane:  $\delta$  = 5.56 (d,  $^2J_{\text{HH},gem} = 1.65$  Hz,  $J_{\text{SnH}} = 145$  Hz, 1H), 5.28 (d,  $^2J_{\text{HH},gem} = 1.65$  Hz,  $J_{\text{SnH}} = 71$  Hz, 1H) ppm.  $^{13}\text{C}\{^1\text{H}\}$  NMR (126 MHz,  $\text{C}_6\text{D}_6$ , 20 °C):  $\delta$  = 155.7, 122.9, 74.5, 35.2, 29.6, 28.0, 27.7, 14.0, 9.8, 8.5 ppm.  $^{119}\text{Sn}$  NMR (187 MHz,  $\text{C}_6\text{D}_6$ , 20 °C):  $\delta$  = -44.0 ppm.



**Entry 17: (*E*)-4-(tributylstannyl)but-3-en-2-one.**  $^1\text{H}$  NMR (300 MHz,  $\text{C}_6\text{D}_6$ , 20 °C):  $\delta$  = 7.45 (d,  $J$  = 19.8 Hz, 1H), 6.69 (d,  $J$  = 19.8 Hz, 1H), 1.94 (s, 3H), 1.75 – 1.56 (m, 6H), 1.47 – 1.27 (m, 6H), 1.03 – 0.83 (m, 15H);  $\alpha$ -isomer:  $\delta$  = 6.26 (d,  $J$  = 1.5 Hz, 1H), 5.95 (d,  $J$  = 1.5 Hz, 1H), 1.94 (s, 3H). Decomposition precluded isolation by chromatography.



**Hydrostannation of Mifepristone.** Colorless residue, (29 mg, 98%, >99%  $\beta$ -isomer).  $^1\text{H}$  NMR (500 MHz,  $\text{C}_6\text{D}_6$ ):  $\delta$  = 7.06 (d,  $J$  = 8.80 Hz, 2 H), 6.63 (d,  $J$  = 8.07 Hz, 2 H), 5.88 (s, 1 H), 5.80 (s,  $J_{\text{SnH}}$  = 77.0 Hz, 1 H), 4.25 (d,  $J$  = 7.34 Hz, 1 H), 2.56 (s, 6 H), 2.40 - 2.53 (m, 2 H), 2.37 (d,  $J$  = 1.47 Hz, 2 H), 2.23 - 2.36 (m, 4 H), 2.07 - 2.20 (m, 3 H), 1.95 - 2.06 (m, 1 H), 1.69 - 1.76 (m, 1 H), 1.48 - 1.69 (m, 9 H), 1.33 - 1.45 (m, 6 H), 1.15 - 1.17 (m, 3 H), 0.89 - 1.09 (m, 15 H), 0.79 (s, 3 H) ppm.  $^{13}\text{C}\{^1\text{H}\}$  NMR (126 MHz,  $\text{C}_6\text{D}_6$ ):  $\delta$  = 197.3, 155.0, 149.0, 145.6, 144.6, 142.8, 132.6, 129.6, 123.6, 113.2, 86.8, 50.8, 48.4, 40.4, 39.9, 39.8, 39.4, 38.8, 37.4, 31.1, 29.8, 28.0, 27.9, 26.2, 24.1, 22.3, 15.5, 14.1, 9.8 ppm.  $^{119}\text{Sn}$  NMR (187 MHz,  $\text{C}_6\text{D}_6$ ):  $\delta$  = -35.6 ppm. HRMS (ESI-TOF, pos. ion; acetonitrile)  $m/z$  calcd for  $[\text{C}_{41}\text{H}_{64}\text{NO}_2\text{Sn}]^+$  ( $\text{M}+\text{H}$ ) $^+$  722.3962; found 722.3970.

## 2.6 Determination of Kinetic Isotope Effect and Hammett Correlations.

### 2.6.1 Kinetic Isotope Effect by Intermolecular Competition

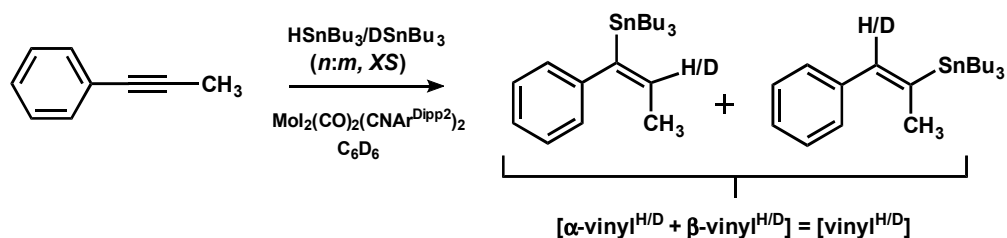


**Figure 2.8.** Hydrostannylation of 1-phenyl-1-propyne gave ratios of vinyl<sup>H</sup> : vinyl<sup>D</sup> with linear dependence on the relative loading of HSnBu<sub>3</sub>/DSnBu<sub>3</sub> in the reaction mixture.

The absence of primary kinetic isotope effect (KIE) has been determined by intermolecular competition experiments (Figure 2.8). Because a wide range of potential energy surfaces give rise to observable KIE in competition experiments, the absence of a primary KIE by this method is more informative than when the same observation is made from independently measured rate-constants (i.e.  $k_{\text{H}}/k_{\text{D}}$ ).<sup>35</sup> Accordingly, the small KIE of 1.108(7) strongly indicates that Sn-H bond cleavage does not occur in the rate-limiting step.

The experiment was carried out at four ratios of HSnBu<sub>3</sub>/DSnBu<sub>3</sub> and these values were plotted versus the ratio of isotopic enrichment in the product (vinyl<sup>H</sup>/vinyl<sup>D</sup>). In this way, the KIE could be extrapolated directly from the slope ( $\text{KIE} = [\text{vinyl}^{\text{H}}/\text{vinyl}^{\text{D}}]/[\text{HSnBu}_3/\text{DSnBu}_3]_0$ ). Although duplicate experiments at 1:1 ratio HSnBu<sub>3</sub>/DSnBu<sub>3</sub> are commonly used for KIE determination (where vinyl<sup>H</sup>/vinyl<sup>D</sup> = KIE), linear regression was favored for two reasons: (1) systematic error due to minor variations in purity of the tin reagents are mitigated, and (2) agreement between KIE values determined by linear regression and the value determined at 1:1 HSnBu<sub>3</sub>/DSnBu<sub>3</sub> would provide added certainty to physical measurements.

*Experimental:* The general procedure (see Section 1.2.3) was modified such that H/D-SnBu<sub>3</sub> was added in three-fold excess relative to alkyne, and the reaction was carried out at ratios

$m:n$  HSnBu<sub>3</sub>/DSnBu<sub>3</sub> ( $m:n = 1:3, 1:1, 3:1$  and  $0:4$ ). Consistent with standard conditions, the alkyne (1-phenyl-propyne, 0.17 mmol, 1 equiv.) and tin reagents were added to a frozen C<sub>6</sub>D<sub>6</sub> solution (1.0 mL) of MoI<sub>2</sub>(CO)<sub>2</sub>CNAr<sup>Dipp</sup><sub>2</sub> (4.7 mg, 0.02 equiv). NMR indicated complete consumption of the alkyne in <10 minutes. Deuterium enrichment of the vinylstannane was determined by NMR as described below.

*Analysis:* NMR was obtained on a JEOL ECA-500 spectrometer. T<sub>1</sub> was estimated from the null-point value, and the relaxation delay was set to five-times T<sub>1</sub>. The FID was phased and a baseline correction was applied. 1-Phenyl-1-propyne was chosen as the acetylenic substrate because the methyl proton resonance at 2.17 ppm provide a convenient internal reference which was used to normalize the integral values of vinylic protons for the  $\alpha,\beta$ -vinylstannane products (vinyl<sup>H/D</sup>).

The integrated spectrum in Figure 2.9 shows the standardized integral value of -CH<sub>3</sub> (int. = 30) and the corresponding values for  $\alpha$ -vinyl<sup>H</sup> and  $\beta$ -vinyl<sup>H</sup> obtained by hydrostannation of 1-phenyl-1-propyne with 1:0 HSnBu<sub>3</sub>/DSnBu<sub>3</sub>. Spectra obtained for each reaction at ratio  $m:n$  HSnBu<sub>3</sub>/DSnBu<sub>3</sub> were similarly normalized to -CH<sub>3</sub> (int. = 30). As the concentration of DSnBu<sub>3</sub> was increased relative to HSnBu<sub>3</sub>, decreased integral values of vinyl<sup>H</sup> relative to -CH<sub>3</sub> were observed due to deuterium incorporation. By subtracting the observed integral value [vinyl<sup>H</sup>] at  $m:n$  HSnBu<sub>3</sub>/DSnBu<sub>3</sub> from the value [vinyl<sup>H</sup>]<sub>0</sub> at 1:0 HSnBu<sub>3</sub>/DSnBu<sub>3</sub>, a normalized integral value [vinyl<sup>D</sup>] was obtained. Taking the ratio of these values [vinyl<sup>H</sup>/vinyl<sup>D</sup>] and plotting against the fractional ratio [HSnBu<sub>3</sub>/DSnBu<sub>3</sub>] (table 5.1) present in the initial reaction mixture gave a line with the value of the slope being the KIE (Figure 2.10).

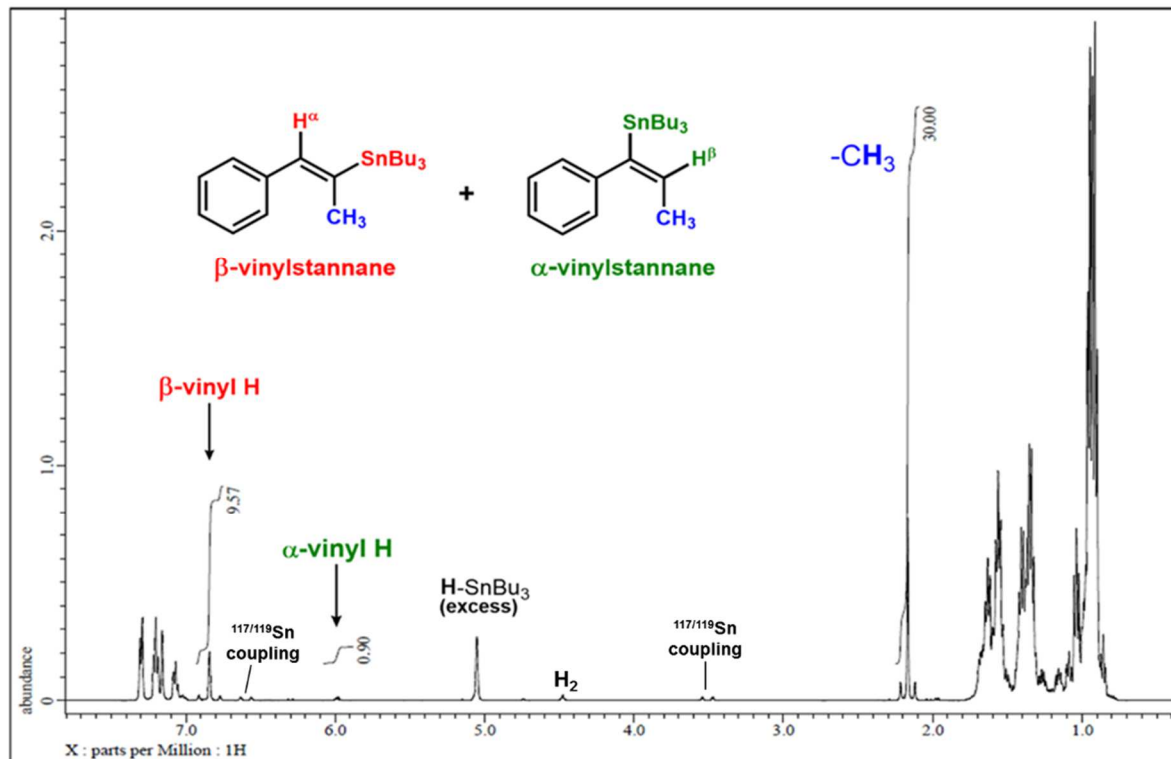


**Figure 2.9.** Reference spectra showing crude  $^1\text{H}$  NMR data for hydrostannation of 1-phenyl-1-propyne with 3 equiv.  $\text{HSnBu}_3$  (1:0  $\text{HSnBu}_3/\text{DSnBu}_3$ ). The sum of  $\alpha$ - and  $\beta$ -vinyl integral values give  $[\text{vinyl}^{\text{H}}]_0$ . Generation of  $\text{H}_2$  ensues upon complete consumption of alkyne.

**Experimental determination of KIE:** As shown in Figure 2.10, least squares fitting shows that the experimentally determined ratio for deuterium enrichment in the final product ( $[\text{vinyl}^{\text{H}}]/[\text{vinyl}^{\text{D}}]$ ) shows the expected linear dependence on the fractional ratio of deuterium in the tin reagent. The near-zero value for the y-intercept indicates a suitable level of precision in the measured values (NMR integration), as the expected ratio  $[\text{vinyl}^{\text{H}}]/[\text{vinyl}^{\text{D}}]$  when only  $\text{DSnBu}_3$  is present is *zero*. The excellent linear-fit ( $R^2 = 0.9999$ ) of the data indicates good precision in addition of tin reagents. High purity of the reagents can be assumed since deviation in purity of the reagents would be expected to cause regular deviation in the  $m:n$  ratio, thus resulting in second-order curvature. The kinetic isotope effect can be extracted from the slope of the line 1.108(7).



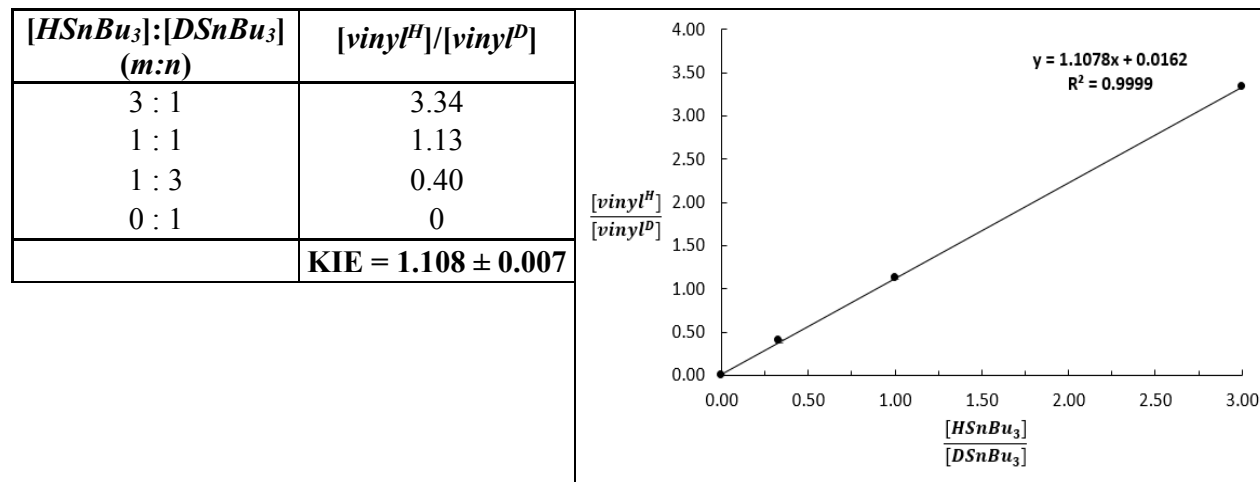


**Figure 2.10.** Experimental values  $[vinyl^H] / [vinyl^D]$  versus ratio of *m:n*  $HSnBu_3/DSnBu_3$ . Analysis by least squares linear regression gives KIE as the slope.

We have proposed that reversible migratory insertion of hydride into the alkyne ligand as a key mechanistic feature by which regioselectivity is derived in Mo-catalyzed hydrostannation. The absence of a primary kinetic isotope effect is consistent with this result. Observation of KIE would indicate rate-limiting cleavage of the Sn-H bond and would therefore place the highest energy barrier before the selectivity determining step – this cannot be the case if the selectivity determining step (migratory insertion) is reversible.

## 2.6.2 Hammett Correlations

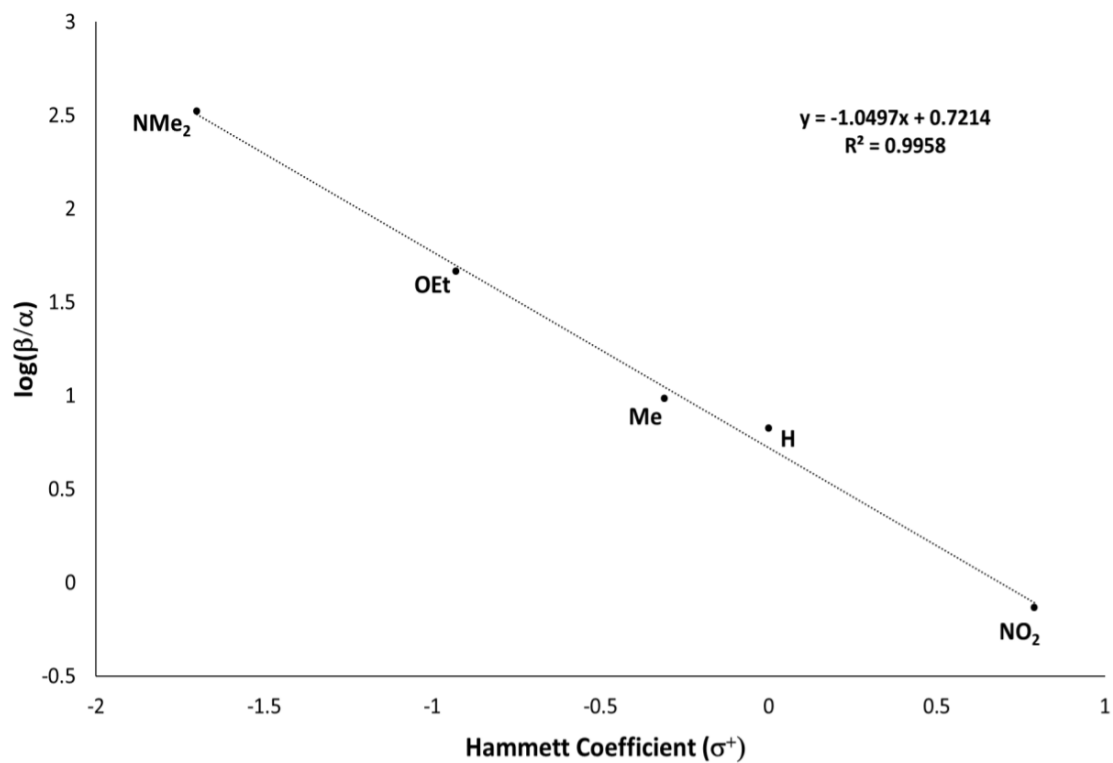


**Figure 2.11** Plot of  $\log(\text{observed selectivity})$  (i.e.  $\log(\beta/\alpha)$ ) vs. Hammett  $\sigma^+$  parameter<sup>36</sup> *para*-substituted aryl alkynes in Table 1.

### 2.6.3 Results of Computational Studies

Results of Computational Studies Density Functional Theory (DFT) calculations were performed with ORCA 3.0.3 program suite<sup>37</sup> using the BP86 functional.<sup>38,39</sup> The all-electron Ahlrichs triple- $\zeta$  basis sets def2-TZVP (standard)<sup>40,41</sup> and def2-TZVP/J (auxiliary)<sup>42-45</sup> were used in all calculations. Relativistic effects were included by use of the zeroth-order regular approximation (ZORA).<sup>41,46-49</sup> Input molecular structures were generated with ChemCraft 1.8.<sup>50</sup>

#### $\beta$ -Intermediates:

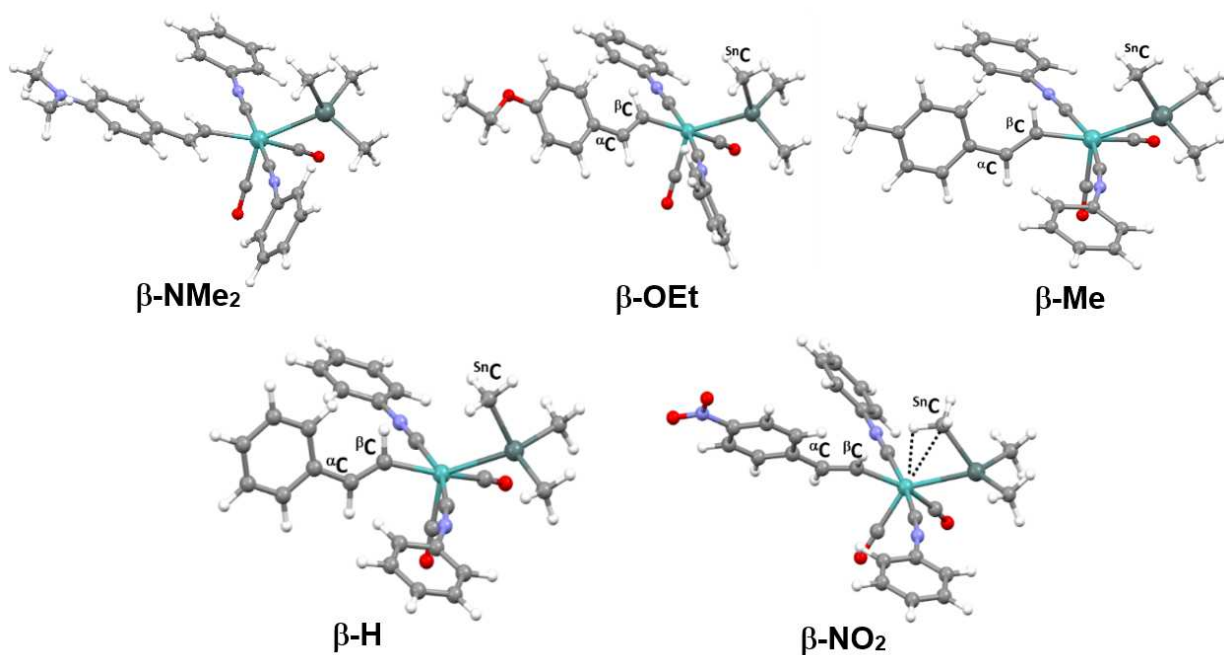


**Figure 2.12.** Optimized  $\beta$ -intermediates,  $\text{Mo}(\text{CO})_2(\text{CNPh})_2(\eta^1\text{-RArCHCH})(\text{SnMe}_3)$ ,  $\text{R} = \text{NMe}_2$ ,  $\text{OEt}$ ,  $\text{Me}$ ,  $\text{H}$ ,  $\text{NO}_2$ . Optimized coordinates of  $\beta$ -H were modified and used as starting coordinates for all  $p$ -functionalized derivatives.

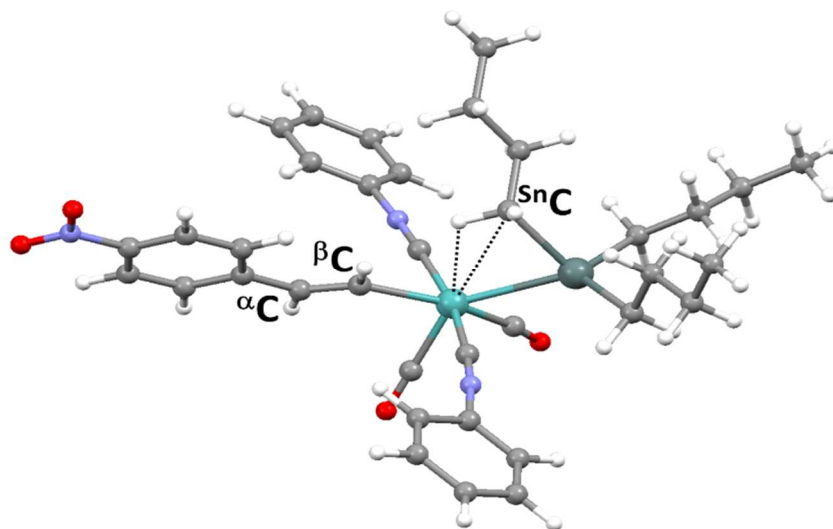


**Figure 2.13.** Optimization of *p*-NO<sub>2</sub>-vinyl complex with SnBu<sub>3</sub> gives an agostic complex analogous to the SnMe<sub>3</sub> complex **β**-NO<sub>2</sub>. Selected bond distances (Å): SnCH–Mo = 2.326, SnC–Mo = 2.905.

**Table 2.2.** Calculated structural parameters for **β**-vinylstannane producing intermediates Mo(η<sup>1</sup>-C–(C(H)=C(H)C<sub>6</sub>H<sub>4</sub>-*p*-X))(SnMe<sub>3</sub>)(CNPh)<sub>2</sub>(CO)<sub>2</sub>.

Intermediate	Hammett Param. (σ <sup>+</sup> )	[ <sup>α</sup> C– <sup>β</sup> C] (Å)	[ <sup>α</sup> C–Mo] (Å)	[ <sup>β</sup> C–Mo] (Å)	[Sn–Mo] (Å)
<b>β</b> -NO <sub>2</sub>	0.79	1.356	3.301	2.201	2.761
<b>β</b> -H	0	1.352	3.298	2.186	2.859
<b>β</b> -Me	-0.31	1.339	3.319	2.187	2.86
<b>β</b> -OEt	-0.93	1.363	3.232	2.187	2.886
<b>β</b> -NMe <sub>2</sub>	-1.70	1.368	3.146	2.165	2.894

**X = NO<sub>2</sub>**

Mo	2.049166	3.016081	-3.482691
C	2.341569	3.915788	-1.720669
N	-1.102328	2.189187	-3.725492
N	5.292276	3.279488	-3.771889
C	-3.689823	-0.254094	-4.632375
H	-3.766287	-1.233396	-5.105745
C	-2.336690	1.599751	-3.871148
C	7.250280	2.808843	-5.088207
C	0.024323	2.557827	-3.631634
C	4.115285	3.210964	-3.652558
C	6.655218	3.354622	-3.936534
C	-3.490042	2.258685	-3.410043
C	2.400120	1.512649	-5.051222
C	-2.437253	0.336841	-4.484333
C	-4.840208	0.397909	-4.176555
H	-5.817403	-0.071209	-4.295226
C	4.164424	-1.606173	-6.216947
H	4.722175	-1.760913	-5.290673
C	3.191060	0.417666	-5.168275
C	8.824235	4.050528	-3.129816
H	9.437270	4.530951	-2.366139
C	7.444319	3.977001	-2.952679
C	-4.734565	1.651347	-3.565766
H	-5.628821	2.161981	-3.206896
C	3.300691	-0.489450	-6.311427
C	9.421894	3.512509	-4.274136
H	10.502871	3.574431	-4.406277
C	8.631653	2.893230	-5.247932
H	9.093846	2.470344	-6.140773
C	2.589066	-0.320537	-7.523144
H	1.913668	0.528856	-7.636756
C	2.729467	-1.210656	-8.576801
H	2.183236	-1.081853	-9.509889
C	3.594156	-2.303549	-8.441179
C	4.315967	-2.507789	-7.262474
H	4.978170	-3.368905	-7.186655
H	-3.394886	3.233809	-2.933842
H	-1.532192	-0.161092	-4.830701
H	6.965002	4.388713	-2.064736
H	6.621564	2.327442	-5.836988
O	2.646701	4.270775	-0.645924
Sn	1.019034	5.576346	-3.402306
C	2.082134	7.323118	-2.663179
H	1.727233	8.215932	-3.193680
H	3.158945	7.198975	-2.828154
H	1.894629	7.442597	-1.589182
C	-1.107637	6.035049	-3.462669
H	-1.241950	7.032213	-3.902067
H	-1.635207	5.291311	-4.069894

H	-1.517327	6.036261	-2.445494
C	1.767364	5.060307	-5.434354
H	2.258875	4.073407	-5.574385
H	2.519947	5.809717	-5.706773
H	0.914623	5.088291	-6.121908
C	2.043775	1.452546	-2.298289
O	2.007829	0.517454	-1.612186
H	3.830830	0.132372	-4.323722
H	1.756594	1.722801	-5.927235
N	3.743909	-3.247648	-9.553503
O	4.518642	-4.203451	-9.403593
O	3.087595	-3.037828	-10.584237

### **X = H**

C	2.688851	4.613514	-1.849941
Mo	2.275961	3.328114	-3.347447
C	2.688851	4.613514	-1.849941
N	-0.749661	2.205165	-3.715584
N	5.529634	3.304383	-3.701017
C	-2.876526	-0.365135	-5.246391
H	-2.793191	-1.177608	-5.969870
C	-1.855551	1.443750	-4.009819
C	7.337675	2.262469	-4.894097
C	0.320592	2.705145	-3.574042
C	4.355740	3.349469	-3.549256
C	6.877924	3.184304	-3.935876
C	-3.085820	1.717723	-3.386688
C	2.595985	1.814190	-4.890925
C	-1.749479	0.395020	-4.942986
C	-4.103260	-0.096273	-4.629781
H	-4.980611	-0.696745	-4.872542
C	2.963259	-1.789824	-5.935932
H	2.796193	-2.200641	-4.937087
C	2.724364	0.469040	-4.929369
C	9.151518	3.853789	-3.466786
H	9.857356	4.471486	-2.910232
C	7.786712	3.981801	-3.217989
C	-4.201374	0.943627	-3.700531
H	-5.154486	1.156055	-3.214895
C	2.962999	-0.389301	-6.101821
C	9.615483	2.941147	-4.419723
H	10.685426	2.846472	-4.609567
C	8.706112	2.148799	-5.127737
H	9.064627	1.433704	-5.869574
C	3.187104	0.110164	-7.402462
H	3.206086	1.189710	-7.566926
C	3.389140	-0.748445	-8.480089
H	3.560802	-0.333735	-9.475435
C	3.379717	-2.136565	-8.295037

C	3.166930	-2.652170	-7.013863
H	3.161055	-3.732203	-6.852254
H	-3.148563	2.531565	-2.664110
H	-0.786319	0.195607	-5.412112
H	7.409669	4.686564	-2.476647
H	6.616388	1.649994	-5.434418
O	3.060551	5.228247	-0.927800
Sn	0.742769	5.735846	-3.499919
C	1.535918	7.621660	-2.738714
H	0.963033	8.445378	-3.185524
H	2.593723	7.726832	-3.008235
H	1.440541	7.663340	-1.646997
C	-1.377452	5.735543	-2.989259
H	-1.791955	6.728761	-3.208688
H	-1.914524	4.981642	-3.575833
H	-1.505828	5.524733	-1.920190
C	0.946117	5.813387	-5.696563
H	1.998297	5.769366	-6.003852
H	0.525827	6.773237	-6.028368
H	0.392133	4.992416	-6.166005
C	2.184375	2.154042	-1.814607
O	2.104756	1.431725	-0.901334
H	2.640734	-0.089413	-3.988339
H	3.541320	-2.806284	-9.141026

### X = Me

Mo	2.285035	3.144274	-3.299326
C	2.686493	4.278001	-1.596986
N	-0.808582	2.142810	-3.914918
N	5.648037	3.405329	-3.712812
C	-3.169784	-0.054354	-5.645594
H	-3.153623	-0.867364	-6.359547
C	-2.003510	1.566090	-4.321061
C	7.521102	2.377344	-4.800243
C	0.233416	2.559046	-3.656855
C	4.517799	3.367337	-3.520905
C	7.010834	3.380834	-3.984007
C	-3.207706	2.037271	-3.810823
C	2.664289	1.640101	-4.950155
C	-1.975597	0.520169	-5.238302
C	-4.379156	0.408678	-5.141236
H	-5.308318	-0.043963	-5.462219
C	2.939101	-1.993135	-5.886326
H	2.682940	-2.371952	-4.903957
C	2.618450	0.301793	-4.979397
C	9.196338	4.319722	-3.714759
H	9.847100	5.074230	-3.292935
C	7.838192	4.354270	-3.437111
C	-4.395241	1.452743	-4.225208

H	-5.335067	1.816130	-3.830684
C	2.955773	-0.615210	-6.101201
C	9.718538	3.322253	-4.528763
H	10.779226	3.299217	-4.742005
C	8.880975	2.353844	-5.069014
H	9.286023	1.575771	-5.702401
C	3.287401	-0.180466	-7.390953
H	3.302893	0.877381	-7.614713
C	3.588159	-1.079821	-8.398148
H	3.834317	-0.702035	-9.384304
C	3.575715	-2.458791	-8.175317
C	3.242670	-2.895503	-6.899385
H	3.215985	-3.957674	-6.685318
H	-3.205930	2.851343	-3.099522
H	-1.026094	0.171672	-5.620271
H	7.416960	5.123272	-2.804889
H	6.855018	1.631465	-5.211210
O	2.976401	4.829648	-0.663158
Sn	0.756905	5.643037	-3.364458
C	1.919018	7.480762	-3.019135
H	1.288294	8.363405	-3.167650
H	2.763628	7.550350	-3.712366
H	2.314863	7.515113	-1.999850
C	-0.966680	5.787988	-2.009791
H	-1.518716	6.715891	-2.190660
H	-1.656411	4.950204	-2.149521
H	-0.643187	5.785771	-0.964496
C	-0.042289	5.854904	-5.406598
H	0.761381	5.859413	-6.149640
H	-0.590771	6.798142	-5.498941
H	-0.725900	5.038062	-5.655702
C	2.115054	1.637143	-1.892293
O	2.005016	0.791172	-1.172757
H	2.310965	-0.236254	-4.084063
H	3.005840	2.099802	-5.887329
C	3.931749	-3.428470	-9.278491
H	5.015676	-3.479043	-9.426256
H	3.583616	-4.437167	-9.046680
H	3.485518	-3.129072	-10.230277

### X = OMe

Mo	2.339811	3.188609	-3.976695
C	2.518622	4.568474	-2.518987
N	-0.713254	2.141134	-4.349983
N	5.594554	3.581074	-4.047200
C	7.795845	2.887338	-4.727359
C	0.382808	2.587657	-4.217268
C	4.413667	3.472436	-4.022921



C	6.956984	3.745662	-3.993942
C	2.889310	1.536064	-5.299654
C	2.072243	-2.033558	-6.227233
H	1.334257	-2.180983	-5.434542
C	2.363111	0.282398	-5.390561
C	8.887667	4.932846	-3.154694
H	9.313322	5.728783	-2.542024
C	7.504955	4.772585	-3.203000
C	2.712220	-0.784047	-6.331422
C	9.727006	4.082435	-3.881887
H	10.809075	4.213668	-3.837156
C	9.176569	3.062120	-4.664341
H	9.827170	2.394525	-5.230776
C	3.662220	-0.636630	-7.369233
H	4.179027	0.316602	-7.491072
C	3.948236	-1.671928	-8.243083
H	4.678449	-1.548940	-9.044544
C	3.295480	-2.913949	-8.115670
C	2.350676	-3.091371	-7.094847
H	1.829871	-4.039273	-6.969617
H	6.838562	5.424619	-2.638936
H	7.352452	2.093977	-5.328844
O	2.757376	5.261018	-1.605679
Sn	0.835965	5.606140	-4.447273
C	1.909749	7.497605	-4.207886
H	1.288850	8.312267	-4.605132
H	2.856403	7.466573	-4.761088
H	2.117856	7.684510	-3.148020
C	-1.088942	5.856005	-3.457040
H	-1.563573	6.774612	-3.828007
H	-1.745454	5.002964	-3.666294
H	-0.941656	5.941916	-2.373429
C	0.478181	5.381668	-6.608111
H	1.422789	5.252520	-7.149854
H	-0.015372	6.296309	-6.965954
H	-0.169116	4.516950	-6.794372
C	2.166446	2.108798	-2.376438
O	2.031217	1.444224	-1.427314
H	1.577020	-0.008216	-4.681064
H	3.722089	1.730222	-5.999173
O	3.649952	-3.867827	-9.028393
C	3.023622	-5.158640	-8.938645
H	1.929423	-5.045361	-9.039241
H	3.231812	-5.600323	-7.947774
C	3.586394	-6.022348	-10.050325
H	4.673998	-6.134757	-9.945439
H	3.375091	-5.580315	-11.033652
H	3.129583	-7.020971	-10.014578
C	-1.974611	1.619053	-4.483528
C	-2.409501	1.143057	-5.734933
C	-2.831457	1.559021	-3.368201

C	-3.692568	0.614969	-5.860319
C	-4.110730	1.026826	-3.513665
C	-4.547634	0.554028	-4.755291
H	-1.732181	1.191067	-6.587481
H	-2.478926	1.927529	-2.405418
H	-4.025767	0.245990	-6.831172
H	-4.771697	0.981251	-2.646895
H	-5.549932	0.138056	-4.860676

**X = NMe<sub>2</sub>**

Mo	2.462755	2.797822	-3.577420
C	2.583926	4.119410	-2.069964
N	-0.679759	1.971167	-3.792845
N	5.653145	3.538301	-3.695653
C	-4.274355	1.561458	-4.433894
H	-5.079070	2.070298	-4.966124
C	-1.947987	1.449640	-3.771282
C	7.918210	3.241664	-4.453334
C	0.469305	2.290098	-3.728470
C	4.496949	3.270589	-3.650775
C	6.969819	3.925833	-3.671444
C	-2.207890	0.259861	-3.062550
C	3.142573	1.113522	-4.754938
C	-2.989984	2.100885	-4.458088
C	-4.534674	0.379166	-3.733912
H	-5.542152	-0.038210	-3.719586
C	1.626836	-1.485416	-7.047961
H	0.601080	-1.362767	-6.691360
C	2.312357	0.232949	-5.393537
C	8.702131	5.398416	-2.848323
H	9.006778	6.239334	-2.223742
C	7.365073	5.008546	-2.863595
C	-3.497907	-0.265145	-3.050502
H	-3.694196	-1.187613	-2.502522
C	2.645887	-0.707351	-6.457581
C	9.648577	4.722583	-3.625329
H	10.693428	5.034501	-3.608078
C	9.251267	3.645294	-4.423576
H	9.985643	3.112943	-5.029406
C	3.952995	-0.906457	-6.954417
H	4.778525	-0.331019	-6.532331
C	4.227386	-1.816444	-7.961705
H	5.256373	-1.931389	-8.298455
C	3.193717	-2.591288	-8.554125
C	1.878510	-2.401908	-8.059636
H	1.048876	-2.977016	-8.467314
H	-1.392607	-0.230871	-2.531660
H	-2.776645	3.022116	-4.999319
H	6.617668	5.524519	-2.261630

H	7.595225	2.403130	-5.070115
O	2.804802	4.783704	-1.130919
Sn	1.114480	5.309244	-4.077299
C	2.344859	7.116358	-3.951911
H	1.760920	7.978465	-4.302804
H	3.239252	7.012274	-4.578589
H	2.650835	7.289535	-2.913259
C	-0.718405	5.755206	-2.983861
H	-1.236614	6.593506	-3.468978
H	-1.382616	4.882532	-2.963717
H	-0.470836	6.035933	-1.952858
C	0.591713	5.079770	-6.205764
H	1.496647	4.937229	-6.808287
H	0.082884	5.997625	-6.533122
H	-0.073463	4.219527	-6.345192
C	2.361194	1.572109	-2.066409
O	2.269420	0.824480	-1.178690
H	1.249358	0.223535	-5.122793
H	4.208748	1.014145	-5.007140
N	3.460648	-3.485869	-9.570364
C	4.829851	-3.718909	-9.996946
H	5.459735	-4.119109	-9.181501
H	4.831369	-4.446198	-10.816260
H	5.301345	-2.793365	-10.367565
C	2.396829	-4.315559	-10.108275
H	2.797151	-4.929673	-10.922708
H	1.967133	-4.991282	-9.346448
H	1.577070	-3.703531	-10.519594

**X = NO<sub>2</sub>, SnBu<sub>3</sub>**

Mo	1.910710	3.744492	-3.137779
C	2.040321	5.069578	-1.638814
N	-1.240208	3.316055	-3.891847
N	5.131748	3.397237	-2.713352
C	-4.057736	1.406593	-5.270648
H	-4.231159	0.507051	-5.862773
C	-2.526389	2.939045	-4.196608
C	7.043373	2.007206	-3.160950
C	-0.102114	3.545676	-3.635158
C	3.968196	3.564969	-2.866642
C	6.470590	3.134673	-2.544709
C	-3.611296	3.708995	-3.739991
C	2.239817	1.821853	-4.164185
C	-2.751628	1.781034	-4.964073
C	-5.139863	2.169786	-4.820431
H	-6.159370	1.868542	-5.063089
C	3.417609	-1.755445	-4.047851
H	3.656241	-1.752034	-2.982060
C	2.765958	0.625232	-3.805068
C	8.612412	3.714282	-1.586503

H	9.222859	4.377858	-0.972251
C	7.257460	3.991767	-1.754631
C	-4.910984	3.317267	-4.054849
H	-5.751328	3.914121	-3.698303
C	2.926530	-0.566932	-4.638726
C	9.187726	2.594208	-2.195235
H	10.248465	2.381555	-2.056659
C	8.399698	1.745607	-2.979657
H	8.843362	0.868893	-3.453173
C	2.624460	-0.606652	-6.021203
H	2.251999	0.291878	-6.515760
C	2.796510	-1.761503	-6.768714
H	2.566833	-1.793111	-7.832753
C	3.282134	-2.917146	-6.143800
C	3.595167	-2.920966	-4.781970
H	3.970114	-3.835450	-4.324986
H	-3.420473	4.598443	-3.139598
H	-1.900531	1.190563	-5.301787
H	6.794543	4.857813	-1.282069
H	6.414869	1.352842	-3.764982
O	2.200044	5.663373	-0.640160
Sn	1.402396	6.385784	-3.913048
C	2.657529	8.078144	-3.272110
H	3.702352	7.751447	-3.387314
H	2.475834	8.186375	-2.191991
C	-0.605404	7.105359	-4.479933
H	-1.304881	6.279625	-4.287751
H	-0.850112	7.913497	-3.773056
C	2.384640	5.248421	-5.578171
H	2.572313	4.176378	-5.325098
H	1.623572	5.206378	-6.371680
C	1.391677	2.608987	-1.625649
O	1.058155	1.925889	-0.748602
H	3.110919	0.486042	-2.773050
H	1.876877	1.878623	-5.208155
N	3.468051	-4.139368	-6.932185
O	3.905880	-5.143633	-6.351764
O	3.177340	-4.102577	-8.137070
C	3.703615	5.858906	-6.065594
H	4.430669	5.890882	-5.236659
H	3.543130	6.908668	-6.365625
C	4.324267	5.094290	-7.245824
H	4.502649	4.048714	-6.943289
H	3.592859	5.052145	-8.071213
C	5.630196	5.718892	-7.746020
H	6.047993	5.150800	-8.589400
H	5.471705	6.753406	-8.086323
H	6.390777	5.743896	-6.950380
C	2.401020	9.395091	-4.009040
H	2.604805	9.276738	-5.088013
H	1.334998	9.672926	-3.932786

C	3.250431	10.558592	-3.472839
H	3.045099	10.684030	-2.395894
H	4.317994	10.288966	-3.549464
C	2.995908	11.878299	-4.205328
H	3.612851	12.690914	-3.795896
H	3.228850	11.791356	-5.277791
H	1.941897	12.184365	-4.118882
C	-0.720343	7.591852	-5.928736
H	0.007063	8.398541	-6.122999
H	-0.460433	6.776243	-6.625500
C	-2.127961	8.103078	-6.276908
H	-2.858284	7.299127	-6.084267
H	-2.390634	8.924924	-5.589051
C	-2.252019	8.580245	-7.726332
H	-3.266953	8.941069	-7.947021
H	-1.552331	9.404144	-7.934440
H	-2.027461	7.767137	-8.433678

## 2.7 Crystallographic Structure Determinations

Single-crystal X-ray structure determinations were carried out at low temperature on Bruker Kappa Diffractometers equipped with a Mo radiation source and a Bruker APEX II detector. Structures were solved by direct methods using SHELXS.<sup>51</sup> All structures were refined by full matrix least-squares procedures utilizing SHELXL<sup>51</sup> within Olex2 small-molecule solution, refinement, and analysis software package.<sup>52</sup> Crystallographic data-collection and refinement data are listed in Table S6.1. Rotation of one *m*-terphenyl isopropyl group resulted in two-site positional disorder of the methyl groups which refined anisotropically with equivalent ADPs. All H-atoms were refined using standard HFIX instructions.

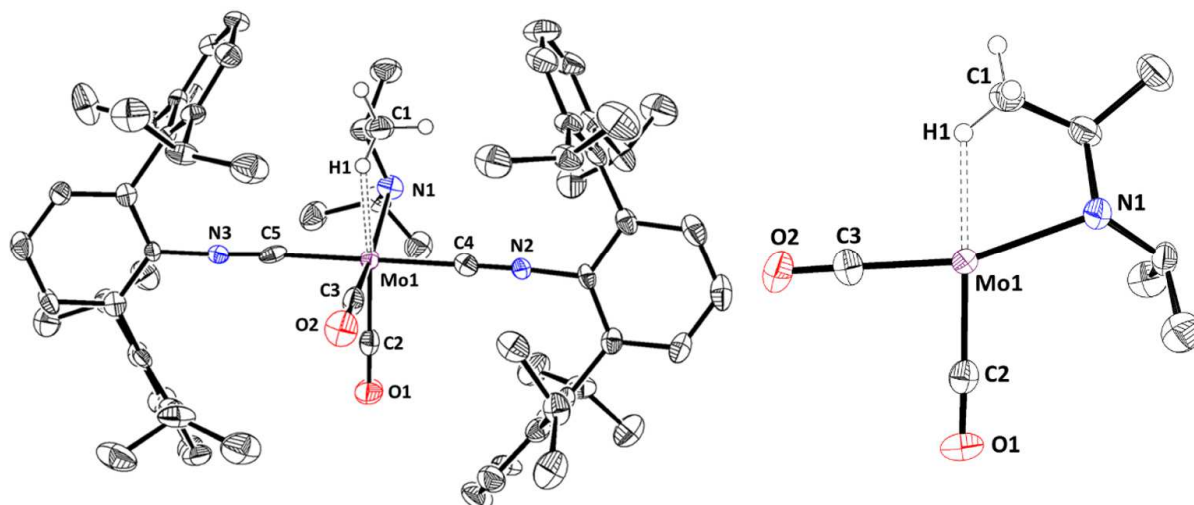


**Figure 2.14.**  $\text{Mo}((\eta^2\text{-}H,C\text{-}(H_3CCH(CH_3))\text{-}\eta^1\text{-}N\text{-}N(H)(i\text{-}Pr))(\text{CO})_2(\text{CNAr}^{\text{Dipp}2})_2$  (**3**). Selected bond lengths (Å) and angles (deg.): Mo1-H1 = 2.1234(5), Mo1-C1 = 2.807(7), Mo1-N1 = 2.326(5), Mo1-C2 = 1.918(6), Mo1-C3 = 1.928(6), Mo1-C4 = Mo1-C5 = 2.061(6), C2-O1 = C3-O2 = 1.163(8), C4-N2 = 1.183(7), C5-N3 = 1.162(7), H1-Mo-N1 = 70.7(16), N1-Mo1-C2 = 110.8(2), C2-Mo1-C3 = 86.5(3), N1-Mo1-C3 = 162.6(2), H1-Mo1-C2 = 175.9(16), H1-Mo1-C3 = 92.2(16), C4-Mo1-C5 = 173.2(2). The methyl protons of C1 were refined using HFIX 137.

**Table 2.3.** Crystallographic data collection and refinement information.

Mo( $\eta^2$ - <i>H,C</i> -(H <sub>3</sub> CCH(CH <sub>3</sub> ))- $\kappa^1$ - <i>N-N</i> (H)( <i>i</i> -Pr))(CO) <sub>2</sub> - (CNAI <sup>Dipp2</sup> ) <sub>2</sub> ( <b>3</b> )	
Formula	C <sub>70</sub> H <sub>89</sub> MoN <sub>3</sub> O <sub>2</sub>
Crystal System	Orthorhombic
Space Group	<i>Pna2</i> <sub>1</sub>
<i>a</i> , Å	31.7613(8)
<i>b</i> , Å	12.9281(4)
<i>c</i> , Å	15.4134(4)
$\alpha$ , deg	90
$\beta$ , deg	90
$\gamma$ , deg	90
<i>V</i> , Å <sup>3</sup>	6328.9(3)
<i>Z</i>	4
Radiation ( $\lambda$ , Å)	Mo-K $\alpha$ , 0.71073
$\rho$ (calcd.), g/cm <sup>3</sup>	1.115
Temp, K	100
$\theta$ max, deg	25.681
data/parameters	12071/708
R <sub>1</sub>	4.03
wR <sub>2</sub>	0.0985
Goof	1.012

## 2.8 $^1\text{H}$ and $^{13}\text{C}$ -NMR Spectra of Isolated Vinylstannanes

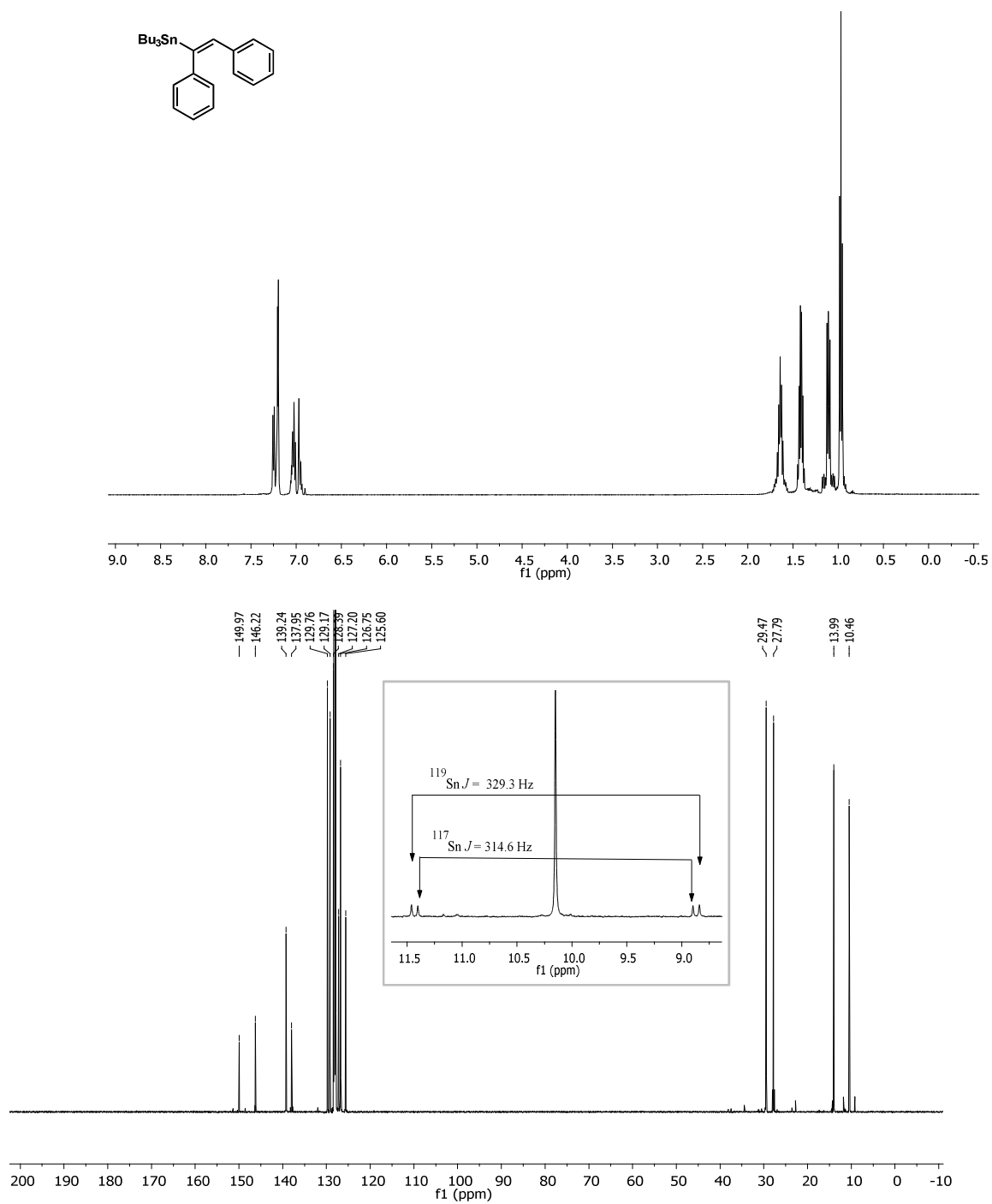


**Figure 2.15.**  $^1\text{H}$  and  $^{13}\text{C}$  NMR of (E)-tributyl(1,2-diphenylvinyl)stannane.



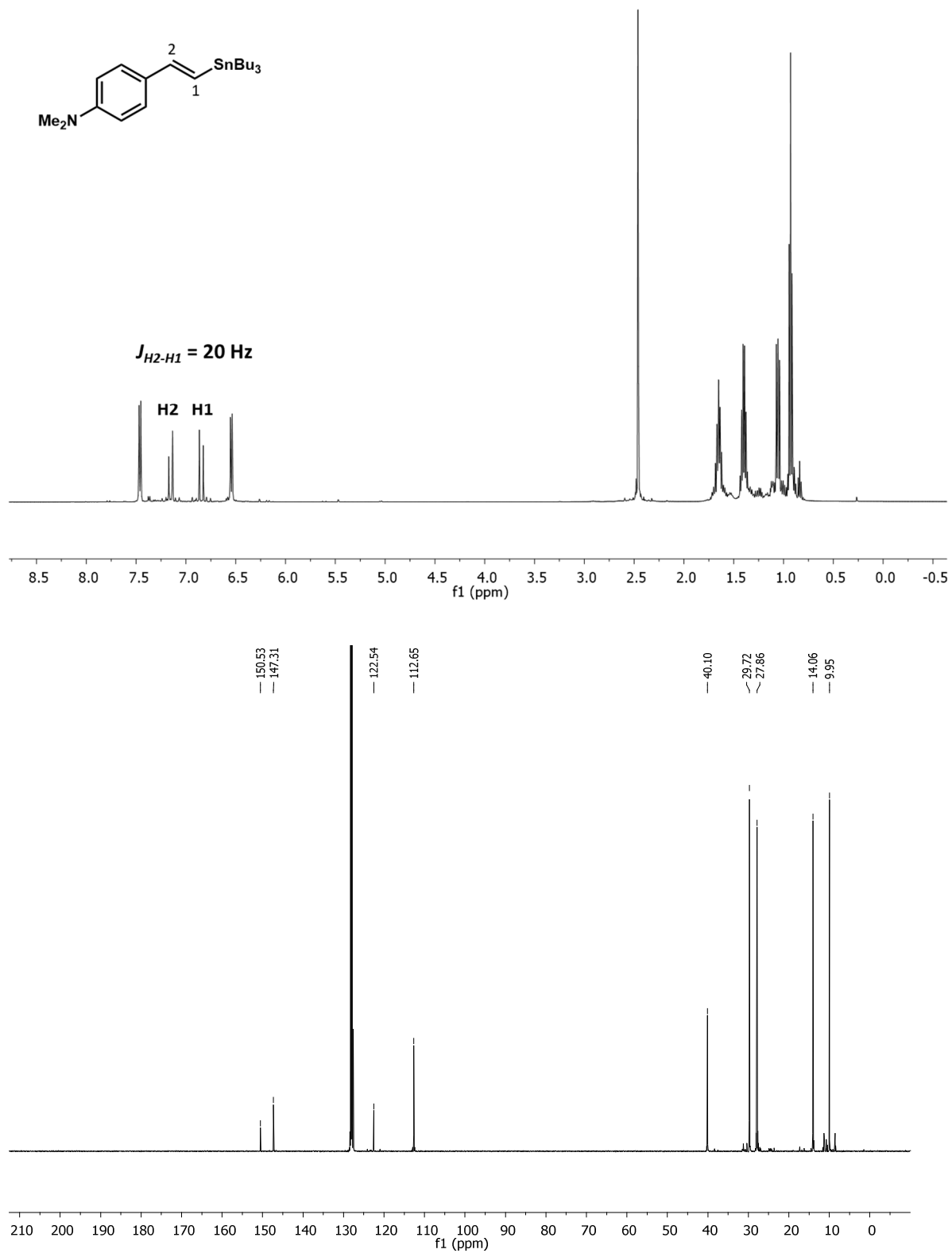


**Figure 2.16.** <sup>1</sup>H and <sup>13</sup>C NMR of (*E*)-*N,N*-dimethyl-4-(2-(tributylstannyl)vinyl)aniline.

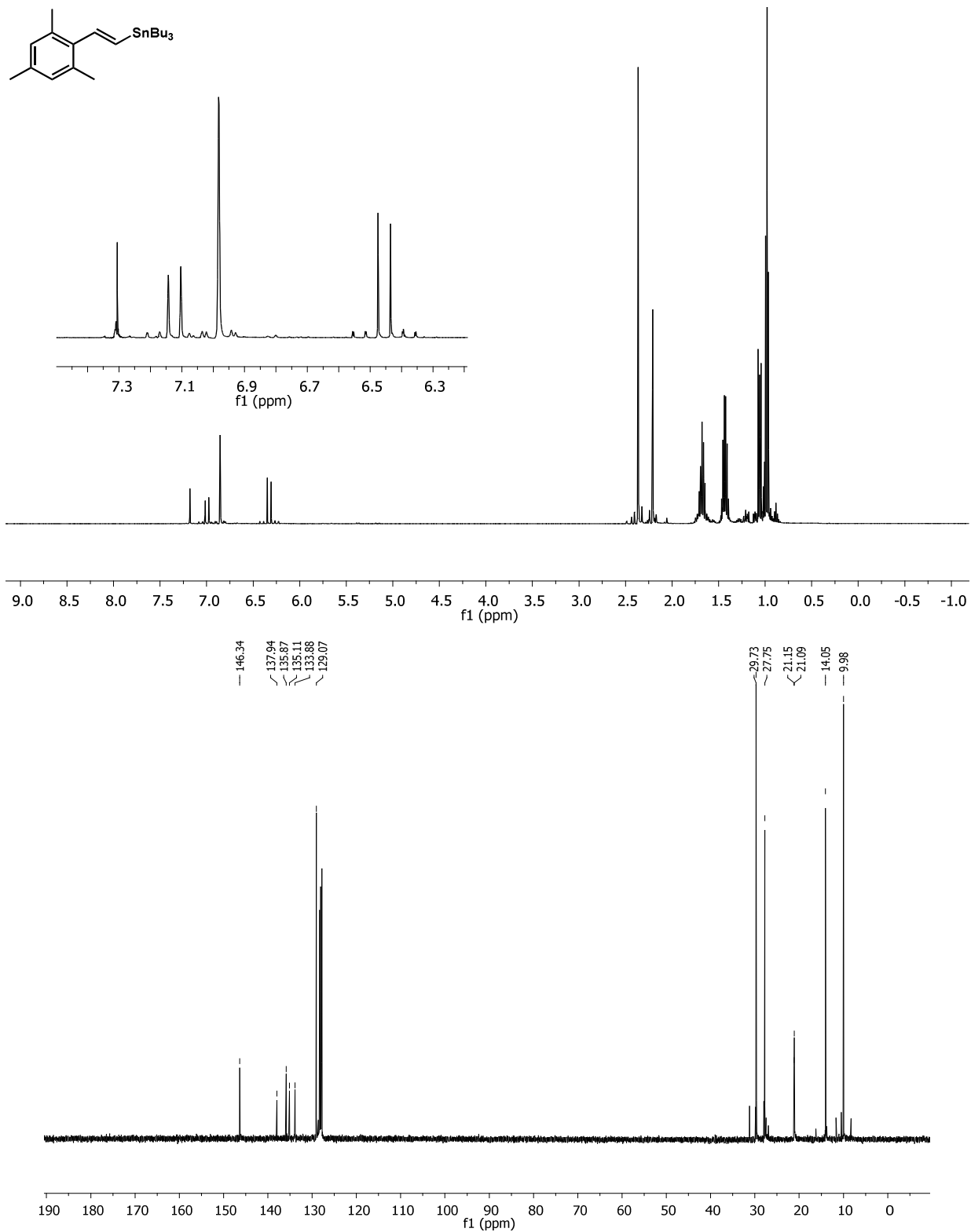


**Figure 2.17.**  $^1\text{H}$  and  $^{13}\text{C}$  NMR of (E)-tributyl(1,3,5-trimethylphenyl)vinylstannane.

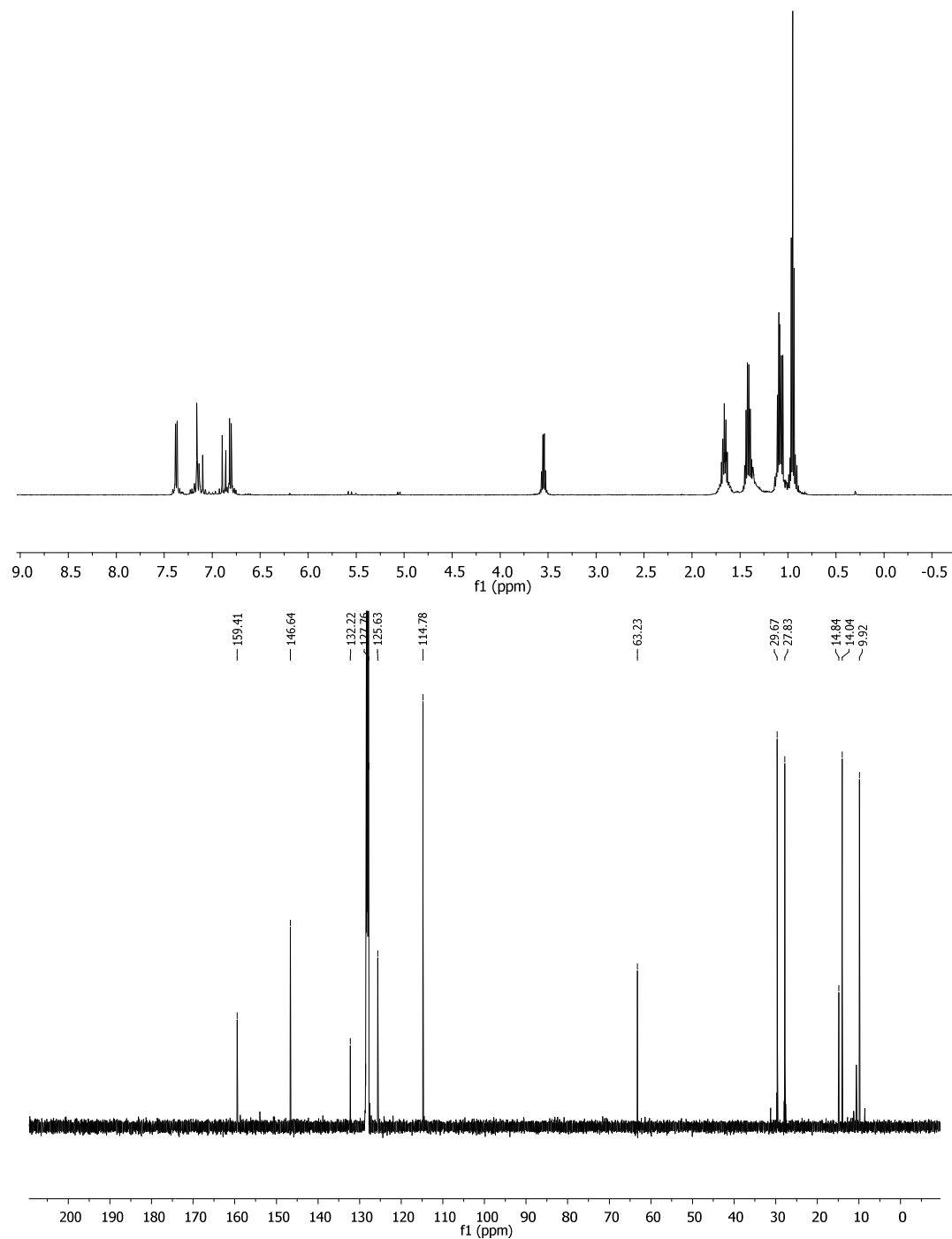
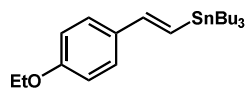


**Figure 2.18.** <sup>1</sup>H and <sup>13</sup>C NMR of (*E*)-tributyl(4-ethoxystyryl)stannane

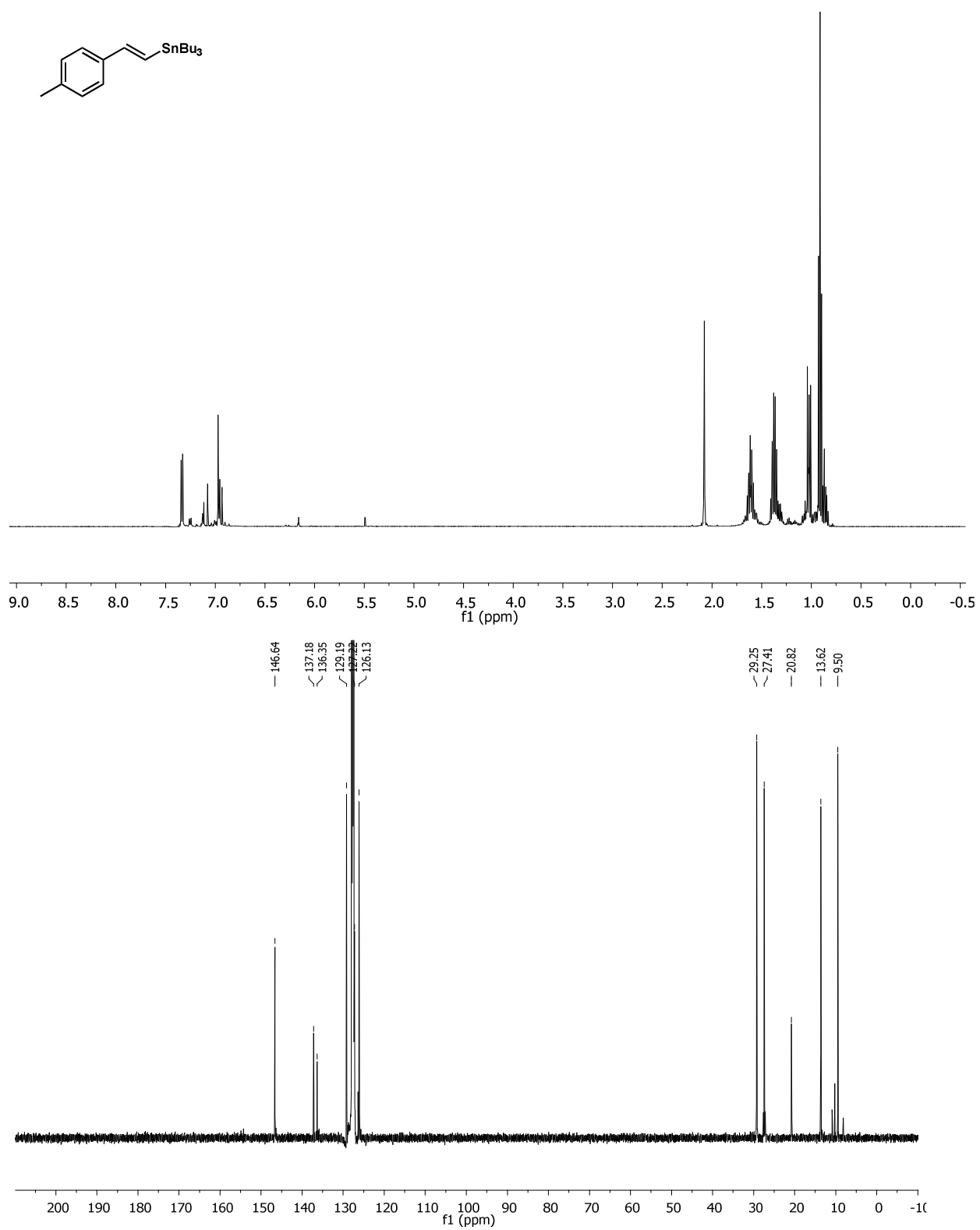


**Figure 2.19.** <sup>1</sup>H and <sup>13</sup>C NMR of (*E*)-tributyl(4-methylstyryl)stannane.

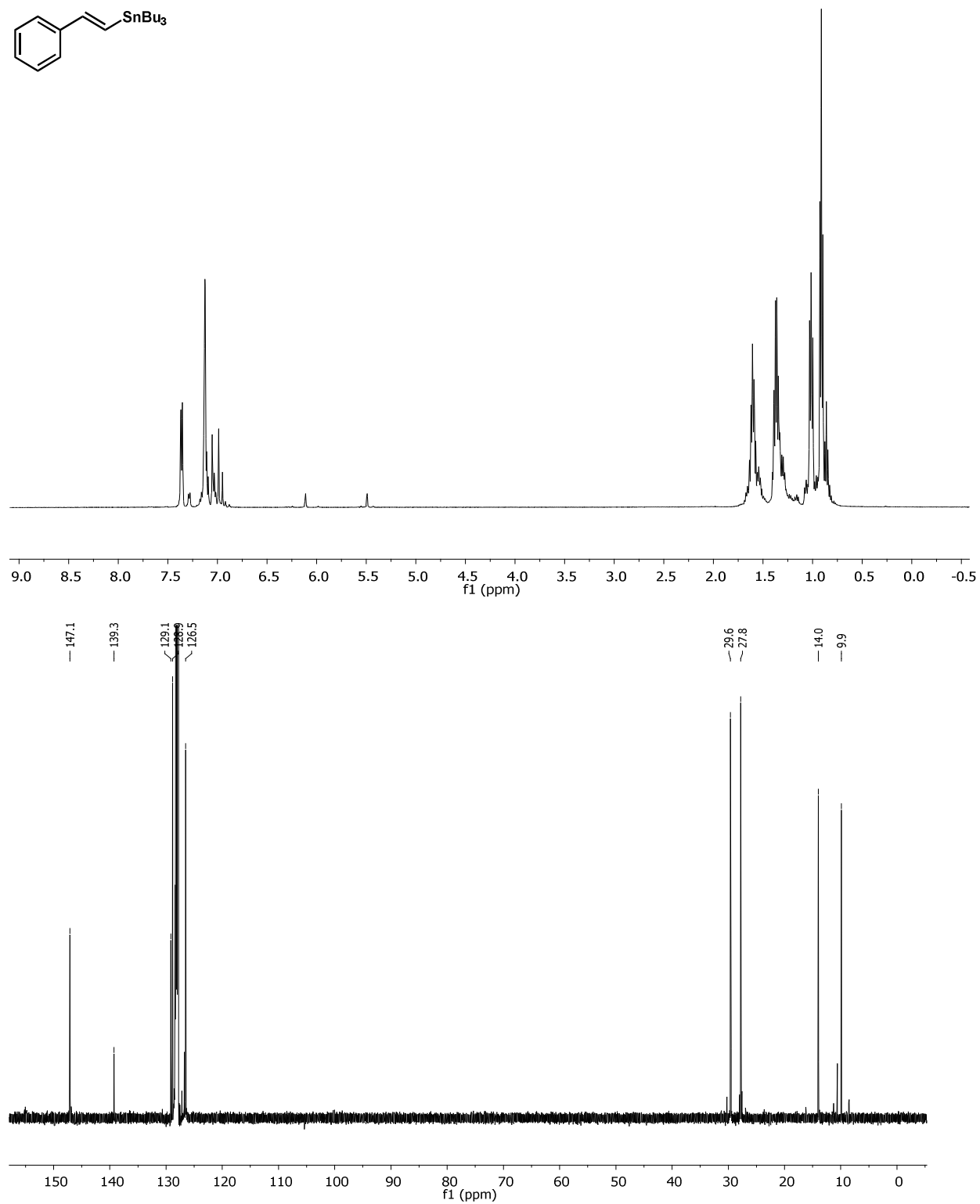
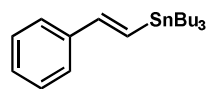


**Figure 2.20.** <sup>1</sup>H and <sup>13</sup>C NMR of (*E*)-tributyl(styryl)stannane.

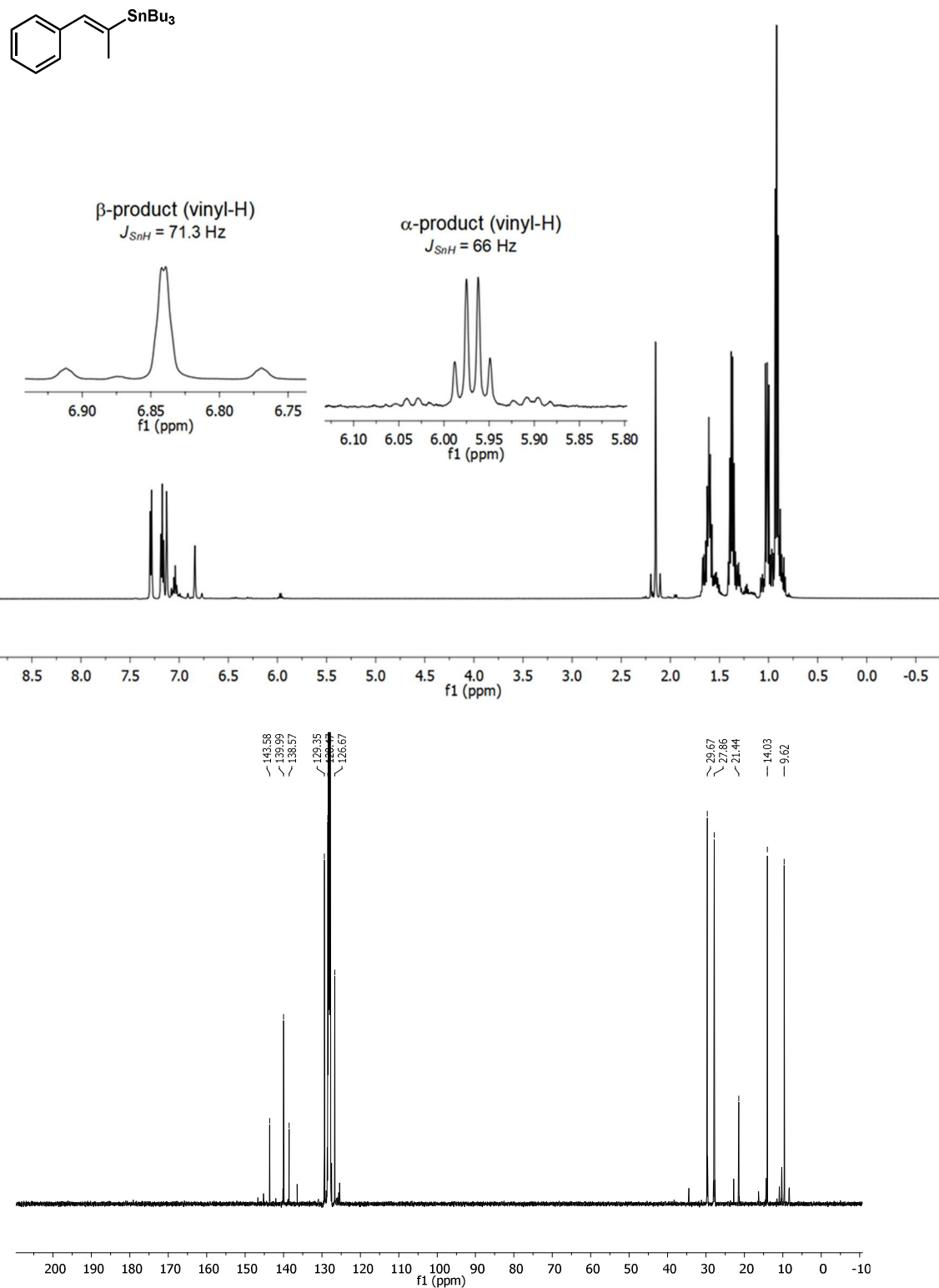


**Figure 2.21.**  $^1\text{H}$  and  $^{13}\text{C}$  NMR of (*E*)-tributyl(1-phenylprop-1-en-2-yl)stannane

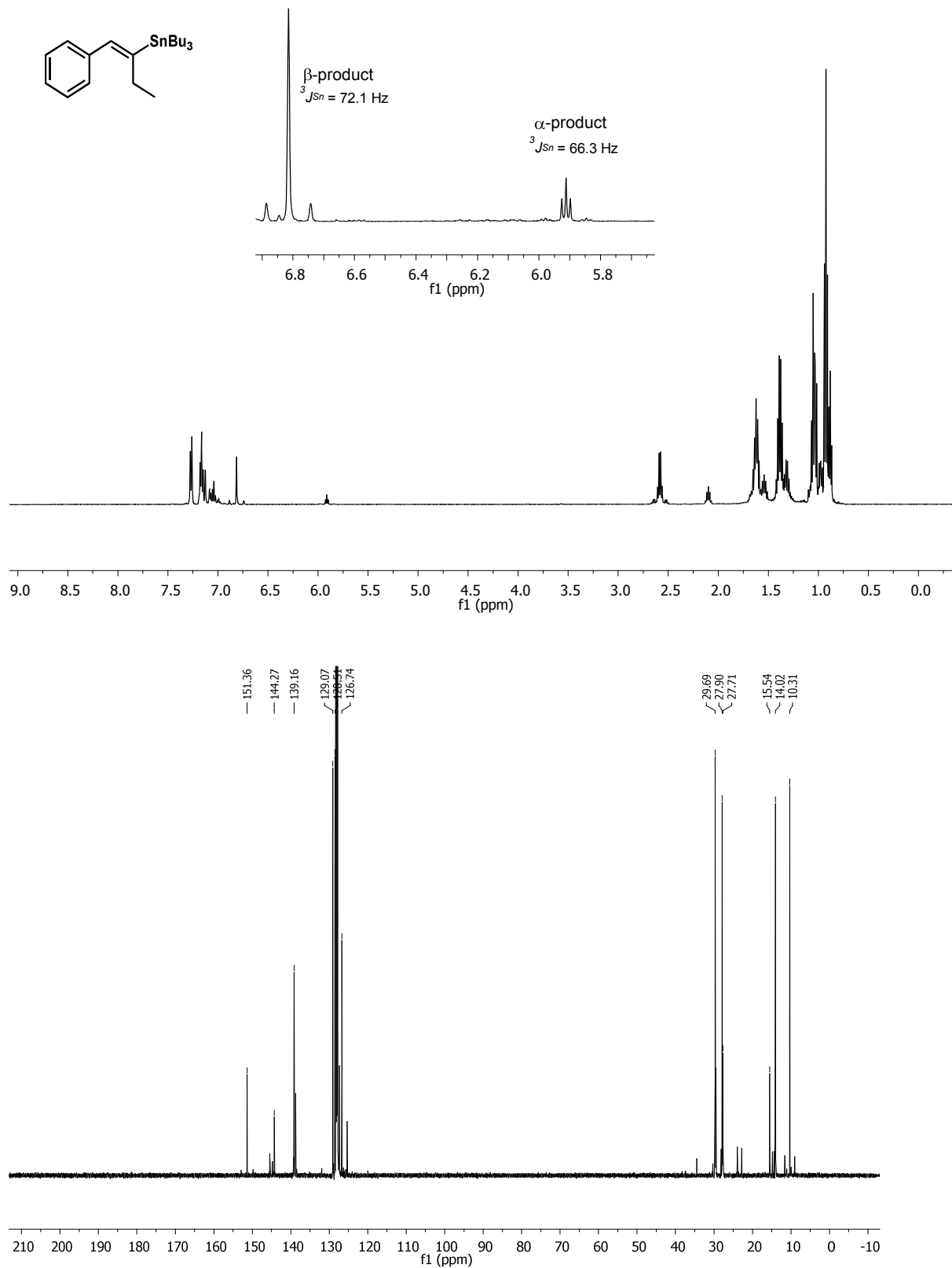


**Figure 2.22.**  $^1\text{H}$  and  $^{13}\text{C}$  NMR of (*E*)-tributyl(1-phenylbut-1-en-2-yl)stannane.

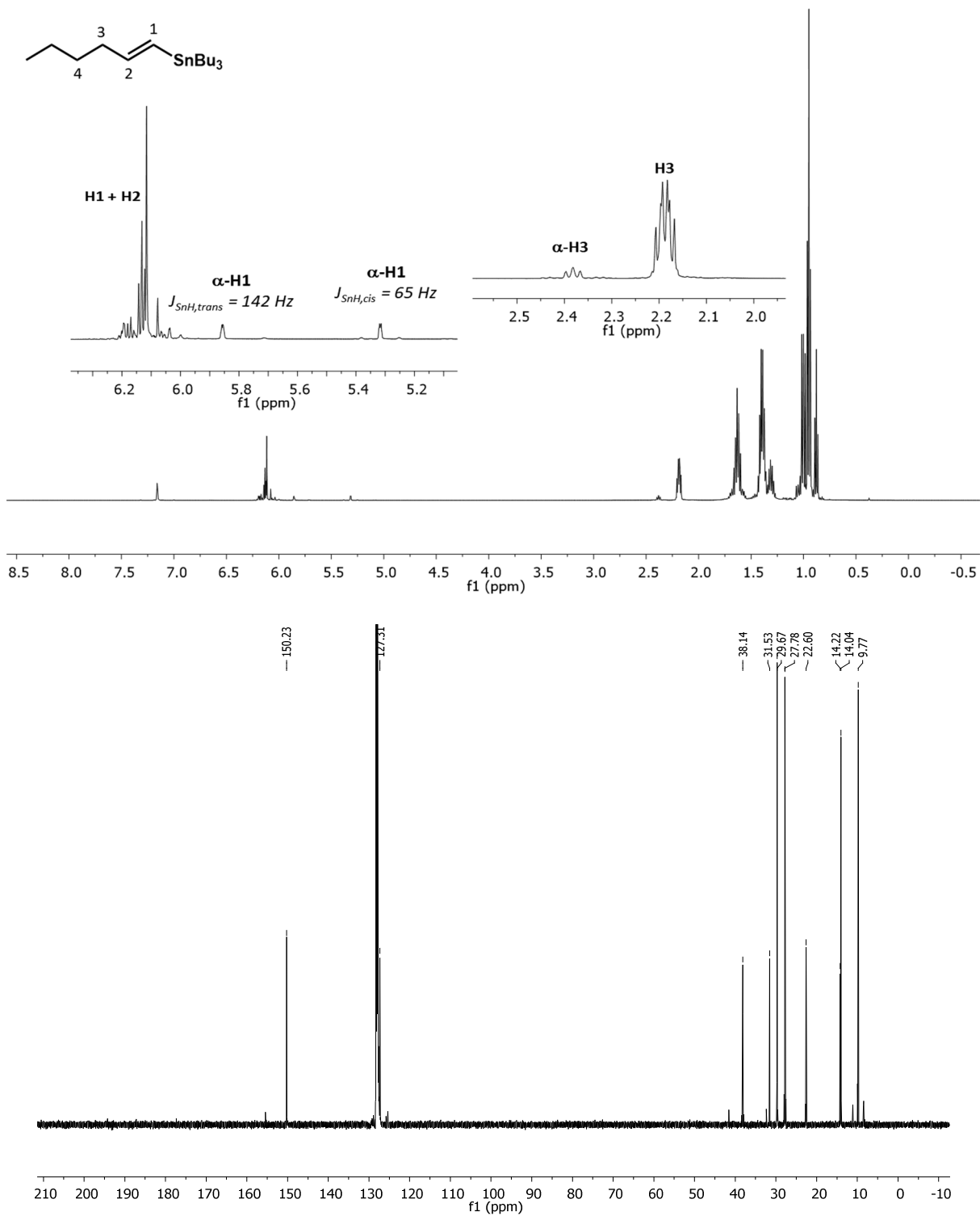
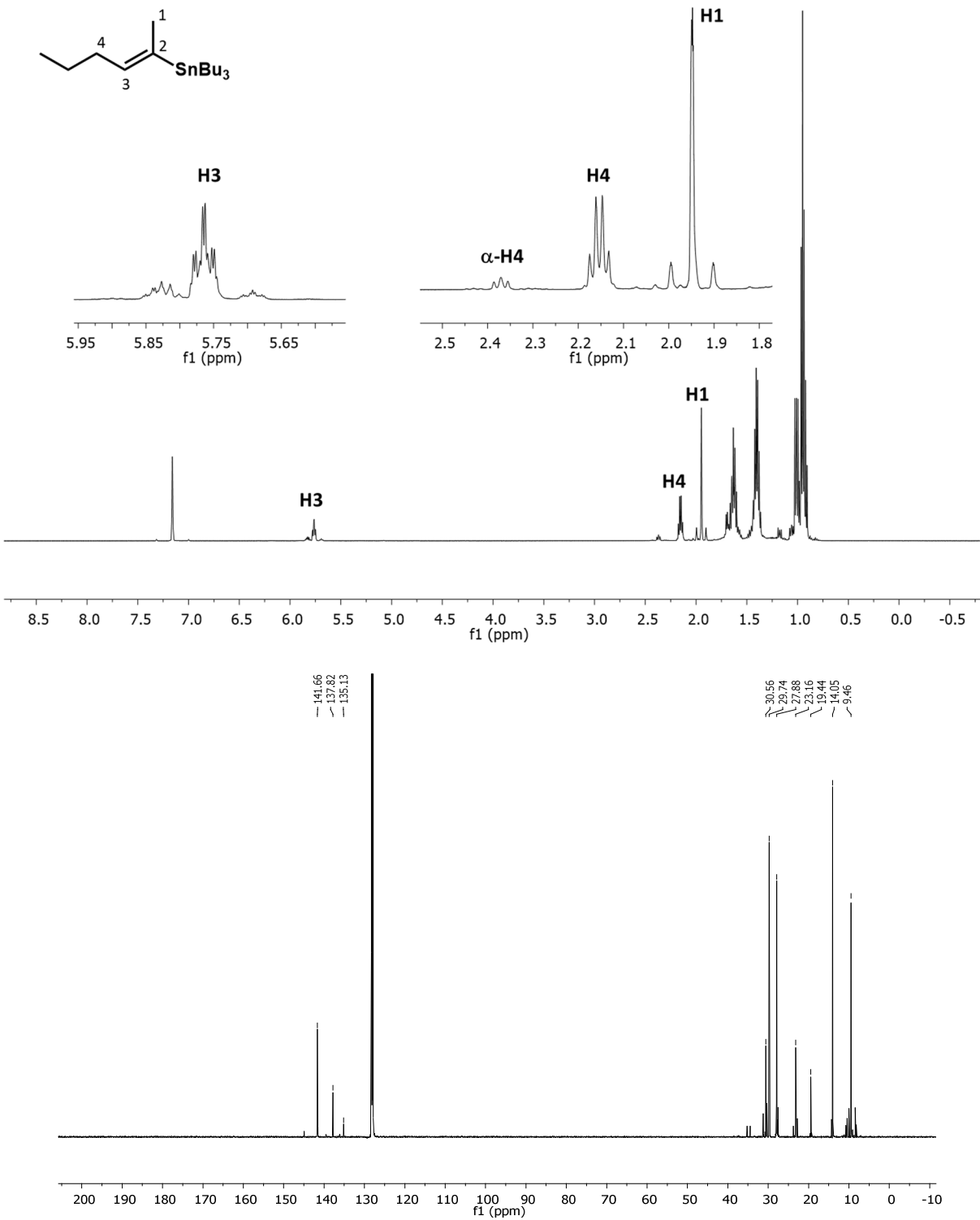
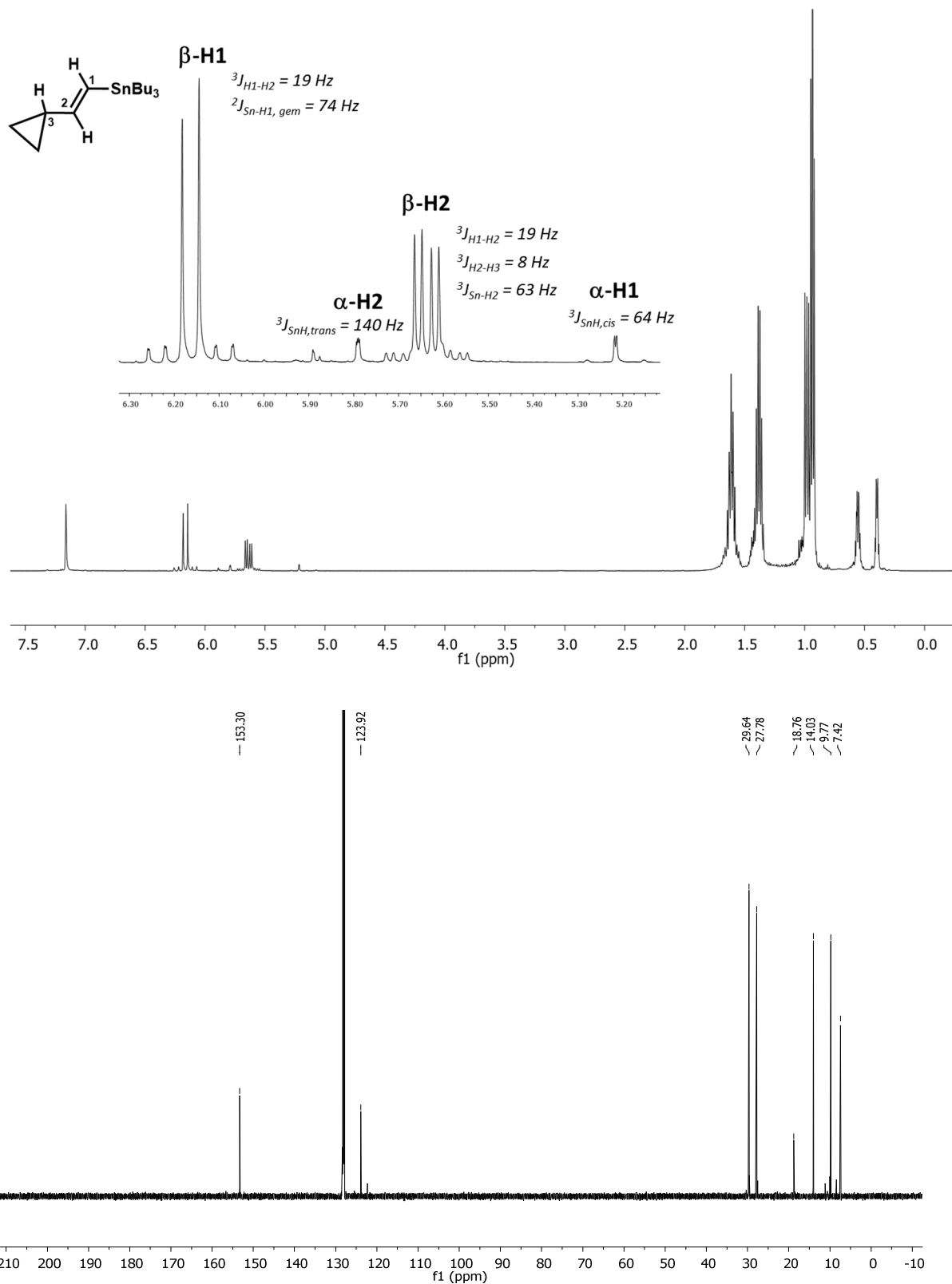


Figure 2.23.  $^1\text{H}$  and  $^{13}\text{C}$  NMR *(E)*-tributyl(hex-1-en-1-yl)stannane.





**Figure 2.24.**  $^1\text{H}$  and  $^{13}\text{C}$  NMR of (*E*)-tributyl(hex-2-en-2-yl)stannane.



**Figure 2.25.** <sup>1</sup>H and <sup>13</sup>C NMR of (*E*)-tributyl(2-cyclopropylvinyl)stannane.

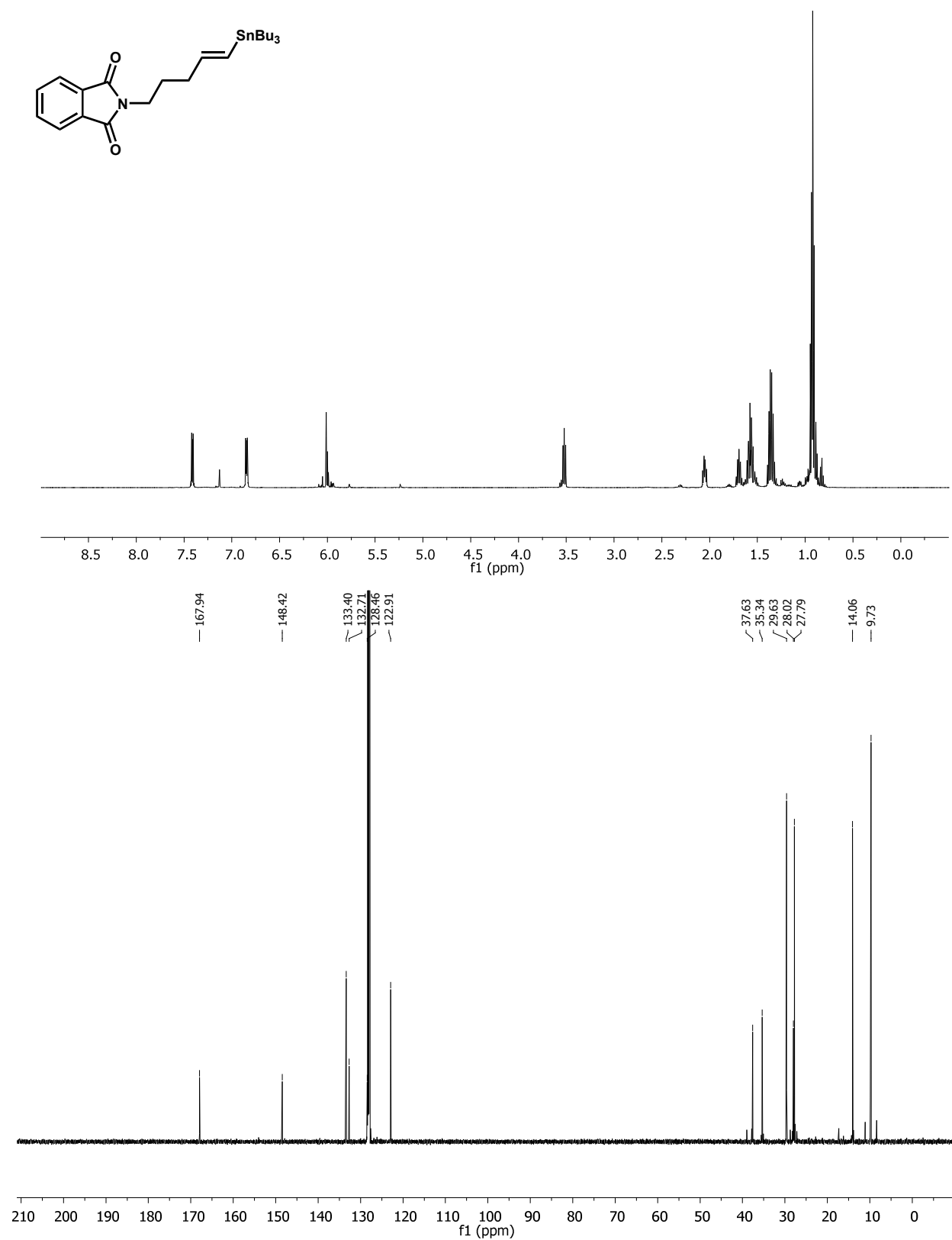


**Figure 2.26.** <sup>1</sup>H and <sup>13</sup>C NMR of *N*-(*E*)-(5-(tributylstannyl)pent-4-en-1-yl)phthalimide.

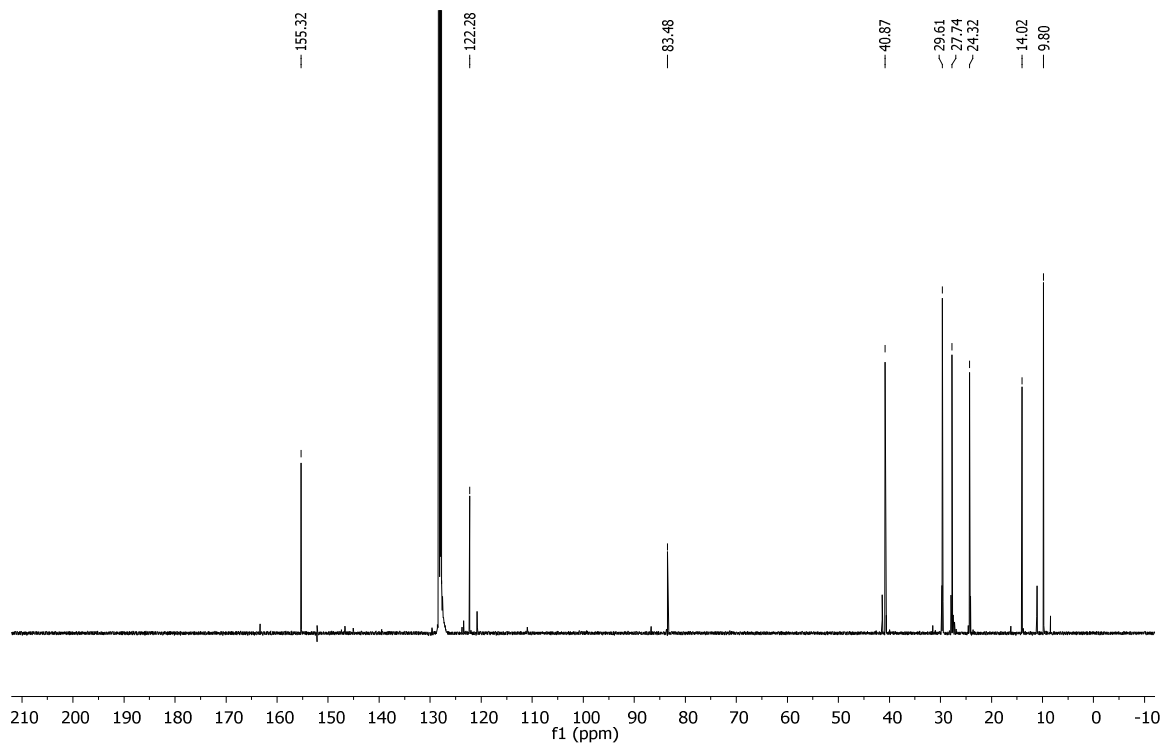
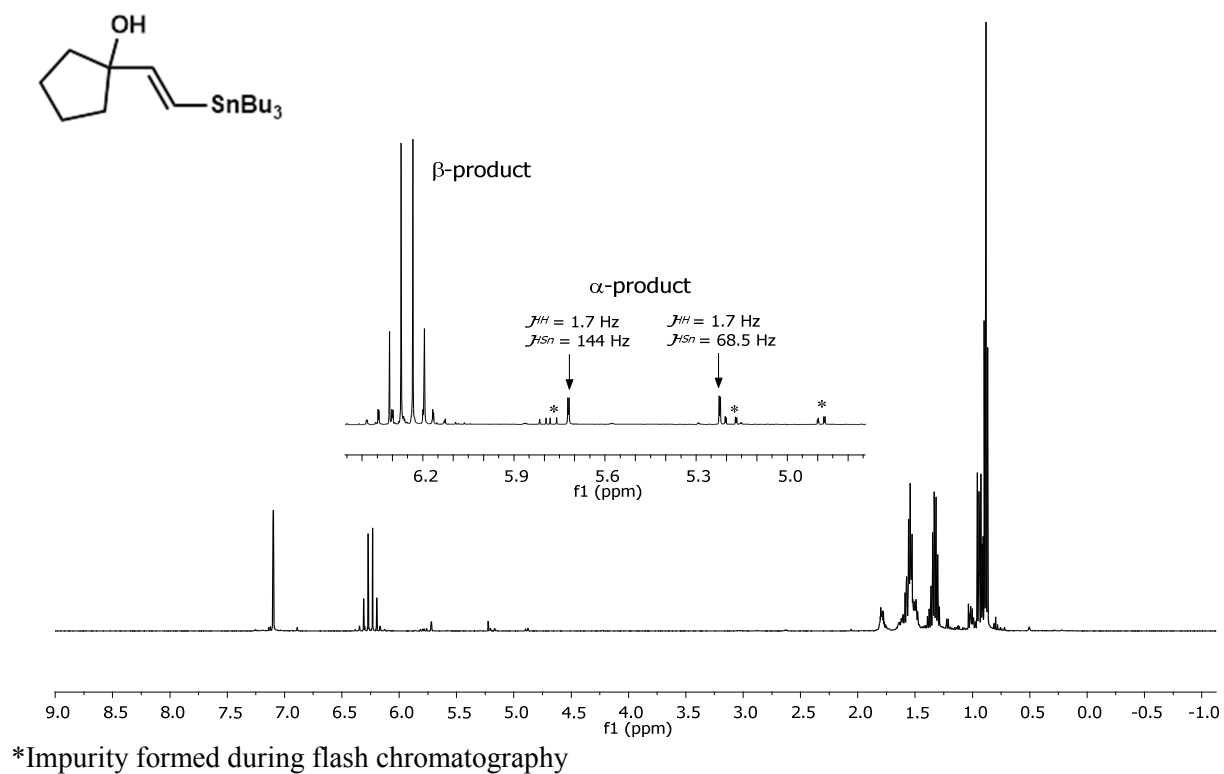


**Figure 2.27.**  $^1\text{H}$  and  $^{13}\text{C}$  NMR of (*E*)-1-(2-(tributylstannyl)vinyl)cyclopentan-1-ol.

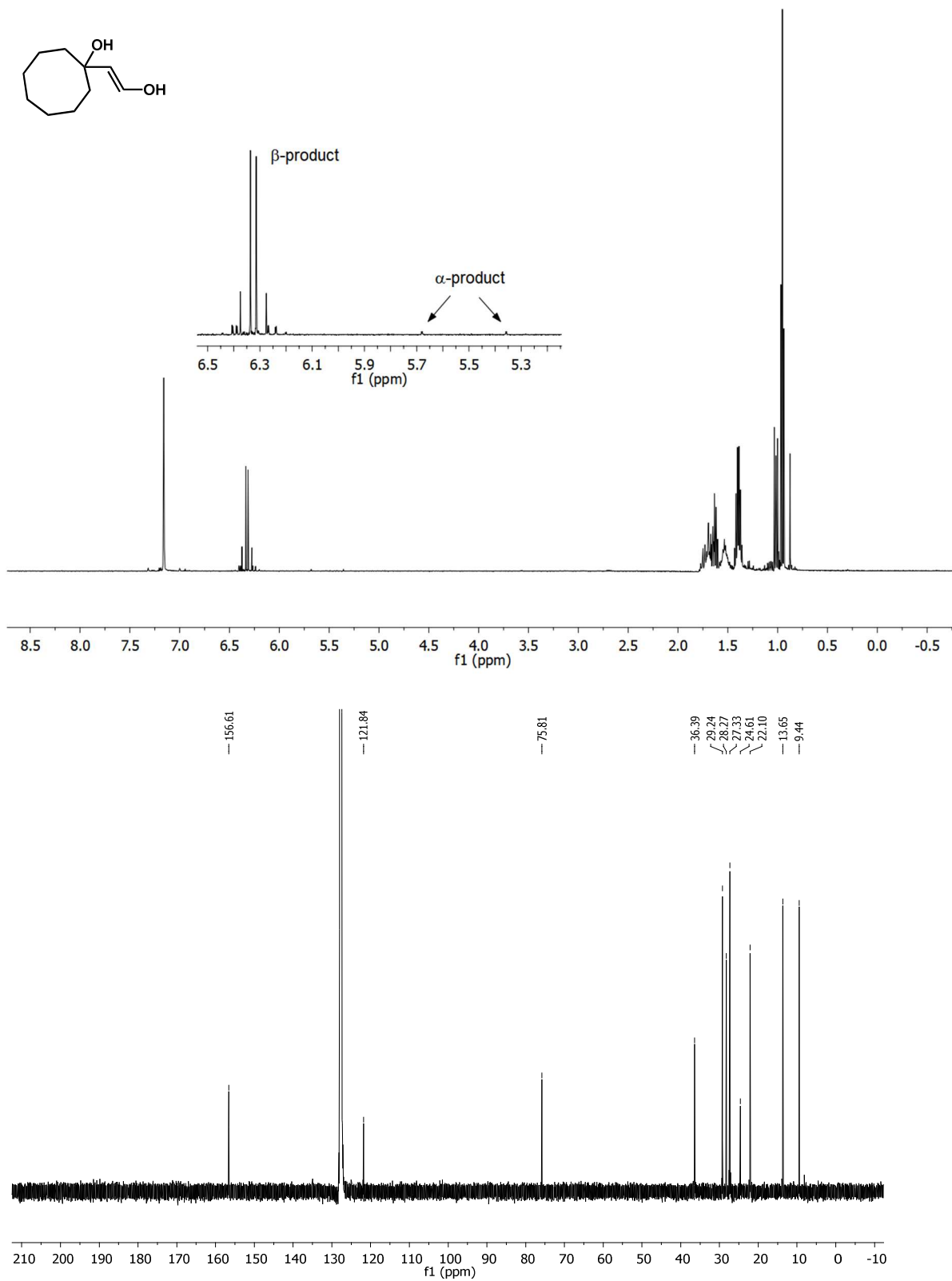


**Figure 2.28.** <sup>1</sup>H and <sup>13</sup>C NMR of *(E)*-1-(2-(tributylstannyl)vinyl)cyclooctan-1-ol.

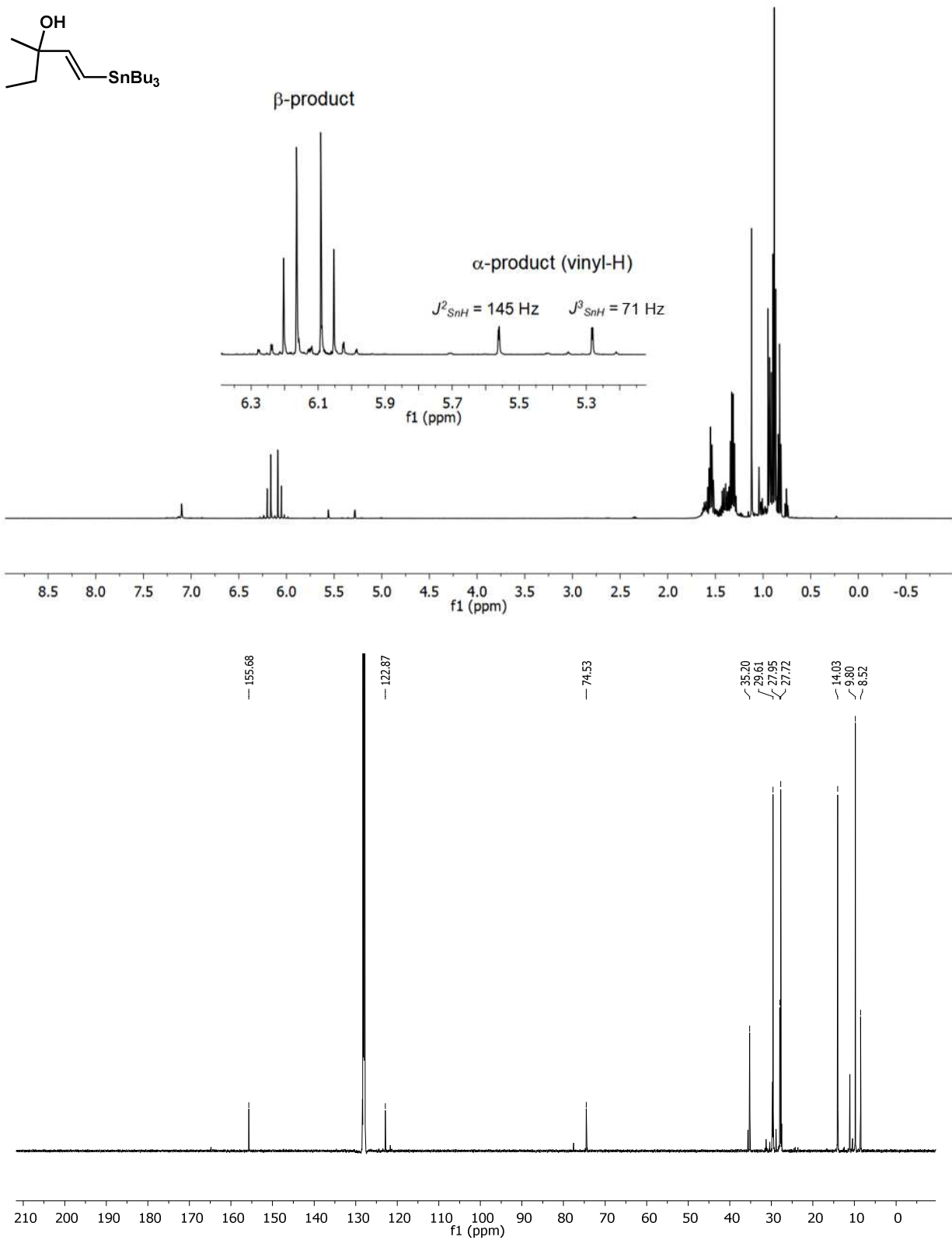


**Figure 2.29.**  $^1\text{H}$  and  $^{13}\text{C}$  NMR of (*E*)-3-methyl-1-(tributylstannyl)pent-1-en-3-ol.

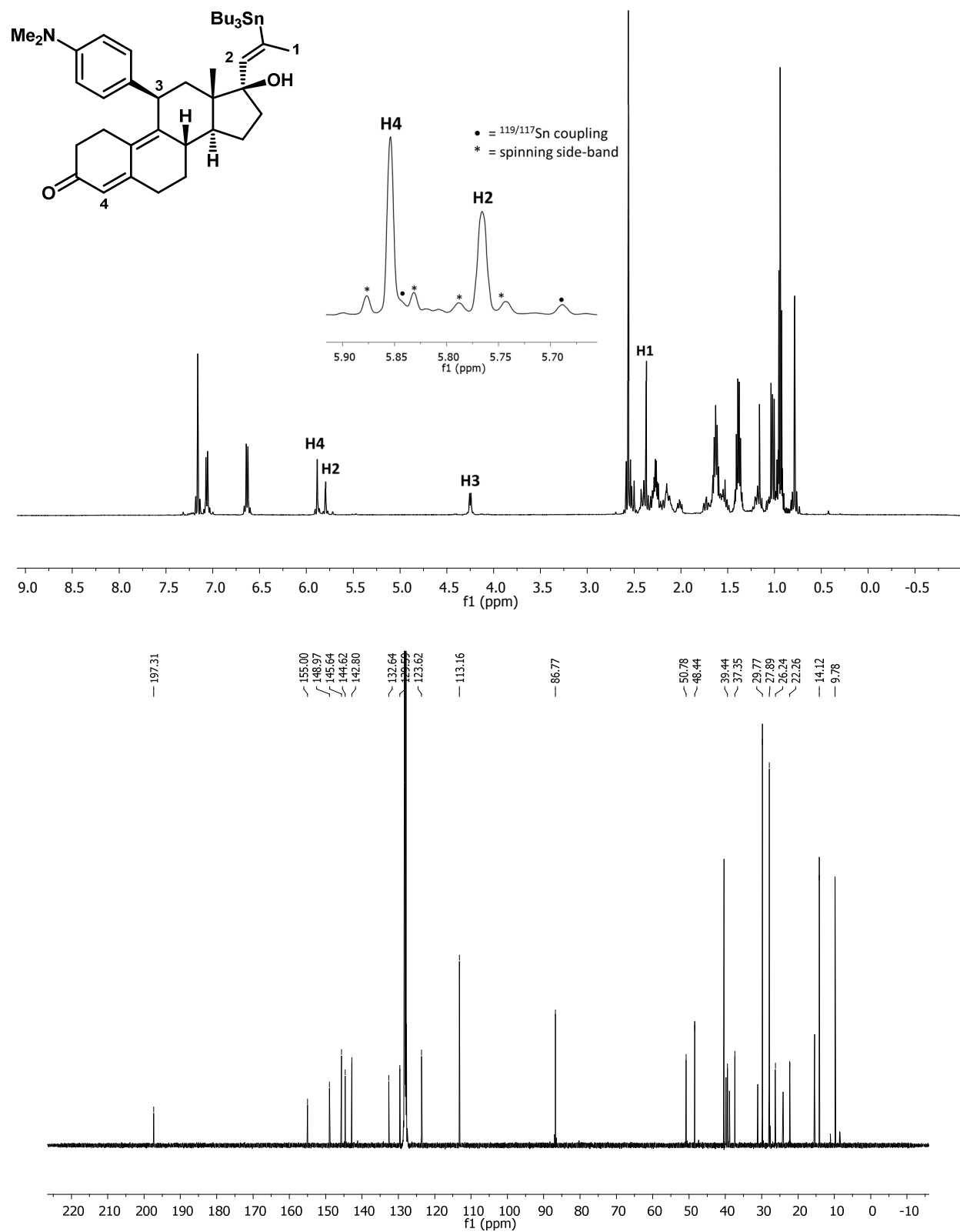


**Figure 2.30.**  $^1\text{H}$  and  $^{13}\text{C}$  NMR of mifepristone hydrostannation.

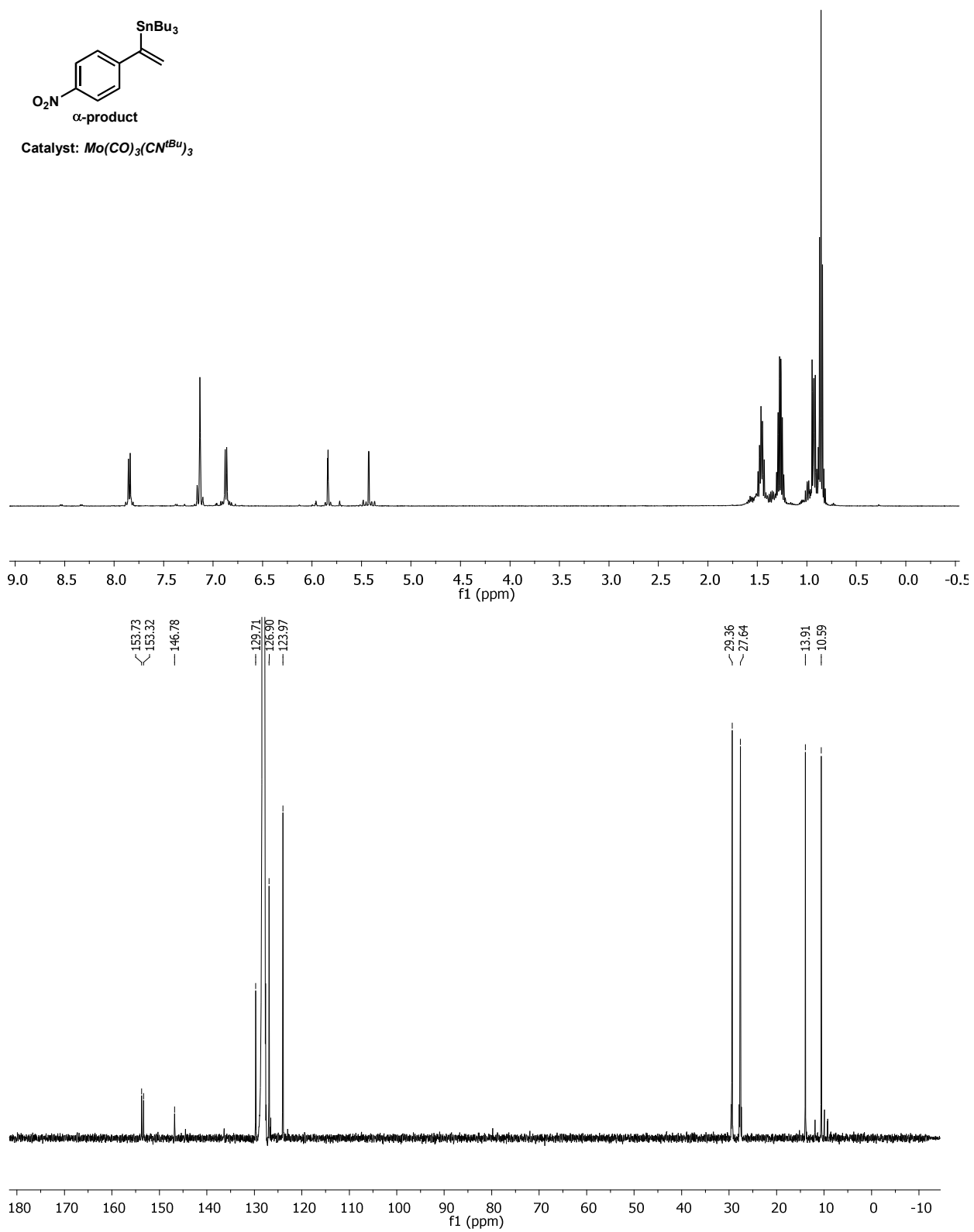


Figure 2.31.  $^1\text{H}$  and  $^{13}\text{C}$  NMR of tributyl(1-(4-nitrophenyl)vinyl)stannane.



## 2.9 Acknowledgements

Chapter 2 is adapted from Kyle A. Mandla, Curtis E. Moore, Arnold L. Rheingold, and Joshua S. Figueroa, “Regioselective Formation of (*E*)- $\beta$ -Vinylstannanes with a Topologically Controlled Molybdenum-Based Alkyne Hydrostannation Catalyst” *Angewandte Chemie, International Edition* **2018**, *57*, 6853-6857. Copyright 2018, Wiley-VCH Verlag GmbH & Co. KGaA, Weinheim. Permission to include published material in this dissertation has been obtained from all coauthors. The dissertation author is the first author of this paper.

## 2.10 References

- (1) Stille, J. K. *Angew. Chemie Int. Ed. English* **1986**, *25* (6), 508–524.
- (2) Stille, J. K.; Groh, B. L. *J. Am. Chem. Soc.* **1987**, *109* (3), 813–817.
- (3) Smith, N. D.; Mancuso, J.; Lautens, M. *Chem. Rev.* **2000**, *100* (8), 3257–3282.
- (4) Trost, B. M.; Ball, Z. T. *Synthesis (Stuttg.)* **2005**, *2005* (6), 853–887.
- (5) Kikukawa, K.; Umekawa, H.; Wada, F.; Matsuda, T.; Matsuda, T. Regioselective Hydrostannation of Terminal Acetylenes under Transition Metal Catalysis <http://www.journal.csj.jp/doi/pdf/10.1246/cl.1988.881> (accessed Jan 3, 2016).
- (6) Kazmaier, U.; Schauss, D.; Pohlman, M. *Org. Lett.* **1999**, *1* (7), 1017–1019.
- (7) Leung, L. T.; Leung, S. K.; Chiu, P. *Org. Lett.* **2005**, *7* (23), 5249–5252.
- (8) Ghosh, B.; Maleczka, R. E. *Tetrahedron Lett.* **2011**, *52* (41), 5285–2587.
- (9) Rummelt, S. M.; Fürstner, A. *Angew. Chemie - Int. Ed.* **2014**, *53* (14), 3626–3630.
- (10) Rummelt, S. M.; Radkowski, K.; Rosca, D.-A.; Fürstner, A.; Rosca, D.-A.; Fürstner, A. *J. Am. Chem. Soc.* **2015**, *137* (16), 5506–5519.
- (11) Roşca, D.-A.; Radkowski, K.; Wolf, L. M.; Wagh, M.; Goddard, R.; Thiel, W.; Fürstner, A.; Roşca, D.-A.; Radkowski, K.; Wolf, L. M.; et al. *J. Am. Chem. Soc.* **2017**, *139* (6), 2443–2455.
- (12) Ichinose, Y.; Oda, H.; Oshima, K.; Utimoto, K. *Bull. Chem. Soc. Jpn.* **1987**, *60* (9), 3468–3470.
- (13) Zhang, H. X. X.; Guibé, F.; Balavoine, G.; Guibe, F.; Balavoine, G. *Tetrahedron Lett.*

- 1988, 29 (6), 619–622.
- (14) Zhang, H. X.; Guibe, F.; Balavoine, G. *J. Org. Chem.* **1990**, 55 (6), 1857–1867.
- (15) Darwish, A.; Lang, A.; Kim, T.; Chong, J. M. *Org. Lett.* **2008**, 10 (5), 861–864.
- (16) Gupta, S.; Do, Y.; Lee, J. H.; Lee, M.; Han, J.; Rhee, Y. H.; Park, J. *Chem. - A Eur. J.* **2014**, 20 (5), 1267–1271.
- (17) Ditri, T. B.; Moore, C. E.; Rheingold, A. L.; Figueroa, J. S.; Ditri, B.; Moore, C. E.; Rheingold, A. L.; Figueroa, J. S. *Inorg. Chem.* **2011**, 50 (20), 10448–10459.
- (18) Ditri, T. B.; Fox, B. J.; Moore, C. E.; Rheingold, A. L.; Figueroa, J. S. *Inorg. Chem.* **2009**, 48 (17), 8362–8375.
- (19) Carpenter, A. E.; Mokhtarzadeh, C. C.; Ripatti, D. S.; Havrylyuk, I.; Kamezawa, R.; Moore, C. E.; Rheingold, A. L.; Figueroa, J. S. *Inorg. Chem.* **2015**, 54 (6), 2936–2944.
- (20) Barnett, B. R.; Labios, L. A.; Stauber, J. M.; Moore, C. E.; Rheingold, A. L.; Figueroa, J. S. *Organometallics* **2017**, 36 (4), 944–954.
- (21) Kazmaier, U.; Pohlman, M.; Schauß, D. *Eur. J. Org. Chem.* **2000**, 3, 2761–2766.
- (22) Braune, S.; Kazmaier, U. *J. Organomet. Chem.* **2002**, 641 (1–2), 26–29.
- (23) Lin, H.; Kazmaier, U. *European J. Org. Chem.* **2007**, 2007 (17), 2839–2843.
- (24) Wesquet, A. 25emO. O.; Kazmaier, U. *Adv. Synth. Catal.* **2009**, 351 (9), 1395–1404.
- (25) Maity, P.; Klos, M. R.; Kazmaier, U. *Org. Lett.* **2013**, 15 (24), 6246–6249.
- (26) Kriley, C. E.; Woolley, C. J.; Krepps, M. K.; Popa, E. M.; Fanwick, P. E.; Rothwell, I. P. *Inorganica Chim. Acta* **2000**, 300–302, 200–205.
- (27) Tyree, W. S.; Vicic, D. A.; Piccoli, P. M. B.; Schultz, A. J.; William S. Tyree, †; David A. Vicic, \*, †; Paula M. B. Piccoli, ‡ and; Arthur J. Schultz\*, ‡. *Inorg. Chem.* **2006**, 45 (22), 8853–8855.
- (28) Chalk, A. J.; Harrod, J. F. *J. Am. Chem. Soc.* **1965**, 87 (1), 16–21.
- (29) Speier, J. L. In *Catalysis and Organic Syntheses*; Elsevier, 1979; Vol. 17, pp 407–447.
- (30) Trebbe, R.; Schager, F.; Goddard, R.; Poerschke, K.-R. *Organometallics* **2000**, 19 (4), 521–526.
- (31) Doherty, N. M.; Bercaw, J. E. *J. Am. Chem. Soc.* **1985**, 107 (9), 2670–2682.
- (32) Pangborn, A. B.; Giardello, M. A.; Grubbs, R. H.; Rosen, R. K.; Timmers, F. J. *Organometallics* **1996**, 15 (5), 1518–1520.

- (33) Albers, M. O.; Coville, N. J.; Uhm, H. L.; Butler, I. S. In *Inorganic Syntheses: Reagents for Transition Metal Complex and Organometallic Syntheses*; Angelicic, R. J., Ed.; Wiley: Hoboken, 1990; p Vol. 28; 140-145.
- (34) Fulmer, G. R.; Miller, A. J. M.; Sherden, N. H.; Gottlieb, H. E.; Nudelman, A.; Stoltz, B. M.; Bercaw, J. E.; Goldberg, K. I. *Organometallics* **2010**, *29* (9), 2176–2179.
- (35) Simmons, E. M.; Hartwig, J. F. *Angew. Chemie - Int. Ed.* **2012**, *51* (13), 3066–3072.
- (36) Hansch, C.; Leo, a; Taft, R. W. *Chem. Rev.* **1991**, *91* (2), 165–195.
- (37) Neese, F. *Wiley Interdiscip. Rev. Comput. Mol. Sci.* **2012**, *2*, 73–78.
- (38) Becke, A. D. *Phys. Rev. A* **1988**, *38* (6), 3098–3100.
- (39) Perdew, J. P. *Phys. Rev. B* **1986**, *33* (12), 8822–8824.
- (40) Lee, C.; Yang, W.; Parr, R. G. *Phys. Rev. B* **1988**, *37* (2), 785–789.
- (41) Pantazis, D. A.; Chen, X.-Y. Y.; Landis, C. R.; Neese, F. *J. Chem. Theory Comput.* **2008**, *4* (6), 908–919.
- (42) Schäfer, A.; Horn, H.; Ahlrichs, R. *J. Chem. Phys.* **1992**, *97* (4), 2571–2577.
- (43) Eichkorn, K.; Treutler, O.; Ohm, H.; Haser, M.; Ahlrichs, R. *Chem. Phys. Lett.* **1995**, *240* (4), 283–290.
- (44) Eichkorn, K.; Treutler O.; Ohm, H.; Haser, M.; Ahlrichs, R. *Chem. Phys. Lett.* **1995**, *242* (6), 652–660.
- (45) Eichkorn, K.; Weigend, F.; Treutler, O.; Ahlrichs, R. *Theor. Chem. Acc.* **1997**, *97*, 119–124.
- (46) Weigend, F.; Ahlrichs, R. *Phys. Chem. Chem. Phys.* **2005**, *7* (18), 3297.
- (47) Lenthe, E. van; Baerends, E. J.; Snijders, J. G. *J. Chem. Phys.* **1993**, *99* (6), 4597–4610.
- (48) Lenthe, E. van; Snijders, J. G.; Baerends, E. J. *J. Chem. Phys.* **1996**, *1051* (10), 6505–154104.
- (49) Werner, H. J.; Manby, F. R.; Knowles, P. J. *J. Chem. Phys.* **2003**, *118* (18), 8149–8160.
- (50) Zhurko, G. A.; Zhurko, D. A. .
- (51) Sheldrick, G. M. *Acta Crystallogr. Sect. A Found. Crystallogr.* **2008**, *A64* (1), 112–122.
- (52) Dolomanov, O.V.; Bourhis, L.J.; Gildea, R.J.; Howard, J.A.K.; Puschmann, H. *J. Appl. Cryst.* **2009**, *42*, 339–341.

## Chapter 3

# Photolytic Reductive Elimination of White Phosphorus from a Mononuclear *cyclo*-P<sub>4</sub> Complex: Bespoke P<sub>4</sub> Release Using Benign Stimulus

### 3.1 Introduction

Among the common allotropes of elemental phosphorus, the synthetic utility of the molecular form, white phosphorus (P<sub>4</sub>), stands out when compared to the more stable polymeric allotropes.<sup>1</sup> Accordingly, P<sub>4</sub> is an essential precursor in industrial-scale synthesis of organophosphorus derivatives and high purity phosphoric acid.<sup>2,3</sup> This importance of P<sub>4</sub> is further underscored by its recent addition to the European Union's list of 27 critical raw materials of high economic importance for which "high supply-risk" is of immediate concern.<sup>4</sup> Adding to challenges in supply chain management, the high reactivity and instability that make P<sub>4</sub> so interesting for chemical transformations also render it challenging to transport and handle. P<sub>4</sub> is the most toxic allotrope of phosphorus, it combusts at room-temperature in air, and it slowly decomposes to polymeric red phosphorus upon exposure to ambient light.<sup>1</sup> Furthermore, stringent regulations for the distribution and transport of even very small quantities of P<sub>4</sub> have greatly limited its commercial availability. Although development of more efficient methods for the derivatization of P<sub>4</sub> remains an important research objective,<sup>5-7</sup> such efforts are becoming increasingly impeded by its restricted accessibility.

To address these challenges, there has been considerable effort aimed at the discovery of air-stable platforms for the safe storage and release of P<sub>4</sub>. The most common strategy involves the encapsulation of P<sub>4</sub> within supramolecular cages or porous materials.<sup>8-12</sup> In an exemplary recent application of this approach, Scheer and co-workers demonstrated that the porous structure of

activated carbon could be intercalated with P<sub>4</sub>. In that work, the resulting phase, P<sub>4</sub>/C, could be used directly as a P<sub>4</sub> source for solution-phase reactions, or induced to release gaseous P<sub>4</sub> when subjected to vacuum.<sup>13</sup> As a complementary strategy, molecular coordination complexes bearing intact P<sub>4</sub> tetrahedra have been envisaged as suitable candidates for P<sub>4</sub> storage and selective release.<sup>14</sup> To this end, it was also recently shown that the P<sub>4</sub>-bridged β-diketimido complex [(LCu)<sub>2</sub>(μ,η<sup>2:2</sup>-P<sub>4</sub>)] (L = [{N(C<sub>6</sub>H<sub>3</sub>iPr<sub>2-2,6</sub>)C(Me)}<sub>2</sub>CH]<sup>-</sup>) released white phosphorus, albeit irreversibly, upon treatment with an excess of pyridine.<sup>15</sup>

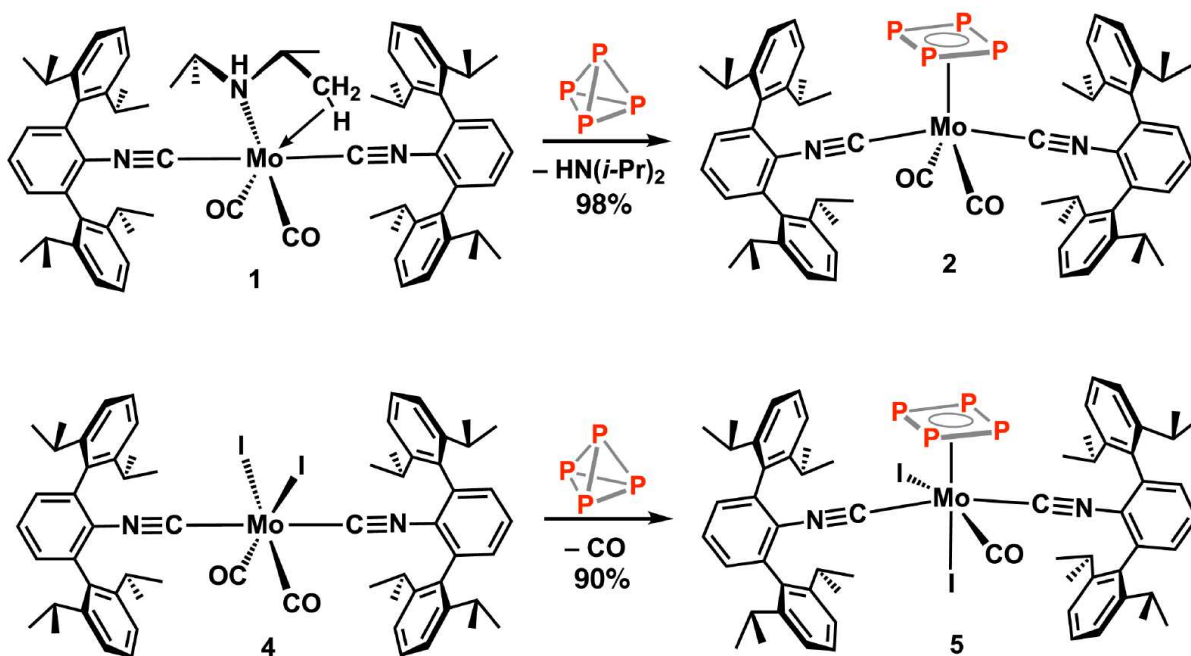
A commonality among these P<sub>4</sub>-storage systems is the preservation of the P<sub>4</sub> tetrahedron. Indeed, the maximal retention P-P bonding for both host-guest and transition metal P<sub>4</sub>-storage systems is a rational design principle when considering the high heat of formation of tetrahedral P<sub>4</sub>.<sup>16,17</sup> However, the long-term stability, retention and safety of white phosphorus as a simple coordinated ligand, or within non-covalent encapsulation, remains an open question due to the lack of detailed information on P<sub>4</sub>-tetrahedra dissociation/release kinetics from metal centers or supramolecular systems, respectively.<sup>18</sup> An intriguing alternative, which can prevent the accidental release of a highly reactive entity, is the storage of the P<sub>4</sub> unit in an activated, kinetically inert form. Furthermore, such an added safety-control would be particularly advantageous if the storage system allowed for bespoke release of tetrahedral P<sub>4</sub> molecules upon application of a benign stimulus. Accordingly, herein we describe a potential storage strategy which sequesters white phosphorus as a kinetically deactivated, planar *cyclo*-P<sub>4</sub> unit covalently linked to a mononuclear molybdenum fragment. Tetrahedral P<sub>4</sub> is released from these (*cyclo*-P<sub>4</sub>)-molybdenum complexes using UV light from readily available light-emitting diode (LED) sources. This approach relies on the advent of straightforward, high-yielding syntheses of mononuclear *cyclo*-P<sub>4</sub> transition metal

complexes and the ability of photo-excited, non-cage P<sub>4</sub> species to undergo rapid unimolecular collapse to the tetrahedral P<sub>4</sub> molecule.<sup>19</sup>

### 3.2 Synthesis and photolytic reactivity of a mononuclear *cyclo*-P<sub>4</sub> complexes

Recently we reported the synthesis of a zero-valent molybdenum-complex, Mo( $\eta^2$ -C,H: $\kappa^1$ -N-(HN(*i*-Pr)<sub>2</sub>)(CO)<sub>2</sub>(CNAr<sup>Dipp2</sup>)<sub>2</sub> (**1**; Ar<sup>Dipp2</sup> = 2,6-(2,6-(*i*-Pr)<sub>2</sub>C<sub>6</sub>H<sub>3</sub>)<sub>2</sub>C<sub>6</sub>H<sub>3</sub>)) which serves as a reactive source of the 14e<sup>-</sup> fragment [Mo(CO)<sub>2</sub>(CNAr<sup>Dipp2</sup>)<sub>2</sub>] by virtue of facile displacement of its  $\eta^2$ -C,H: $\kappa^1$ -N-diisopropylamine chelate.<sup>20</sup> Treatment of **1** with 1.0 equiv of white phosphorus in *n*-pentane/toluene mixture proceeds in near-quantitative yield with the exclusive formation of a single diamagnetic product, as assayed by <sup>1</sup>H and <sup>31</sup>P{<sup>1</sup>H} NMR spectroscopy. Structural characterization of orange crystals of this product revealed the mononuclear complex ( $\eta^4$ -P<sub>4</sub>)Mo(CO)<sub>2</sub>(CNAr<sup>Dipp2</sup>)<sub>2</sub> (**2**), which possesses symmetrical  $\eta^4$ -coordination of a planar *cyclo*-P<sub>4</sub> unit to the Mo center (Scheme 3.1; Figure 3.1). While several dinuclear, bridging *cyclo*-P<sub>4</sub> complexes (*i.e.* ( $\mu_2$ -( $\eta^4$ : $\eta^4$ -*cyclo*-P<sub>4</sub>)M<sub>2</sub>)) have now been reported,<sup>6,7,21–27</sup> it is notable that mononuclear *cyclo*-P<sub>4</sub> complexes are limited only to the Group 5 species Cp<sup>R2</sup>M( $\eta^4$ -P<sub>4</sub>)(CO)<sub>2</sub> (M = V, R = Me; Nb, R = Me; Ta, R = *t*-Bu)<sup>28–30</sup> and the iron complex Fe( $\eta^4$ -P<sub>4</sub>)(<sup>Ph</sup>PP<sub>2</sub><sup>Cy2</sup>) recently reported by Mézailles (<sup>Ph</sup>PP<sub>2</sub><sup>Cy2</sup> = PhP(CH<sub>2</sub>CH<sub>2</sub>PCy<sub>2</sub>)<sub>2</sub>).<sup>31</sup> DFT calculations on **2** revealed the presence of two occupied non-bonding d-orbitals on the Mo center, consistent with a d<sup>4</sup> electronic configuration. In addition, the calculations show that the interaction between the *cyclo*-P<sub>4</sub> unit and the Mo center is best described as three-fold, a+2e molecular orbital framework, such that the complex is best formulated as featuring the coordination of an ostensible aromatic, six  $\pi$ -electron [*cyclo*-P<sub>4</sub>]<sup>2-</sup> dianion (see Section 3.4.4, Figure 3.13).<sup>32,33</sup> Most importantly however, complex **2** possesses high-lying filled molecular orbitals that are P-P  $\sigma$ -bonding in character, in addition to

several low-lying empty orbitals featuring substantial anti-bonding character between the *cyclo*-P<sub>4</sub> unit and the Mo center. We hypothesized that these electronic features would potentially allow for an energetically accessible ligand-to-metal charge-transfer (LMCT) excitation that resulted in extrusion of the P<sub>4</sub> from the metal center. In addition, complex **2** is stable for days in air and resists thermal degradation up to 90 °C (24 h) in C<sub>6</sub>D<sub>6</sub> solution. Accordingly, this property rendered complex **2** a viable candidate for a storage/photolytic-release system for white phosphorus.



**Scheme 3.1.** Synthesis of  $\eta^4$ -(*cyclo*-P<sub>4</sub>) complexes **2** and **5**.

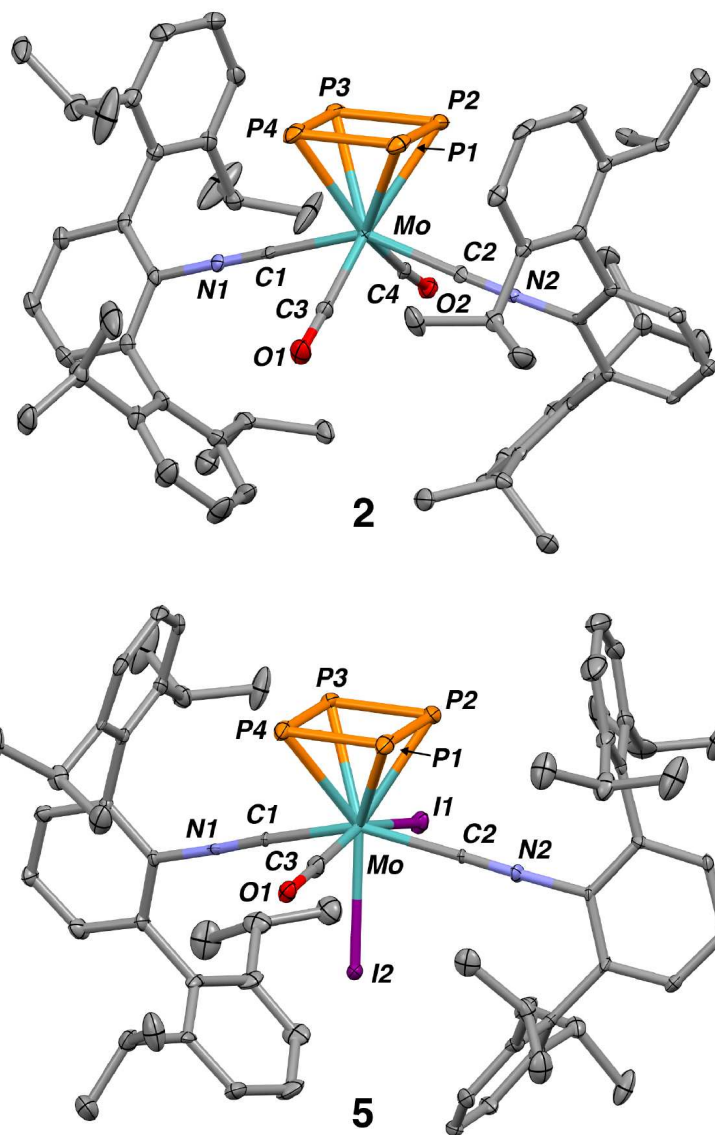


**Figure 3.1.** Molecular structures of  $\eta^4$ -(*cyclo*-P<sub>4</sub>) complexes **2** (top) and **5** (bottom).

To test the applicability of complex **2** as a white phosphorus release reagent, its photochemical properties were investigated. When dissolved in 1,2-dimethoxyethane (DME), complex **2** showed no evidence of reaction when exposed to 385-396 nm violet light. However, upon irradiation with a 284 nm light source for 1 h, the solution became turbid and  $^{31}\text{P}\{^1\text{H}\}$  NMR spectroscopy indicated complete disappearance of the resonance of **2** located at  $\delta = +113$  ppm. However, this  $^{31}\text{P}\{^1\text{H}\}$  spectrum was completely devoid of resonances between -1000 and +1000



ppm. While these experimental conditions did not establish the suitability of complex **2** as a source of P<sub>4</sub>, the absence of detectable <sup>31</sup>P{<sup>1</sup>H}NMR signals following irradiation is consistent with release of the *cyclo*-P<sub>4</sub> unit followed by photo-induced catenation to red phosphorus.<sup>19,34</sup> Importantly, when irradiated at wavelengths less than 300 nm, white phosphorus is known to undergo photo-dissociation to two P<sub>2</sub> molecules, which rapidly polymerize to red phosphorus.<sup>34,35</sup> The formation of insoluble products upon 284 nm irradiation of **2** was thus hypothesized to proceed after reductive elimination of the P<sub>4</sub> from the Mo center. In support of this notion, <sup>1</sup>H NMR analysis of the reaction mixture after irradiation of **2** revealed the presence of the zero-valent, tetracarbonyl complex Mo(CO)<sub>4</sub>(CNAr<sup>Dipp2</sup>)<sub>2</sub> (**3**) as well as the free isocyanide CNAr<sup>Dipp2</sup> as exclusive products.<sup>34-35</sup> Notably, the formation of **3** and CNAr<sup>Dipp2</sup> have been previously established as the products of rapid ligand redistribution when the reactive 14e<sup>-</sup> species [Mo(CO)<sub>2</sub>(CNAr<sup>Dipp2</sup>)<sub>2</sub>] is generated in solution.<sup>36,37</sup> Accordingly, the formation of the zero-valent complex **3** upon irradiation of complex **2**, as well as the formation of particulate matter, provide strong evidence for photo-reductive release of the *cyclo*-P<sub>4</sub> unit from the Mo center in complex **2**. To our knowledge, photo-dissociation of coordinated *cyclo*-P<sub>n</sub> ligands from transition metal centers has not been reported previously.

Given that the short wavelengths of light required to release P<sub>4</sub> from **2** also induce P<sub>4</sub> catenation, we reasoned that an electronic modification, where the metal center was formally oxidized relative to complex **2**, could result in lower-lying vacant d-orbitals for a P<sub>4</sub>-releasing LMCT, thereby enabling photolytic-P<sub>4</sub> extrusion at longer wavelengths.<sup>38</sup> Satisfying this criterion, we found that the divalent, diiodide complex MoI<sub>2</sub>(CO)<sub>2</sub>(CNAr<sup>Dipp2</sup>)<sub>2</sub> (**4**),<sup>37</sup> which is the precursor to complex **2**, also reacts cleanly with white phosphorus to produce the mononuclear *cyclo*-P<sub>4</sub> complex, (η<sup>4</sup>-P<sub>4</sub>)MoI<sub>2</sub>(CO)(CNAr<sup>Dipp2</sup>)<sub>2</sub> (**5**), concomitant with loss of one CO ligand in 90% yield

(Scheme 3.1. Synthesis of  $\eta^4(\text{cyclo-P}_4)$  complexes **2** and **5**). Remarkably, complex **5** also remains unchanged upon standing as a solid in air for several days and retains its integrity for at least two days when heated to 80 °C in C<sub>6</sub>D<sub>6</sub> solution. Structural characterization of **5** revealed a  $\eta^4(\text{cyclo-P}_4)$  unit and retention of both iodide ligands, with one occupying the position *trans* to the *cyclo-P*<sub>4</sub> ring centroid (Figure 3.1). This particular orientation de-symmetrizes the <sup>31</sup>P{<sup>1</sup>H} NMR signal of the  $\eta^4\text{-P}_4$  unit into an AA'BB' spin pattern centered at +75 ppm ( $J_{AA'} = 298$  Hz,  $J_{BB'} = 339$  Hz,  $J_{AB} = 278$  Hz,  $J_{AB'} = 1$  Hz; Figure 3.2, top). In addition, DFT calculations revealed that the highest-lying, filled molecular orbital manifold for complex **5** consists predominantly orbitals with both iodide lone pair and P-P  $\sigma$ -bonding character (*see* Section 3.4.4. Figure 3.14). Correspondingly, the lowest-lying unoccupied orbitals for **5** possess significant  $\eta^4\text{-P}_4/\text{Mo}$  antibonding character, which, when coupled with its formally d<sup>2</sup> electronic configuration, signifies that lower-energy P<sub>4</sub>-releasing LMCTs relative to complex **2** may be accessible.

To evaluate this hypothesis, the photolytic behavior of complex **5** was evaluated. Irradiation of a 2.5 mM C<sub>6</sub>D<sub>6</sub>/DME solution (85:15 v/v%) of **5** with an 18W violet LED (385-395 nm) for 30 min, followed by analysis of the reaction mixture by <sup>31</sup>P{<sup>1</sup>H} NMR spectroscopy, revealed the complete consumption of the starting material and formation of a single peak centered at -525 ppm (*see* Section 3.3.2., Figure 3.5). Remarkably, the latter is indicative of white phosphorus, and notably, no significant formation of other phosphorus-containing by-products were observed in this spectrum of the post-photolysis reaction mixture. In addition, integration of the white phosphorus signal obtained after photolysis versus an internal standard (PPh<sub>3</sub>) revealed greater than 95% retention of phosphorus in a soluble form, thereby indicating that 385-395 nm irradiation did not lead to substantial catenation of P<sub>*n*</sub> units under these conditions. Analysis of the post-photolysis reaction mixture by <sup>1</sup>H NMR spectroscopy showed the clean

formation of a single new  $\text{CNAr}^{\text{Dipp}^2}$ -containing product. Structural determination of crystals of this product revealed it to be the  $16e^- \kappa^1\text{-O}$  DME-adduct,  $\text{MoI}_2(\text{CO})(\kappa^1\text{-O-DME})(\text{CNAr}^{\text{Dipp}^2})_2$  (**6**), thereby strongly suggesting that photo-reductive elimination of  $\text{P}_4$  from complex **5** produces the  $14e^-$  species,  $[\text{MoI}_2(\text{CO})(\text{CNAr}^{\text{Dipp}^2})_2]$ , which is efficiently trapped by the DME solvent. Most notably however, post-photolysis mixtures of white phosphorus and complex **6** remain unchanged when left standing in the dark for up to 2 h. However, heating this mixture to  $80^\circ\text{C}$  for 45 min, results in the complete reversion to the  $\eta^4\text{-P}_4$  complex **5**, thereby establishing that white phosphorus can be easily and reversibly re-incorporated onto the Mo center in this system (Figure 3.2).

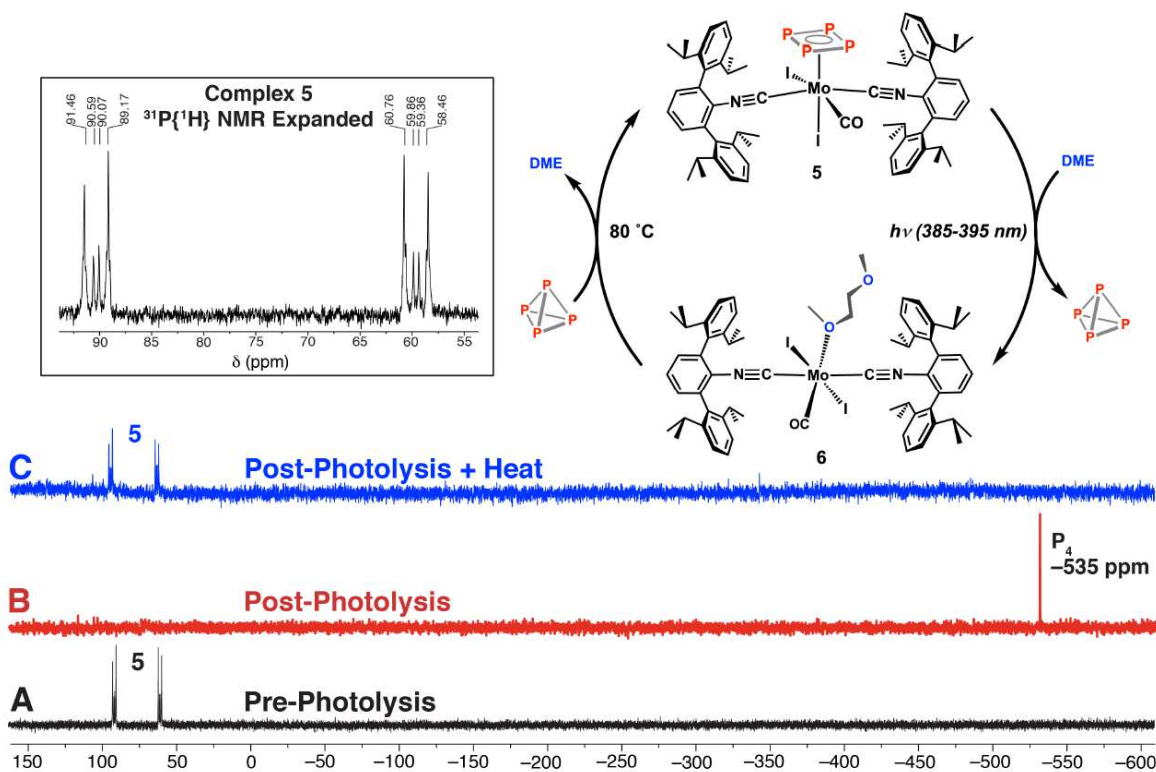


**Figure 3.2** Photolytic release and recapture of white phosphorus ( $\text{P}_4$ ). Top left: Expanded  $^{31}\text{P}\{^1\text{H}\}$  NMR spectrum of complex **5** showing AA'BB' coupling pattern. Top right: Release/recapture cycle for  $\text{P}_4$  via photolysis of complex **5** and thermolysis of the DME-complex **6** in the presence of liberated  $\text{P}_4$ . Bottom:  $^{31}\text{P}\{^1\text{H}\}$  NMR stack showing complex **5** before photolysis with violet-light LEDs (A). The post-photolysis mixture showing exclusive formation of white phosphorus ( $\delta = -535$  ppm) (B). Regeneration of complex **5** via heating ( $80^\circ\text{C}$ ; 30 min) the post-photolysis mixture of DME complex **6** and liberated of white phosphorus (C).

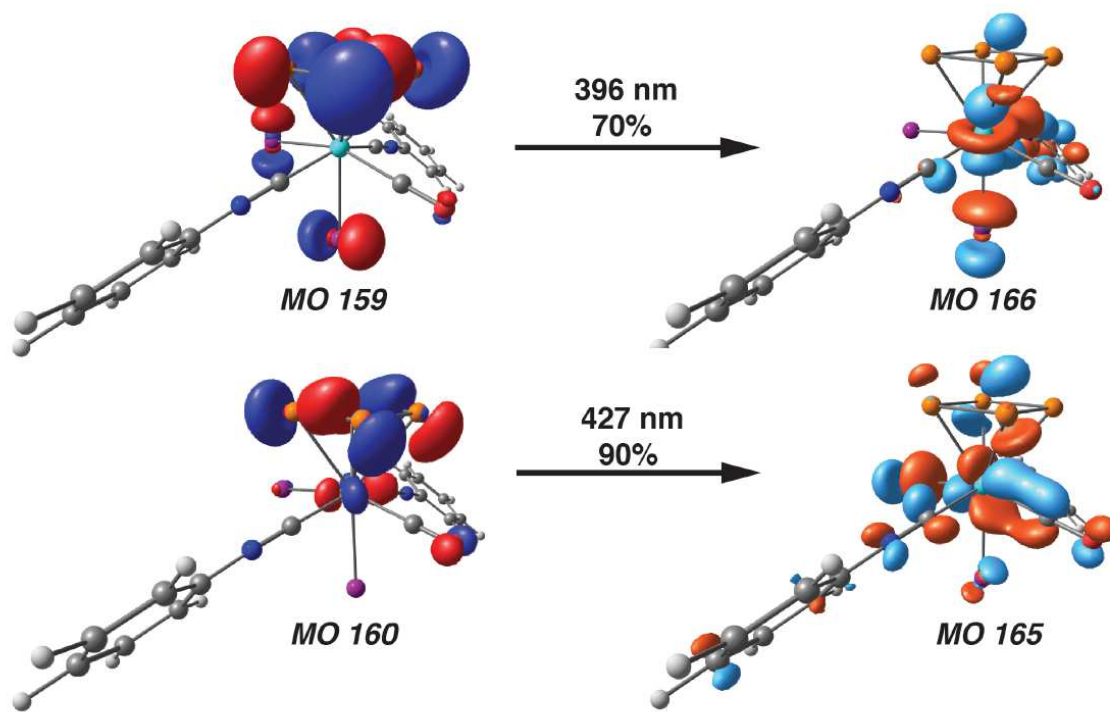


**Figure 3.3.** Major TD-DFT calculated excitations for model 5m corresponding to P<sub>4</sub>-releasing LMCTs.

Insight into the specific photo-induced excited states involved in reductive elimination of white phosphorus were obtained by UV-Vis spectroscopy and time-dependent density functional theory (TD-DFT) calculations. The lowest energy absorptive feature in the UV-vis spectrum of **5** is a broad tailing-absorption extending from 425 to 550 nm (*see* Section 3.4.1 Figure 3.10). The feature is well reproduced in the TD-DFT calculations, and is attributed to LMCT transitions involving electron-transfer from iodine lone pairs into the d-orbital manifold of molybdenum. To the blue of this feature is a comparatively intense shoulder at 350-425 nm, and the TD-DFT calculations reveal two high-extinction absorptive features in this region corresponding to electron-transfer from the *cyclo*-P<sub>4</sub>  $\sigma$ -bonding framework into the an Mo/ $\eta^4$ -P<sub>4</sub> anti-bonding orbital possessing significant d-orbital character (Figure 3.3). We believe promotion of an electron in one or both of these singlet LMCT excited states are the initial perturbation by which subsequent

relaxation pathways make accessible the release of the *cyclo*-P<sub>4</sub> unit for the ultimate production of tetrahedral white phosphorus.<sup>19</sup> Accordingly, from a conceptual standpoint, we contend that this photo-elimination approach from a deactivated P<sub>4</sub> unit serves as a method and/or potential guide post for the transport and on-demand utilization of white phosphorus, while minimizing the hazards associated with the native, bulk material.

### 3.3 Synthetic Procedures and Characterization Data

#### 3.3.1 General considerations.

All manipulations were carried out under an atmosphere of purified dinitrogen using standard Schlenk and glovebox techniques. Unless otherwise stated, reagent-grade starting materials were purchased from commercial sources and either used as received or purified by standard procedures.<sup>39</sup> Solvents were dried and deoxygenated according to standard procedures.<sup>40</sup> Benzene-d<sub>6</sub> (Cambridge Isotope Laboratories) was distilled from NaK alloy/benzophenone ketyl and stored over 4 Å molecular sieves under N<sub>2</sub> for at least 24 h prior to use. Celite 405 (Fisher Scientific) was dried under vacuum (24 h) at a temperature above 250 °C and stored in the glovebox prior to use. KBr (FTIR grade from Aldrich) was stirred overnight in anhydrous THF, filtered and dried under vacuum at a temperature above 250 °C prior to use. The *m*-terphenyl isocyanide CNAr<sup>Dipp</sup><sub>2</sub> was prepared as previously reported.<sup>41</sup>

General photolysis experiments were carried out using an iLumen8 (100 LEDs, 18W, 385-395 nm). Shortwave photolysis experiments were carried with a 254 nm Hg lamp. UV-Vis spectra were obtained on a Shimadzu UV-3600. Solution <sup>1</sup>H, <sup>13</sup>C{<sup>1</sup>H}, <sup>31</sup>P NMR spectra were recorded on a Bruker Avance 300, a Jeol ECA 500, or a Varian X-SENS 500 spectrometer. <sup>1</sup>H and <sup>13</sup>C{<sup>1</sup>H} chemical shifts are reported in ppm relative to SiMe<sub>4</sub>. (<sup>1</sup>H and <sup>13</sup>C δ = 0.0 ppm) with reference to residual solvent resonances of 7.16 ppm (<sup>1</sup>H) and 128.06 ppm (<sup>13</sup>C) for C<sub>6</sub>D<sub>6</sub>. <sup>31</sup>P chemical shifts

are reported in ppm relative to H<sub>3</sub>PO<sub>3</sub> with reference to PPh<sub>3</sub> as an internal standard with a resonance of -6.00 ppm. FTIR spectra were recorded on a Thermo-Nicolet iS10 FTIR spectrometer. FTIR samples were prepared as C<sub>6</sub>D<sub>6</sub> or THF solutions injected into a ThermoFisher solution cell equipped with KBr windows. Solvent peaks were digitally subtracted from all spectra by comparison with an authentic spectrum obtained immediately prior to that of the sample. The following abbreviations were used for the intensities and characteristics of important IR absorption bands: vs = very strong, s = strong, m = medium, w = weak, vw = very weak; br = broad, sh = shoulder. Combustion analyses were performed by Midwest Laboratories of Indianapolis, IN (USA).

### 3.3.2 Synthesis of ( $\eta^4$ -P<sub>4</sub>)Mo(CO)<sub>2</sub>(CNAr<sup>Dipp2</sup>)<sub>2</sub> (**2**).

To a cold pentane solution of Mo(CO)<sub>2</sub>(CNAr<sup>Dipp2</sup>)<sub>2</sub>(*N,CH*-HN*i*Pr<sub>2</sub>) (**1**, 0.0991 g, 90.1  $\mu$ mol, 1.0 equiv, 10 mL, -40 °C) was added a toluene solution of P<sub>4</sub> (0.012 g, 96.4  $\mu$ mol, 1.07 equiv, 1 mL). The reaction mixture was stirred at room temperature for 1 h, at which time a pale orange color persisted in solution. The reaction mixture was concentrated in vacuo to give **2** (0.0992 g, 88.3  $\mu$ mol, 98% yield) as the sole reaction product as estimated by <sup>1</sup>H and <sup>31</sup>P NMR. To obtain analytically pure samples, the solid was taken up in 3:2 mixture of Et<sub>2</sub>O/pentane (10 mL), the solution was filtered and the volume was reduced in vacuo to ca. 0.400 mL and placed in the freezer at -40 °C to afford **2** as an orange crystalline solid suitable for X-ray diffraction. Yield: 0.068 g, 60.4  $\mu$ mol, 67%. Analytically pure samples were obtained <sup>1</sup>H NMR (500 MHz, C<sub>6</sub>D<sub>6</sub>)  $\delta$  7.38 (t, *J* = 7.8 Hz, 4H), 7.20 (d, *J* = 7.8 Hz, 8H), 6.92 (d, *J* = 7.2 Hz, 4H), 6.87 – 6.83 (m, 2H), 2.62 (sept, 6.8, 8H), 1.28 (d, *J* = 6.8 Hz, 24H), 1.07 (d, *J* = 6.8 Hz, 24H) ppm; <sup>13</sup>C{<sup>1</sup>H} NMR (126 MHz, C<sub>6</sub>D<sub>6</sub>)  $\delta$  ppm 227.2, 177.6, 146.2, 139.0, 134.5, 130.36, 129.9, 128.1, 123.7, 31.4, 24.8, 24.3 ppm; <sup>31</sup>P{<sup>1</sup>H} NMR (121 MHz, C<sub>6</sub>D<sub>6</sub>)  $\delta$  113.6 (s) ppm. FTIR (KBr windows, C<sub>6</sub>D<sub>6</sub>, 25 °C):

$\nu(\text{C}\equiv\text{N}) = 2130$  (s),  $2101$  (vs),  $\nu(\text{C}=\text{O}) = 2001$  (m),  $1941$  (vs), other:  $1461$ ,  $1414$ ,  $1385$ ,  $1363$ ,  $2962$ ,  $2928$ ,  $2906$ ,  $2868$ ,  $1057$ ,  $757$   $\text{cm}^{-1}$ . Anal. Calcd. for  $\text{C}_{64}\text{H}_{74}\text{MoN}_2\text{O}_2\text{P}_4$ : C 68.44; H, 6.64; N, 2.49. Found: C, 67.94; H 6.80; N, 2.60.

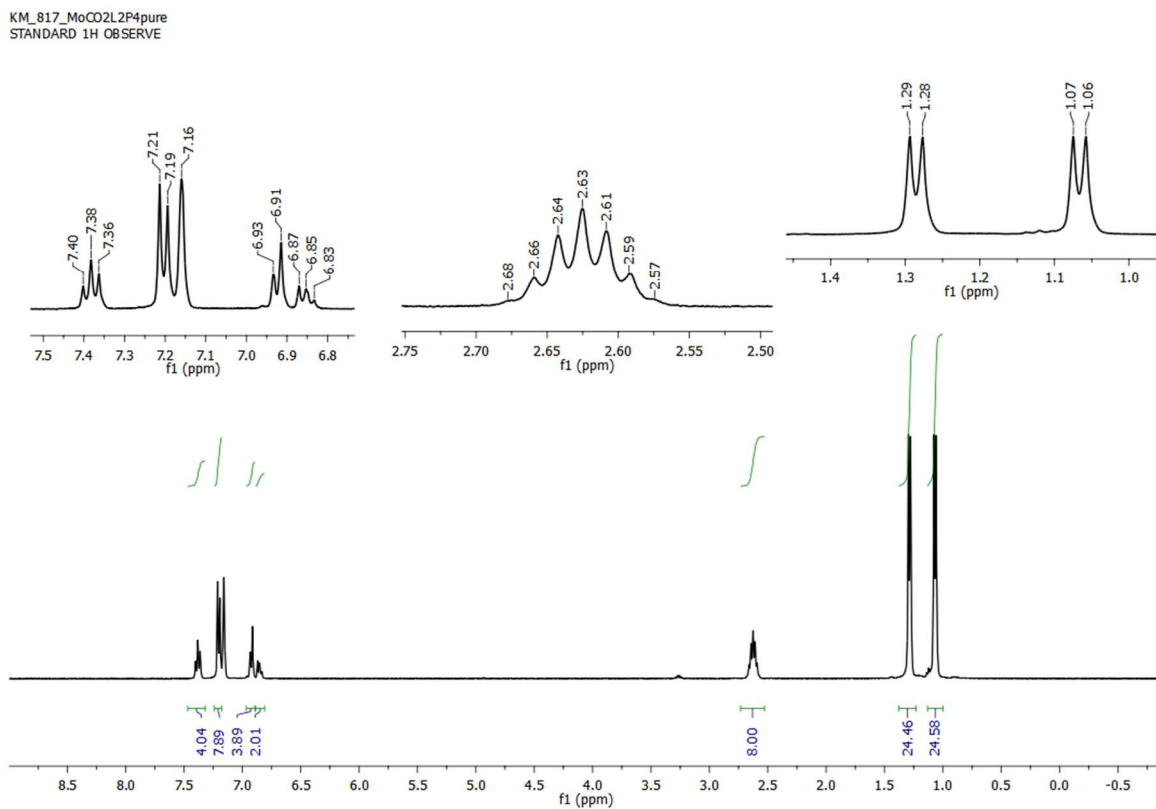


**Figure 3.4.**  $^1\text{H}$  NMR (500.0 MHz,  $\text{C}_6\text{D}_6$ ,  $20^\circ\text{C}$ ) spectrum of of **5**.

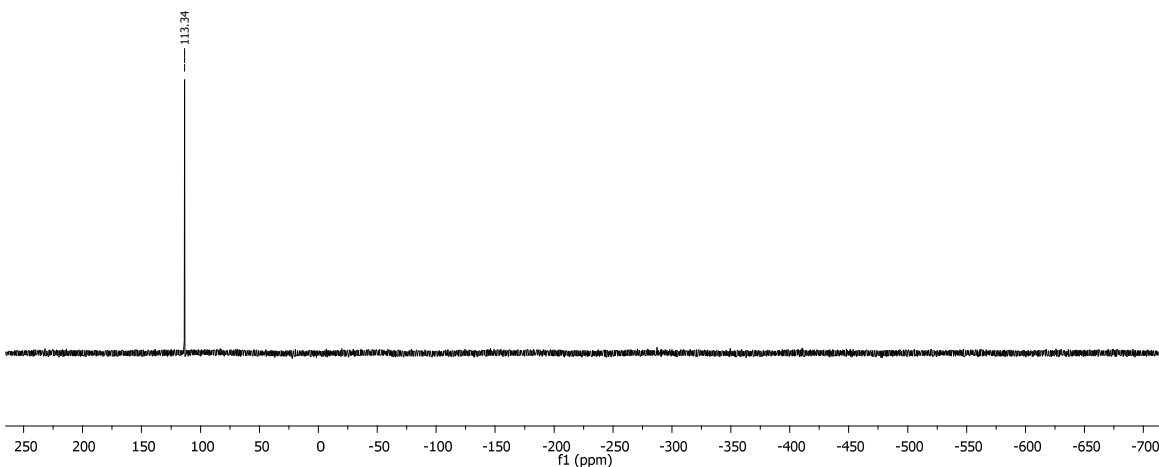


**Figure 3.5.**  $^{31}\text{P}\{^1\text{H}\}$  NMR (121.4 MHz, C6D6, 20 °C) spectrum of **2**

### 3.3.3 Synthesis of $(\eta^4\text{-P}_4)\text{MoI}_2(\text{CO})(\text{CNAr}^{\text{Dipp}2})_2$ (**5**).

Synthesis of  $(\eta^4\text{-P}_4)\text{MoI}_2(\text{CO})(\text{CNAr}^{\text{Dipp}2})_2$  (**5**). A 4:1 toluene/DME solution of  $\text{MoI}_2(\text{CO})_2(\text{CNAr}^{\text{Dipp}2})_2$  (**1**, 0.030 g, 0.024 mmol, 1 equiv, 5 mL) and  $\text{P}_4$  (0.0035 g, 0.029 mmol, 1.2 equiv) was stirred in a sealed 25 mL Schlenk ampoule at 80 °C for 4 h. To the reaction mixture was added 2 mL *n*-pentane, and the solution was chilled at -40 °C for 30 min and then filtered. The filtered solution was concentrated, then washed with cold *n*-pentane (*ca.* 5 mL, -40 °C) to give **5** as a yellow solid (0.029 g, 0.022 mmol, 90%). X-ray diffraction quality crystals were grown from a concentrated  $\text{Et}_2\text{O}$  solution at -40 °C. Analytically pure crystals were grown from a 1:1  $\text{Et}_2\text{O}$ /toluene mixture and were obtained as a solvate with two molecules of toluene per unit **5**.  $^1\text{H}$  NMR (300.0 MHz, C6D6, 20 °C):  $\delta$  = 7.46 (q,  $J$  = 7.5 Hz, 4H), 7.23 (d,  $J$  = 7.8 Hz, 8H), 6.91–6.83 (m, 4H), 6.78 (dd,  $J$  = 8.6, 6.3 Hz, 2H), 2.62 / 2.60 (m), 1.43 (t,  $J$  = 6.3 Hz, 24H), 0.99 (dd,  $J$



= 6.7, 3.3 Hz, 24H);  $^{13}\text{C}\{^1\text{H}\}$  NMR (126.0 MHz,  $\text{C}_6\text{D}_6$ , 20 °C):  $\delta$  = 203.0, 153.3, 146.6, 146.5, 140.2, 134.8, 131.1, 129.9, 124.3, 124.0, 31.5, 31.4, 25.18, 24.9, 24.3, 24.2;  $^1\text{P}\{^1\text{H}\}$  NMR (121.0 MHz,  $\text{C}_6\text{D}_6$ , 20 °C):  $\delta$  = 90.3 (m) and 59.6 (m) ppm ( $A A' B B'$   $J_{A A'}$  = 298 Hz,  $J_{B B'}$  = 339 Hz,  $J_{A B}$  = 278 Hz,  $J_{A B'}$  = 1 Hz). FTIR (KBr windows,  $\text{C}_6\text{D}_6$ , 25 °C):  $\nu(\text{C}\equiv\text{N})$  = 2142 (s), 2104 (w),  $\nu(\text{C}=\text{O})$  = 2007 (s)  $\text{cm}^{-1}$ , also 2961, 2928, 2868, 1179, 794, 757  $\text{cm}^{-1}$ . Anal. Calcd. for  $\text{C}_{77}\text{H}_{90}\text{N}_2\text{O MoI}_2\text{P}_4$  ( $6 \cdot 2(\text{C}_7\text{H}_8)$ ): C, 60.32; H, 5.92; N, 1.83. Found: C, 60.31; H, 6.13; N, 2.06.

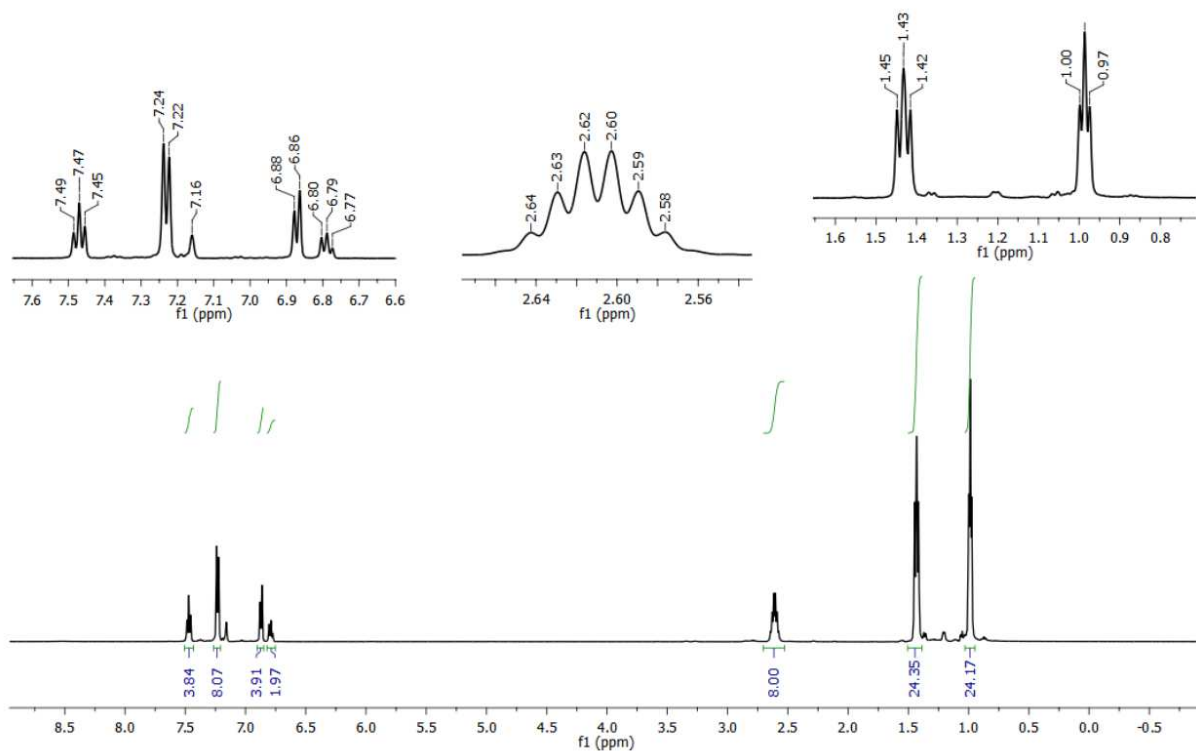


**Figure 3.6.**  $^1\text{H}$  NMR (500.0 MHz,  $\text{C}_6\text{D}_6$ , 20 °C) spectrum of of **5**.

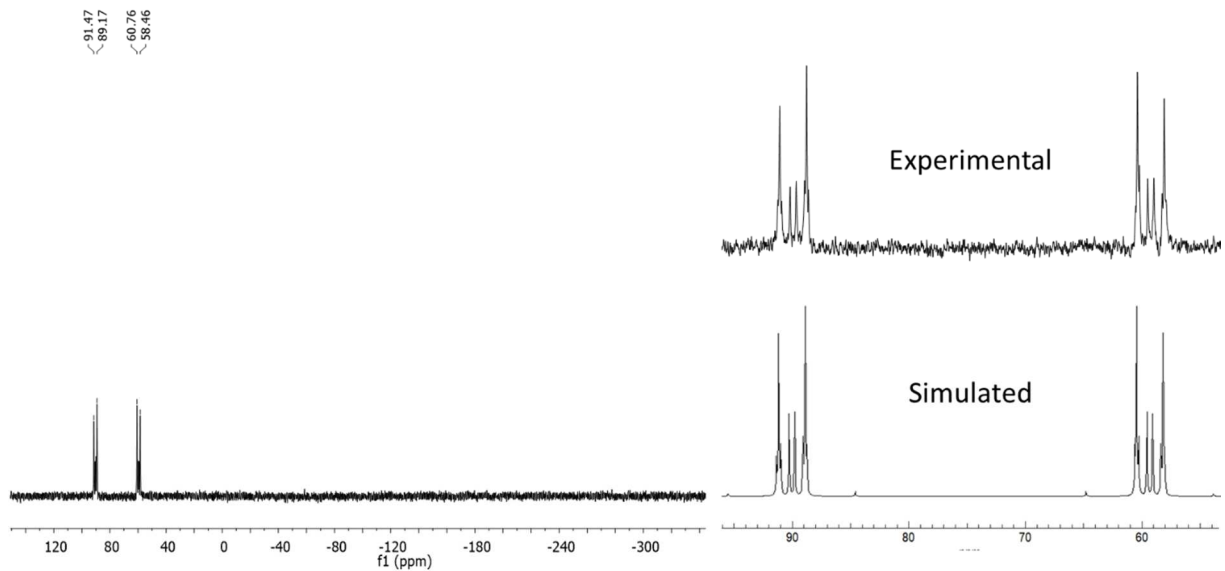


**Figure 3.7.**  $^{31}\text{P}\{^1\text{H}\}$  NMR (121.4 MHz,  $\text{C}_6\text{D}_6$ , 20 °C) spectrum of **5** and evaluation of homonuclear coupling: WinDNMR<sup>42</sup> simulated AA'BB' spectrum gives  $J_{AA'} = 298$  Hz,  $J_{BB'} = 339$  Hz,  $J_{AB} = 278$  Hz,  $J_{AB'} = 1$  Hz.

### 3.3.4 Variable Temperature (VT) $^{31}\text{P}$ NMR Analysis of $\text{MoI}_2(\text{CO})(\text{CNAr}^{\text{Dipp}^2})_2$ (**5**)

Hindered rotation of *cyclo*- $\text{P}_4$  is apparent by  $^{31}\text{P}$  NMR of **5**. Accordingly, the  $\text{C}_s$  symmetric complex gives rise to two independent chemical shifts within a distinctive AA'BB' spin system (Figure 3.7). Variable Temperature (VT)-NMR up to 75 °C ( $\text{C}_6\text{D}_6$ , 202.4 Hz) did not show coalescence, however, line-broadening characteristic of hindered rotation is observed.

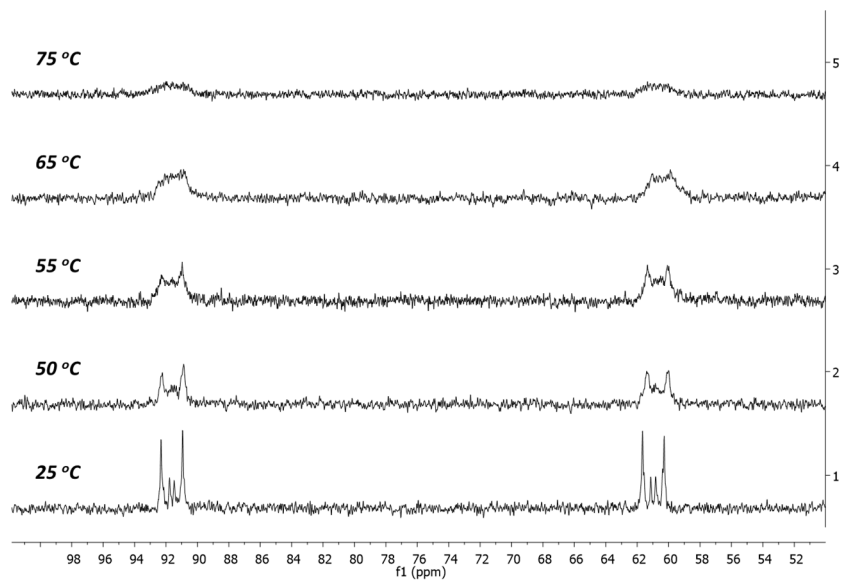


**Figure 3.8.** VT  $^{31}\text{P}$ -NMR (202.404 MHz,  $\text{C}_6\text{D}_6$ ) of **5** indicates hindered rotation of *cyclo*- $\text{P}_4$  is persistent up to 75 °C.

### 3.3.5 Photolytic Reductive Elimination of White Phosphorus, and Thermal Regeneration of (*cyclo*- $\text{P}_4$ ) $\text{MoI}_2(\text{CO})(\text{CNAr}^{\text{Dipp}^2})_2$ (**5**)

**Experimental procedure.** A 25 mL ampoule was charged with a 1.0 mM solution of **5** (2% DME in  $\text{C}_6\text{H}_6$ , 6 mL) under  $\text{N}_2$  atmosphere. The sealed ampoule was irradiated (385-395 nm, LED) while stirring for 20 min.  $^{31}\text{P}$  NMR showed consumption of **5** with release of  $\text{P}_4$  (Figure 3.9, middle). *cyclo*- $\text{P}_4$  complex **5** was regenerated (93% yield by NMR vs. internal standard of  $\text{PPh}_3$ , *not shown*) upon heating the irradiated solution for 30 min at 70 °C (Figure 3.9, bottom).

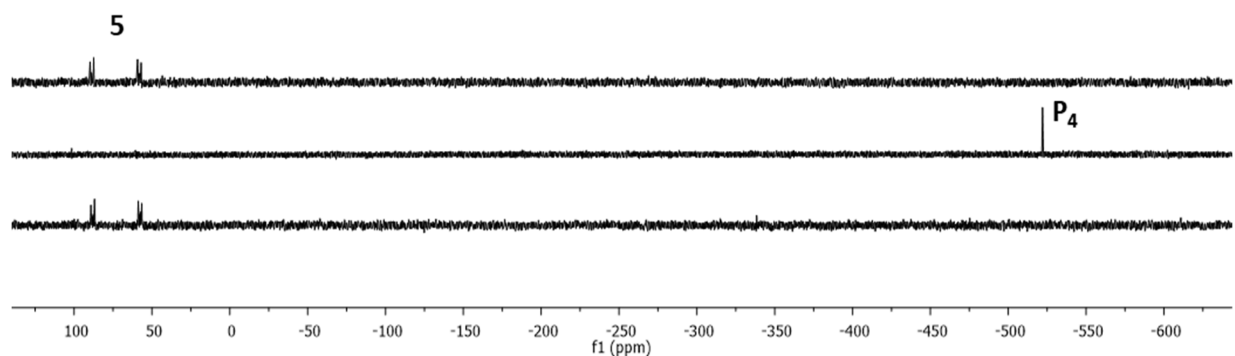
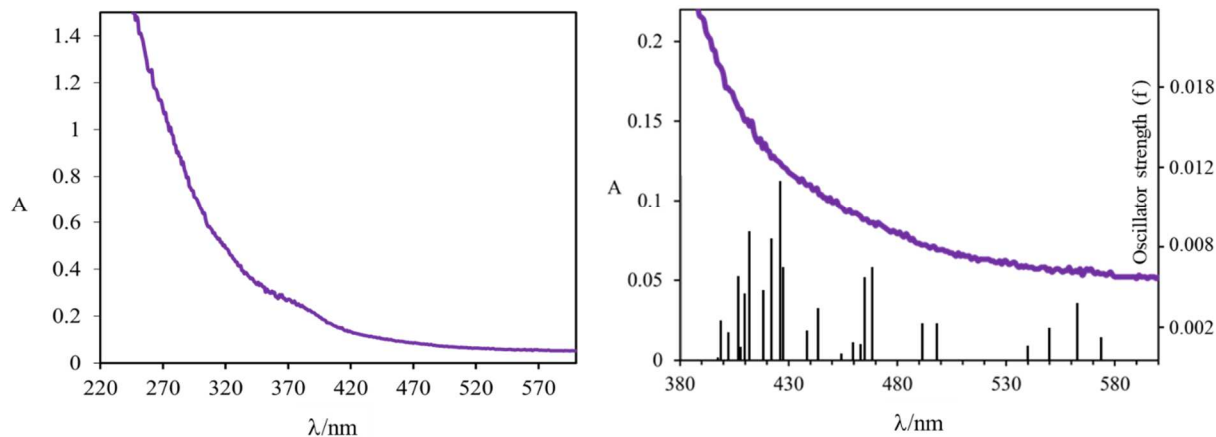


**Figure 3.9.**  $^{31}\text{P}$  NMR showing **5** prior to photolysis (top), after 20 min photolysis (middle), and thermal regeneration of **5** at 70 °C.

### 3.4 Analysis of Electronic Structure: UV-vis Spectroscopy, TD-DFT Analysis, and Structural Optimizations

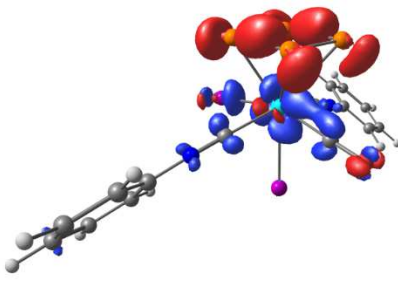
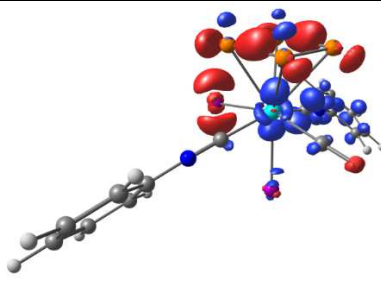
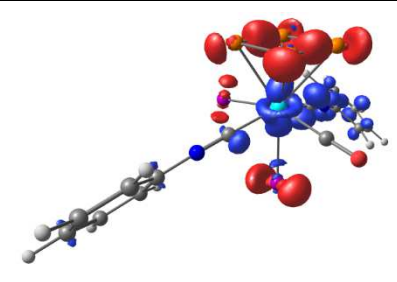
**Methods.** Density Functional Theory (DFT) calculations were performed with ORCA 4.0.0 program suite<sup>43</sup> at the BP86 level of theory.<sup>44,45</sup> Relativistic effects were accounted for by zeroth-order regular approximation (ZORA).<sup>46–50</sup> The relativistic recontracted Ahlrichs triple- $\zeta$  basis set ZORA-def2-TZVP was used with a segmented all-electron relativistically contracted SARC/J auxiliary basis set.<sup>46,51</sup> Atomic coordinates obtained by single-crystal XRD used as the starting point for optimizations, however, structures were truncated with phenyl isocyanide (CNPh) in place of  $\text{CNAr}^{\text{Dipp}2}$ . *ChemCraft 1.8* was used for visualization of geometry optimized structures and molecular orbitals (MO).<sup>52</sup>

### 3.4.1 UV-vis Spectroscopy and TD-DFT Calculations.



**Figure 3.10.** Experimental UV-vis spectrum of **5** (left) and zoomed-in view of UV-vis with calculated vertical transitions represented by black bars (right).

**Table 3.1.** TD-DFT difference density plots (red = ground state, blue = excited state) and the corresponding orbital transitions.

 <p>State 14 (transition, weight):            160a → 165a, 0.903            162a → 167a, 0.0564</p>	 <p>State 21 (transition, weight):            160a → 166a, 0.619            162a → 168a, 0.014            163a → 171a, 0.302            164a → 170a, 0.013            164a → 171a, 0.017</p>	 <p>State 24 (transition, weight):            159a → 166a, 0.704            162a → 168a, 0.187            162a → 169a, 0.031            163a → 171a, 0.021            164a → 171a, 0.025</p>
--	---	---

### 3.4.2 Example ORCA input file for geometry optimization

```
! RKS Opt BP86 ZORA ZORA-def2-TZVP SARC/J KeepDens VerySlowConv
TightSCF
%basis
NewGTO Mo "old-ZORA-TZVP" end
NewGTO I "old-ZORA-TZVP" end
end

%output
Print[ P_Basis ] 2
Print[ P_MOs ] 1
end

* xyz 0 1
I      -1.764806      7.553053      12.608138
I      -1.118485      9.801704      9.655824
I      -1.764806      7.553053      12.608138
Mo      0.419455      9.228118      11.937475
P       2.926667      8.907011      12.566388
P       1.549457      7.543662      13.490519
P       1.949251     10.575033      13.542520
P       0.579301      9.194346      14.482547
N      -1.659539     11.446428      13.052225
C       0.963061      4.448178      7.043893
H       0.446332      4.269799      6.266019
C      -3.542893     12.923736     12.658504
C       2.839011      3.902766      8.424145
H       3.594074      3.354103      8.603667
C       2.504175      4.924962      9.296275
C      -2.739383     12.544476     14.945058
C      -4.538926     13.718376     13.160684
H      -5.153365     14.132293     12.566433
C       2.083717      3.682434      7.305383
H       2.333645      2.993878      6.698949
C       0.578962      5.466762      7.895222
C      -3.769640     13.340922     15.407123
H      -3.864663     13.490043     16.339767
C      -4.663125     13.926066     14.524594
H      -5.365064     14.473537     14.857697
C      -2.682401     12.316920     13.564806
C       1.396251      5.706960      9.022899
C      -0.891994     10.716804     12.677819
C       1.520100     10.500084     10.832530
O       2.148134     11.236932     10.201090
C       0.895965      7.626738     10.626012
N       1.080332      6.745410      9.889085
H      -3.430298     12.774036     11.594872
H      -2.011048     12.116859     15.618164
H       3.099973      5.109202     10.178024*
```

### 3.4.3 Geometry optimized of *cyclo*-P<sub>4</sub> model complexes 2M and 5M

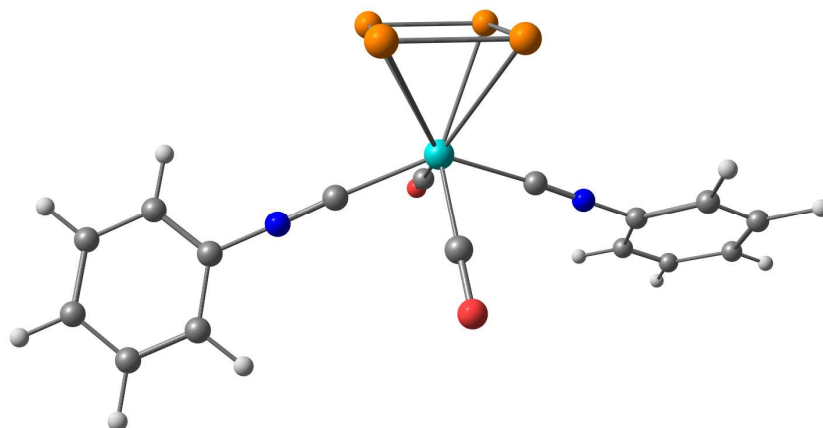


**Figure 3.11.** Optimized model complex  $(\eta^4\text{-P}_4)\text{Mo}(\text{CO})_2(\text{CNPh})_2$  (**2M**).

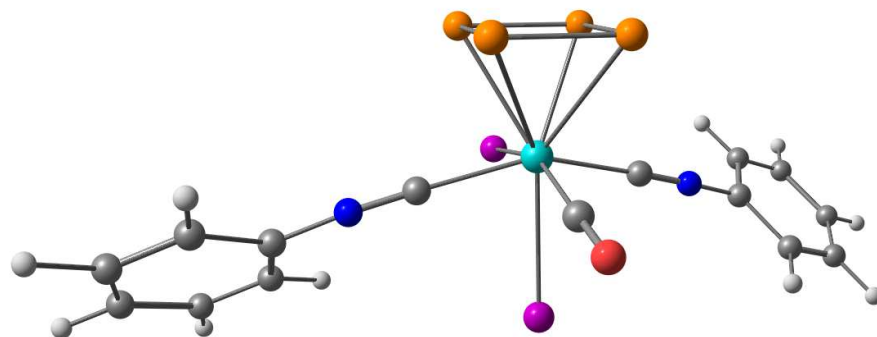


**Figure 3.12.** Optimized model complex  $(\eta^4\text{-P}_4)\text{Mo}_2(\text{CO})(\text{CNPh})_2$  (**5M**).

### 3.4.4 Molecular orbital analysis of *cyclo*-P<sub>4</sub> complexes 2M and 5M

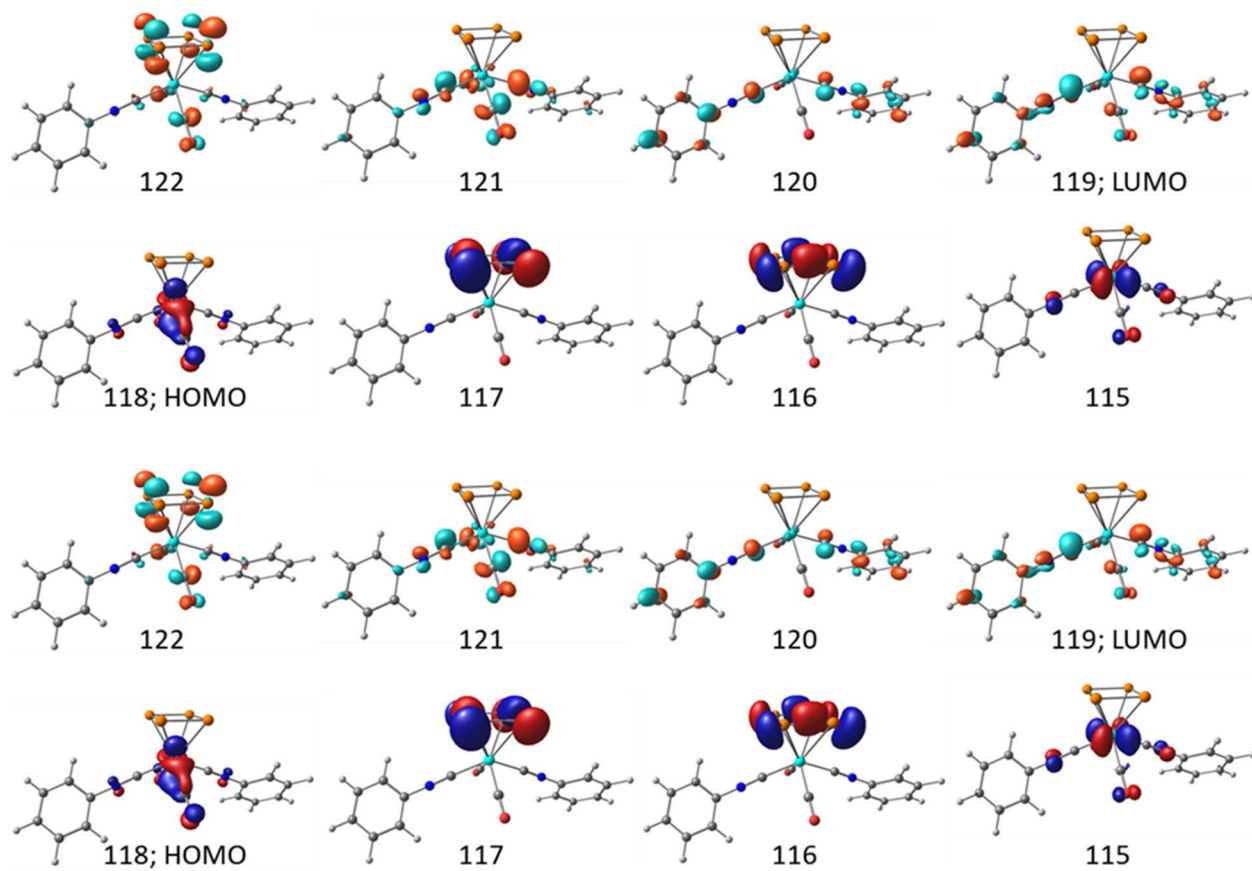


**Figure 3.13.** Molecular Orbitals Calculated for  $(\eta^4\text{-P}_4)\text{Mo}(\text{CO})_2(\text{CNPh})_2$  (2M).



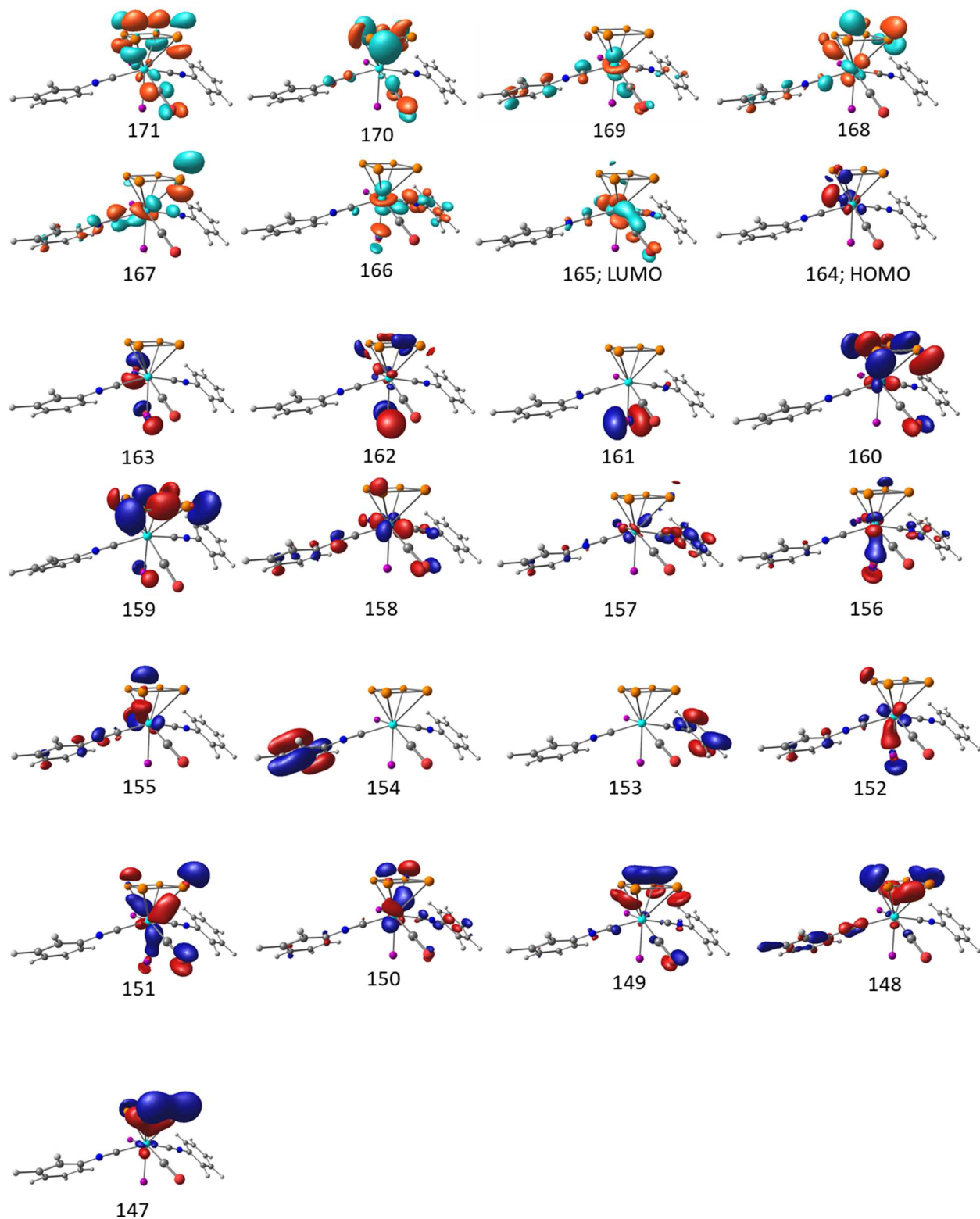


**Figure 3.14.** Molecular orbitals calculated for  $(\eta^4\text{-P}_4)\text{Mo}_2(\text{CO})(\text{CNPh})_2$  (**5M**).

### 3.4.5 Geometry Optimized Coordinates

#### ( $\eta^4$ -P<sub>4</sub>)Mo(CO)<sub>2</sub>(CNPh)<sub>2</sub> (**2M**)

Mo	13.00873877	13.6560661	16.59656447
P	13.05853934	15.17328834	18.73165746
P	14.56155805	13.60111343	18.70896928
P	11.4695764	13.65351571	18.71947963
P	12.97264079	12.08162237	18.68961664
N	10.90690135	15.87377824	15.47378327
N	15.10599406	11.47332412	15.39896737
O	14.91798491	15.51749065	14.8840022
O	11.08561673	11.842108	14.84891889
C	15.99175453	10.55285318	14.88760871
C	9.928989728	18.06595009	15.63397899
C	17.03509523	8.377217385	14.98817004
H	17.1502889	7.407667969	15.47439093
C	16.13669157	9.302850673	15.51414562
C	11.65857587	15.07497717	15.9150223
C	9.309422563	16.5624788	13.81259161
C	14.35719302	12.25858969	15.868547
C	16.74193627	10.8697691	13.74213446
C	10.05157759	16.82975245	14.97590665
C	17.6324588	9.929107084	13.22901116
H	18.21323733	10.1715656	12.33817495
C	17.78272805	8.683986908	13.84718161
H	18.48199632	7.952646029	13.4398643
C	8.451266866	17.5393361	13.31194405
H	7.877572035	17.33570403	12.40697875
C	14.21336824	14.82955676	15.49529768
C	9.06301451	19.02850159	15.11989036
H	8.966313787	19.98798797	15.62969278
C	8.32462092	18.771634	13.96052154
H	7.650849048	19.53172648	13.56305995
C	11.79665464	12.51332247	15.47115864
H	10.51140179	18.25128542	16.53589192
H	9.417420782	15.59736002	13.31837749
H	15.54668687	9.078272082	16.40218183
H	16.61595657	11.84463912	13.27199574

### **( $\eta^4$ -P<sub>4</sub>)MoI<sub>2</sub>(CO)(CNPh)<sub>2</sub> (5M)**

I	-1.50463869	7.33524229	12.85397306
Mo	0.59029921	9.23708057	12.03684502
P	1.81279360	7.55526193	13.53532052
P	3.15179726	9.03925004	12.61175866
P	2.11326887	10.63919142	13.66199678
P	0.76792950	9.16611212	14.59058173
N	1.39410672	6.76754466	10.02852629
C	1.13727225	7.65395449	10.75901450
N	-1.64358559	11.40369661	13.07846019
C	-2.94318534	13.40045620	12.76017742
C	2.88348754	4.24241085	7.81895863
H	3.86709412	3.92530417	7.47125993
C	2.78236974	5.31079008	8.70768257
C	0.47423289	3.98960225	7.82223002
H	-0.42306798	3.47445995	7.47782837
C	-3.42018682	11.88811752	14.62042840
C	-4.45471625	12.72904729	15.02394893
H	-5.04515561	12.46871237	15.90314720
C	0.35107785	5.05419157	8.71195361
C	-3.98283284	14.22749682	13.17944978
H	-4.20436402	15.13592981	12.61826769
C	1.73470167	3.58094601	7.37497991
H	1.82208130	2.74490132	6.67978071
C	-2.66686520	12.23067327	13.48587796
C	1.51242204	5.71170785	9.15042003
C	-0.81844105	10.64573066	12.71877927
C	-4.73789404	13.89680342	14.30865056
H	-5.55042666	14.54953165	14.63039338
C	1.52455054	10.61286968	10.87956497
O	2.07558936	11.39784533	10.23725473
I	-1.08906565	9.65885311	9.70661101
H	-3.18931741	10.96992610	15.15979430
H	-2.34723593	13.63776927	11.87940179
H	-0.62042832	5.38772365	9.07495551
H	3.66706460	5.83899621	9.06194828

## **3.5 Crystallographic Structure Determinations**

**General.** Single X-ray structure determinations were performed at 100 K on Bruker Kappa diffractometers equipped with a Mo radiation source and an APEX-II CCD area detector. All

structures were solved via direct methods with SHELXS<sup>13</sup> and refined by full-matrix least-squares procedures using SHELXL<sup>13</sup> within the Olex2<sup>14</sup> software. All hydrogen atoms were omitted for clarity. Crystallographic data collection and refinement information is listed in Table 3.2.

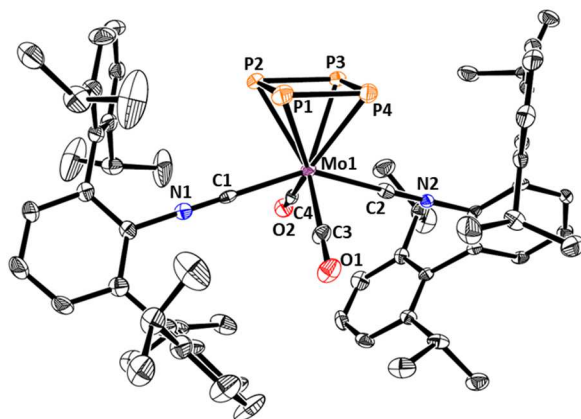


**Figure 3.15.** Molecular structure of  $(\eta^4\text{-P}_4)\text{Mo}(\text{CO})_2(\text{CNAr}^{\text{Dipp}2})_2$  (**2**). Selected bond distances (Å) and angles (deg). Mo-P1 = Mo-P2 = 2.574(2), Mo-P3 = Mo-P4 = 2.582(2), Mo-P4(centroid) = 2.075, Mo-C1 = 2.005(5), Mo-C2 = 2.022(6), Mo-C3 = 2.115(5), Mo-C4 = 2.013, C1-O1 = 1.142(6), C2-O2 = 1.136(7), C3-N1 = 1.153(6), C4-N2 = 1.152(6), P1-P2 = 2.152(2), P1-P4 = 2.173(2), P2-P3 = 2.180(2), P3-P4 = 2.148(2), C3-Mo-C4 = 147.4(2), C2-Mo-C1 = 111.6(2), P1-P2-P3 = 90.07(8), P1-P4-P3 = 90.38(8), P2-P3-P4 = 89.73(8).

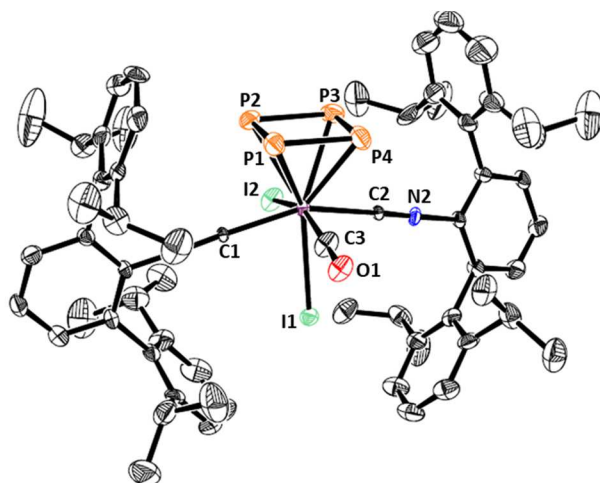


**Figure 3.16.** Molecular structure of  $(\eta^4\text{-P}_4)\text{MoI}_2(\text{CO})(\text{CNAr}^{\text{Dipp}2})_2$  (**5**). Selected bond distances (Å) and angles (deg): Mo-P1 = Mo-P4 = 2.599(5), Mo-P2 = Mo-P3 = 2.552(4), Mo-C1 = Mo-C2 = 2.12(1), Mo-C3 = 2.01(2), Mo-I1 = 2.8109(9), Mo-I2 = 2.833(2), C3-O1 = 1.15(3), P1-P2 = 2.147(6), P1-P4 = 2.166(5), P2-P3 = 2.156(5), P3-P4 = 2.160(6), P1-P2-P3 = P2-P3-P4 = P2-P1-P4 = 90.2(3), P3-P4-P1 = 89.4(2). C1-Mo-C2 = 152.1(4), C3-Mo-I1 = 74.0(5), C3-Mo-I2 = 157.7(5).

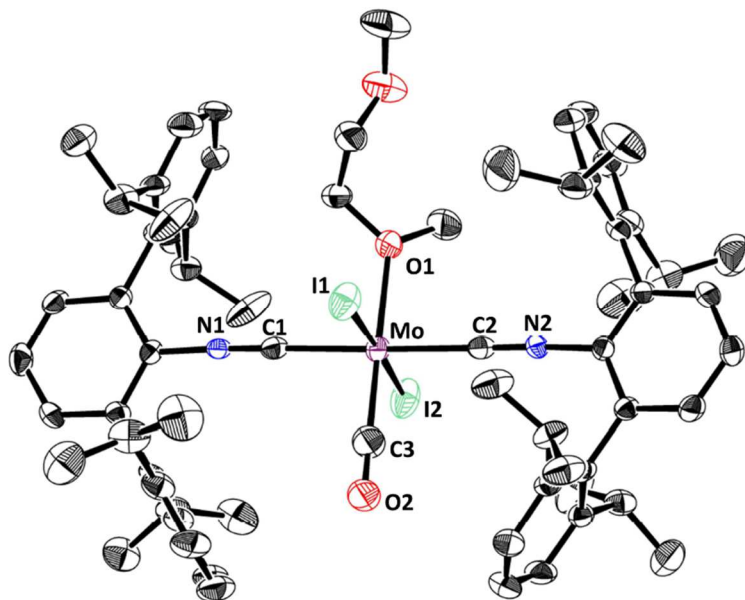


**Figure 3.17.** Molecular structure of  $\text{MoI}_2(\text{CO})_2(\text{CNAr}^{\text{Dipp}2})_2(\text{DME})$  (**6**).  $\text{C1-Mo} = \text{C2-Mo} = 2.142(8)$ ,  $\text{Mo-O1} = 2.271(4)$ ,  $\text{Mo-I1} = \text{Mo-I2} = 2.731(1)$ ,  $\text{C1-Mo-C2} = 178.5(2)$ ,  $\text{O1-Mo-C3} = 179.5(3)$ ,  $\text{I1-Mo-I2} = 178.01(3)$ .

**Table 3.2.** Crystallographic Data Collection and Refinement Information

	$(\eta^4\text{-P}_4)\text{Mo}(\text{CO})_2$ $(\text{CNAr}^{\text{Dipp}2})_2$ ( <b>2</b> )	$(\eta^4\text{-P}_4)\text{MoI}_2(\text{CO})$ $(\text{CNAr}^{\text{Dipp}2})_2 \cdot 0.32 \text{Et}_2\text{O}$ ( <b>5</b> )	$\text{MoI}_2(\text{CO})_2(\text{CNAr}^{\text{Dipp}2})_2$ ( <b>6</b> )
Formula	$\text{C}_{69}\text{H}_{84}\text{MoN}_2\text{O}_2\text{P}_4$	$\text{C}_{63.6}\text{H}_{75.5}\text{I}_2\text{MoN}_2\text{O}_{1.2}\text{P}_4$	$\text{C}_{74.9}\text{H}_{102}\text{I}_2\text{MoN}_2\text{O}_{6.9}$
Crystal System	Monoclinic	Monoclinic	Triclinic
Space Group	$P2_1/c$	$C2$	$P-1$
$a$ , Å	17.3171(9)	25.103(4)	12.745(2)
$b$ , Å	17.4470(11)	18.060(3)	16.4561(18)
$c$ , Å	21.4553(12)	17.710(5)	18.975(3)
$\alpha$ , deg	90	90	104.653(3)
$\beta$ , deg	90.034(2)	122.973(3)	94.687(3)
$\gamma$ , deg	90	90	98.460(4)

V, Å <sup>3</sup>	6482.3(6)	6736(2)	3778.8(9)
Z	4	4	2
Radiation (λ, Å)	Mo-Kα, 0.71073	Mo-Kα, 0.71073	Mo-Kα, 0.71073
ρ (calcd.), g/cm <sup>3</sup>	1.223	1.327	1.312
Temp, K	100	100	100
θ max, deg	25.377	20.9	25.079
data/parameters	11464/722	12464/660	13391/830
R <sub>1</sub>	0.0574	0.0525	0.0549
wR <sub>2</sub>	0.1398	0.1157	0.1440
GooF	1.009	0.991	1.008

### 3.6 Acknowledgements

Chapter 3 was adapted with permission from Mandla, K. A.; Moore, C. E.; Rheingold, A. L.; Figueroa, J. S. “Photolytic Reductive Elimination of White Phosphorus from a Mononuclear *cyclo*-P<sub>4</sub> Transition Metal Complex: Bespoke P<sub>4</sub> Release Using Benign Stimulus,” *Angewandte Chemie, International Edition*, **2018**, *Accepted*. Copyright 2018 Wiley-VCH, Weinheim. The dissertation author is the first author of this paper.

### 3.7 References

- (1) Greenwood, N. N. 1997th ed.; Earnshaw, A., Ed.; Elsevier, 1997.
- (2) Corbridge, D. Elsevier: Amsterdam, 2000.
- (3) Quin, L. D. Wiley: New York, 2000.
- (4) European Commission. EU List of Critical Raw Materials, European Commission, Brussels, 2017.

- (5) Scheer, M.; Balázs, G.; Seitz, A. *Chem. Rev* **2010**, *110*, 4236–4256.
- (6) Cossairt, B. M.; Piro, N. A.; Cummins, C. C. *Chem. Rev.* **2010**, *110* (7), 4164–4177.
- (7) Caporali, M.; Gonsalvi, L.; Rossin, A.; Peruzzini, M. *Chem. Rev.* **2010**, *110* (7), 4178–4235.
- (8) Mal, P.; Breiner, B.; Rissanen, K.; Nitschke, J. R. *Science*. **2009**, *324* (5935), 1697–1699.
- (9) Schwarzmaier, C.; Schindler, A.; Heindl, C.; Scheuermayer, S.; Peresyphina, E. V.; Virovets, A. V.; Neumeier, M.; Gschwind, R.; Scheer, M. *Angew. Chemie Int. Ed.* **2013**, *52* (41), 10896–10899.
- (10) Choi, W.; Ohtsu, H.; Matsushita, Y.; Kawano, M. *Dalt. Trans.* **2016**, *45* (15), 6357–6360.
- (11) Yang, D.; Zhao, J.; Yu, L.; Lin, X.; Zhang, W.; Ma, H.; Gogoll, A.; Zhang, Z.; Wang, Y.; Yang, X.-J.; et al. *J. Am. Chem. Soc.* **2017**, *139* (20), 7130.
- (12) Yang, D.; Zhao, J.; Yu, L.; Lin, X.; Zhang, W.; Ma, H.; Gogoll, A.; Zhang, Z.; Wang, Y.; Yang, X.-J.; et al. *J. Am. Chem. Soc.* **2017**, *139* (16), 5946–5951.
- (13) Seitz, A. E.; Hippauf, F.; Kremer, W.; Kaskel, S.; Scheer, M. *Nat. Commun.* **2018**, *9*, 361.
- (14) Krossing, I. *J. Am. Chem. Soc.* **2001**, *123* (19), 4603–4604.
- (15) Spitzer, F.; Sierka, M.; Latronico, M.; Mastroilli, P.; Virovets, A. V.; Scheer, M. *Angew. Chemie Int. Ed.* **2015**, *54* (14), 4392–4396.
- (16) NIST Chemistry WebBook, NIST Standard Reference Database Number 69, National Institute of Standards and Technology, Gaithersburg MD, 20899, <http://webbook.nist.gov>.
- (17) Chase, M. W. *J. Chem. Phys* **1998**, *9*, 1938.
- (18) Peruzzini, M.; Gonsalvi, L.; Romerosa, A. *Chem. Soc. Rev.* **2005**, *34* (12), 1038.
- (19) Wang, L.-P.; Tofan, D.; Chen, J.; Voorhis, T. Van; Cummins, C. C. *RSC Adv.* **2013**, *3*, 23166–23171.
- (20) Mandla, K. A.; Moore, C. E.; Rheingold, A. L.; Figueroa, J. S. *Angew. Chemie Int. Ed.* **2018**, *57* (23), 6853–6857.
- (21) Scheer, M.; Herrmann, E.; Sieler, J.; Oehme, M. *Angew. Chemie Int. Ed. English* **1991**, *30* (8), 969–971.
- (22) Scheer, M.; Becker, U.; Huffman, J. C.; Chisholm, M. H. *J. Organomet. Chem.* **1993**, *461* (1–2), C1–C3.

- (23) Velian, A.; Cummins, C. C. *Chem. Sci.* **2012**, 3 (4), 1003.
- (24) Camp, C.; Maron, L.; Bergman, R. G.; Arnold, J. J. *Am. Chem. Soc.* **2014**, 136 (50), 17652–17661.
- (25) Yao, S.; Lindenmaier, N.; Xiong, Y.; Inoue, S.; Szilvási, T.; Adelhardt, M.; Sutter, J.; Meyer, K.; Driess, M. *Angew. Chemie Int. Ed.* **2014**, 54 (4), 1250–1254.
- (26) Spitzer, F.; Graßl, C.; Balázs, G.; Zolnhofer, E. M.; Meyer, K.; Scheer, M. *Angew. Chemie Int. Ed.* **2016**, 55 (13), 4340–4344.
- (27) Pelties, S.; Maier, T.; Herrmann, D.; Bruin, B.; Rebreyend, C.; Gärtner, S.; Shenderovich, I. G.; Wolf, R. *Chem. - A Eur. J.* **2016**, 23 (25), 6094–6102.
- (28) Scherer, O. J.; Vondung, J.; Wolmershäuser, G. *Angew. Chemie Int. Ed. English* **1989**, 28 (10), 1355–1357.
- (29) Scherer, O. J.; Winter, R.; Wolmershäuser, G. *Z. anorg. allg. Chem.* **1993**, 619 (5), 827–835.
- (30) Herberhold, M.; Frohmader, G.; Milius, W. *J. Organomet. Chem.* **1996**, 522 (2), 185–196.
- (31) Cavaillé, A.; Saffon-Merceron, N.; Nebra, N.; Fustier-Boutignon, M.; Mézailles, N. *Angew. Chemie Int. Ed.* **2018**, 57 (7), 1874–1878.
- (32) Kraus, F.; Aschenbrenner, J. C.; Korber, N. *Angew. Chemie Int. Ed.* **2003**, 42 (34), 4030–4033.
- (33) Jiménez-Halla, J. O. C.; Matito, E.; Robles, J.; Solà, M. *J. Organomet. Chem.* **2006**, 691 (21), 4359–4366.
- (34) Rathenau, G. *Physica* **1937**, 4 (6), 503–514.
- (35) Tofan, D.; Cummins, C. C. *Angew. Chemie - Int. Ed.* **2010**, 49 (41), 7516–7518.
- (36) Mandla, K. A.; Moore, C. E.; Rheingold, A. L.; Figueroa, J. S. *Angew. Chemie Int. Ed.* **2018**, 57 (23), 6853–6857.
- (37) Ditri, T. B.; Moore, C. E.; Rheingold, A. L.; Figueroa, J. S.; Ditri, B.; Moore, C. E.; Rheingold, A. L.; Figueroa, J. S. *Inorg. Chem.* **2011**, 50 (20), 10448–10459.
- (38) Lever, A. *J. Chem. Ed.* **1974**, 51, 612–614.
- (39) Armarego, W. L. F.; Chai, C. L. L. 5th ed.; Elsevier, 2003.
- (40) Pangborn, A. B.; Giardello, M. A.; Grubbs, R. H.; Rosen, R. K.; Timmers, F. J.



*Organometallics* **1996**, *15* (5), 1518–1520.

- (41) Fox, B. J.; Sun, Q. Y.; DiPasquale, A. G.; Fox, A. R.; Rheingold, A. L.; Figueroa, J. S. *Inorg. Chem.* **2008**, *47* (19), 9010–9020.
- (42) Reich, H. J. *J. Chem. Educ.* **1995**, *72* (12), 1086.
- (43) Neese, F. *Wiley Interdiscip. Rev. Comput. Mol. Sci.* **2012**, *2* (1), 73–78.
- (44) Becke, A. D. *Phys. Rev. A* **1988**, *38* (6), 3098–3100.
- (45) Perdew, J. P. *Phys. Rev. B* **1986**, *33* (12), 8822–8824.
- (46) Pantazis, D. A.; Chen, X.-Y. Y.; Landis, C. R.; Neese, F. *J. Chem. Theory Comput.* **2008**, *4* (6), 908–919.
- (47) Weigend, F.; Ahlrichs, R. *Phys. Chem. Chem. Phys.* **2005**, *7* (18), 3297.
- (48) Lenthe, E. van; Baerends, E. J.; Snijders, J. G. *J. Chem. Phys.* **1993**, *99* (6), 4597–4610.
- (49) Lenthe, E. van; Snijders, J. G.; Baerends, E. J. *J. Chem. Phys.* **1996**, *1051* (10), 6505–154104.
- (50) Werner, H. J.; Manby, F. R.; Knowles, P. J. *J. Chem. Phys.* **2003**, *118* (18), 8149–8160.
- (51) Lee, C.; Yang, W.; Parr, R. G. *Phys. Rev. B* **1988**, *37* (2), 785–789.
- (52) Zhurko, G. A.; Zhurko, D. A. ChemCraft 2014, [www.chemcraftprog.com](http://www.chemcraftprog.com).

## Chapter 4

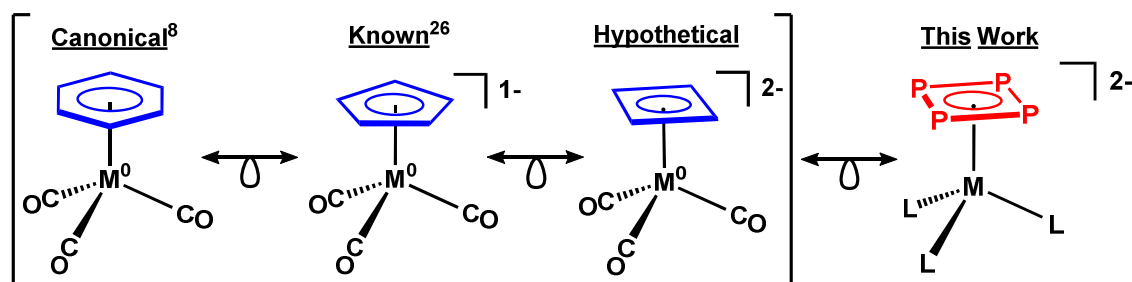
### A *cyclo-P<sub>4</sub>* Analog of Mo(CO)<sub>3</sub>( $\eta^6$ -benzene)

#### 4.1 Introduction

Nearly 70 years ago, Peter L. Pauson and Thomas J. Kealy confounded the field of inorganic chemistry with a report describing the unintended synthesis of a compound with the formula Fe(C<sub>5</sub>H<sub>5</sub>)<sub>2</sub>.<sup>1,2</sup> The subsequent discovery that all six  $\pi$ -electrons from each cyclopentadienyl ligand were engaged in chemical bonds with the Fe(II) metal-center marked a renaissance in the understanding of chemical structure and bonding.<sup>3-6</sup> A short time later, Fischer and co-workers showed that the same principles were applicable in the coordination of neutral aromatic ligands with the preparation of ( $\eta^6$ -C<sub>6</sub>H<sub>6</sub>)Cr( $\eta^6$ -C<sub>6</sub>H<sub>6</sub>)<sup>7</sup> and ( $\eta^6$ -C<sub>6</sub>H<sub>6</sub>)Cr(CO)<sub>3</sub>.<sup>8</sup> This concept was further extended with an interesting proposal by Orgel and Longuet-Higgins suggesting that cyclobutadiene, despite being antiaromatic, could be stabilized in transition metal complexes by donation of its 4n  $\pi$ -electrons.<sup>9</sup>

It followed, therefore, that when this prediction came to fruition<sup>10-12</sup> cyclobutadiene (Cb) ligands were regarded as being transition-metal-stabilized antiaromatic species which were otherwise analogous to other *cis*-dienes.<sup>13-15</sup> Purporting to support this view was the ligand-based reactivity toward nucleophiles,<sup>10,14,16,17</sup> and the release of neutral cyclobutadiene from Fe(CO)<sub>3</sub>(Cb), which was thought to result from metal-based oxidation.<sup>14,18,19</sup> Contrasting this notion, however, were structural and spectroscopic investigations showing the four C-H groups of Fe(CO)<sub>3</sub>(Cb) to be equivalent,<sup>20</sup> suggesting instead that cyclobutadiene was aromatic. This view became widely accepted following investigations showing participation of ligated cyclobutadiene in electrophilic aromatic substitution.<sup>21,22</sup>

Two common interpretations describing the origins of aromaticity have been offered. With respect to  $\text{Fe}(\text{CO})_3(\text{Cb})$ , Bursten and Fenske suggested  $d^8$ -configuration is retained, and Hückel's  $4n+2$  rule is satisfied due to a high degree of covalency between iron and the degenerate  $\pi$ -orbitals of cyclobutadiene.<sup>23</sup> Conversely, Clack and Warren suggested that cyclobutadiene becomes aromatic in what can be considered a formal two-electron metal-to-ligand charge transfer. In their analysis of electron distribution in  $\text{CpCoCb}$ , they suggest Cb is best regarded as a dianionic ligand interacting with a  $d^6$ -metal center to give an overall electronic structure resembling ferrocene.<sup>24</sup> By this interpretation, the interactions of a metal-center with the six  $\pi$ -electrons of cyclobutadiene should be analogous to interactions with benzene. Admittedly, the distinction between these two explanations may be relegated to a matter of formalisms, however, this view neglects the conceptual importance of charge distribution in covalent metal-ligand interactions. Indeed, the conceptual formalism by which Cp came to be understood as an anionic, six-electron donor has provided an important basis for pursuit and discovery of anionic Cp-metallates supported by otherwise neutral ligand fields while also helping to confirm the analogy between coordination complexes of benzene and Cp (Scheme 4.1).<sup>25-27</sup> Absent from the literature are dianionic cyclobutadienyl complexes which would serve as an important step toward inclusion of 4-membered rings into the well-established analogy between  $\eta^5$ -cyclopentadiene and  $\eta^6$ -benzene (Scheme 4.1).



**Scheme 4.1.** Isolobal analogy of  $n$ -membered aromatic rings with Group 6 carbonyls.

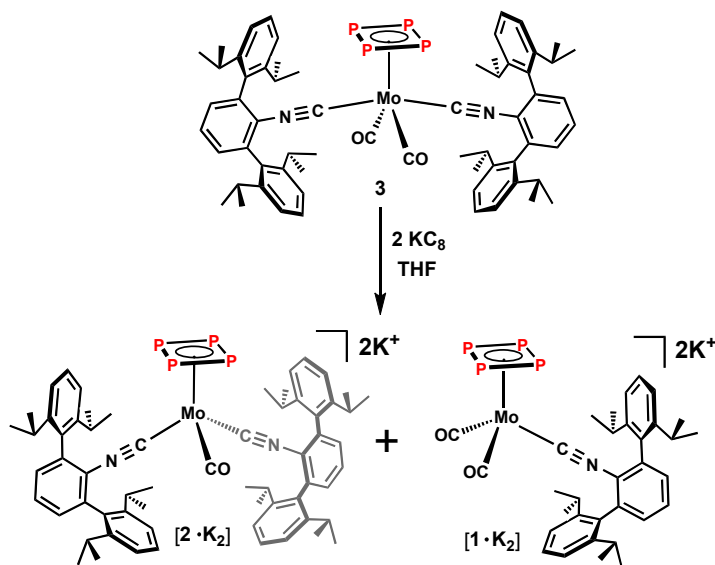
Hindering this objective is the large extent of charge localization in all-carbon cyclobutadiene ligands preventing substantial  $\pi$ -backdonation from the metal-center. The challenge has been overcome in this work by utilizing the enhanced  $\pi$ -acceptance<sup>28</sup> of a carbon-free analog to cyclobutadiene, tetraphospha-cyclobutadiene (*cyclo*-P<sub>4</sub>). Providing further kinetic stabilization of the highly reduced metal complexes in this work are kinetically stabilizing *m*-terphenyl isocyanide ligands CNAr<sup>Dipp2</sup> (2,6-(2,6-(*i*-Pr)<sub>2</sub>C<sub>6</sub>H<sub>3</sub>)<sub>2</sub>C<sub>6</sub>H<sub>3</sub>) which are isolobal to CO. By applying these strategies, unlikely analogs to the canonical Group 6  $\eta^6$ -benzene complexes,<sup>8</sup> M(CO)<sub>3</sub>( $\eta^6$ -C<sub>6</sub>H<sub>6</sub>), have been prepared. Reported herein is the synthesis of *cyclo*-P<sub>4</sub> dianions [( $\eta^4$ -P<sub>4</sub>)Mo(CO)<sub>3-n</sub>(CNAr<sup>Dipp2</sup>)<sub>n</sub>]<sup>2-</sup>, n = 1 [**1**·K<sub>2</sub>], n = 2 [**2**·K<sub>2</sub>].

## 4.2 Results and Discussion

### 4.2.1 Synthesis and characterization of dianionic *cyclo*-P<sub>4</sub> complexes [**1**·K<sub>2</sub>] and [**2**·K<sub>2</sub>]

In the previous chapter, syntheses of the first examples of mononuclear Group 6 *cyclo*-P<sub>4</sub> complexes, ( $\eta^4$ -P<sub>4</sub>)Mo(CO)<sub>2</sub>(CNAr<sup>Dipp2</sup>)<sub>2</sub> (**3**) and ( $\eta^4$ -P<sub>4</sub>)MoI<sub>2</sub>(CO)(CNAr<sup>Dipp2</sup>)<sub>2</sub> (**4**). In that work, spectroscopy and DFT investigations were consistent with coordination of a formally dianionic *cyclo*-P<sub>4</sub> ligand to transition to formally di- and tetravalent metal centers, respectively. Importantly, these complexes provided the first examples demonstrating the ability of *cyclo*-P<sub>4</sub> to support a metal in multiple oxidation states. In consideration of this fact and previous work whereby *cyclo*-P<sub>5</sub> ligands were found to support highly reduced analog to titanocene dianion,<sup>28</sup> we sought to determine if *cyclo*-P<sub>4</sub> would provide similar stabilization of highly reduced species. When a thawing THF solution of **3** was allowed to react with 2.1 equivalents of KC<sub>8</sub> the color deepened from orange to dark red. <sup>31</sup>P NMR (THF, 122 MHz) of the crude reaction mixture

showed two independent chemical shifts in a 2:1 ratio at 105 and 121 ppm, thus indicating the formation of two new products wherein the *cyclo*-P<sub>4</sub> substituent had remained intact without undergoing further activation. Confirmation of a metal-based reduction was obtained by FTIR (THF, KBr windows), which showed a large bathochromic shift of CO stretching frequencies as low as 1635 cm<sup>-1</sup>. Also observed by FTIR, however, was the presence of free isocyanide at 2116 cm<sup>-1</sup>. <sup>1</sup>H NMR provided additional insight into the distribution of isocyanide containing products by analysis of septet peaks corresponding to methine proton resonances of the CNAr<sup>Dipp</sup><sub>2</sub> isopropyl groups. Interestingly, <sup>1</sup>H NMR (300 MHz) in C<sub>6</sub>D<sub>6</sub> showed only two soluble products: the major phosphorus-containing product, with two magnetically inequivalent isopropyl groups at 3.10 and 3.05 ppm, and free isocyanide at 2.70 ppm. Noting that magnetic inequivalence of the isocyanide isopropyl groups likely suggested bis-isocyanide coordination in the major product, the integration of the <sup>1</sup>H CNAr<sup>Dipp</sup><sub>2</sub> methine resonances corresponded to a 2:1 molar ratio of the major product to free CNAr<sup>Dipp</sup><sub>2</sub> – the same ratio as was observed between the major and minor phosphorus-containing species by <sup>31</sup>P NMR in THF.



**Scheme 4.2.** Synthetic pathway for synthesis of *cyclo*-P<sub>4</sub> dianions [2·K<sub>2</sub>] and [1·K<sub>2</sub>] (gives 2:1 ratio), and rectification of [1·K<sub>2</sub>] by thermolysis in presence of CO.

Conveniently, solubility differences enabled facile separation of the three spectroscopically observed products. First, free ligand was removed by extracting an acetonitrile solution of the crude reaction mixture with pentane. The acetonitrile phase, containing both phosphorus containing products, was concentrated and dissolved in a 2%-THF/pentane solution. The resulting solution was stored 3h at -40 °C to afford the minor dicarbonyl dianion  $[(\eta^4\text{-P}_4)\text{Mo}(\text{CO})(\text{CNAr}^{\text{Dipp}_2})_2][\text{K}_2]$  ( $[\mathbf{2}\cdot\mathbf{K}_2]$ ), as confirmed by X-ray crystallography (Figure 4.1), as a pure, yellow, microcrystalline product in 11% yield. Reduction of the solution phase afforded the major product as an analytically pure amorphous red solid. Spectroscopy and combustion analysis of this material were consistent with formulation of  $[\mathbf{2}\cdot\mathbf{K}_2]$  as the mono-decarbonylated product  $[(\eta^4\text{-P}_4)\text{Mo}(\text{CO})(\text{CNAr}^{\text{Dipp}_2})_2][\text{K}_2]$ , obtained in 64% yield.

Consistent with other zero-valent metallates were broad  $\text{C}\equiv\text{N}$  and  $\text{C}\equiv\text{O}$  stretching frequencies by FTIR of . We attribute complexity in the FTIR data to exchanging interactions between and the potassium counterions. Supporting this assessment, X-ray crystallography of  $[\mathbf{1}\cdot\mathbf{K}_2]$  (Figure 4.1) showed the presence of two non-equivalent potassium ions in the asymmetric unit; one formed close-ion-interactions with a flanking 2,6-diisopropyl arene of the ligand, a P-atom lone pair, and the CN  $\pi$ -electrons; the other cation interacted primarily with the O-atom of the CO ligand. Interestingly, the extended structure reveals that each potassium cation forms an additional bridging interaction with the *cyclo*-P<sub>4</sub> ring of an adjacent molecule. Crystals of  $[\mathbf{1}\cdot\mathbf{K}_2]$  are thus comprised of linear metallopolymer with each monomer forming two symmetrically inequivalent linkages through 1,1'-(*P,P*) and 3,3'-(*P,P*) bridging interactions of adjacent *cyclo*-P<sub>4</sub> rings with the cation Figure 4.2. Despite the apparent fluxionality these interactions in THF, as indicated by the presence of a single ligand environment by <sup>1</sup>H and <sup>31</sup>P NMR, it is interesting to note that unlike the amorphous material in the crude reaction mixture, crystals of  $[\mathbf{1}\cdot\mathbf{K}_2]$  are

completely insoluble in C<sub>6</sub>D<sub>6</sub>. Even when an amorphous solid of [1·K<sub>2</sub>] is prepared by concentrating a solution in which crystals were dissolved in THF, the solubility in C<sub>6</sub>D<sub>6</sub> remains negligible. It is thus likely that, although fluxional, the presence of four ionic linkages per monomeric unit (Figure 4.2, bottom) of crystalline [1·K<sub>2</sub>] are sufficient to retain some connectivity in the solution phase.

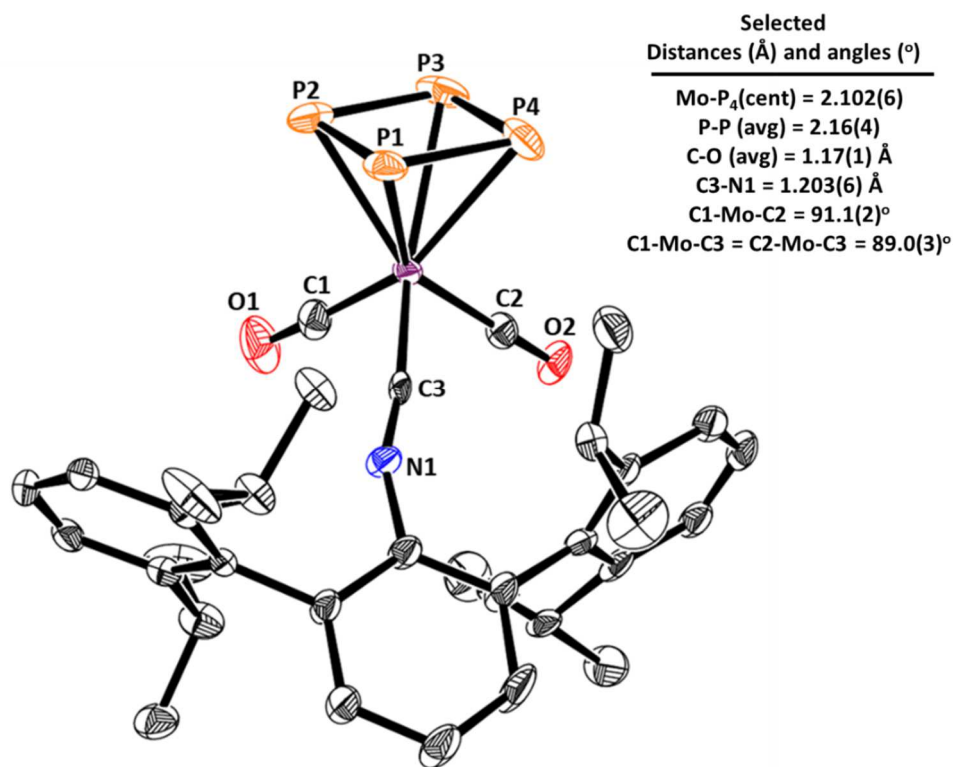


**Figure 4.1.** Molecular structure of [1]<sup>2-</sup> (K<sup>+</sup> and THF excluded for clarity).





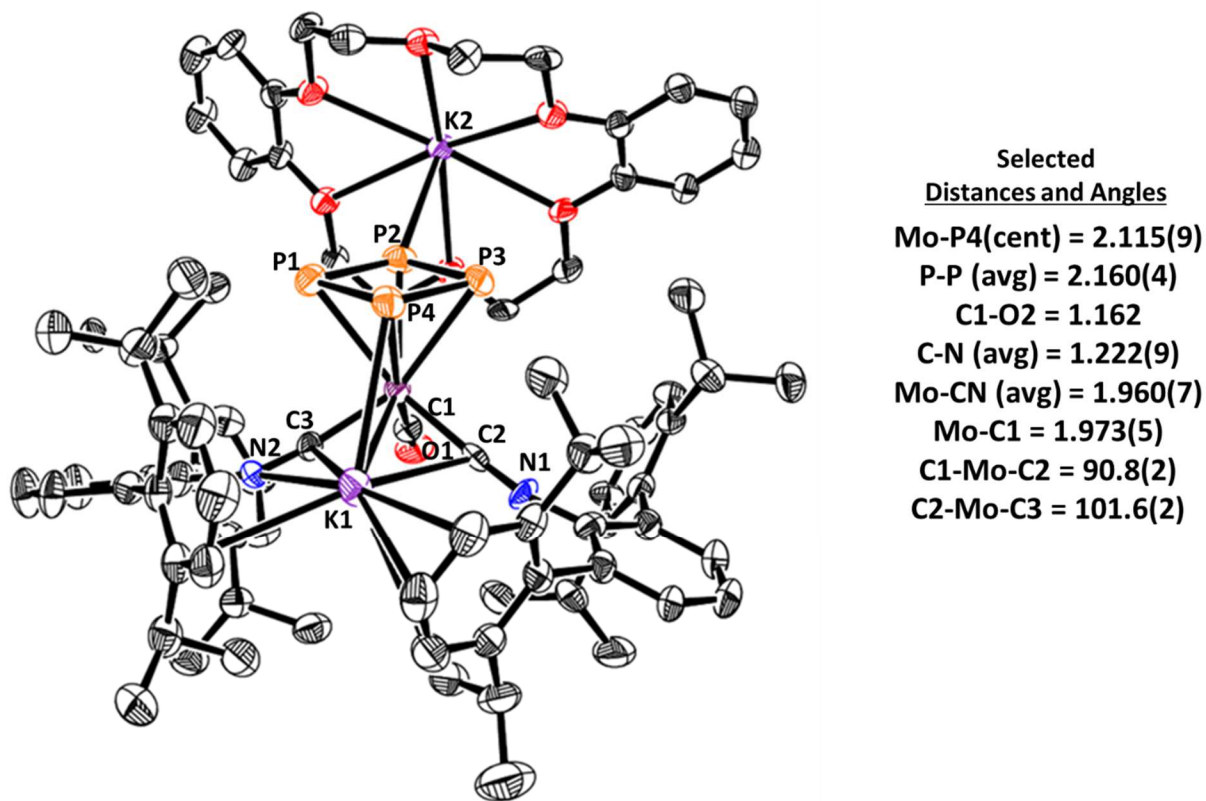


**Figure 4.3.** Molecular structure of [(db18-C-6)·K][2·K].

Although spectroscopic data and combustion analysis confirmed isolation of  $[2 \cdot K_2]$ , multiple attempts to obtain diffraction quality crystals of the *bis*-isocyanide dianion only afforded an amorphous red solid. Noting the polymeric structure of crystalline  $[1 \cdot K_2]$ , it is likely that the presence of two isocyanide ligands hinder organization of bridging interactions required for nucleation. To obtain structural data, therefore, we sought to prepare the discrete anion by sequestration of bridging cations. Treatment of a THF solution of  $[2 \cdot K_2]$  with 1 equiv dibenzo-18-crown-6 (db-18-C-6) showed an expected blue shift of CNAr and CO stretching frequencies as is consistent with the loss of  $K^+ \cdots \pi_{CO/CN}$  interactions.<sup>29</sup> Satisfyingly, overnight storage of the reaction mixture at  $-40$  °C afforded bright-red, diffraction quality crystals. X-ray crystallography revealed that sequestration of a single cation provided  $[(db18-C-6) \cdot K][2 \cdot K]$  as discrete molecular

species (Figure 4.3). The molecular structure of [(db18-C-6)·K][2·K] was consistent with NMR evidence indicating two Ar<sup>Dipp2</sup> magnetic environments by <sup>1</sup>H NMR. Accordingly, intramolecular interactions between two Ar<sup>Dipp2</sup> groups with K<sup>+</sup> appear to fix the *m*-terphenyl framework into position. The presence of two well-defined septets in the <sup>1</sup>H NMR suggests this interaction is not fluxional on the NMR timescale. This is further supported by the inability of up to 4 equiv db-18-C-6 to affect sequestration of the second cation after 24 h at rt.

It is important to note that molecular structures of both [1·K<sub>2</sub>] (Figure 4.1) and [(db18-C-6)·K][2·K] (Figure 4.3) corroborate spectroscopic data suggesting coordination of a dianionic *cyclo*-P<sub>4</sub> ligand<sup>30</sup> to a formally zero-valent metal center. Accordingly, increased  $\pi$ -backdonation in (db18-C-6)·K][2·K] and [1·K<sub>2</sub>] is indicated by shortening of M-CO and M-CN bond lengths by ca. 0.1 Å compared to **3**. Increased backdonation to ligand  $\pi^*$ -orbitals is also reflected in small bond elongation of C=O and C≡N bond lengths (Figure 4.1 and Figure 4.3), however, the measured distances remain consistent with sustained triple bond character for both CNAr<sup>Dipp2</sup> and CO ligands. Although redox noninnocence has been observed previously in *cyclo*-P<sub>4</sub> complexes, as was exemplified by Driess and co-workers with [Co- $\eta^4$ , $\eta^4$ -P<sub>4</sub>-Co] inverse sandwich complexes,<sup>30</sup> this can be ruled out in [1·K<sub>2</sub>] and [(db18-C-6)·K][2·K] by comparison of P-P bond distances which remained ca. 2.16 Å after reduction. Instead, increased repulsion between the Mo<sup>0</sup> and [*cyclo*-P<sub>4</sub>]<sup>2-</sup> give longer Mo-P<sub>4</sub>(centroid) distances in the dianionic complexes, e.g. [1·K<sub>2</sub>] = Mo-P<sub>4</sub>(cent) = 2.1959(3) Å] compared to the neutral complex **3** [2.0749(9) Å]. The structural parameters are thus strongly consistent with sustained dianionic character of the cyclophosphabutadiene ligand irrespective of metal valency. Noting that the two additional electrons are expected to fill the degenerate P<sub>4</sub>- $\pi$ -orbitals of e<sub>g</sub> parentage, a clear analogy to the six  $\pi$ -electrons of benzene emerges.

#### 4.2.2 DFT investigation of isolobal analogy between dianionic *cyclo*-P<sub>4</sub> complexes and ( $\eta^6$ -C<sub>6</sub>H<sub>6</sub>)Mo(CO)<sub>3</sub>.

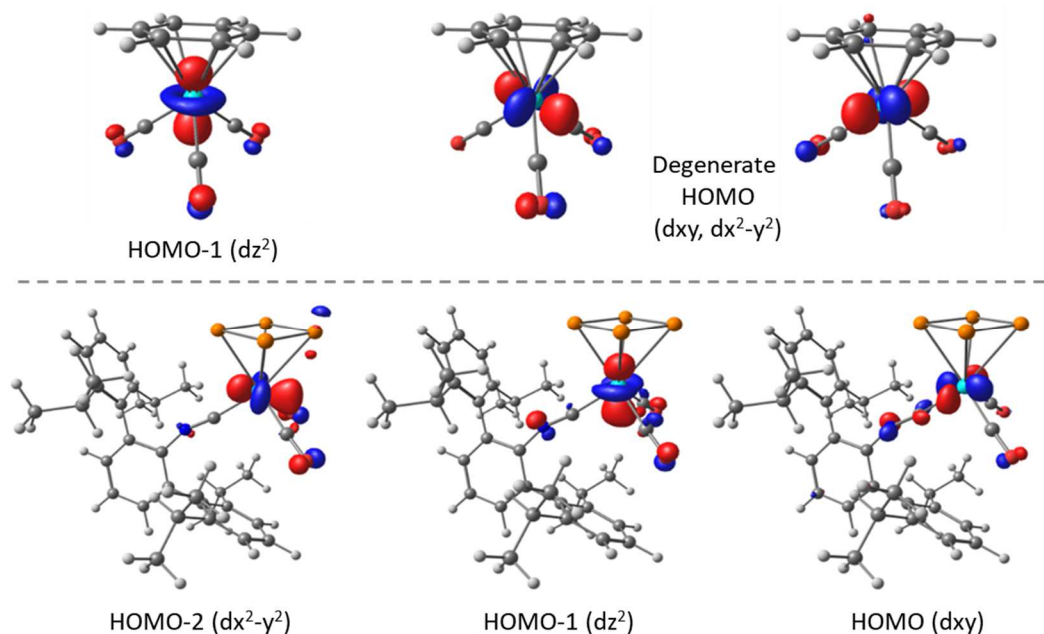


**Figure 4.4.** Filled d-orbitals of ( $\eta^6$ -C<sub>6</sub>H<sub>6</sub>)Mo(CO)<sub>3</sub> (top) and [1]<sup>2-</sup> (bottom).

Density functional theory (DFT) investigations provided a more detailed picture of the isolobal relationship between *cyclo*-P<sub>4</sub> dianions and ( $\eta^6$ -C<sub>6</sub>H<sub>6</sub>)Mo(CO)<sub>3</sub>. Accordingly, Figure 4.4 shows nearly perfect overlap in the symmetry adapted linear combinations of frontier d-orbitals for (C<sub>6</sub>H<sub>6</sub>)Mo(CO)<sub>3</sub> and [1]<sup>2-</sup>. Indeed, the only notable difference in the decomposition of d-orbitals between (C<sub>6</sub>H<sub>6</sub>)Mo(CO)<sub>3</sub> and [1]<sup>2-</sup> is the presence of a greater  $\delta$ -backbonding interaction [Mo( $dx^2-y^2$ ) $\rightarrow$ P( $\pi^*$ )] in [1]<sup>2-</sup> which stabilizes  $dx^2-y^2$  by 0.37 eV relative to  $dxy$ . The similar electronic structure of [1]<sup>2-</sup> and ( $\eta^6$ -C<sub>6</sub>H<sub>6</sub>)Mo(CO)<sub>3</sub> becomes even more apparent in an analysis of the ligand  $\pi$ -systems (Figure 4.5). Both complexes meet Huckel's criteria for aromaticity with  $4n+2$  electrons occupying the three ligand-based  $\pi$ -orbitals. Aromaticity in [1]<sup>2-</sup> was further

supported by the presence of diatropic ring current 1 Å above the P<sub>4</sub>-plane, as indicated by the NICS value of -6.98 ppm.<sup>31-33</sup> Expectedly, stronger σ-donation of the dianionic *cyclo*-P<sub>4</sub> ligand is

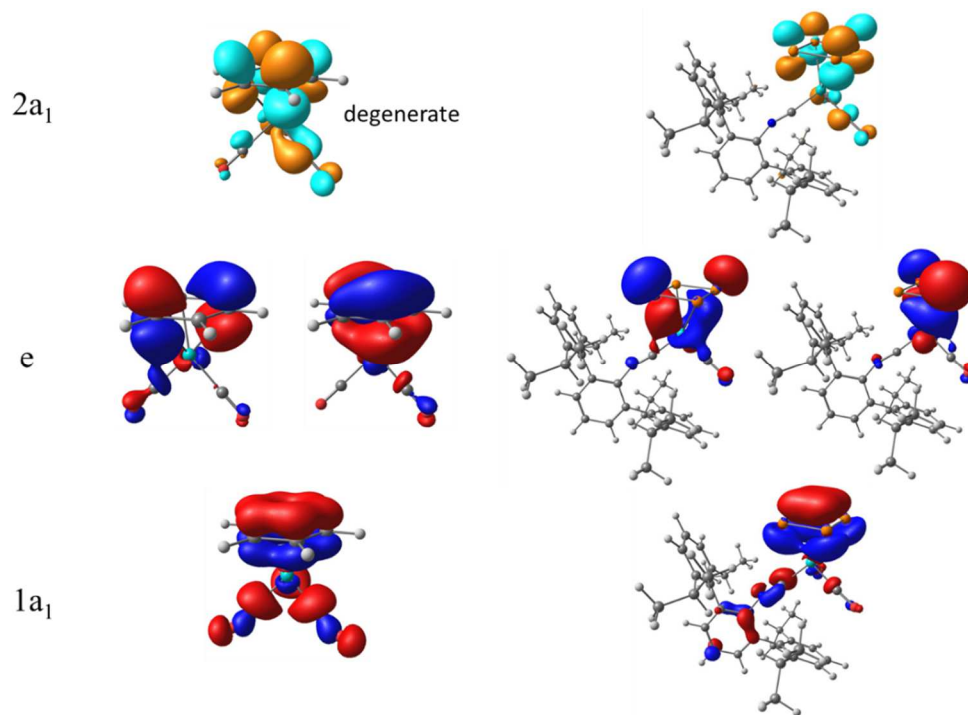


**Figure 4.5.** Aromatic  $\pi$ -orbitals of  $\text{Mo}(\text{CO})_3(\eta^6\text{-benzene})$  and  $[\mathbf{1}]^{2-}$ .

apparent by the increased hybridization in the orbitals of e-parentage compared to  $(\eta^6\text{-C}_6\text{H}_6)\text{Mo}(\text{CO})_3$  (Figure 4.5). Accordingly, an evaluation of combined e-orbital electron-distributions in  $(\eta^6\text{-C}_6\text{H}_6)\text{Mo}(\text{CO})_3$  showed greater retention of electron density within the arene, giving an 85:15 distribution between  $\text{C}_6\text{H}_6$  and Mo, respectively. The more strongly donating *cyclo*-P<sub>4</sub> ligand shed more electron density to give a more even 70:30 distribution between P<sub>4</sub> and Mo. Apart from subtle differences, however, the interactions between  $[\text{Mo}(\text{CO})_3]$  and the three filled  $\pi$ -orbitals of *cyclo*-P<sub>4</sub> in  $[\mathbf{1}]^{2-}$  are analogous to those with benzene in  $\text{Mo}(\text{CO})_3(\eta^6\text{-C}_6\text{H}_6)$ .

### 4.3 Conclusions

The establishment of cyclopentadiene as an aromatic, monoanionic ligand in coordination complexes was achieved relatively early following the discovery of ferrocene.<sup>2,3,34</sup> Interestingly, the natural extension of this idea to the four-membered rings of cyclobutadienyl complexes has been slower to develop. This work exploits the enhanced  $\pi$ -accepting properties of the all-phosphorus cyclobutadiene ligand, *cyclo*-P<sub>4</sub>, to provide the first examples of dianionic cyclobutadienyl complexes. DFT confirmed interactions of *cyclo*-P<sub>4</sub> with a zero-valent metal center in [1]<sup>2-</sup> to be analogous to those with benzene in ( $\eta^6$ -C<sub>6</sub>H<sub>6</sub>)Mo(CO)<sub>3</sub>.

## 4.4 Experimental

### 4.4.1 Synthesis and isolation of [( $\eta^4$ -P<sub>4</sub>)Mo(CO)(CNAr<sup>Dipp2</sup>)<sub>2</sub>][K<sub>2</sub>] (**[2·K<sub>2</sub>]**) and [( $\eta^4$ -P<sub>4</sub>)Mo(CO)<sub>2</sub>(CNAr<sup>Dipp2</sup>)<sub>2</sub>][K<sub>2</sub>] (**[1·K<sub>2</sub>]**) from a 3:1 [2·K<sub>2</sub>]/[1·K<sub>2</sub>] mixture

To a thawing THF solution (10 mL) of 3-P<sub>4</sub> (143 mg, 0.127 mmol, 1 equiv) was added a suspension of finely dispersed KC<sub>8</sub> (39 mg, 0.289 mmol, 2.25 equiv) in THF (2 mL). The reaction mixture was shaken rigorously for ca. 5 min. while warming to r.t. The resulting graphite suspension was filtered then concentrated to a solid. <sup>31</sup>P and <sup>1</sup>H NMR indicated a 2:1:1 ratio of [2·K<sub>2</sub>], [1·K<sub>2</sub>], and free isocyanide ligand (CNAr<sup>Dipp2</sup>), respectively. To remove liberated CNAr<sup>Dipp2</sup>, the solid was taken up in acetonitrile (3 mL) and washed with pentane (5 x 1 mL). The acetonitrile phase was then concentrated, and solids were then taken up in 0.2 mL THF, and 10 mL of pentane were added. After 1 h at -40 °C, microcrystalline [1·K<sub>2</sub>] was isolated as a pale yellow solid by filtration and subsequent drying in vacuo (0.010 g, 12.9  $\mu$ mol, 11% yield); X-ray quality crystals of [1·K<sub>2</sub>] were obtained by storage of a THF solution at -40 °C for four weeks. The solution phase was concentrated to give analytically pure [2·K<sub>2</sub>] as an amorphous red solid (0.096 g, 85  $\mu$ mol, 64% yield). <sup>1</sup>H NMR (500 MHz, C<sub>6</sub>D<sub>6</sub>) <sup>1</sup>H NMR (500 MHz, cdcl<sub>3</sub>)  $\delta$  7.54 – 7.40 (m, 4H), 7.39 – 7.22 (m, 8H), 6.90 (d,  $J$  = 7.4 Hz, 4H), 6.82 (t,  $J$  = 7.5 Hz, 2H), 3.13 – 2.97

(br m, 4H), 2.96 – 2.86 (sept,  $J = 6.9$  Hz, 4H), 1.57 (br, 12H), 1.28 – 1.21 (d,  $J = 6.5$  Hz, 12H), 1.17 (d,  $J = 6.6$  Hz, 12H), 1.11 – 1.04 (d,  $J = 6.2$  Hz, 12H);  $^{13}\text{C}\{^1\text{H}\}$  NMR (126 MHz,  $\text{C}_6\text{D}_6$ )  $\delta$  226.4 ( $^{13}\text{C}\equiv\text{O}$ , m), 148.5, 147.9, 139.7, 134.9, 130.9, 128.8, 123.5, 123.2, 122.2, 31.6, 31.4, 31.3, 25.3, 25.0, 24.4, 24.0.  $^{31}\text{P}$  NMR (162 MHz,  $\text{C}_6\text{D}_6$ )  $\delta$  105.5 (br m). FTIR (KBr windows,  $\text{C}_6\text{D}_6$ , 25 °C):  $\nu(\text{C}\equiv\text{N}) = 1981$  (s, br), 1935 (sh), 1915 (vs)  $\text{cm}^{-1}$ ,  $\nu(\text{C}\equiv\text{O}) = 1760$  (vs, br), 1679 (vs, br)  $\text{cm}^{-1}$ , other: 3059 (w, br), 2961 (m), 2929 (w), 2904 (vw), 2867 (w), 1572 (m), 1461 (w), 1410 (m), 1109 (vw), 1057 (vw), 789 (vw), 766 (w), 756 (w)  $\text{cm}^{-1}$ . Anal. Calcd for  $\text{C}_{71}\text{H}_{90}\text{K}_2\text{MoN}_2\text{O}_3\text{P}_4$ : C, 64.72; H, 6.89; N, 2.13. Found: C, 64.32; H, 6.67; N, 2.08.

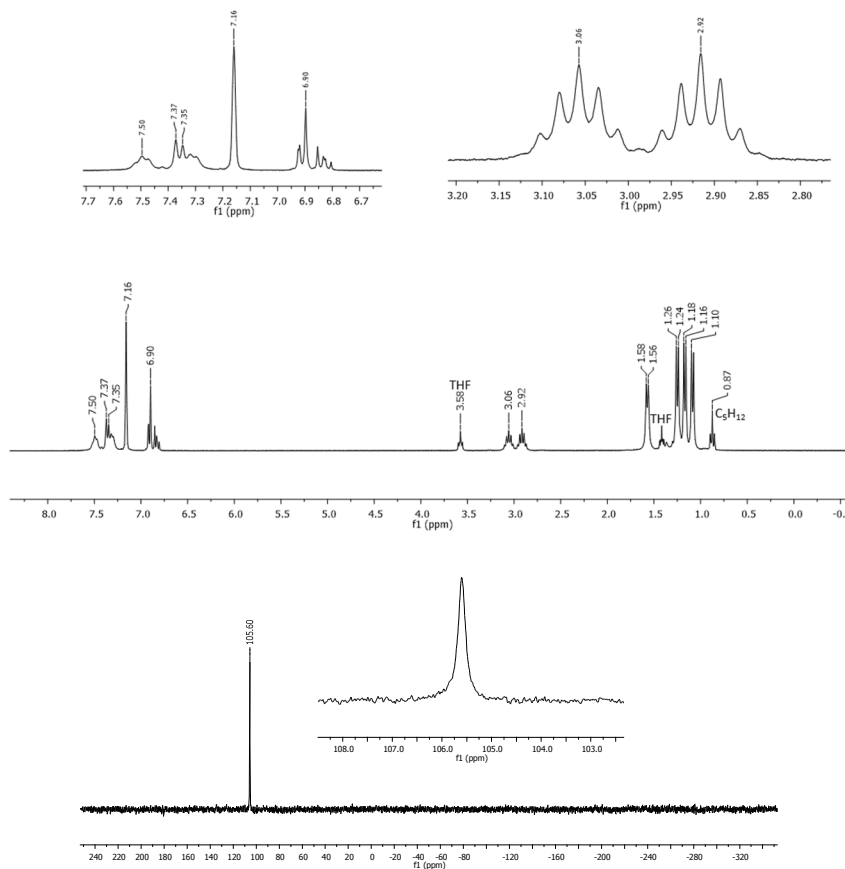


**Figure 4.6.**  $^1\text{H}$  (300 MHz,  $\text{C}_6\text{D}_6$ , top) and  $^{31}\text{P}$  NMR (122 MHz,  $\text{C}_6\text{D}_6$ , bottom) of  $[2\cdot\text{K}_2]$ .

#### 4.4.2 $[(\eta^4\text{-P}_4)]\text{Mo}(\text{CO})_2(\text{CNAr}^{\text{Dipp}^2})\text{2K} ([\mathbf{1}\cdot\mathbf{K}_2])$

To a 50 mL Schlenk ampoule charged with a THF solution of 6-P<sub>4</sub> (50 mg, 0.064 mol, 1 equiv., 10 mL) was added 1 atm CO. The sealed reaction vessel was then heated at 90 °C for 6 h. The solution volume was then reduced by ca. 75% *in vacuo*, layered in pentane (5 mL) and stored at -40 °C for 18 h. Filtration afforded  $[\mathbf{1}\cdot\mathbf{K}_2]$  as a yellow solid (0.022 g, 28.8 mol, 45% yield). <sup>31</sup>P NMR (162 MHz, THF/d<sub>8</sub>) 120.4 ppm. <sup>1</sup>H NMR (300 MHz, THF) δ 7.21 (m, 5H), 6.98 (m, 4H), 2.92 (sept, 4H), 1.32 (d, *J* = 6.8 Hz, 6H), 1.12 (d, *J* = 6.8 Hz, 6H). δ 7.22 (dd, *J* = 8.8, 6.1 Hz, 3H), 7.19 – 7.16 (m, 4H), 6.96 (td, *J* = 8.7, 3.2 Hz, 3H), 2.89 (sept, *J* = 6.8 Hz, 4H), 1.26 (d, *J* = 6.8 Hz, 13H), 1.08 (d, *J* = 6.8 Hz, 6H). <sup>13</sup>C NMR (126 MHz, thf) δ 147.7, 140.2, 136.1, 130.3, 130.1, 128.3, 123.6, 121.2, 31.7, 27.6, 26.4.

#### 4.4.3 $[(\eta^4\text{-P}_4)\text{Mo}(\text{CO})(\text{CNAr}^{\text{Dipp}^2})_2][\mathbf{2K}(\text{dibenzo-18-crown-6})] ([(\text{db18-C-6})\cdot\mathbf{K}][\mathbf{2}\cdot\mathbf{K}])$

To a toluene solution of  $[\mathbf{2}\cdot\mathbf{K}_2]$  (50 mg, 0.043 μmol, 1 equiv, 5 mL) was added dibenzo-18-crown-6 (0.16 g, 0.044 μmol, 1.04 equiv). The reaction mixture was allowed to stir 18 h at r.t., then concentrated to a red solid, taken up in Et<sub>2</sub>O/pentane (3:1, 4 mL) and filtered to remove the unreacted crown-ether as an insoluble solid. Volatiles were removed *in vacuo* to afford  $[(\text{db18-C-6})\mathbf{K}][\mathbf{2}\cdot\mathbf{K}]$  as a dark red solid (0.063 g, 0.41 μmol, 96%). <sup>1</sup>H NMR (500 MHz, C<sub>6</sub>D<sub>6</sub>) δ 7.38 – 7.24 (m, 8H), 7.09 (d, *J* = 6.9 Hz, 4H), 7.01 (d, *J* = 7.5 Hz, 4H), 6.90 – 6.79 (m, 6H), 6.49 (m, 4H), 3.97 (br, 8H), 3.62 (br, 8H), 3.14 (sept, *J* = 6.8 Hz, 4H), 3.03 (sept, *J* = 6.8 Hz, 4H), 1.56 (d, *J* = 6.8 Hz, 12H), 1.18 (br, 12H), 1.14 (d, *J* = 6.8 Hz, 24H). <sup>13</sup>C {<sup>1</sup>H} NMR (126 MHz, C<sub>6</sub>D<sub>6</sub>) δ 239.2 (<sup>13</sup>C≡O), 147.7, 147.2, 146.7, 140.1, 139.5, 137.2, 134.7, 130.7, 129.7, 129.6, 129.3, 125.7, 123.4, 123.2, 122.8, 121.4, 120.3, 111.6, 69.2, 67.7, 31.5, 31.2, 31.6, 25.5, 25.1, 24.9, 24.7, 24.5, 24.3 ppm. <sup>31</sup>P NMR (161.9 MHz, C<sub>6</sub>D<sub>6</sub>) 112.4 ppm. FTIR(KBr windows, C<sub>6</sub>D<sub>6</sub>, 25 °C): ν(C≡N) = 1877 (vs, br), 1780 (vs, br) cm<sup>-1</sup>, ν(C≡O) = 1654 (vs, br), 1635 (vs, br) cm<sup>-1</sup>, other: 3065 (vw), 3039 (vw), 2960

(s), 2927(m), 2866 (m), 1558 (vs), 1506 (vs), 1455 (vs), 1406 (vs), 1251 (vs), 1217 (s), 1128 (vs), 1059 (m), 957 (w), 944 (w), 753 (w), 742 (w)  $\text{cm}^{-1}$ . Anal. Calcd for  $\text{C}_{83}\text{H}_{94}\text{K}_2\text{MoN}_2\text{O}_7\text{P}_4$ : C, 66.24; H, 6.94; N, 1.83. Found: C, 64.85; H, 6.65; N, 1.69.

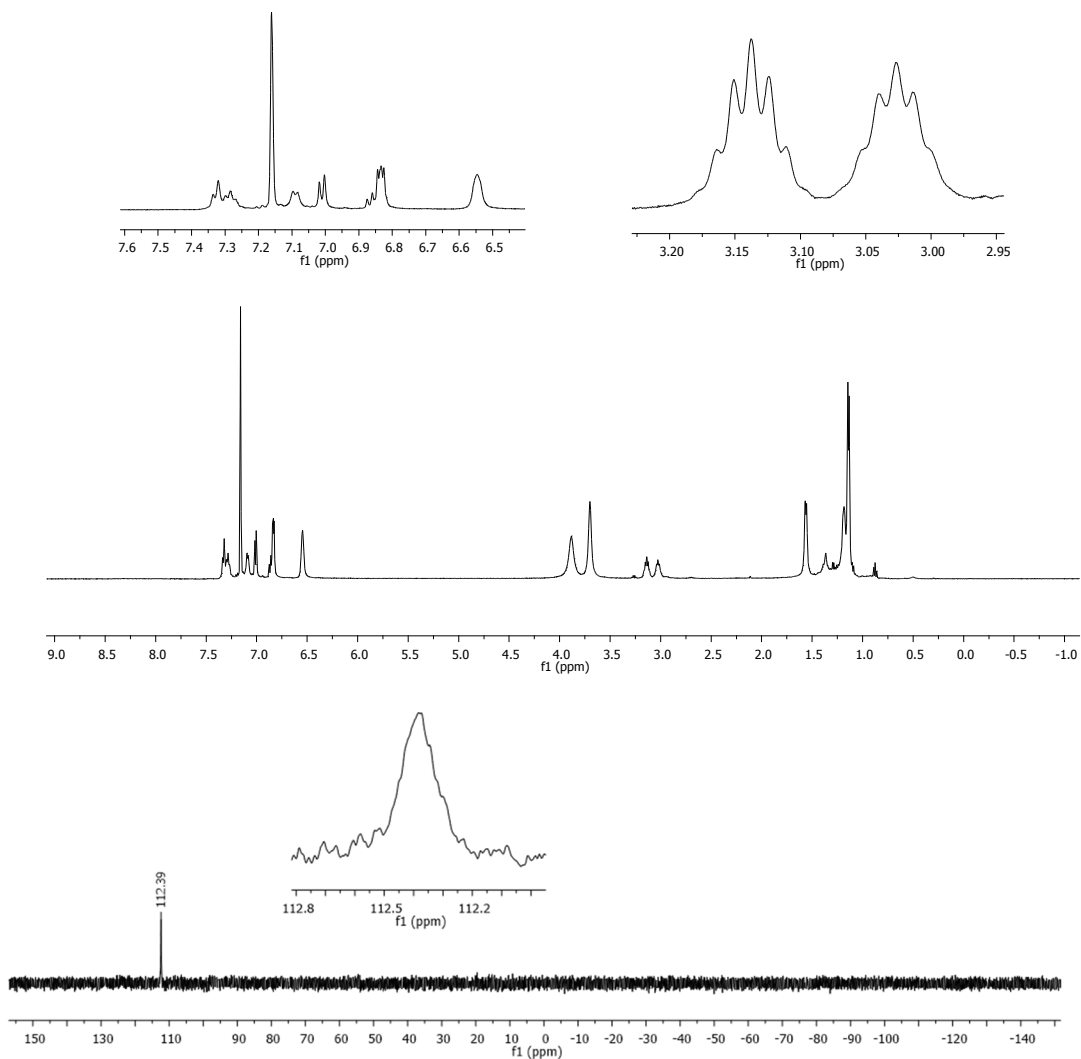


**Figure 4.7.**  $^1\text{H}$  (300 MHz,  $\text{C}_6\text{D}_6$ , top) and  $^{31}\text{P}$  NMR (122 MHz,  $\text{C}_6\text{D}_6$ , bottom) of  $[(\text{db18-C-6})\cdot\text{K}][2\cdot\text{K}]$ .



#### 4.4.4 Molecular orbital correlation diagram of $(\eta^6\text{-C}_6\text{H}_6)\text{Mo}(\text{CO})_3$ and $[(\eta^4\text{-P}_4)\text{Mo}(\text{CO})_2\text{-(CNAr}^{\text{Dipp}2})]^{2-}$

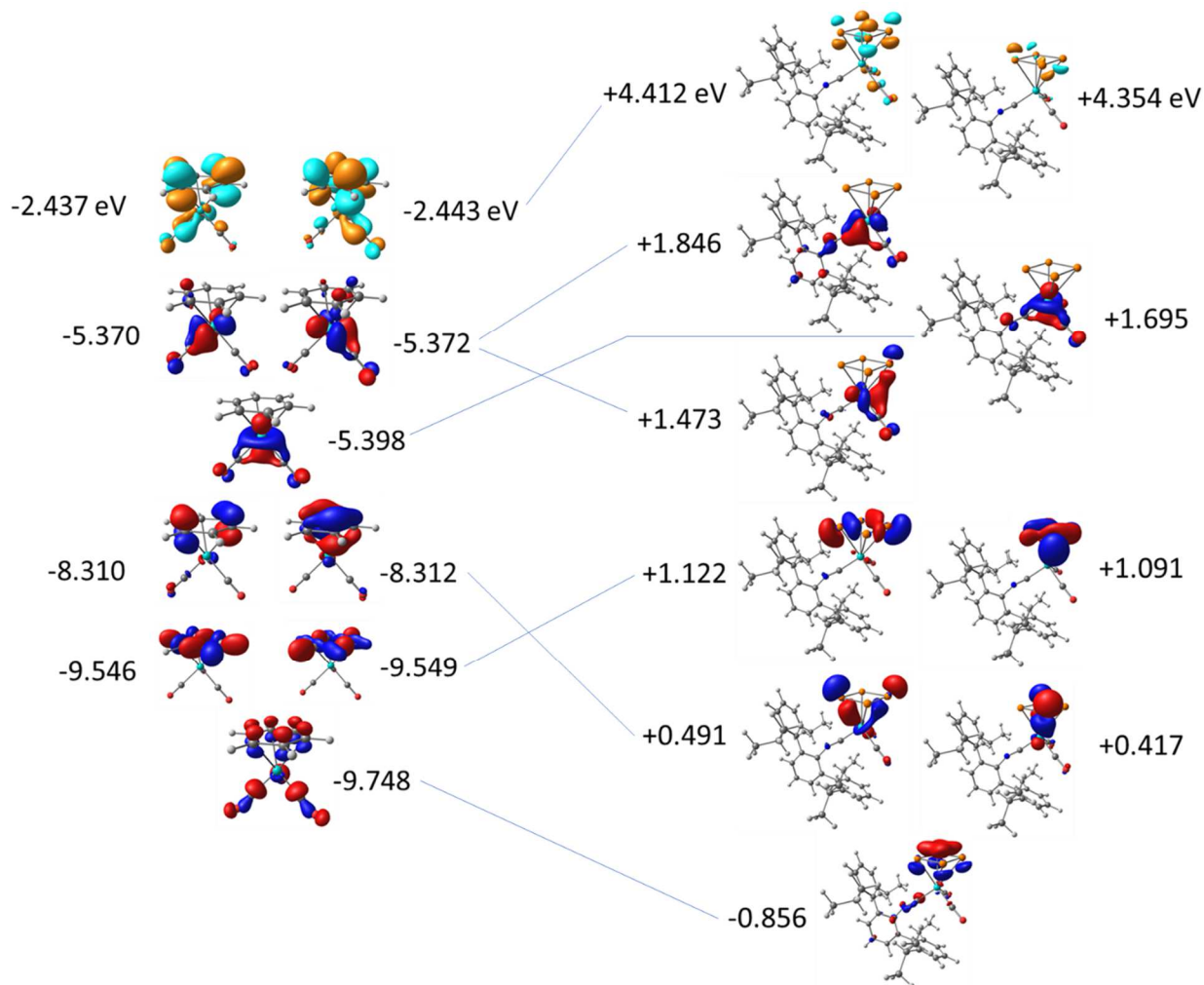


**Figure 4.8** MO correlation diagram of  $(\eta^6\text{-C}_6\text{H}_6)\text{Mo}(\text{CO})_3$  (left) and  $[(\eta^4\text{-P}_4)\text{Mo}(\text{CO})_2\text{-(CNAr}^{\text{Dipp}2})]^{2-}$  (right).

#### 4.4.5 Geometry Optimized Coordinates

$(\eta^6\text{-C}_6\text{H}_6)\text{Mo}(\text{CO})_3$

Mo	0.20763554459187	-0.40565877575475	-1.75950217079973
O	-1.42390124942505	1.86714111461542	-3.18719435269776
O	2.33231912126108	-0.15903077627440	-4.05990450198079
C	1.53229629970061	-0.24923503825065	-3.21919196918340
O	-1.33197669280719	-2.45483407757600	-3.57456947667530
C	-0.81220469911667	1.01931709358743	-2.67464772755506
C	-0.75645197597012	-1.68486571110915	-2.91761650768514
C	-0.75458949251895	-1.09621634141087	0.32245848673375
C	-0.53969042302847	0.29705328927620	0.38716141717341

C	0.34216172642225	-1.96600006348066	0.03027054508444
H	-1.37632694166801	0.96632832019218	0.58284693825618
H	0.17398728314964	-3.03979343148286	-0.04543635981885
C	0.77276081544836	0.83685537375920	0.20751899875410
C	1.64197284458009	-1.44388256854773	-0.14643916681659
H	0.93423286661185	1.91197675576124	0.26338880488019
H	2.47619323810385	-2.10888741096462	-0.36274745392888
C	1.84889203145388	-0.03020709444327	-0.08014642643199
H	2.84549143652103	0.37779415545248	-0.24323267680250
H	-1.75321364631005	-1.50513413834918	0.46387535849392

$(\eta^4\text{-P}_4)\text{Mo}(\text{CO})_2(\text{CNAr}^{\text{Dipp2}})_2 ([\mathbf{1}]^{2-})$

Mo	13.443390	6.538117	11.683976
O	10.381703	7.004862	11.152243
N	14.455253	9.539683	11.892590
C	13.963552	8.403844	11.775496
C	16.629313	10.486555	14.579972
O	13.947836	6.471281	8.581341
C	15.656947	11.522121	12.487830
C	16.710145	10.712566	13.184369
C	11.539425	6.871105	11.348642
C	17.687558	9.839146	15.232806
H	17.624079	9.657816	16.308464
C	14.539810	10.874053	11.842535
C	18.855557	9.569935	13.146126
H	19.709803	9.180368	12.586876
C	15.398923	10.897264	15.379281
H	14.666631	11.287669	14.656906
C	17.820157	10.217014	12.457839
C	13.754647	6.501220	9.748017
C	14.757078	9.692165	16.089236
H	14.562176	8.873095	15.383335
H	13.803177	9.986194	16.554710
H	15.408856	9.298588	16.886777
C	15.781596	12.910193	12.457509
H	16.641726	13.363315	12.958835
C	17.901418	10.343502	10.941441
H	16.994340	10.871388	10.612929
C	18.801795	9.392072	14.526944
H	19.612559	8.875760	15.047205
C	11.184453	10.932000	11.177814
C	12.384272	11.153495	10.459096
C	13.583239	11.716999	11.160013
C	11.264795	10.473228	8.412662
H	11.294771	10.266409	7.340324
C	10.078906	10.272012	9.114996
H	9.189053	9.906417	8.597458
C	12.427724	10.904403	9.064958
C	10.045548	10.495353	10.488369
H	9.126759	10.293184	11.042542
C	11.101875	11.169146	12.681650

H	12.117855	11.412233	13.025228
C	15.711417	12.028693	16.375688
H	16.463674	11.709007	17.115392
H	14.802679	12.324986	16.924709
H	16.104077	12.916889	15.858695
C	13.709699	11.105947	8.262811
H	14.530576	11.199370	8.990289
C	14.843644	13.722053	11.802514
H	14.953207	14.808385	11.790128
C	19.109720	11.187628	10.497145
H	19.081647	12.190793	10.947231
H	19.119047	11.303152	9.401318
H	20.059319	10.712212	10.792281
C	14.036391	9.914633	7.347262
H	14.051429	8.966370	7.900309
H	15.025185	10.058533	6.882044
H	13.304563	9.813707	6.529022
C	13.761242	13.102437	11.163239
H	13.011329	13.714253	10.652717
C	17.904373	8.961601	10.264422
H	18.803399	8.382937	10.534687
H	17.892680	9.071798	9.168525
H	17.024201	8.372883	10.557878
C	13.660071	12.416107	7.453748
H	12.830453	12.394144	6.727448
H	14.597549	12.564589	6.892186
H	13.513661	13.285001	8.111428
C	10.211373	12.383736	13.006825
H	10.587738	13.294850	12.517042
H	10.185169	12.564723	14.093882
H	9.175848	12.220778	12.666846
P	14.891238	5.937676	13.782589
P	15.282375	4.660850	12.052416
P	13.238702	3.870354	12.160725
P	12.842943	5.171314	13.883590
C	10.644329	9.917427	13.447141
H	9.617265	9.627464	13.177387
H	10.665140	10.107938	14.532564
H	11.297775	9.060232	13.231777

## 4.5 Crystal Structure Data

**Table 4.1.** Crystallographic Data Collection and Refinement Information

	$[(\eta^4\text{-P}_4)\text{Mo}(\text{CO})_2(\text{CNAr}^{\text{Dipp}2})][\text{K}_2(\text{THF})_3][\mathbf{1}\cdot\mathbf{K}_2]$	$[(\eta^4\text{-P}_4)\text{Mo}(\text{CO})_2(\text{CNAr}^{\text{Dipp}2})][\text{K}_2(\text{dibenzo-18-crown-6})_2]\cdot 3.5(\text{C}_6\text{H}_6)\cdot 0.5(\text{C}_5\text{H}_{12})[(\text{db18-C-6})\cdot\mathbf{K}][\mathbf{2}\cdot\mathbf{K}]$
Formula	$\text{C}_4\text{H}_5\text{K}_2\text{MoNO}_5\text{P}_4$	$\text{C}_{106.5}\text{H}_{124.1}\text{K}_2\text{MoN}_2\text{O}_7\text{P}_4$
Crystal System	Triclinic	Triclinic
Space Group	<i>P-1</i>	<i>P-1</i>
<i>a</i> , Å	12.502(2)	14.4244(10)
<i>b</i> , Å	13.836(2)	26.5836(17)
<i>c</i> , Å	16.348(3)	28.7659(18)
$\alpha$ , deg	82.769(5)	109.476(2)
$\beta$ , deg	68.987(5)	104.353(2)
$\gamma$ , deg	66.288(5)	98.248(2)
<i>V</i> , Å <sup>3</sup>	2416.3(7)	9761.0(11)
<i>Z</i>	2	4
Radiation ( $\lambda$ , Å)	Mo-K $\alpha$ , 0.71073	Mo-K $\alpha$ , 0.71073
$\rho$ (calcd.), g/cm <sup>3</sup>	1.355	1.254
Temp, K	100	100
$\theta$ max, deg	25.101	25.751
data/parameters	8517/649	37091/2248
<i>R</i> <sub>1</sub>	0.0520	0.0793
w <i>R</i> <sub>2</sub>	0.1282	0.1874
Goof	1.002	1.174

## 4.6 Acknowledgements

Chapter 4 was adapted with permission from Mandla, K. A.; Moore, C. E.; Rheingold, A. L.; Figueroa, J. S. “A *cyclo*-P<sub>4</sub> Analog of Mo(CO)<sub>3</sub>(η<sup>6</sup>-benzene).” *Manuscript in progress*. The dissertation author is the first author of this paper.

## 4.7 References

- (1) Kealy, T. J.; Pauson, P. L. *Nature* **1951**, *168*, 1039–1040.
- (2) Werner, H. *Angew. Chem. Int. Ed.* **2012**, *51*, 6052–6058.
- (3) Fischer, E. O.; Jira, R. *J. Organomet. Chem.* **2001**, 7–12.
- (4) Fischer, E. O.; Pfab, W. B. *Naturforsch.* **1952**, *7*, 377 – 379.
- (5) Ruch, E.; Fischer, E. O. *Z. Naturforsch. B* **1952**, *7*, 676.
- (6) Wilkinson, G.; Rosenblum, M.; Whiting, M.; Woodward, R. *J. Am. Chem. Soc* **1952**, *74* (8), 2125–2126.
- (7) Fischer, E. O.; Hafner, W. *Z. Naturforschg* **1955**, *10b*, 665–668.
- (8) Fischer, E. O.; Öfele, K. *Chem. Ber.* **1957**, *90* (11), 2532–2535.
- (9) Longuet-Higgins, H. C.; Orgel, L. E. *J. Chem. Soc.* **1956**, *0*, 1969.
- (10) Criegee, R.; Förg, F.; Brune, H.-A.; Schönleber, D. *Chem. Ber.* **1964**, *97* (12), 3461–3468.
- (11) Dunitz, J. D.; Mez, H. C.; Mills, O. S.; Shearer, H. M. M. *Helv. Chim. Acta* **1962**, *45*, 647.
- (12) Dodge, R. P.; Shomaker, V. *Nature* **1960**, *186*, 798–799.
- (13) Bally, T.; Masumune, S. *Tetrahedron* **1980**, *36*, 343–370.
- (14) Maitlis, P. *Adv. Organomet. Chem.* **1966**, *4*, 95–143.
- (15) Hoffmann, R. *Nobel Lect.* **1981**, 34–66.
- (16) Criegee, R.; Ludwig, P. *Chem. Ber.* **1961**, *94* (8), 2038–2043.
- (17) Oberhansli, W.; Dahl, L. F. *Inorg. Chem.* **1965**, *4* (2), 150–157.

- (18) Pettit, R.; GF, E. *Adv. Organomet. Chem.* **1964**, *1*, 31.
- (19) Reeves, P. C.; Henery, J.; Pettit, R. *J. Am. Chem. Soc.* **1969**, *91* (21), 5888–5890.
- (20) DODGE, R. P.; SCHOMAKER, V. *Nature* **1960**, *186* (4727), 798–799.
- (21) Kraus, F.; Korber, N. *Chem. - A Eur. J.* **2005**, *11* (20), 5945–5959.
- (22) Fitzpatrick, J. D.; Watts, L.; Emerson, G. F.; Pettit, R. *J. Am. Chem. Soc.* **1965**, *87* (14), 3254–3255.
- (23) Bursten, B. E.; Fenske, R. F. *Inorg. Chem.* **1979**, *18* (7), 1760–1765.
- (24) Clack, D.; Warren, K. *Inorganica Chim. Acta* **1978**, *27*, 105–108.
- (25) Crotty, D. E.; Corey, E. R.; Anderson, T. J.; Click, M. D.; Oliver, J. P. 1977; Vol. 16.
- (26) Sanger, I.; Kuckmann, T. I.; Dornhaus, F.; Bolte, M.; Wagner, M.; Lerner, H.-W. *Dalt. Trans.* **2012**, *41*, 6671–6676.
- (27) Janta, R.; Albert, W.; Robner, H.; Malisch, W.; Langenbach, H.-J.; Rottinger, E.; Vahrenkamp, H. *Chem. Ber.* **1980**, *113* (8), 2729–2738.
- (28) Urnezus, E.; Brennessel, W. W.; Cramer, C. J.; Ellis, J. E.; Schleyer, P. von R. *Science* (80-.). **2002**, *295*, 832–834.
- (29) Dougherty, D. A. *Acc. Chem. Res.* **2013**, *46* (4), 885–893.
- (30) Yao, S.; Lindenmaier, N.; Xiong, Y.; Inoue, S.; Szilvasi, T.; Adelhardt, M.; Sutter, J.; Meyer, K.; Driess, M. *Angew. Chemie Int. Ed.* **2015**, *54* (4), 1250–1254.
- (31) Von, P.; Schleyer, R.; Kiran, B.; Simion, D. V; Sorensen, T. S. *J. Am. Chem. Soc* **1999**, *122* (3), 510–513.
- (32) Chen, Z.; Wannere, C. S.; Corminboeuf, C.; Puchta, R.; Von, P.; Schleyer, R. .
- (33) Stanger, A. *J. Org. Chem.* **2005**, *71* (3), 883–893.
- (34) Woodward, R.; Rosenblum, M.; Whiting, M. *J. Biol. Chcv* **1952**, *74*, 3458.

## Chapter 5

# The Electrochemistry of Molybdenum *cyclo*-P<sub>4</sub> Complexes and Isolation of the First Mononuclear *cyclo*-P<sub>4</sub> Radical

### 5.1 Introduction

The first example of transition-metal-mediated activation of white phosphorus, marked by the synthesis of  $\text{RhCl}(\text{PPh}_3)(\eta^2\text{-P}_4)$ ,<sup>1,2</sup> opened new frontiers in chemical research which have persisted to now, nearly 50 years later. Since that discovery, intense research has revealed remarkable electronic and structural diversity accessible to all-phosphorus ligands derived from elemental sources. In addition to fundamentally interesting coordination chemistries accessed upon activation of P<sub>4</sub>, interest in transition metal mediated activation has been sustained, in large part, by the goal of developing cost-effective strategies for the derivatization of phosphorus directly from elemental sources.<sup>3,4</sup> Paradoxically, however, the diverse topologies, coordination modes, and degradation pathways that have rendered the subject of P<sub>4</sub>-activation so interesting also present a significant challenge in building the conceptual framework required for developing scalable, industrially relevant processes.

Further complicating this objective, even where well-defined P<sub>4</sub>-activation modes have been established, reactivity of the resulting metal-phosphide intermediates remains intertwined with fundamental M-P interactions defined by each complex's electronic structure. In chapter 3, the oxidation state of molybdenum was found to be critical for efficient photolytic reductive elimination of P<sub>4</sub> from *cyclo*-P<sub>4</sub> complexes. Accordingly, the tetra-valent oxidation state of  $(\eta^4\text{-P}_4)\text{MoI}_2(\text{CO})(\text{CNAr}^{\text{Dipp}2})_2$  (**1**) provided unoccupied d-orbitals which were readily populated by photoexcitation from high-lying P-P  $\sigma$ -bonding orbitals. In that system, therefore, photolysis with violet light (385 nm) gave tetrahedral-P<sub>4</sub> and the divalent solvento-complex

$\text{MoI}_2(\text{CO})(\text{CNAr}^{\text{Dipp}2})_2(\text{DME})$ . Despite the identical *cyclo*- $\text{P}_4$  ligand topology in the divalent complex  $(\eta^4\text{-P}_4)\text{Mo}(\text{CO})_2(\text{CNAr}^{\text{Dipp}2})_2$  (**2**), the absence of low-lying d-orbitals prevented efficient reductive elimination of  $\text{P}_4$ . Divergent reactivity of has also been found in investigations of cyclo- $\text{P}_3$  group transfer. In those studies, treatment of  $[(\eta^3\text{-P}_3)\text{Nb}(\text{ODipp})_3]^-$  with  $\text{AsCl}_3$  resulted in *cyclo*- $\text{P}_3$  transfer to give  $\text{AsP}_3$ , whereas the neutral tungsten valence analog  $(\eta^3\text{-P}_3)\text{W}(\text{ODipp})_3$  resisted group-transfer, giving instead the ligand exchange product  $(\eta^3\text{-P}_3)\text{W}(\text{Cl})(\text{ODipp})_2(\text{THF})$ .<sup>5,6</sup> It is thus apparent that a complete survey of chemical reactivity for a given  $\text{P}_n$ -ligand topology requires accessibility to a diverse library of coordination complexes spanning a range of oxidation states, metal-centers, and coordination geometries.

Although recent progress has expanded accessibility of *cyclo*- $\text{P}_4$  complexes to include  $\text{Fe}(\eta^4\text{-P}_4)(\text{PhPP}_2^{\text{Cy}2})$  ( $\text{PhPP}_2^{\text{Cy}2} = \text{PhP}(\text{CH}_2\text{CH}_2\text{PCy}_2)_2$ )<sup>31</sup> and  $\text{CoCp}(\eta^4\text{-P}_4)$  in addition to Scherer's seminal reports of the Group 5 sandwich complexes  $\text{Cp}^{\text{R}2}\text{M}(\eta^4\text{-P}_4)(\text{CO})_2$  ( $\text{M} = \text{Group 5}$ ),<sup>28-30</sup> limited access has restricted investigation of reactivity and redox properties. In this work, cyclic voltammetry (CV) studies reveal rich redox chemistry accessible to *cyclo*- $\text{P}_4$  complexes **1** and **2**. Parallel synthetic efforts enabled isolation of intermediates observed by CV, including the first radical *cyclo*- $\text{P}_4$  complex  $(\eta^4\text{-P}_4)\text{MoI}(\text{CO})(\text{CNAr}^{\text{Dipp}2})_2$ . The accessibility of new *cyclo*- $\text{P}_4$  complexes with diversified coordination geometries and metal oxidation-states is thus expected to provide a firm platform by which new methodologies for functionalization of white phosphorus can be developed.



## 5.2 Results and Discussion

### 5.2.1 Redox properties of $(\eta^4\text{-P}_4)\text{Mo}(\text{CO})_2(\text{CNAr}^{\text{Dipp}2})_2$ (**2**)

Sweeping of a 1 mM THF solution of **2** toward negative potentials resulted a large reduction wave at -2.48 vs  $\text{Fc}^+/\text{Fc}$  which is followed by a major and minor overlapping feature at -3.08 and 3.21 V vs  $\text{Fc}^+/\text{Fc}$ , respectively (Figure 5.1, see Figure 5.2 for DPV). Previously, we reported that treatment of **2** with 2 equiv  $\text{KC}_8$  resulted in simultaneous formation of the highly reduced mono and dicarbonyl *cyclo*- $\text{P}_4$  dianions  $[(\eta^4\text{-P}_4)\text{Mo}(\text{CO})(\text{CNAr}^{\text{Dipp}2})_2]2\text{K}$  (**[3]** $[\text{K}_2]$ ) and  $[(\eta^4\text{-P}_4)\text{Mo}(\text{CO})_2(\text{CNAr}^{\text{Dipp}2})_2]2\text{K}$  (**[4]** $[\text{K}_2]$ ) in a 1:3 ratio. Importantly, CV of **[3]** $[\text{K}_2]$  (1 mM, THF, 100 mV/s) showed no reductive features in the solvent window of THF, suggesting that the two over-lapping features at -3.08 and -3.21 V vs  $\text{Fc}^+/\text{Fc}$  can be attributed to the formation of **[4]** $^-$  and **[3]** $^-$ . It can thus be surmised that the first reductive feature at -2.48 V vs  $\text{Fc}^+/\text{Fc}$  arises by single electron reduction of **2**. Furthermore, irreversibility of this feature is consistent with rapid dissociation of either CO or  $\text{CNAr}^{\text{Dipp}2}$  from the  $19\text{ e}^-$  intermediate **[2]** $^-$  (Scheme 5.1). Furthermore, the presence of CO or  $\text{CNAr}^{\text{Dipp}2}$  dissociation likely follows the first reduction is consistent with the presence of two overlapping cathodic features in the second reduction wave. Importantly, as a consequence of increased  $\sigma$ -donation and decreased  $\pi$ -acceptance of isocyanides relative to carbonyls,<sup>9-13</sup> isocyanide for CO ligand substitution has been shown to facilitate oxidation of metal complexes at lower potentials.<sup>14,15</sup> By the same effect, increased  $\pi$ -backbonding in dicarbonyl species **[4]** $^-$  would be expected to undergo reduction at less negative potentials than the monocarbonyl. It is, therefore, informative that the minor feature ( $E_{\text{red}} = 3.08\text{ V vs Fc}^+/\text{Fc}$ ) is formed at less reducing potentials than that of the major feature ( $E_{\text{red}} = -3.21\text{ vs Fc}^+/\text{Fc}$ ), as this observation is corroborates synthetic studies showing that formation of the *bis*-isocyanide monocarbonyl dianion **[3]** $^-$  is favored by a ratio of 2:1 **[3]** $^-$ /**[4]** $^-$ .

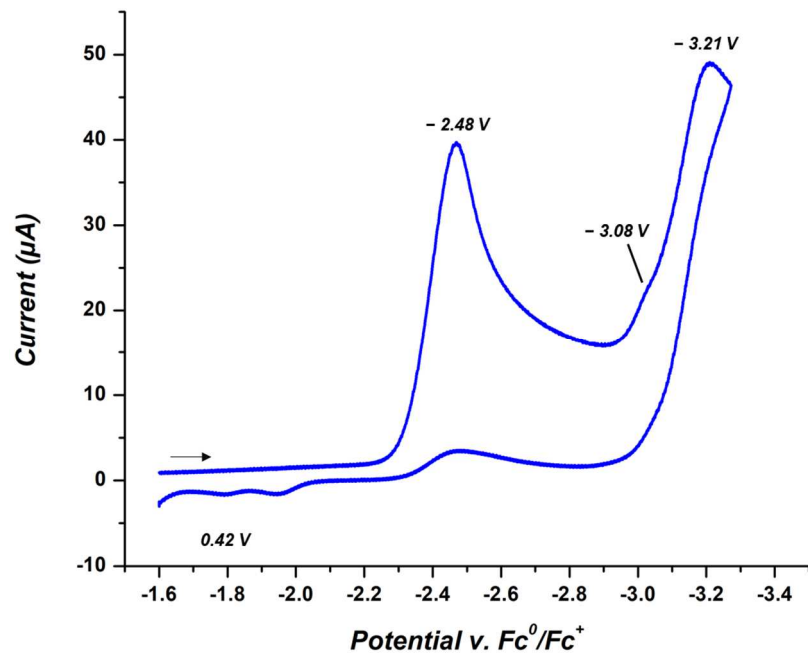


**Figure 5.1.** CV of *cyclo*-P<sub>4</sub> complex **2** (0.3M [NBu<sub>4</sub>][PF<sub>6</sub>] THF solution,  $v = 100$  mV/s).

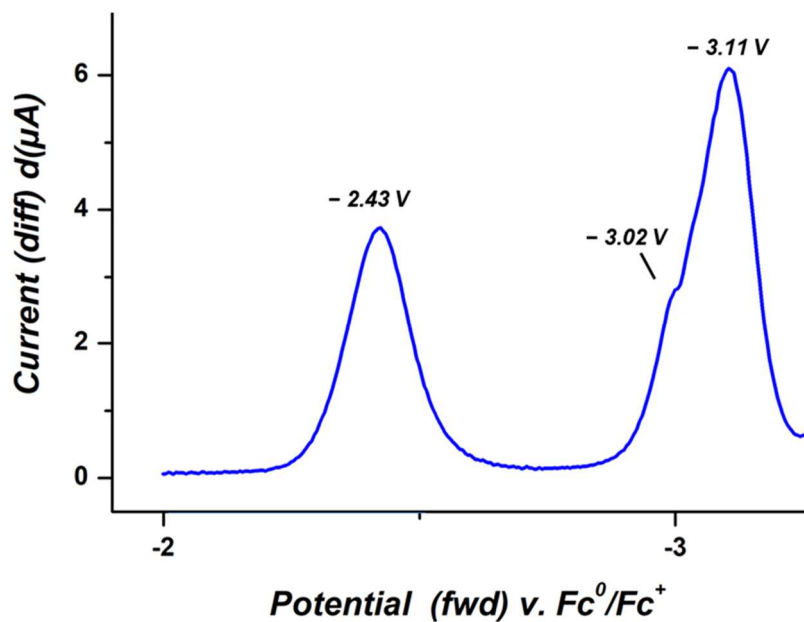
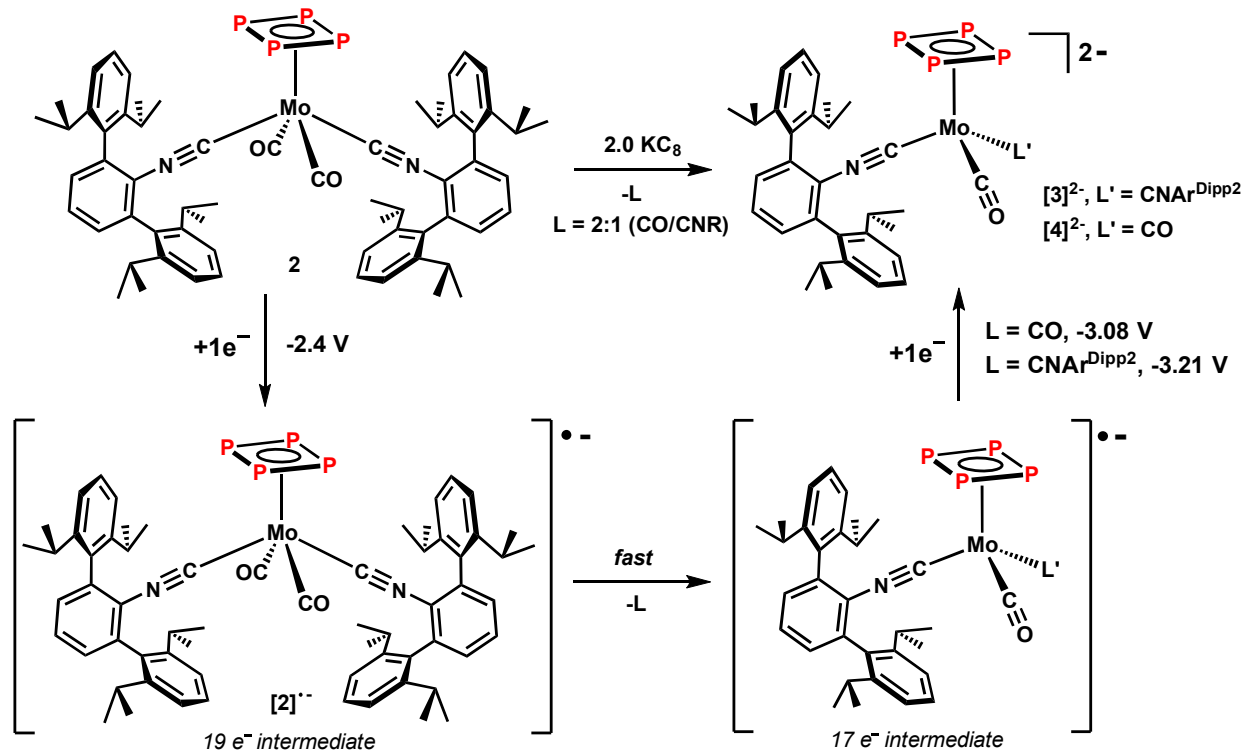


**Figure 5.2.** DPV of **2** (1.0 mM complex, 0.3M [NBu<sub>4</sub>][PF<sub>6</sub>], THF solution).



**Scheme 5.1.** Proposed mechanism for the formation of dianionic cyclo-P<sub>4</sub> complexes.

### 5.2.2 Redox properties of $(\eta^4\text{-P}_4)\text{MoI}_2(\text{CO})(\text{CNAr}^{\text{Dipp}2})_2$ (**1**)

With assignment of the reductive processes of **2** in hand, we next sought to investigate the redox chemistries accessible to **1** (Figure 5.3). Following an initial reduction wave at -2.43 vs Fc<sup>+</sup>/Fc are two sequential one-electron cathodic events at -2.79 and -3.16 V vs Fc<sup>+</sup>/Fc consistent with the Mo(II) → Mo(I) → Mo(0) transitions observed in the reduction of **2** (Figure 5.1). Importantly, the shift of the Mo(II) → Mo(I) process to negative potentials in **1** (2.8 vs Fc<sup>+</sup>/Fc compared to 2.48 vs Fc<sup>+</sup>/Fc with **2**) reflects the less π-accepting coordination environment of the monocarbonyl analyte **1** compared to dicarbonyl complex **2**. Furthermore, the observation of a single, non-overlapping reduction at -3.16 vs Fc<sup>+</sup>/Fc further supports our assignment of that transition to  $[(\eta^4\text{-P}_4)\text{Mo}(\text{CO})(\text{CNAr}^{\text{Dipp}2})_2]^{1-} \rightarrow [(\eta^4\text{-P}_4)\text{Mo}(\text{CO})(\text{CNAr}^{\text{Dipp}2})_2]^{2-}$  since the presence of only three L-type ligands in **1** precludes formation of the related dicarbonyl species.

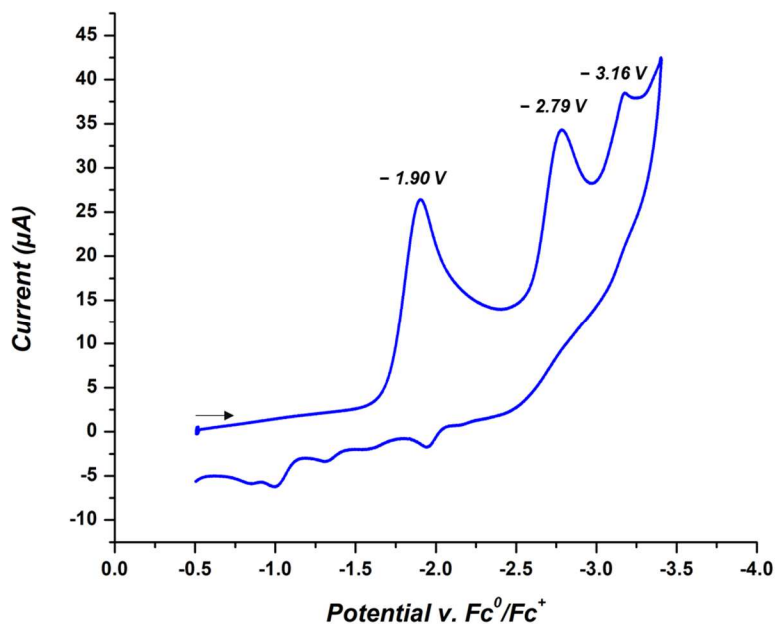


**Figure 5.3.** CV of *cyclo*-P<sub>4</sub> complex **1** (1.0 mM complex, 0.3M [NBu<sub>4</sub>][PF<sub>6</sub>], THF solution, scan rate 100 mV/s).

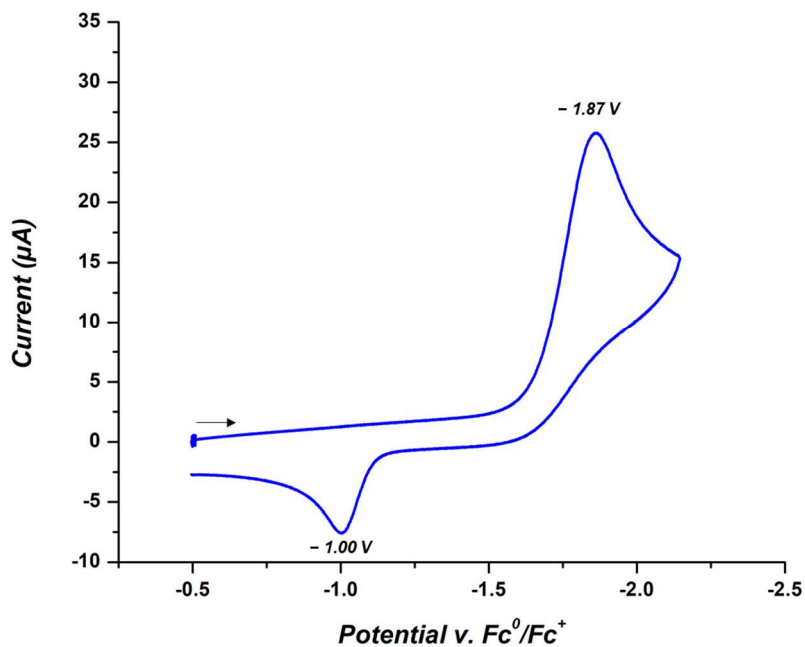
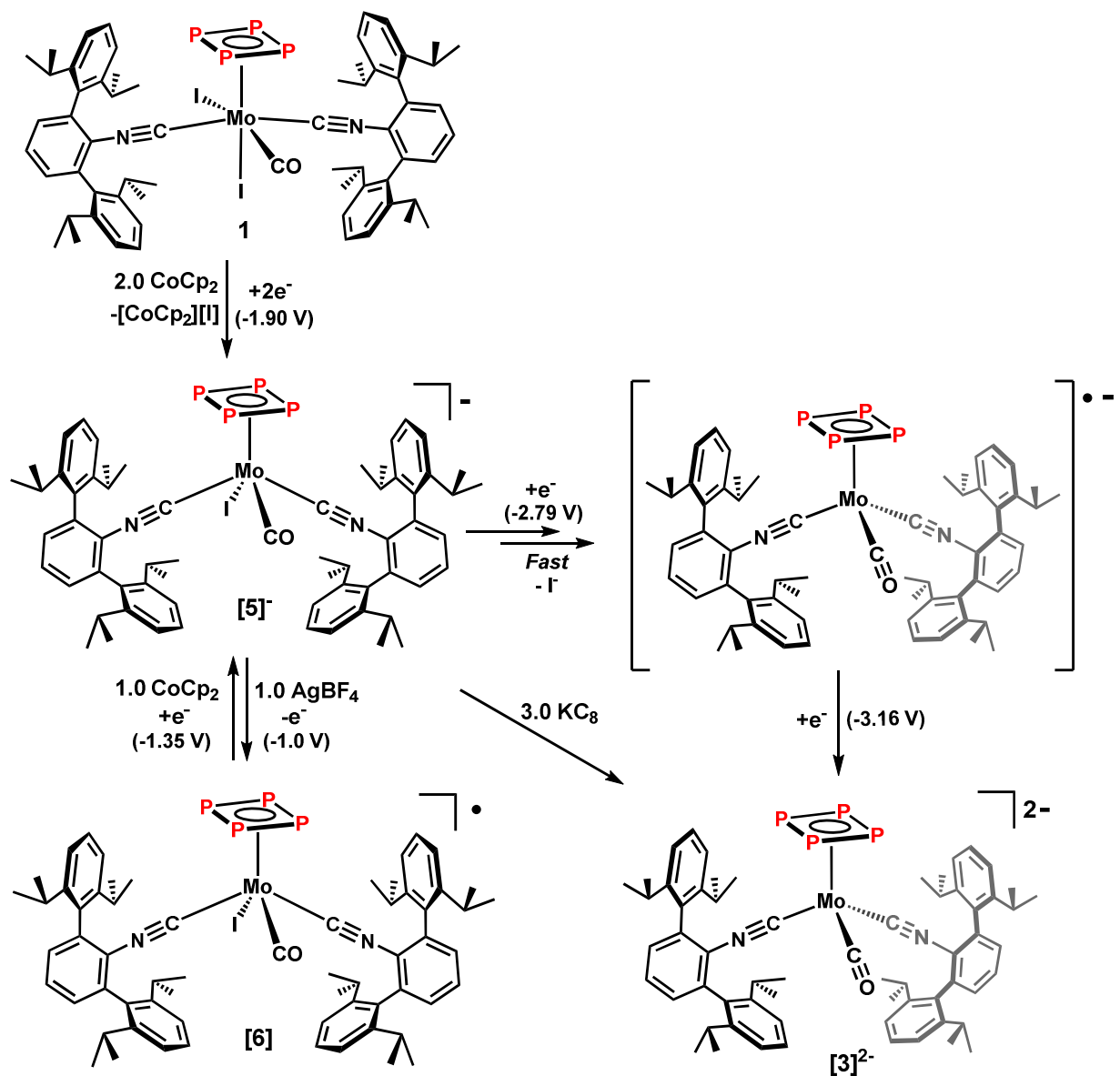


**Figure 5.4.** Resolution of oxidative feature at -1.00 V by reversing sweep after the first cathodic event (1.0 mM complex **1**, 0.3M [NBu<sub>4</sub>][PF<sub>6</sub>], THF solution, scan rate 100 mV/s).



**Scheme 5.2.** Summary of electrochemical processes accessible to **1** (CV potentials vs  $\text{Fc}^+/\text{Fc}$  in parenthesis) and chemical reagents utilized in synthetic routes.

Of particular interest in the redox chemistry of **1** was the two-electron irreversible wave associated with a  $\text{Mo(IV)} \rightarrow \text{Mo(II)}$  transition at  $-1.87 \text{ V}$  vs  $\text{Fc}^+/\text{Fc}$  and an anodic event at  $-1.00$  vs  $\text{Fc}^+/\text{Fc}$  (Figure 5.4).<sup>16,17</sup> Previously, we showed that reduction of the related mixed carbonyl-isocyanide,  $\text{XMn(CO)}_3(\text{CNAr}^{\text{Dipp}2})_2$  ( $\text{X} = \text{halide}$ ) exhibited similar irreversible two-electron cathodic wave which was separated from an accompanying oxidative feature by  $1.1 \text{ V}$ .<sup>18</sup>

Importantly, this oxidation was attributed to single electron oxidation of the electrochemically generated  $[\text{Mn}(\text{CO})_3(\text{CNAr}^{\text{Dipp}2})_2]^-$  to give the neutral radical  $\text{Mn}(\text{CO})_3(\text{CNAr}^{\text{Dipp}2})_2$ . We thus considered the possibility that the anodic process in Figure 5.4 arose through an analogous single-electron oxidation of an anionic *cyclo*-P<sub>4</sub> intermediate. Noting that synthesis of the Mn-radical by chemical oxidation of  $\text{Na}[\text{Mn}(\text{CO})_3(\text{CNAr}^{\text{Dipp}2})_2]$  with 1.0 equiv TlOTf closely resembled the electrochemical pathway,<sup>19</sup> we were encouraged to pursue a similar synthetic strategy toward isolation of a radical *cyclo*-P<sub>4</sub> complex.

As an entryway to this oxidative strategy, we initially sought to isolate the intermediate generated electrochemically in the first reduction of **1**. Satisfyingly, treatment with 2.0 equiv CoCp<sub>2</sub> resulted in complete consumption of **1** and a single CO stretching frequency at 1884 cm<sup>-1</sup> in the FTIR (C<sub>6</sub>D<sub>6</sub>, 25 °C) which was revealed to be the cobaltocenium salt  $[\text{CoCp}_2][(\eta^4\text{-P}_4)\text{MoI}(\text{CO})(\text{CNAr}^{\text{Dipp}2})_2]$  (**5**)[CoCp<sub>2</sub>] by X-ray crystallography (Figure 5.5). Consistent with the 2e<sup>-</sup> reductive process observed by CV, treatment of **1** with 1.0 equiv CoCp<sub>2</sub> in thawing THF resulted in only partial consumption of the starting complex and formation of **5**[CoCp<sub>2</sub>] as the major product. Insight into the 2e<sup>-</sup> reductive process of **1** was obtained by comparison to the cyclic voltammogram of **5**[CoCp<sub>2</sub>] (Figure 5.6). The electrochemical oxidation of **5**[CoCp<sub>2</sub>] shows two reversible features completely reversible (Scheme 5.2). Furthermore, reversible 1e<sup>-</sup> oxidation of **5** supported our hypothesis that the 17e<sup>-</sup> radical would be accessible by double reduction of **1** followed by a 1 e<sup>-</sup> oxidation.

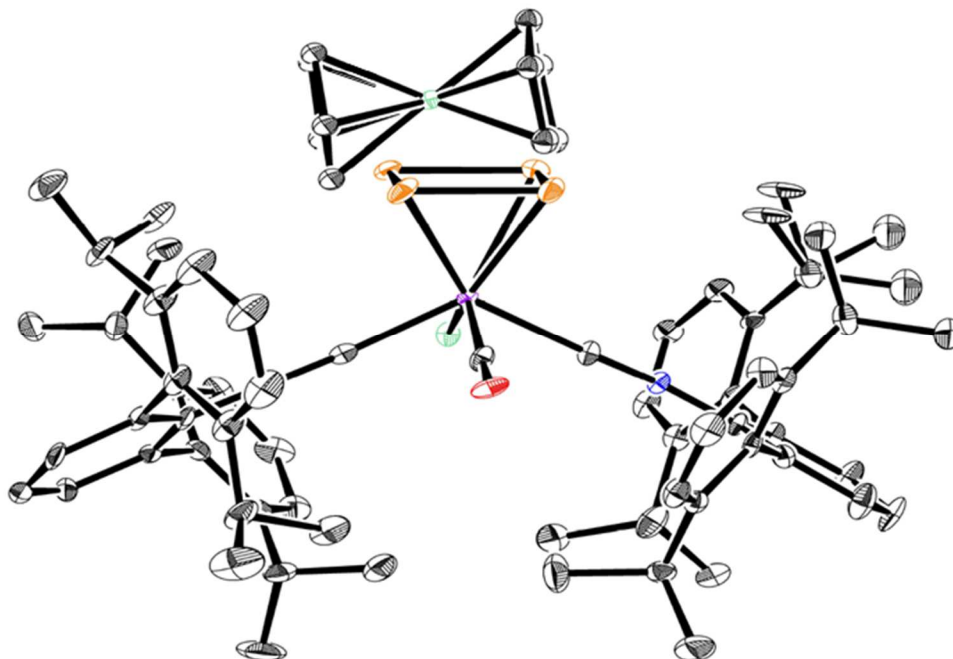


**Figure 5.5.** Molecular structure of  $[\text{CoCp}_2][(\eta^4\text{-P}_4)\text{MoI}(\text{CO})(\text{CNAr}^{\text{Dipp}2})_2]$  (**[5][CoCp<sub>2</sub>]**).

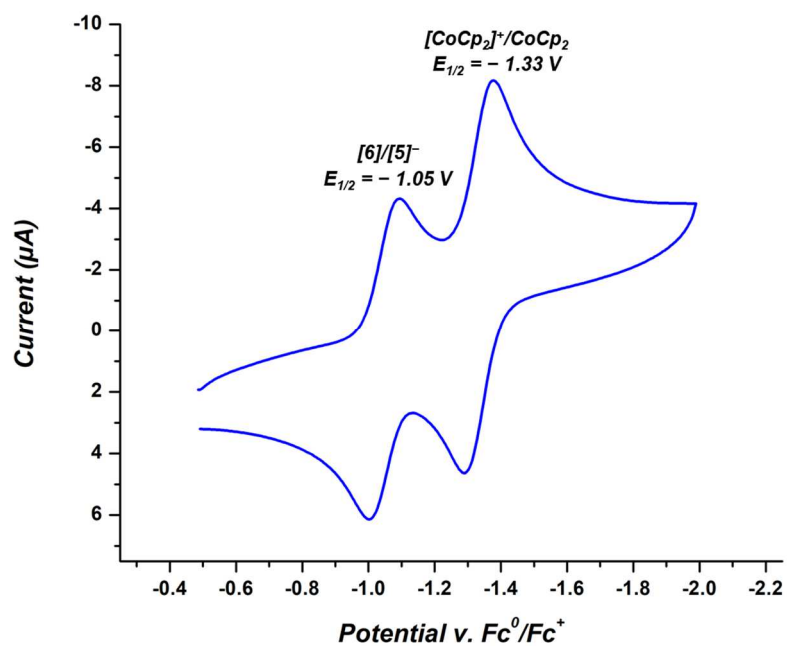
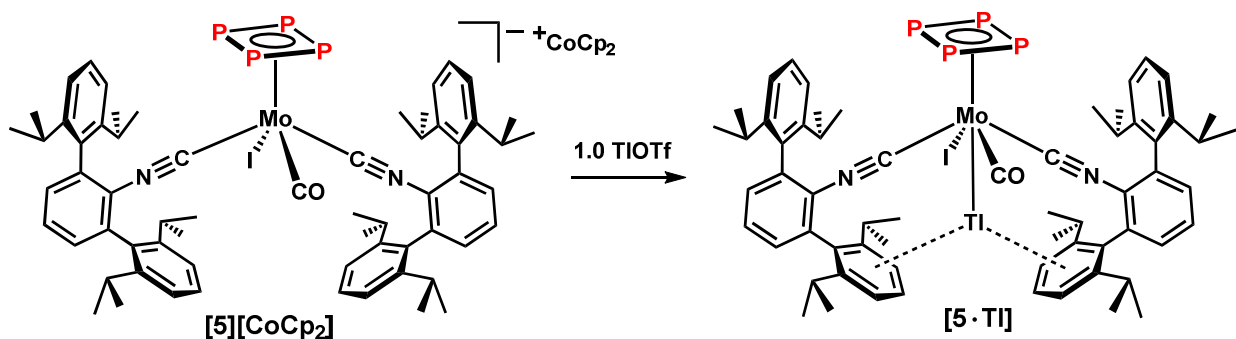


**Figure 5.6.** Cyclic voltammetry of **[5][CoCp<sub>2</sub>]** (1.0 mM complex, 0.3M  $[\text{NBu}_4][\text{PF}_6]$ , THF solution, scan rate 100 mV/s).

With  $[5][\text{CoCp}_2]$  in hand, we again considered the strategy wherein TlOTf was used as a mild oxidant for the preparation of  $\text{Mn}(\text{CO})_3(\text{CNAr}^{\text{Dipp}})_2$ .<sup>20</sup> Interestingly, however, spectroscopic analysis of the reaction between TlOTf and  $[5][\text{CoCp}_2]$  revealed only a small shift in the CO stretching frequency to  $1893\text{ cm}^{-1}$ , which is inconsistent with oxidation of the Mo metal-center. We initially suspected  $\text{Tl}^+$  coordination with *cyclo*- $\text{P}_4$  similar to observations by Scheer and co-workers in the preparation of soluble coordination polymers linked by  $\mu^2-(\eta^1, \eta^5)\text{-}(\text{cyclo-P}_5)$ <sup>21</sup> and  $\mu^2-(\eta^1, \eta^2)\text{-}(\text{cyclo-P}_3)$ <sup>22</sup> interactions with  $\text{Tl}^+$ . To our surprise, however, X-ray crystallography revealed the product to be thallium adduct  $[5\cdot\text{Tl}]$  which contains an exceedingly rare  $\text{Mo} \rightarrow \text{Tl}^+$  Z-type interaction whereby thallium is situated in the cleft formed by *m*-terphenyl arenes (Figure 5.7, Scheme 5.3). A CSD search of Group 6 metals with  $\text{M}\cdots\text{Tl}$  bonding interactions indicates only three structural motifs are known to support the Z-type interaction. Among these are  $\text{Tl}^{3+}$  adducts with  $[\text{CpM}(\text{CO})_3]^-$  ( $\text{M} = \text{Cr}, \text{Mo}$ )<sup>23-25</sup> and  $[\text{Cr}(\text{CO})_5]^-$  ligating fragments,<sup>26</sup> and one  $\text{Tl}^+$  adduct with the dianionic metallaborane  $[(\text{nido-7,8-C}_2\text{B}_9\text{H}_{11})\text{Mo}(\text{CO})_3]$ .<sup>2-27</sup>



**Scheme 5.3.** Synthesis of thallium adduct  $[5\cdot\text{Tl}]$

Due to Z-type character of the  $\text{M}\cdots\text{Tl}$  bonding interaction, the CO stretching frequency of  $[5\cdot\text{Tl}]$  showed a  $+26\text{ cm}^{-1}$  blue-shift in the FTIR, as is consistent with donation of electron density from the d-manifold of the metal-center into  $\text{Tl}^+$ . This is further supported by the precise  $180.00^\circ$



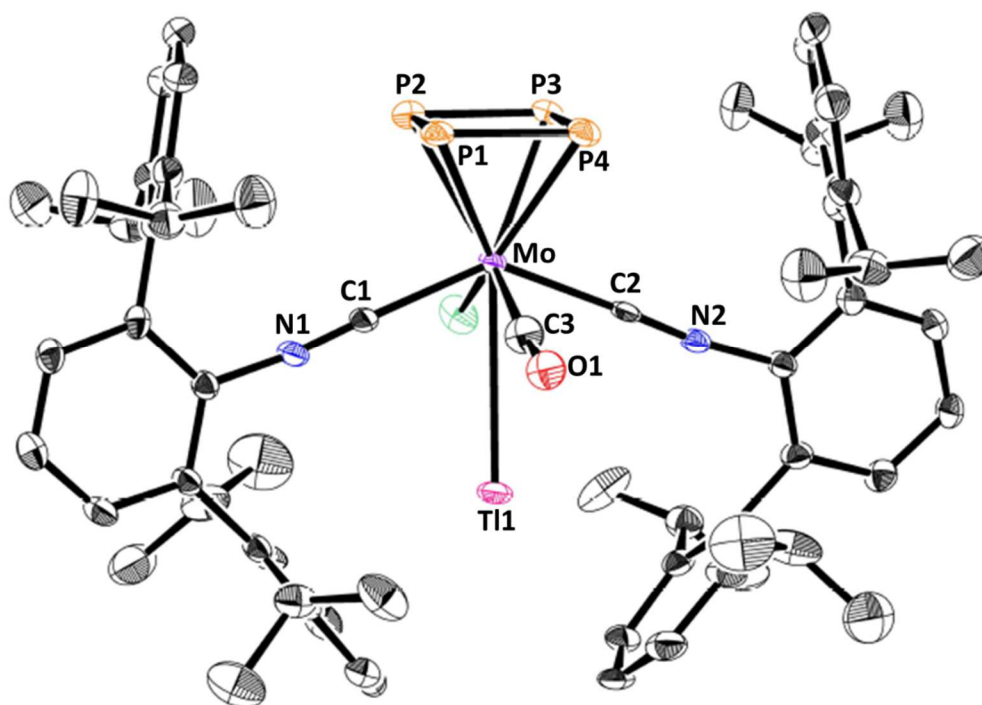


**Figure 5.7** Molecular structure of  $(\eta^4\text{-P}_4)\text{MoI}(\text{CO})(\text{CNAr}^{\text{Dipp}2})_2(\text{Tl})$  ([**5•Tl**]).

$\text{Tl}^+\text{-Mo-}[\text{cyclo-P}_4]$  (centroid) bond angle which orients the cation directly across from the strongly donating *cyclo-P*<sub>4</sub> group. Notwithstanding, however, the measured Mo-Tl bond distance of 3.269(8) Å was longer than expected for an unsupported M-Tl bond. Providing insight into Mo-Tl bond elongation was the presence of two uncharacteristically distinct magnetic shielding environments for the flanking arene rings of the  $\text{CNAr}^{\text{Dipp}2}$  ligands by <sup>1</sup>H NMR (500 MHz, C<sub>6</sub>D<sub>6</sub>). Accordingly, the methine protons of the  $\text{CNAr}^{\text{Dipp}2}$  isopropyl groups showed two independent septets separated by 0.06 ppm. We thus propose that stabilization of the Mo-Tl bond is bolstered by secondary intramolecular cation- $\pi$  interactions with the flanking arene rings of the *m*-terphenyl groups. Supporting this assessment is the alignment of both  $\text{CNAr}^{\text{Dipp}2}$  in such a way as to minimize the two  $\text{Tl}^+\cdots\text{Ar}^{\text{Dipp}}$  distances to 3.25 Å. Importantly, the agreement of spectroscopic

features with structural data indicate that  $\text{Mo}\cdots\text{Ti}^+$  and the accompanying  $\text{Ti}^+\cdots\text{Ar}^{\text{Dipp}}$  cation- $\pi$  interactions are persistent in solution.

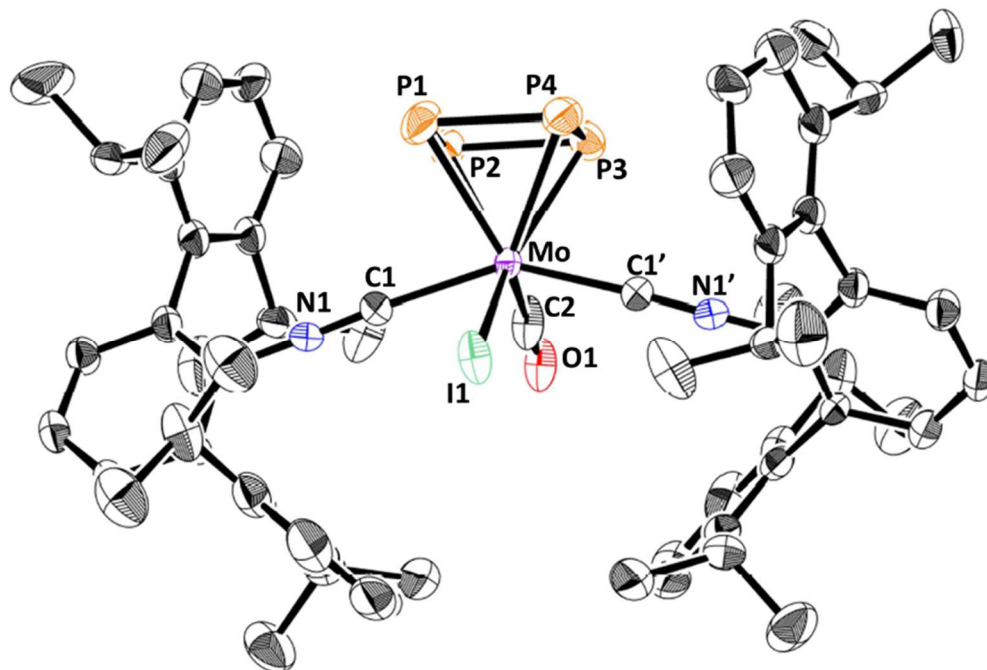


**Figure 5.8.** Molecular structure of  $(\eta^4\text{-P}_4)\text{MoI}(\text{CO})(\text{CNAr}^{\text{Dipp}2})_2$  (**6**).

In contrast to M-M adduct formation in  $[\mathbf{5}\cdot\text{Ti}]$ , treatment of  $[\mathbf{5}][\text{CoCp}_2]$  with 1 equiv  $\text{AgBF}_4$  in THF resulted in large  $100\text{ cm}^{-1}$  blue shift in the CO stretching frequency to  $1984\text{ cm}^{-1}$  indicating a metal-based oxidation. X-ray crystallography confirmed the structure to be the neutral *cyclo-P*<sub>4</sub> complex **6** (Figure 5.8. **Molecular** structure of  $(\eta^4\text{-P}_4)\text{MoI}(\text{CO})(\text{CNArDipp}_2)_2$  (**6**). The broad, featureless <sup>1</sup>H NMR spectrum provided initial evidence of radical character with Evans method giving  $\mu_{\text{eff}} = 1.71(3)\ \mu_{\text{B}}$ , as is consistent with the presence of a single unpaired electron. EPR analysis at 5 K in (10 mM, THF) provided further insight into the magnetic properties of **6** giving a rhombic signal centered at  $g = 2.0$ , consistent with a spin- $1/2$  complex of low-symmetry. Although resolution of hyperfine splitting was limited by significant line broadening, resolved features on the high field feature confirms spin-density at phosphorus as predicted by DFT [Figure

5.10(b)]. Furthermore, comparison of the SOMO to the calculated spin-density surface in Figure 5.10 reveals minimal spin-polarization so as to maintain localized spin density within the SOMO. Most importantly, **6** provides the first example of a *cyclo*-P<sub>n</sub> complex supported by a d<sub>3</sub> metal center, and the first example of a mononuclear *cyclo*-P<sub>4</sub> radical.

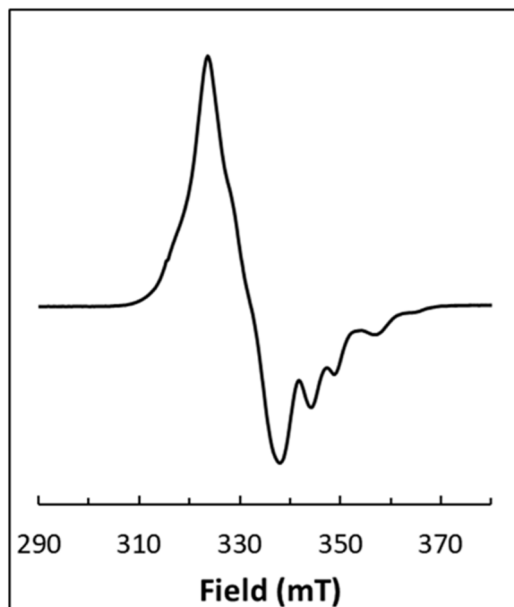


**Figure 5.9.** EPR of **6** (10 mM complex in THF, 5K, 9.64 GHz)

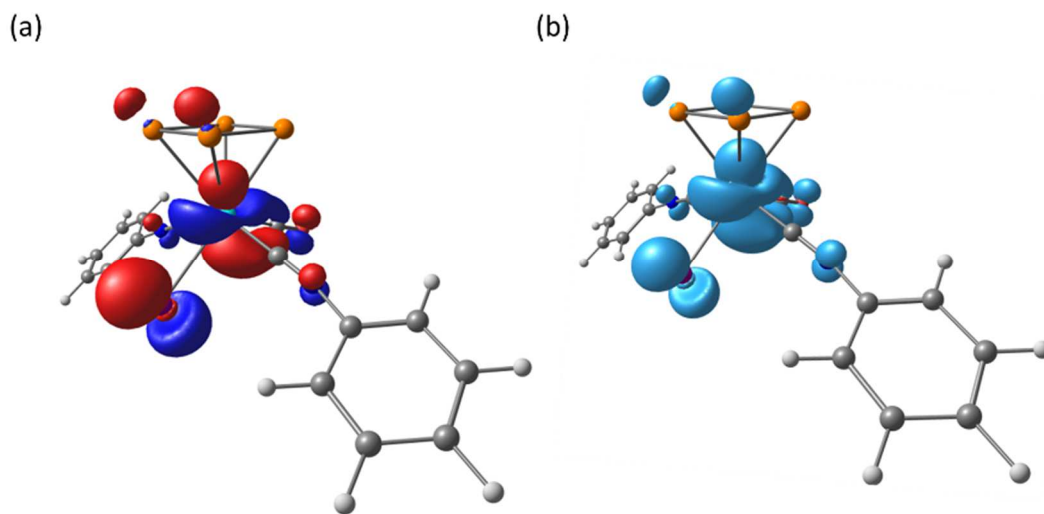


**Figure 5.10.** DFT optimized (BP86, ZORA-def2-TZVP) structure of **6** showing SOMO (a) and spin-density-surface (b).

**Table 5.1.** Selected bond parameters for **6** (XRD and DFT), [5][CoCp<sub>2</sub>], and [5•Tl].

		<b>6</b>		[5][CoCp <sub>2</sub> ]	[5•Tl]
Method		Calculated	XRD	XRD	XRD
NC-Mo-CN	deg	145.3	147(4)	121.9(5)	136.0(4)
OC-Mo-I	deg	120.3	124(1)	134.2(4)	132.4(5)
I-Mo-P4(cent.)	deg	129.4	128	112.98(11)	115.94(3)
OC-Mo-P4(cent)	deg	110.2	107	134.2(4)	111.6(5)
Mo-P4(cent)	Å	2.082	2.022	2.051 (2)	2.047(2)
Mo-I	Å	2.831	2.815(5)	2.871(1)	2.733(1)
Mo-CNAr	Å	2.086	2.093(9)	2.066(16)	2.096(7)

Interestingly, the identical coordination environment of **6** to the anion [5][CoCp<sub>2</sub>] provided a basis of comparison for the consequences of the singly occupied orbital on geometric parameters. As shown in Table 5.1 The most noticeable structural change in the **6** is an opening of the ArCN-Mo-CNAr bond angle from 129° in [5][CoCp<sub>2</sub>] to 147° in the radical species (**6**), which is accompanied by a tightening of the OC-Mo-I bond angle from 134° to 124°, and a slight constriction in the Mo-I bond length (Table 5.1, Figure 5.5). Taken together, these structural features are consistent with the removal of a single electron from the metal-centered SOMO, which is primarily dz<sup>2</sup> in character [Figure 5.10(a)]. Accordingly, decreased electron density of the dz<sup>2</sup> relaxes  $\pi$ -backbonding interactions with the CN  $\pi^*$ , thus allowing the encumbering isocyanides to take more-sterically favored positions with the ligands approaching trans positions as backdonation from the SOMO to one CO ligand is sufficient to compensate for the lost CN  $\pi^*$  interactions. It is interesting to note that decreased localization of electron density in dz<sup>2</sup>-orbital due to the Z-type interaction with Tl<sup>+</sup> appears to have a similar effect on the NC-Mo-CN bond angle. Further reflecting increased  $\pi$ -backdonation into the CO  $\pi^*$  is a shortening of the Mo-I

bond. Accordingly, polarization of the  $dz^2$  orbital in the direction of CO reduces the Mo-I antibonding interaction with a the  $\pi_1$ -orbital of the iodine lone pair [Figure 5.10(a)].

### 5.3 Synthetic procedures, characterization data, and calculations

**General considerations.** All manipulations were carried out under an atmosphere of purified dinitrogen using standard Schlenk and glovebox techniques. Unless otherwise stated, reagent-grade starting materials were purchased from commercial sources and either used as received or purified by standard procedures.<sup>29</sup> Solvents were dried and deoxygenated according to standard procedures.<sup>30</sup> Benzene- $d_6$  (Cambridge Isotope Laboratories) was distilled from NaK alloy/benzophenone ketyl and stored over 4 Å molecular sieves under  $N_2$  for at least 24 h prior to use. Celite 405 (Fisher Scientific) was dried under vacuum (24 h) at a temperature above 250 °C and stored in the glovebox prior to use. KBr (FTIR grade from Aldrich) was stirred overnight in anhydrous THF, filtered and dried under vacuum at a temperature above 250 °C prior to use. The *m*-terphenyl isocyanide  $CNAr^{Dipp2}$  was prepared as previously reported.<sup>31</sup>

Solution  $^1H$ ,  $^{13}C\{^1H\}$ ,  $^{31}P$  NMR spectra were recorded on a Bruker Avance 300, a Jeol ECA 500, or a Varian X-SENS 500 spectrometer.  $^1H$  and  $^{13}C\{^1H\}$  chemical shifts are reported in ppm relative to  $SiMe_4$  ( $^1H$  and  $^{13}C$   $\delta = 0.0$  ppm) with reference to residual solvent resonances of 7.16 ppm ( $^1H$ ) and 128.06 ppm ( $^{13}C$ ) for  $C_6D_6$ , 7.26 ppm ( $^1H$ ). FTIR spectra were recorded on a Thermo-Nicolet iS10 FTIR spectrometer. FTIR samples were prepared as  $C_6D_6$  or THF solutions injected into a ThermoFisher solution cell equipped with KBr windows. Solvent peaks were digitally subtracted from all spectra by comparison with an authentic spectrum obtained immediately prior to that of the sample. The following abbreviations were used for the intensities and characteristics of important IR absorption bands: vs = very strong, s = strong, m = medium, w = weak, vw = very weak; br = broad, sh = shoulder. Combustion analyses were performed by

Midwest Laboratories of Indianapolis, IN (USA) or or Robertson Microlit Laboratories of Madison, NJ (USA).

All cyclic voltammetry (CV) and differential pulse voltammetry (DPV) were performed at room temperature under dinitrogen atmosphere with a Gamry Interface 1010E potentiostat. A single-compartment cell was used for all experiments. Voltammograms were recorded in 0.3M [NBu<sub>4</sub>][PF<sub>6</sub>] THF solution at  $v = 100$  mV/s with a 3mm glassy carbon working electrode, a Pt wire counter electrode and a silver wire pseudoreference electrode (separated from the bulk solution by a Vycor tip). Potentials were calibrated against the Fc/Fc<sup>+</sup> redox couple (internal standard). Mo complex concentrations ranged from 1-1.5 mM.

**[( $\eta^4$ -P<sub>4</sub>)MoI(CO)(CNAr<sup>Dipp2</sup>)<sub>2</sub>][CoCp<sub>2</sub>] ([5][CoCp<sub>2</sub>]).** To a thawing 2:1 THF/pentane solution of ( $\eta^4$ -P<sub>4</sub>)MoI<sub>2</sub>(CO)(CNAr<sup>Dipp2</sup>)<sub>2</sub> (0.100 g, 74  $\mu$ mol, 1 equiv, 2 mL) was added a thawing THF solution of CoCp<sub>2</sub> (0.029 g, 153  $\mu$ mol, 2.07 equiv, 1 mL). The reaction mixture was stirred at r.t. for 1 h, stored overnight at -40 °C, filtered, and concentrated in vacuo. The resulting solid was taken up in toluene (0.5 mL), layered with pentane, and recrystallized at -40 °C to afford black crystalline needles (0.079 g, 56  $\mu$ mol, 74%). <sup>1</sup>H NMR (500 MHz, THF/d<sub>8</sub>)  $\delta$  7.18 (t,  $J = 7.5$  Hz, 2H), 7.14 (t,  $J = 7.7$  Hz, 4H), 7.08 (d,  $J = 7.5$  Hz, 4H), 7.05 (d,  $J = 7.7$  Hz, 4H), 7.01 (d,  $J = 7.5$  Hz, 4H), 5.13 (br, 10H, <sup>+</sup>Co(C<sub>5</sub>H<sub>5</sub>)<sub>2</sub>), 2.60 (sept,  $J = 6.5$  Hz, 8H), 1.18 (m,  $J = 5.4$  Hz, 24H), 0.99 (d,  $J = 6.8$  Hz, 24H). <sup>13</sup>C NMR (126 MHz, THF/d<sub>8</sub>)  $\delta$  146.6, 146.5, 139.2 (br), 136.5, 130.9, 129.0, 126.1, 123.6, 123.5, 31.6, 25.1, 25.0 (CO and CNAr<sup>Dipp2</sup> signals could not be resolved even after scanning for long durations). <sup>31</sup>P{<sup>1</sup>H} (161.9 MHz, THF/d<sub>8</sub>, 55-80 (br, m) ppm. FTIR (KBr windows, C<sub>6</sub>D<sub>6</sub>, 25 °C):  $\nu$ (C $\equiv$ N) = 2077 (sh), 2050 (vs), 1997(sh),  $\nu$ (C $\equiv$ O) = 1884, other: 2960 (s), 2928(m), 1579 (vw), 1413(w), 1007 (w), 757 (w).

**( $\eta^4$ -P<sub>4</sub>)MoI(CO)(CNAr<sup>Dipp2</sup>)<sub>2</sub>(TI) ([5•TI]).** To a thawing DME solution of [5][CoCp<sub>2</sub>] (0.100 g, 71  $\mu$ mol, 1 equiv, 3 mL) was added a thawing DME solution of TIOTf (0.026 g, 74  $\mu$ mol, 1.04 equiv, 1 mL). The reaction mixture was stirred at r.t. for 1 h, stored overnight at -40 °C, filtered, and concentrated in vacuo. The resulting solid was taken up in toluene (0.5 mL), layered with pentane, and recrystallized at -40 °C to afford large red crystals (0.076 g, 51  $\mu$ mol, 74%). <sup>1</sup>H NMR (500 MHz, C<sub>6</sub>D<sub>6</sub>)  $\delta$  7.43 (t, *J* = 7.7 Hz, 4H), 7.22 (d, *J* = 7.1 Hz, 4H), 7.18 (d, *J* = 7.7 Hz, 4H), 6.89 – 6.82 (m, 4H), 6.80 – 6.73 (m, 2H), 2.68 (sept, *J* = 6.8 Hz, 4H), 2.60 (sept, *J* = 6.8 Hz, 4H), 1.44 (d, *J* = 6.9 Hz, 12H), 1.35 (d, *J* = 6.9 Hz, 12H), 0.98 (d, *J* = 6.7 Hz, 12H), 0.97 (d, *J* = 6.6 Hz, 12H). <sup>13</sup>C NMR (126 MHz, C<sub>6</sub>D<sub>6</sub>)  $\delta$  147.8, 147.2, 138.3, 135.8, 130.9, 130.0, 129.0, 127.4(br), 124.1 (br), 31.4, 25.83, 24.9, 24.2 (br) (CO and CNAr<sup>Dipp2</sup> signals could not be resolved even after scanning for long durations). <sup>31</sup>P{<sup>1</sup>H} 145-182 (br, m). FTIR (KBr windows, C<sub>6</sub>D<sub>6</sub>, 25 °C):  $\nu$ (C $\equiv$ N) = 2048 (vs), 2071 (sh), 1994 (w),  $\nu$ (C $\equiv$ O) = 1893 (s), other: 2962 (s), 2931 (m), 2866(m), 1068 (m), 914 (w), 914 (m), 760 (m) cm<sup>-1</sup>.

**( $\eta^4$ -P<sub>4</sub>)MoI(CO)(CNAr<sup>Dipp2</sup>)<sub>2</sub> (6).** To a thawing DME solution of [5][CoCp<sub>2</sub>] (0.100 g, 71  $\mu$ mol, 1 equiv, 3 mL) was added a thawing DME solution of AgBF<sub>4</sub> (0.014 g, 72  $\mu$ mol, 1.01 equiv, 1 mL). The reaction mixture was stirred at r.t. for 1 h, stored at -40 °C overnight, filtered, and concentrated in vacuo. It was then taken up in Et<sub>2</sub>O (0.5 mL) and recrystallized at -40 °C to afford dark red crystals (0.052 g, 42.4  $\mu$ mol, 60%). <sup>1</sup>H NMR (300 MHz)  $\delta$  11.47, 7.57, 7.27, 7.17, 7.12, 7.05, 3.12, 1.68, 1.29 (all signals are broad). FTIR (KBr windows, C<sub>6</sub>D<sub>6</sub>, 25 °C):  $\nu$ (C $\equiv$ N) = 2137 (sh), 2121 (s),  $\nu$ (C $\equiv$ O) = 1984 (s), other: 2962 (s), 2927 (m), 2870 (w), 1469 (w), 1447 (w), 1412 (w), 1385(w), 1321 (w), 1056 (w), 801 (w), 757 (m), 438(w) cm<sup>-1</sup>.

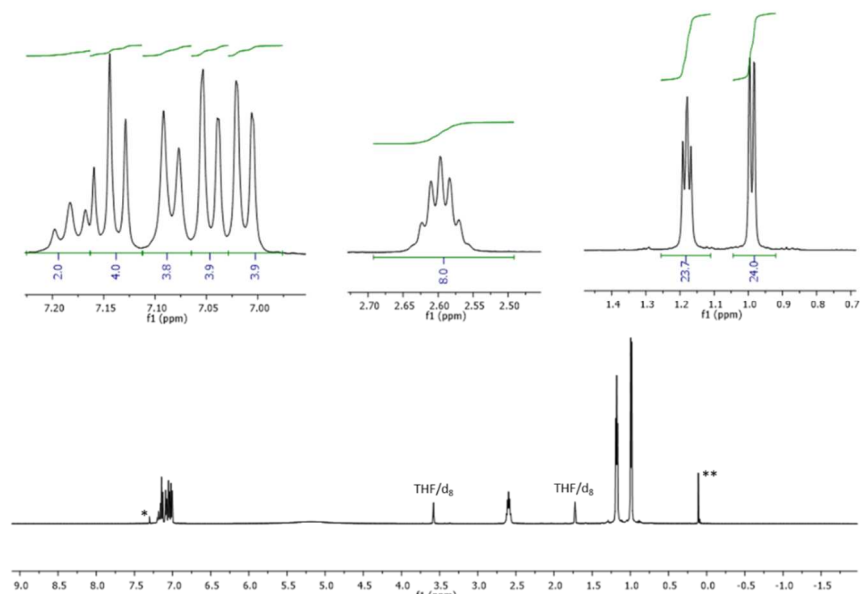


**Figure 5.11.**  $^1\text{H}$  NMR (500 MHz, THF/ $d_8$ ) of  $[(\eta^4\text{-P4})\text{MoI}(\text{CO})(\text{CNAr}^{\text{Dipp2}})_2][\text{CoCp}_2]$  (**[5]** $[\text{CoCp}_2]$ ). Rapid ion exchange in THF enables resolution of coupling constants and the time-averaged cobaltocenium ( $^+\text{CoCp}_2$ ) chemical shift (br, 5.6 – 4.8 ppm). \* $\text{C}_6\text{H}_6$ , \*\*Si-grease

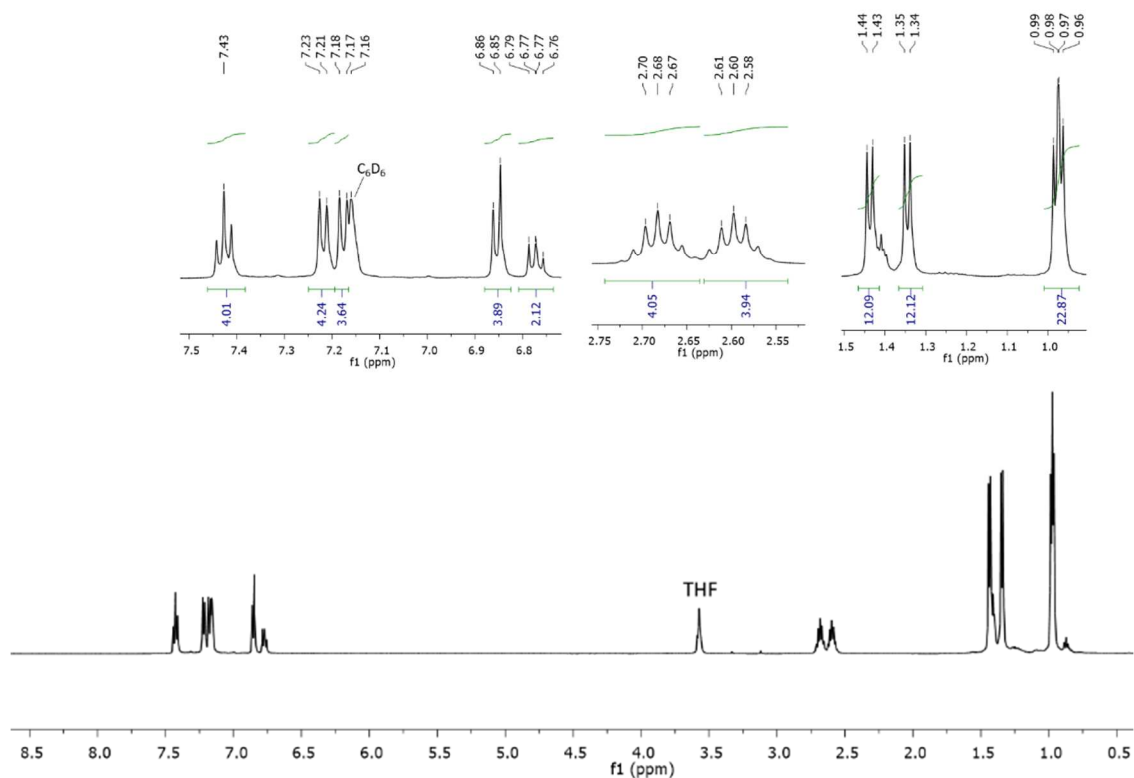


**Figure 5.12.**  $^1\text{H}$  NMR (500 MHz,  $\text{C}_6\text{D}_6$ ) of  $(\eta^4\text{-P4})\text{MoI}(\text{CO})(\text{CNAr}^{\text{Dipp2}})_2(\text{Tl})$  (**[5•Tl]**), THF solvated crystals). \*Si-grease present in the instrument probe.



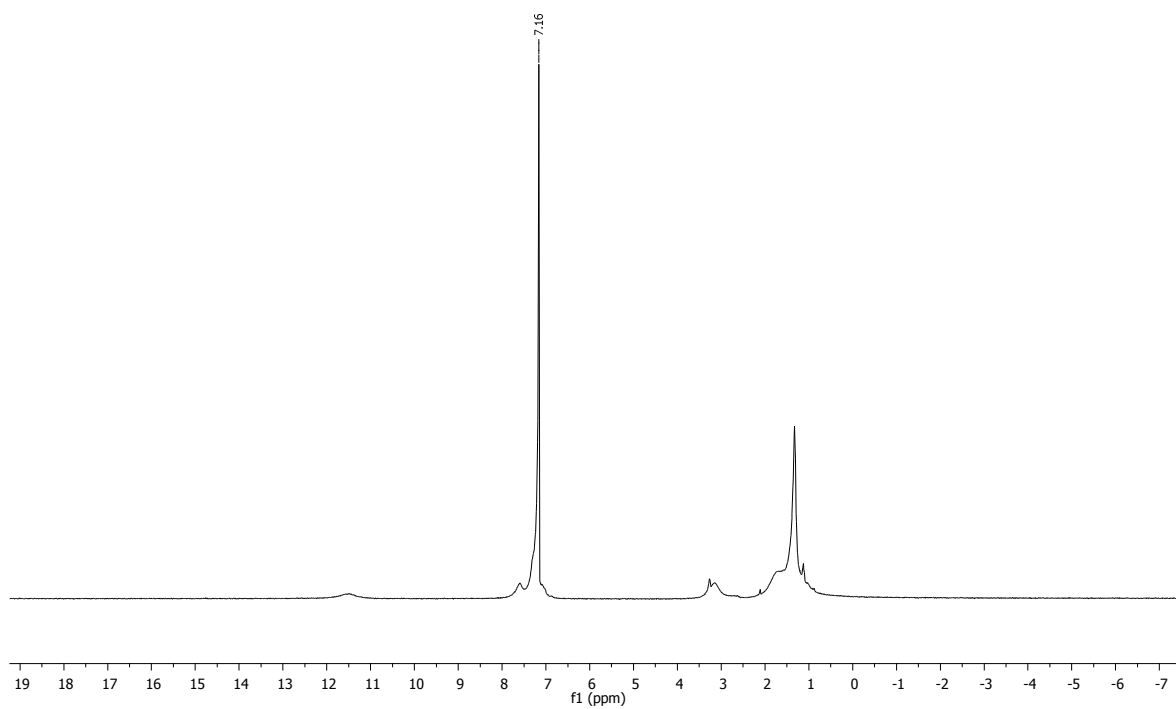


**Figure 5.13.**  $^1\text{H}$  NMR ( $\text{C}_6\text{D}_6$ , 300 MHz) of  $(\eta^4\text{-P}_4)\text{MoI}(\text{CO})(\text{CNAr}^{\text{Dipp}2})_2$  (**6**).

#### 5.4 Details of DFT computational studies

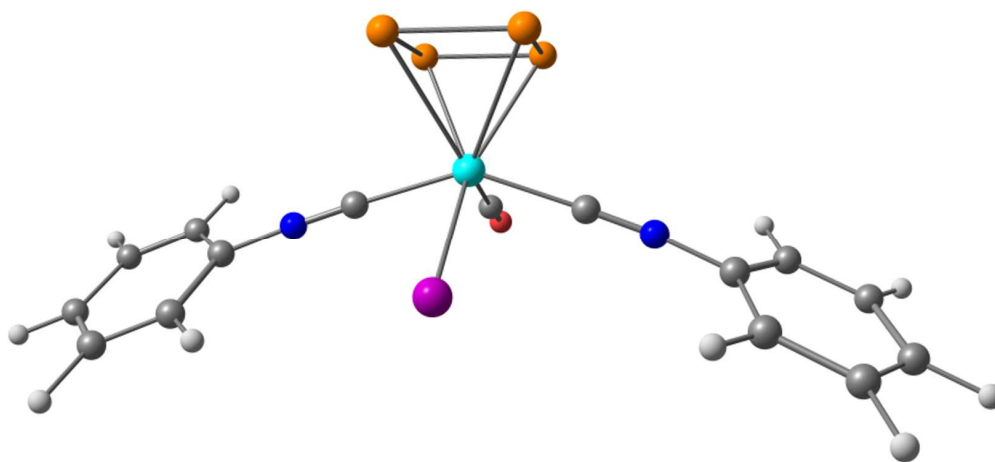


**Figure 5.14.** Optimized coordinates for model *cyclo*- $\text{P}_4$  radical complex **6M**.

### 5.4.1 Geometry optimized coordinates

( $\eta^4$ -P<sub>4</sub>)MoI(CO)(CNPh)<sub>2</sub> (6M)

Mo	13.45702853271695	14.38550246113488	16.62422124582854
I	11.67988355836503	12.64113790286165	15.27818784857020
N	15.41324637697775	11.96212836005349	15.63963590957479
C	17.45438331703170	10.83914134320485	15.03412805160577
C	16.05296403956130	10.85527886753850	15.12937441149356
C	18.08708891395993	9.71329086868521	14.51097265365850
H	19.17521636719389	9.69613086597995	14.43409886131454
C	17.33565397920454	8.61349694129658	14.08442516819603
H	17.83738171286499	7.73565999075131	13.67551728674726
C	15.28894152032466	9.75396801391929	14.70482481942484
C	15.94047336980099	8.63904494944923	14.18221208080061
H	15.35265938810458	7.78296220156228	13.84877687665016
C	14.70395816973928	12.82639172660938	16.02083686960735
P	13.74907958826891	16.19380288610505	18.46230070979239
O	15.38671813368406	16.30548198750885	15.01748733715941
C	14.67095793109859	15.59324797269585	15.58398422661331
P	15.28587937321956	14.63607684419530	18.44605789129183
P	12.21740445145211	14.67281588373263	18.88858943232018
P	13.74929964250500	13.12044386673075	18.87205318462824
N	11.05012689876249	16.38639926716964	15.68836479279771
C	8.91263398040813	16.36240383709873	14.59415106478450
C	9.94833125286197	17.07099087765804	15.22826090241692
C	7.80152587736946	17.06093424122457	14.12755758310998
H	6.99514709039177	16.51610970904930	13.63444335819717
C	7.71426719368095	18.44745722558282	14.29145615354897
H	6.83904799080641	18.98555939349638	13.92533177274789
C	9.87160441315312	18.46390123196372	15.39380140780620
C	8.74900061359422	19.14319401894453	14.92471025314584
H	8.68291737957594	20.22432056003755	15.05522862335246
C	11.90815203814946	15.66148038481922	16.05277585522258
H	14.20275770069214	9.79553614953487	14.78944397189986
H	18.02435787613746	11.70527356366123	15.36992167233980
H	8.99969085550409	15.28172227948864	14.47900790287698
H	10.68822453283843	18.99080705425568	15.88716980947571

### 5.5 Crystallographic determination of molecular structures

Positional disorder of the [ $\eta^4$ -P<sub>4</sub>)MoI(CO)(TI)] fragment was refined over two positions with 63% and 37% occupancy of the major and minor component, respectively. EADP was applied to adjacent disorder components where required. The PLATON SQUEEZE procedure was applied to remove residual electron density from disordered benzene and pentane (134 electrons found in solvent accessible volume, corresponding to ca. 4.5 equiv benzene).

Complex 6: Disorder of  $[\text{Mo}(\text{CO})(\eta^4\text{-P}_4)]$  was resolved over two positions, related by 2-fold rotation, with 50% occupancy. The corresponding positions of iodine were located at 44.6% occupancy, with the remaining balance being accounted for by two additional symmetry-related positions (5.4% occupancy). C- and O-atom positions of carbon monoxide were refined with *dfix* instructions due to instability of refinement imparted by overlapping electron density of iodine. Disorder of  $\text{CNAr}^{\text{Dipp}^2}$  flanking rings and isopropyl groups were also resolved with 50% occupancy. EADP was applied to adjacent disorder components where required. Residual electron density from heavily disordered pentane was removed with PLATON SQUEEZE (217 electrons in solvent-accessible void, corresponding to ca. 8 equiv pentane in the unit cell).

**Table 5.2.** Crystallographic Data Collection and Refinement Information

	$[(\eta^4\text{-P}_4)\text{MoI}(\text{CO})$ $(\text{CNAr}^{\text{Dipp}^2})_2][\text{CoCp}_2]\cdot$ $(\text{THF})_3$ $([\mathbf{5}][\text{CoCp}_2])$	$(\eta^4\text{-P}_4)\text{MoI}(\text{CO})$ $(\text{CNAr}^{\text{Dipp}^2})_2(\text{TI})$ $([\mathbf{5}\cdot\text{TI}])$	$(\eta^4\text{-P}_4)\text{MoI}(\text{CO})$ $(\text{CNAr}^{\text{Dipp}^2})_2$ $(\mathbf{6})$
Formula	$\text{C}_{81.6}\text{H}_{95.8}\text{CoIMoN}_2\text{O}_{2.9}\text{P}_4$	$\text{C}_{63}\text{H}_{74}\text{IMoN}_2\text{OP}_4\text{TI}$	$\text{C}_{63}\text{H}_{74}\text{IMoN}_2\text{OP}_4$
Crystal System	Triclinic	Monoclinic	Orthorhombic
Space Group	P-1	$\text{P2}_1$	Pccn
<i>a</i> , Å	19.2750(8)	11.8836(5)	17.248
<i>b</i> , Å	21.6259(9)	20.7901(11)	18.535
<i>c</i> , Å	23.3225(9)	14.3040(5)	21.558
$\alpha$ , deg	116.406(2)	90	90
$\beta$ , deg	93.467(2)	90.448(2)	90
$\gamma$ , deg	108.130(2)	90	90
<i>V</i> , Å <sup>3</sup>	8046.1(6)	3533.9(3)	6892
<i>Z</i>	4	2	4
Radiation ( $\lambda$ , Å)	Cu-K $\alpha$ , 1.54184	Cu-K $\alpha$ , 1.54184	Cu-K $\alpha$ , 1.54184
$\rho$ (calcd.), g/cm <sup>3</sup>	1.343	1.340	1.178
Temp, K	100	100	100
$\theta$ max, deg	138.924	117.68	59.048
data/parameters	30075/1807	6392/705	4955/385
<i>R</i> <sub>1</sub>	0.1307	0.0473	0.0842
w <i>R</i> <sub>2</sub>	0.3019	0.1281	0.2437
GooF	1.260	1.049	1.028

## 5.6 Acknowledgements

Chapter 5 was adapted with permission from Mandla, K. A.; Moore, C. E.; Gembicky, M.; Rheingold, A. L.; Figueroa, J. S. “The Electrochemistry of Molybdenum *cyclo*-P<sub>4</sub> Complexes and Isolation of the First Mononuclear *cyclo*-P<sub>4</sub> Radical.” *Manuscript in progress*. The dissertation author is the first author of this paper.

## 5.7 References

- (1) Ginsberg, A. P.; Lindsell, W. E. *J. Am. Chem. Soc.* **1971**, *93* (8), 2082–2084.
- (2) Ginsberg, A. P.; Lindsell, W. E.; Silverthorn, W. E. *Trans. N. Y. Acad. Sci.* **1971**, *33* (3 Series II), 303–312.
- (3) Caporali, M.; Gonsalvi, L.; Rossin, A.; Peruzzini, M. *Chem. Rev.* **2010**, *110* (7), 4178–4235.
- (4) Cossairt, B. M.; Piro, N. A.; Cummins, C. C. **2010**, 4164–4177.
- (5) Breunig, J. M.; Tofan, D.; Cummins, C. C. *Eur. J. Inorg. Chem.* **2014**, 1605–1609.
- (6) Cossairt, B. M.; Diawara, M.; Cummins, C. C. 2–3.
- (7) Cossairt, B. M.; Diawara, M.; Cummins, C. C. *Science (80-. )*. **2009**, *323*, 602.
- (8) Pinter, B.; Smith, K. T.; Kamitani, M.; Zolnhofer, E. M.; Tran, B. L.; Fortier, S.; Pink, M.; Wu, G.; Manor, B. C.; Meyer, K.; et al. *J. Am. Chem. Soc.* **2015**, *137* (48), 15247–15261.
- (9) King, R. B.; Saran, M. S. *Inorg. Chem.* **1974**, *13* (1), 74–78.
- (10) Sarapu, A. C.; Fenske, R. F. *Inorg. Chem.* **1975**, *14* (2), 247–253.
- (11) Yamamoto, Y. *Coord. Chem. Rev.* **1980**, *32* (3), 193–233.
- (12) Sarapu, A. C.; Fenske, R. F. *Inorg. Chem.* **1972**, *11* (12), 3021–3025.
- (13) Matare, C. J.; Foo, D. M.; Kane, K. M.; Zehnder, R.; Wagener, M.; Shapiro, P. J.; Concolino, T.; Rheingold, A. L. *Organometallics* **2000**, *19* (8), 1534–1539.
- (14) Lyons, L. J.; Pitz, S. L.; Boyd, D. C. *Inorg. Chem.* **1995**, *34* (1), 316–322.

- (15) Essenmacher, G. J.; Treichel, P. M. *Inorg. Chem.* **1977**, *16* (4), 800–806.
- (16) Evans, D. H. *Chem. Rev.* **2008**, *108*, 2113–2144.
- (17) Bard, A. J.; Merz, A.; Merzlb, A. *J. Am. Chem. Soc.* **1979**, *101* (11), 2959–2965.
- (18) Agnew, D. W.; Sampson, M. D.; Moore, C. E.; Rheingold, A. L.; Kubiak, C. P.; Figueroa, J. S. **2016**.
- (19) Agnew, D. W.; Moore, C. E.; Rheingold, A. L.; Figueroa, J. S. *Angew. Chem. Int. Ed. Engl.* **2015**, *54* (43), 12673–12677.
- (20) Vanýsek, P. Marcel Dekker, 1978; Vol. 18.
- (21) Welsch, S.; Gregoriades, L. J.; Sierka, M.; Zabel, M.; Virovets, A. V.; Scheer, M. *Angew. Chemie Int. Ed.* **2007**, *46* (48), 9323–9326.
- (22) Fleischmann, M.; Welsch, S.; Gregoriades, L. J.; Gröger, C.; Scheer, M. **2014**, *69*, 1348–1356.
- (23) Rajaram, J.; Ibers, J. A. *Inorg. Chem.* **1973**, *12* (6), 1313–1317.
- (24) Clarkson, L. M.; Clegg, W.; Hockless, D. C. R.; Norman, N. C.; Marder, T. B. *J. Chem. Soc., Dalton Trans.* **1991**, *0*, 2229–2239.
- (25) Richard, P.; Zrineh, A.; Guillard, R.; Habbou, A.; Lecomte, C.; IUCr. *Acta Crystallogr. Sect. C Cryst. Struct. Commun.* **1989**, *45* (8), 1224–1226.
- (26) Curnow, O. J.; Schiemenz, B.; Huttner, G.; Zsolnai, L. *J. Organomet. Chem.* **1993**, *459* (1–2), 17–20.
- (27) Do, Y.; Knobler, C. B.; Hawthorne, M. F. *J. Am. Chem. Soc.* **1987**, *109* (6), 1853–1854.
- (28) Mädl, E.; Balázs, G.; Peresyphkina, E. V.; Scheer, M. *Angew. Chemie Int. Ed.* **2016**, *55* (27), 7702–7707.
- (29) Armarego, W. L. F.; Chai, C. L. L. 5th ed.; Elsevier, 2003.
- (30) Pangborn, A. B.; Giardello, M. A.; Grubbs, R. H.; Rosen, R. K.; Timmers, F. J. *Organometallics* **1996**, *15* (5), 1518–1520.
- (31) Fox, B. J.; Sun, Q. Y.; DiPasquale, A. G.; Fox, A. R.; Rheingold, A. L.; Figueroa, J. S. *Inorg. Chem.* **2008**, *47* (19), 9010–9020.

## Chapter 6

# Reactivity of *cyclo*-P<sub>4</sub> Opens New Routes to Phosphaallenes and *cyclo*-P<sub>3</sub>

### 6.1 Introduction

A longstanding objective of organometallic chemistry has been the development of new methodologies for the derivatization of white phosphorus. Today, P<sub>4</sub> remains a critical source of phosphorus used in the preparation of organophosphorus products for food, pharmaceuticals, detergents, and other specialty products. Currently, the derivatization of phosphorus into valuable consumer products typically begins with oxidation of P<sub>4</sub> with Cl<sub>2</sub>-gas to deliver PCl<sub>3</sub>, which may then be submitted to multistep synthesis for further derivatization.<sup>1,2</sup> The ability of transition metals to activate the P<sub>4</sub>-tetrahedron of elemental phosphorus has thus motivated a large body of work with the goal of developing direct synthetic routes to valuable phosphorus-containing derivatives.

In the preceding chapters, the synthesis of stable, mononuclear *cyclo*-P<sub>4</sub> complexes was described. The unique electronic structure of ( $\eta^4$ -P<sub>4</sub>)MoI<sub>2</sub>(CO)(CNAr<sup>Dipp2</sup>)<sub>2</sub> **1** with P-P sigma bonding orbitals lying above the three  $\pi$ -orbitals together with low-lying vacant d-orbitals was found to enable photolytic reductive elimination to regenerate tetrahedral P<sub>4</sub> as a free species in solution. In chapter 4 and 5, the redox chemistry of **1** and ( $\eta^4$ -P<sub>4</sub>)Mo(CO)<sub>2</sub>(CNAr<sup>Dipp2</sup>)<sub>2</sub> (**2**) revealed the *cyclo*-P<sub>4</sub> fragment to be surprisingly resilient, enabling isolation of the first *cyclo*-P<sub>4</sub> radical species ( $\eta^4$ -P<sub>4</sub>)MoI(CO)(CNAr<sup>Dipp2</sup>)<sub>2</sub> and highly reduced *cyclo*-P<sub>4</sub> analogs to Mo(CO)<sub>3</sub>( $\eta^6$ -C<sub>6</sub>H<sub>6</sub>) complexes, i.e. [ $\eta^4$ -P<sub>4</sub>)Mo(CO)<sub>n</sub>(CNAr<sup>Dipp2</sup>)<sub>3-n</sub>]<sup>2-</sup>. Importantly, these investigations have provided high yielding synthetic routes to five unique structural motifs bearing the *cyclo*-P<sub>4</sub> unit –

more than double the number of known mononuclear *cyclo*-P<sub>4</sub> complexes.<sup>3-6</sup> Yet to be described, here or in the literature, is the utility of these systems for further derivatization of phosphorus.

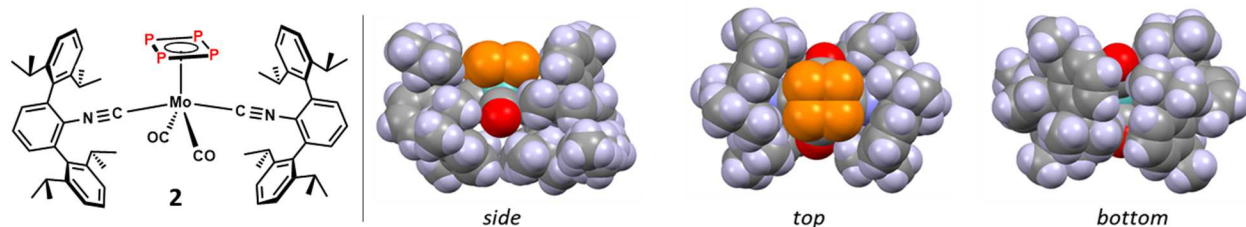
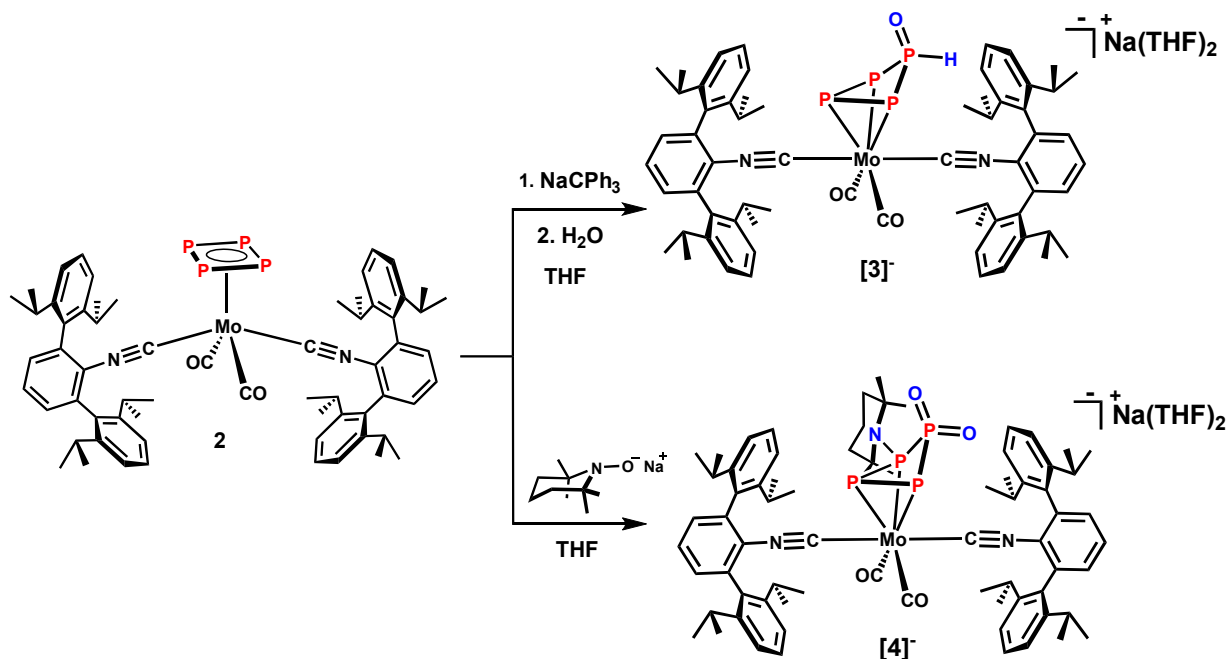


**Figure 6.1.** Space-filling model of **2**.

In this work, the sterically encumbered complex **2** (Figure 6.1) was used to interrogate the ligand-based reactivity of *cyclo*-P<sub>4</sub>. Despite excellent kinetic and thermodynamic stability, **2** readily undergoes nucleophilic addition with oxygen nucleophiles to give anionic  $\eta^3$ -cyclophosphaallyl complexes. In a departure from the addition of nucleophiles to carbon-based cyclobutadiene ligands,<sup>7-9</sup> the presence of open coordination-sites at phosphorus enable electron density to be dispersed in what can be regarded as intramolecular oxidative addition of O-H and N-O bonds to give the functionalized  $\eta^3$ -phosphaallyls, e.g. P<sub>3</sub>P(O)H and RN-P(P<sub>2</sub>)PO<sub>2</sub>. The reactivity of **2** was also investigated with electrophiles. Lewis acidic metal fragments were found to link two equivalents of **2** through coordination of the phosphorus lone pairs without disruption of P-P bonding. Interestingly, similar reactivity has been utilized previously in the construction of remarkable supramolecular structures with fullerene topology.<sup>10</sup> More intriguing was the formation of  $(\eta^3\text{-P}_3)\text{MoI}(\text{CO})_2(\text{CNAr}^{\text{Dipp}2})_2$  (**3**) upon treatment of **2** with 1 equiv I<sub>2</sub>. Interrogation of the mechanism revealed the formation of cyclo-P<sub>3</sub> to be a large thermodynamic driving force enabling the loss of one equivalent of iodophosphinidine (PI). Importantly, the successful trapping of P-I with 1,2-bis(diphenylphosphino)ethane (dppe) suggests this process may be a useful source of mono-valent phosphorus.

## 6.2 Results and discussion

### 6.2.1 Activation of *cyclo*-P<sub>4</sub> with Nucleophiles



**Scheme 6.1** Nucleophilic addition reactions with **2**.

Recent investigations by Scheer and co-workers have demonstrated the functionalization of *cyclo*-P<sub>5</sub> ligands with main group nucleophiles.<sup>11</sup> In that work, addition of strong nucleophiles resulted in puckered cyclic phosphides whereby the functionalized P-atom was released from the plane of the ring with the functional group occupying that single substituent occupying the however. As an entry to these investigations, NaOH was generated in situ by treatment of **2** with 1.3 equiv NaCPh<sub>3</sub> followed immediately by H<sub>2</sub>O (1.3 equiv) to give a rare<sup>12</sup> phosphidoallyl motif in complex **[3]<sup>-</sup>** (Scheme 6.1 Nucleophilic addition reactions with **2**.. Although the hydrogen atom could not be located at phosphorus in the difference map by XRD (Figure 6.2), the resulting product showed clear evidence of P-H bond formation by <sup>31</sup>P NMR with a doublet-of-triplet-of-doublets at 38 ppm ( $J_{PH} = 412$  Hz) collapsing to a triplet of doublets (td) in the proton decoupled



spectrum (Figure 6.3 **Figure 6.3**). Initially, we considered the possibility that  $[3]^-$  had been generated by electron transfer from trityl anion since the trianionic ligand would be expected to rapidly protonate upon addition of  $H_2O$ . Inconsistent with this notion, however,  $^1H$  NMR showed no reaction between **2** and  $NaCPh_3$  on the timescale in which this reaction was carried out. Furthermore, the direct addition of hydroxide was achieved by treatment of **2** with a THF solution containing 1.5 equiv KOH and dibenzo-18-crown-6, as indicated by the identical coupling pattern by  $^{31}P$  NMR. We thus speculated that nucleophilic addition of  $^-OH$  was followed by a rapid intramolecular proton-transfer as shown in Figure 6.4.

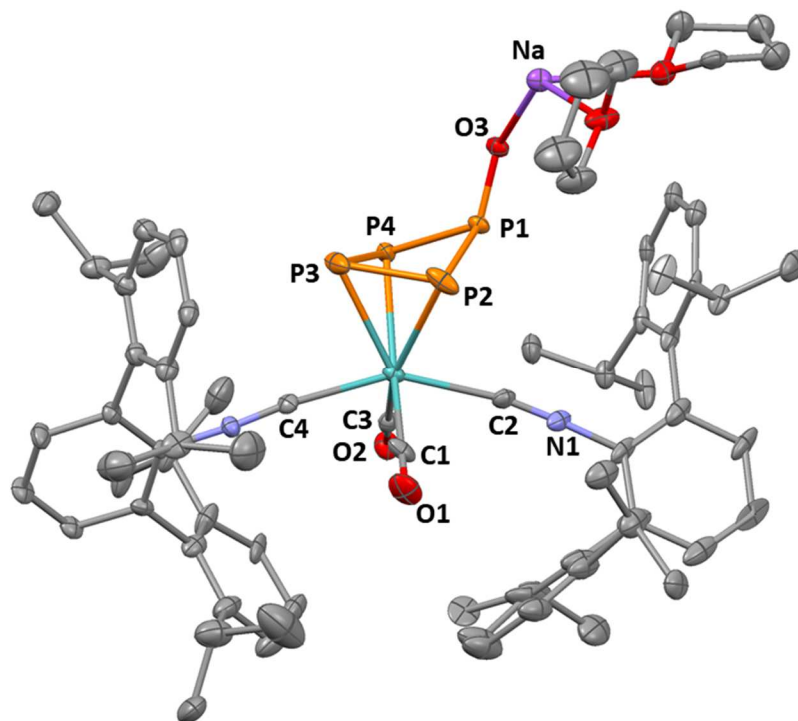


**Figure 6.2.** Molecular structure of  $[3]^-$ .

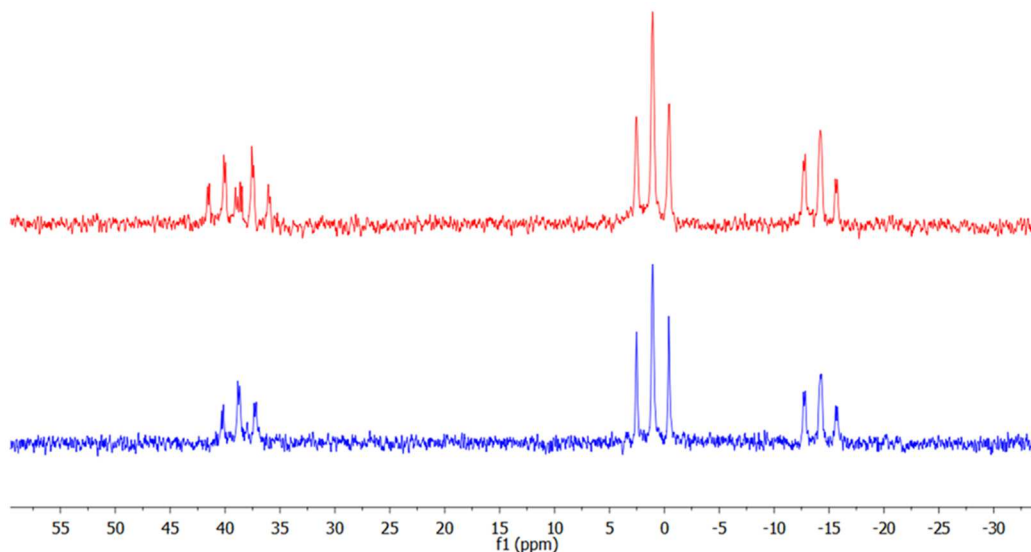


**Figure 6.3** Bottom: Proton-decoupled spectrum of  $[3]^-$ ,  $^{31}\text{P}\{^1\text{H}\}$  NMR (161.9 MHz,  $\text{C}_6\text{D}_6$ ). Top:  $^{31}\text{P}$  NMR (161.9 MHz,  $\text{C}_6\text{D}_6$ ) showing  $^1\text{H}/^{31}\text{P}$  coupling of peak at 38 ppm ( $^1J_{\text{P-H}} = 412$  Hz).

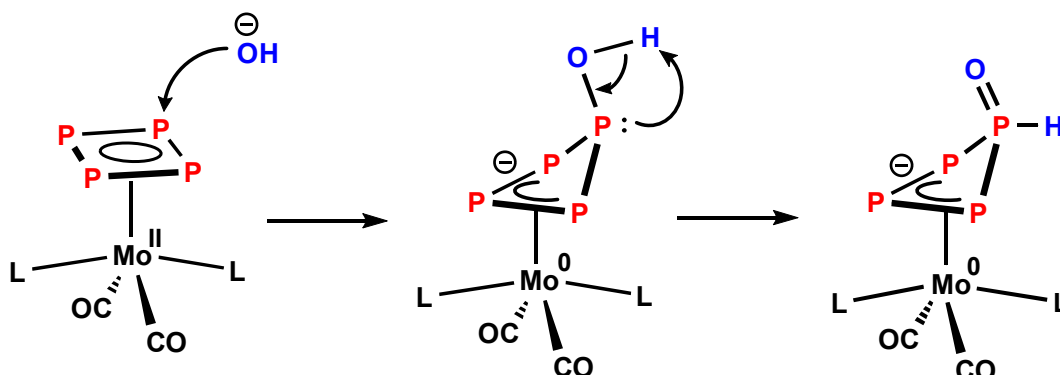


**Figure 6.4** Proposed reaction mechanism for the formation of  $[3]^-$ .

In further investigations of reactivity with nucleophilic oxygen species, treatment of **2** with 3-fold excess  $[\text{TEMPO}][\text{Na}]$  was found to result in a sudden darkening of solution to dark violet. Remarkably X-ray crystallography revealed the product to be phosphallene  $[4]^-$ . Interestingly, despite the transfer of two O-atoms and a piperidine group to phosphorus,  $[3]^-$  is only monoanionic. This complicates the mechanistic picture indicating electron-transfer equilibria in solution likely generate small quantities of the TEMPO radical which participate in O-atom

transfer following nucleophilic addition of  $[\text{TEMPO}]^-$  to phosphorus, as is supported by the large excess of NaTEMPO required to reach completion. Although mechanistic insight remains limited, the reaction **2** and  $[\text{TEMPO}][\text{Na}]$  provide an intriguing example of the divergent reactivity uniquely accessible to *cyclo*-P<sub>4</sub>.

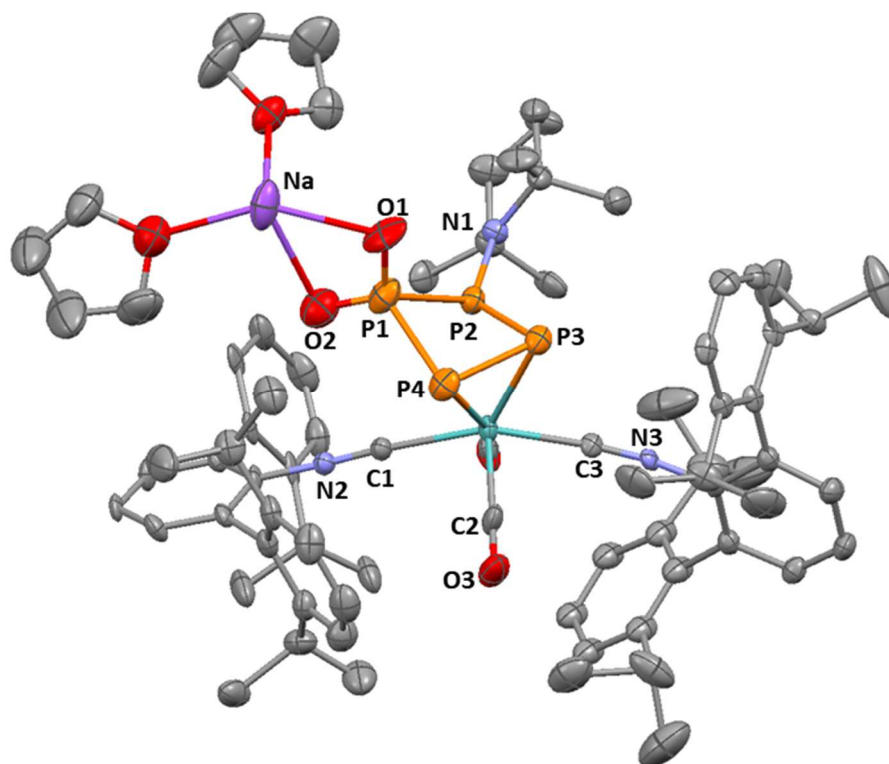


**Figure 6.5.** Molecular structure of  $[4]^-$ .

### 6.2.2 Complexation through *cyclo*-P<sub>4</sub> lone pairs

Treatment of **2** with 3 equiv  $\text{Mo}(\text{CO})_3(\text{ACN})_3$  in acetonitrile resulted in ligand rearrangement of the tris-acetonitrile complex to give the bis- $[\text{Mo}(\text{CO})_4]$  linked dimer **5**. Notably, previous work by Scheer and co-workers demonstrated the ability of *cyclo*-P<sub>4</sub> to serve as a 12 electron donor by pentanuclear coordination in which the phosphorus lone pairs of a  $[\text{W}(\text{CO})_4(\textit{cyclo}\text{-P}_4)]$  unit were capped by four  $[\text{W}(\text{CO})_5]$  fragments.<sup>13</sup> Interestingly, despite utilization of a pseudo-trivalent precursor  $\text{Mo}(\text{CO})_3(\text{ACN})_3$ , the sterically encumbering

isocyanides allowed for only two P-atoms from each ring to engage in coordination with  $\text{Mo}(\text{CO})_n$ . Interestingly, the dimerization suggests that cis-phosphide coordination has a sufficient thermodynamic driving force so as to overcome what is likely a significant entropic barrier.

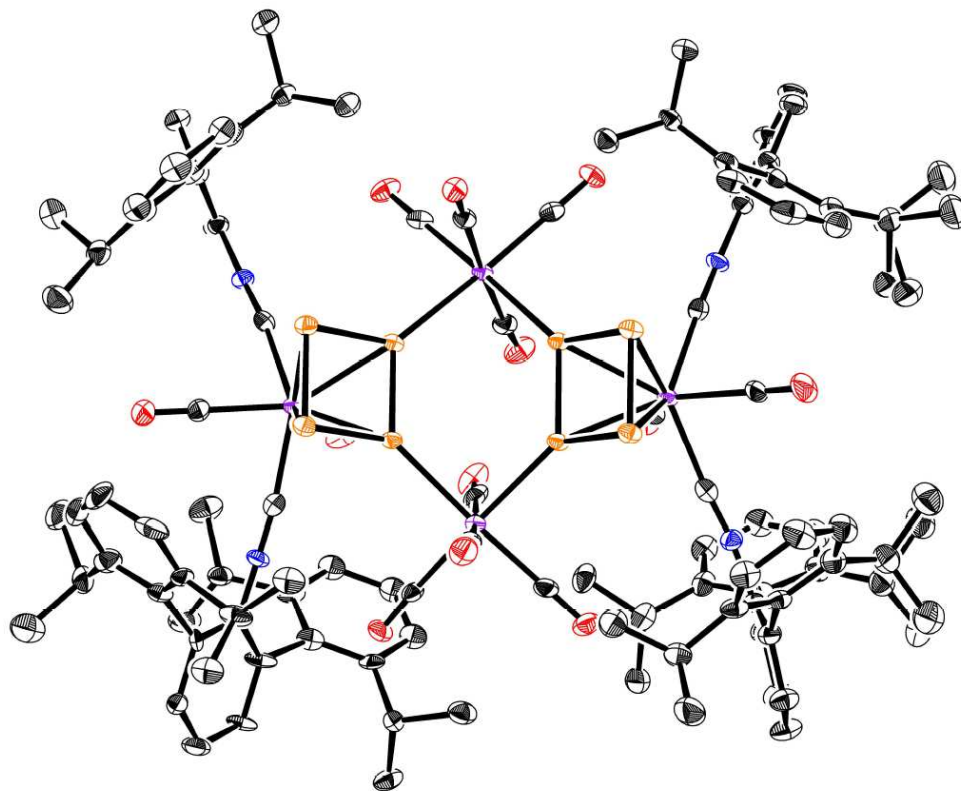


**Figure 6.6.** Molecular structure of **5**.

### 6.2.3 Synthesis of $(\eta^3\text{-P}_3)\text{MoI}(\text{CO})(\text{CNAr}^{\text{Dipp}2})_2$

As shown in Chapter 3, the molecular orbital picture of *cyclo*- $\text{P}_4$  in  $(\eta^4\text{-P}_4)\text{MoI}_2(\text{CO})(\text{CNAr}^{\text{Dipp}2})_2$  (**1**) and  $(\eta^4\text{-P}_4)\text{Mo}(\text{CO})_2(\text{CNAr}^{\text{Dipp}2})_2$  (**2**) unexpectedly reveals the  $b_{2u}$  P-P  $\sigma$ -bonding interactions to be higher in energy than the  $\pi$ -system. In that work, photolytic reduction elimination of tetrahedral  $\text{P}_4$  from **1** was initiated by promotion of an electron from the  $\sigma$ -bonding framework of the *cyclo*- $\text{P}_4$  ligand into the metal center. Importantly, it is by this initial perturbation in the electronic structure of *cyclo*- $\text{P}_4$  and the ensuing relaxation processes that the

P<sub>4</sub>-tetrahedron is restored and released from the metal-center as white phosphorus. A remarkable aspect of this process, especially when considering the proclivity of phosphorus to form complex catenates, is the origami-like control required to generate a highly strained, highly reactive species in high yield. Indeed, the high yields of P<sub>4</sub> in this process suggests that reconstruction of the P<sub>4</sub>-tetrahedron occurs through a well-defined process within the steric protection of the *m*-terphenyl ligands. Furthermore, the absence of catenates in solution is strong evidence against dissociation of a P<sub>4</sub>-diradical species<sup>14</sup> which then must undergo bicyclic ring closure. Noting that the sequence of events leading to formation of white phosphorus were initiated by the photo-oxidation of *cyclo*-P<sub>4</sub>, we were thus intrigued by the possibility that chemical oxidants could induce similar well-behaved structural reconfigurations.

Initial attempts to affect oxidation of **2** by stoichiometric metal-based oxidants (AgBF<sub>4</sub>, AgOTf) resulted in consumption of less than 10% of starting material, while the presence of large excess of the oxidizing species resulted in intractable mixtures. Gratifyingly, however, treatment with 1 equiv I<sub>2</sub> in C<sub>6</sub>D<sub>6</sub> resulted in rapid consumption of starting material by <sup>1</sup>H NMR and the appearance of a single sharp singlet at -341 ppm by <sup>31</sup>P NMR. Importantly, the high field resonance indicated an oxidatively induced re-organization of the phosphide ligand scaffold. Crystallographic structure determination of the product obtained from the reaction of **2** and I<sub>2</sub> established the product as the mononuclear *cyclo*-P<sub>3</sub> product (η<sup>3</sup>-P<sub>3</sub>)Mo(CO)<sub>2</sub>(CNAr<sup>Dipp2</sup>)<sub>2</sub> (**6-P<sub>3</sub>**, Figure 6.7). The product was obtained as an orange crystalline solid in 76% yield by washing the concentrated reaction mixture with pentane, followed by crystallization at -40 °C from an acetonitrile-layered solution of toluene. Importantly, in addition to demonstrating the ability of sterically encumbering ligands to direct chemical oxidation to the *cyclo*-P<sub>4</sub> ligand, isolation of the

resulting P-atom extruded product **6-P<sub>3</sub>** establishes *cyclo-P<sub>4</sub>* as a well-defined precursor to *cyclo-P<sub>3</sub>*.

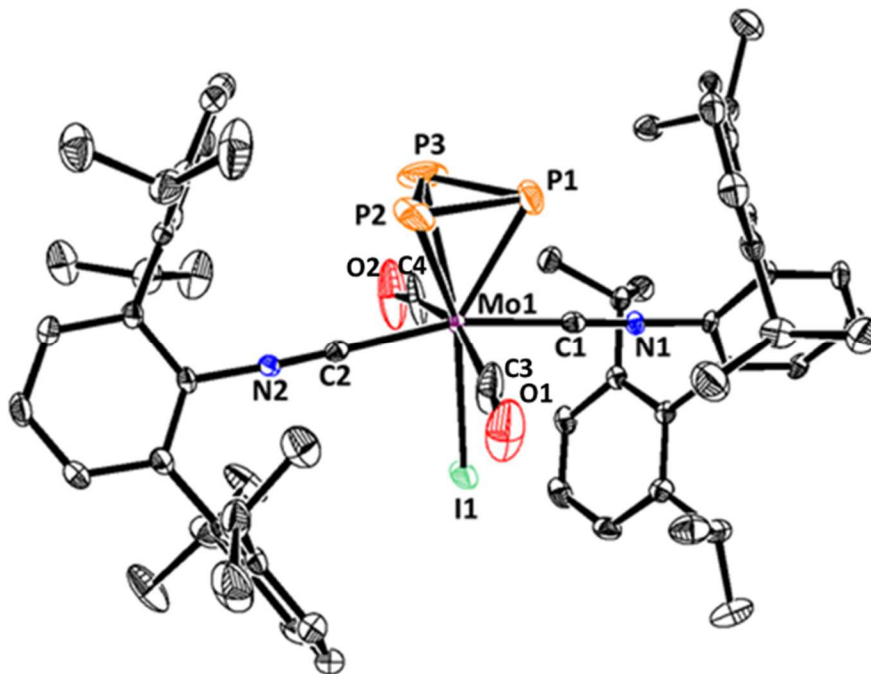


**Figure 6.7.** Molecular structure of  $(\eta^3\text{-P}_3)\text{MoI}(\text{CO})_2(\text{CNAr}^{\text{Dipp}2})_2$  (**6-P<sub>3</sub>**). Selected bond distances (Å) and angles (deg), Mo-P (avg) = 2.53(4), Mo- $[\eta^3\text{-P}_3]$  (centroid) = 2.444, Mo-C2 = 2.061(6), Mo-C3 = 2.061(6), Mo-C4 = 2.013(7), Mo-I = 2.7975(9), C1-N1 = 2.163(5), C2-N2 = 1.155(5), C3-O1 = 1.140(7), C4-O2 = 1.13(1). P-P (avg) = 2.11(9), C1-Mo-C2 = 164.5(1), C4-Mo-I = 75.8(2), C4-Mo-I = 83.8(2), C1-Mo- $[\eta^3\text{-P}_3]$ (cent) = C2-Mo- $[\eta^3\text{-P}_3]$  (cent) = 97.7(2), I-Mo- $[\eta^3\text{-P}_3]$ (cent) = 176.87.

#### 6.2.4 Synthesis of $[(\eta^3\text{-P}_3)\text{Mo}(\text{CO})(\text{CNAr}^{\text{Dipp}2})_2]\text{K}$

As noted previously, significant interest in *cyclo-P<sub>3</sub>* complexes has been derived from the portability of the P<sub>3</sub>-group for synthesis of atomically precise reagents.<sup>15</sup> In that work, anionic *cyclo-P<sub>3</sub>* complexes were found to be suitable for group transfer due to the increased electron density at phosphorus. We thus sought to determine if *cyclo-P<sub>3</sub>* metallates could be supported in our system. To that end, **6-P<sub>3</sub>** was treated with 1.1 equiv KC<sub>8</sub> in thawing THF. Following filtration, diffraction quality crystals were grown from pentane. Structural determination revealed

the resulting product to be  $7\text{-P}_3^-$  crystallized in a trimeric donut structure. Investigations are underway to determine if  $7\text{-P}_3^-$  is a suitable source of *cyclo*- $\text{P}_3$ .

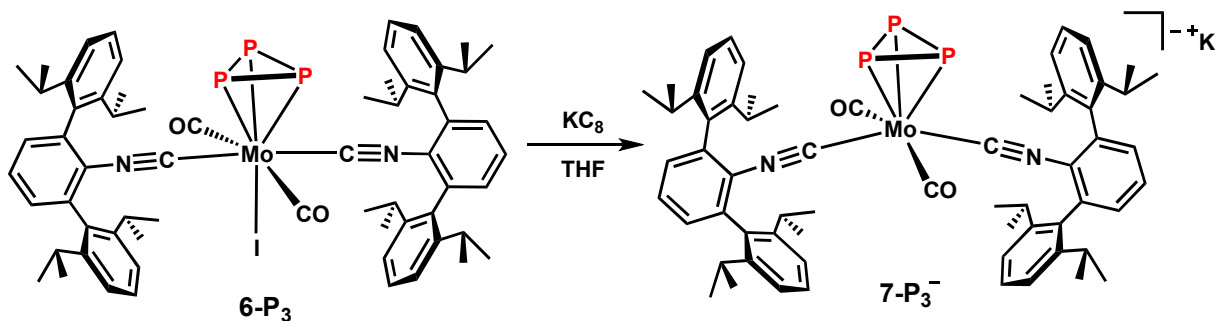


**Figure 6.8.** Synthesis of *cyclo*- $\text{P}_3$  anion  $7\text{-P}_3^-$ .

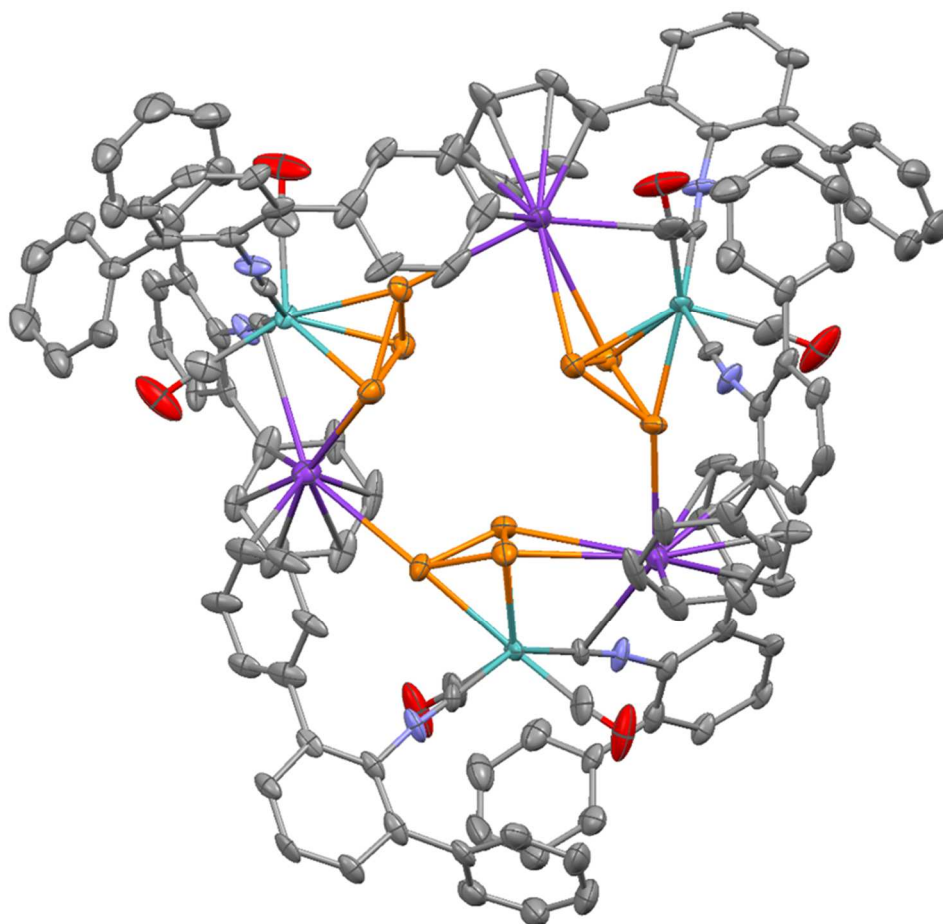


**Figure 6.9.** Expanded view of  $7\text{-P}_3^-$  showing trimeric structure with  $\text{P}\cdots\text{K}^+$  linkages (isopropyl groups excluded for clarity).

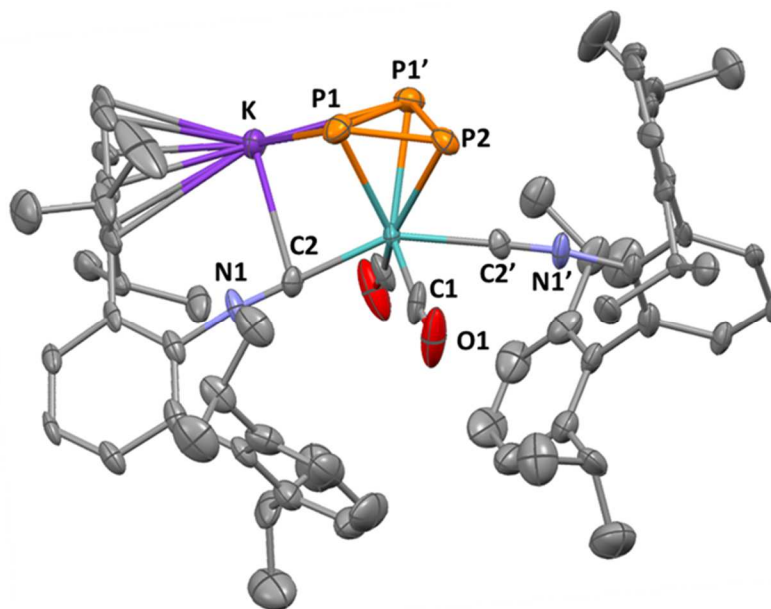


**Figure 6.10.** Molecular structure of a  $7\text{-P}_3^-$  monomeric unit. Mo-C1 = 1.99(1) Mo-C2 = 2.062(8), Mo-P1 = 2.580(5), Mo-P2 = 2.571(3), C1-O1 = 1.118(2), C2-N1 = 1.162(10), P1-P1' = 2.177(5), P1'-P2 = 2.197(4), P1-P2 = 2.058(5), P2-P1 = 2.058(5), Mo-P<sub>3</sub> (cent) = 2.256(3), P1-K = 3.331(4), P1'-K = 3.294(4), C1-Mo-C1' = 1.741(17), C2-Mo-C2' = 150.0(6), C1-Mo-P<sub>3</sub> (cent) = 107.9(4), C1'-Mo-P<sub>3</sub> (cent) = 132.2(4).

### 6.2.5 Analysis of Electronic Structure in *cyclo*-P<sub>3</sub> complexes

In order to determine the elementary steps leading to the structural reconfiguration from *cyclo*-P<sub>4</sub> to *cyclo*-P<sub>3</sub>, we sought to establish the distribution of electrons between the [ML<sub>4</sub>] (L = CO, CNAr<sup>Dipp2</sup>) fragment and *cyclo*-P<sub>3</sub>. While the electronic structure of *cyclo*-P<sub>3</sub> complexes have been analyzed previously, there remains ambiguity regarding the nature of the *cyclo*-P<sub>3</sub> ligand. With respect to formalisms, this section addresses ambiguity in the assignment of *cyclo*-P<sub>3</sub> as either a trianionic “3X” ligand or a monoanionic, 3e<sup>-</sup> donor, “LX”-type ligand (here, X refers to an anionic 1e<sup>-</sup> donor, while L is a neutral two-electron donor in accordance with the neutral electron counting method). For our purposes, such designation of *cyclo*-P<sub>3</sub> in **6-P<sub>3</sub>** provides a basis by which to determine if the P-atom extrusion is attributed to metal- or P<sub>4</sub>-based oxidation events.



Previously, molecular orbital analysis of high-valent *cyclo*-P<sub>3</sub> complexes ( $\eta^3$ -P<sub>3</sub>)Mo(N[*i*Pr]Ar')<sub>3</sub> and (nacnac)V( $\eta^3$ -P<sub>3</sub>)(Ntoly<sub>2</sub>) led Mindiola and co-workers to designate *cyclo*-P<sub>3</sub> as a trianionic 3X ligand.<sup>16</sup> Despite similar bond parameters to these, and other *cyclo*-P<sub>3</sub> complexes, our analysis suggests that *cyclo*-P<sub>3</sub> in **6-P<sub>3</sub>** should be formally regarded as an LX-donor ligand coordinated to the d<sup>4</sup>, 15e<sup>-</sup> metal fragment [Mo<sup>II</sup>I(CO)<sub>2</sub>(CNAr<sup>Dipp2</sup>)<sub>2</sub>]. Intuitively, the existence of **6-P<sub>3</sub>** as a stable dicarbonyl complex is inconsistent with assignment of the metal center as a d<sup>2</sup>, Mo<sup>IV</sup> species. Although d<sup>2</sup> metal-carbonyls have been reported for early transition metals with strongly-donating anionic ligands, the interest in these complexes typically stems from atypical reactivity and lability of CO in these systems.<sup>17-21</sup> Furthermore, the presence of  $\pi$ -accepting isocyanide ligands has been shown to facilitate oxidative decarbonylation of complexes related to **6-P<sub>3</sub>**.<sup>22</sup> It is significant, therefore, that **6-P<sub>3</sub>** is stable for weeks at room-temperature, and shows no decomposition after 24 h at 90 °C in C<sub>6</sub>D<sub>6</sub>.

To probe the electronic structure of the metal-center more directly, the CO stretching frequency of **6-P<sub>3</sub>** was evaluated by FTIR. Because of the sensitivity of the CO stretching frequency to  $\pi$ -backdonation into the CO  $\pi^*$  orbital,<sup>23-26</sup> CO ligands have been well-established spectroscopic as reporter ligands for assessment of the distribution of electron density between metal and ligand.<sup>27</sup> Accordingly, the CO stretching frequency of **6-P<sub>3</sub>** is expected to resemble that of other formally divalent complexes. Importantly, the **6-P<sub>3</sub>** CO stretching frequency of 1983 cm<sup>-1</sup> is similar to the related complexes MoI<sub>2</sub>(CO)<sub>2</sub>(CNAr<sup>Dipp2</sup>)<sub>2</sub> ( $\nu_{\text{CO}}$  = 2004 and 1994 cm<sup>-1</sup>) and to MoI<sub>2</sub>(THF)(CO)<sub>2</sub>(CNAr<sup>Dipp2</sup>)<sub>2</sub> ( $\nu_{\text{CO}}$  = 1969 and 1947 cm<sup>-1</sup>),<sup>22</sup> thus supporting our assessment that **6-P<sub>3</sub>** should formally be regarded as a 3e<sup>-</sup> LX-donor ligand coordinated to the d<sup>4</sup>, 15e<sup>-</sup> metal fragment [Mo<sup>II</sup>I(CO)<sub>2</sub>(CNAr<sup>Dipp2</sup>)<sub>2</sub>].

The electronic structure of **6-P<sub>3</sub>** and **7-P<sub>3</sub>** was further assessed by density functional theory (DFT: BP86, ZORA-def2-TZVP). Orbital analysis of **7-P<sub>3</sub>** was clearly consistent with coordination of a monoanionic ligand to a zero-valent d<sup>6</sup> metal center as indicated by the presence of three filled d-orbitals in Figure 6.11. The distribution of electrons in **6-P<sub>3</sub>** is more challenging to assess due to hybridization of filled-orbitals of e-parentage. Importantly though, the relative contribution of the Mo and P the d( $\pi$ )-P( $\pi^*$ ) interactions are opposite of those calculated in the high-valent systems.<sup>16</sup> Accordingly, d $\pi$ -stabilization of CO and CNAr<sup>Dipp</sup><sub>2</sub> gives mainly d-orbital contribution, forming  $\sigma$ -backbonding interactions with the  $\pi^*$ -orbitals of *cyclo*-P<sub>3</sub> (Figure 6.12, 1e-orbitals). These findings are consistent with the isolobal analogy between *cyclo*-P<sub>3</sub> and the hydrocarbon analog *cyclo*-C<sub>3</sub>H<sub>3</sub> in coordination complexes (references include examples of isolobal complexes of Ni<sup>28-30</sup> and Mo<sup>31,32</sup>). Further supporting our assessment that *cyclo*-P<sub>3</sub> should be regarded as an anionic 3e- donor is the presence of three, metal-based d-orbitals in the anionic *cyclo*-P<sub>3</sub> complex. Interestingly, in the dianion the NC-Mo-CN bond angle is constrained to 126°, while the OC-Mo-CO bond angle is 153°. This change, which resembles a C<sub>4v</sub>→C<sub>2v</sub> distortion in the MO diagram, isolates the Mo→P  $\sigma$ -backbonding interaction to a single orbital at E = -1.34 eV, which is significantly stabilized in comparison to the other Mo-based orbitals.

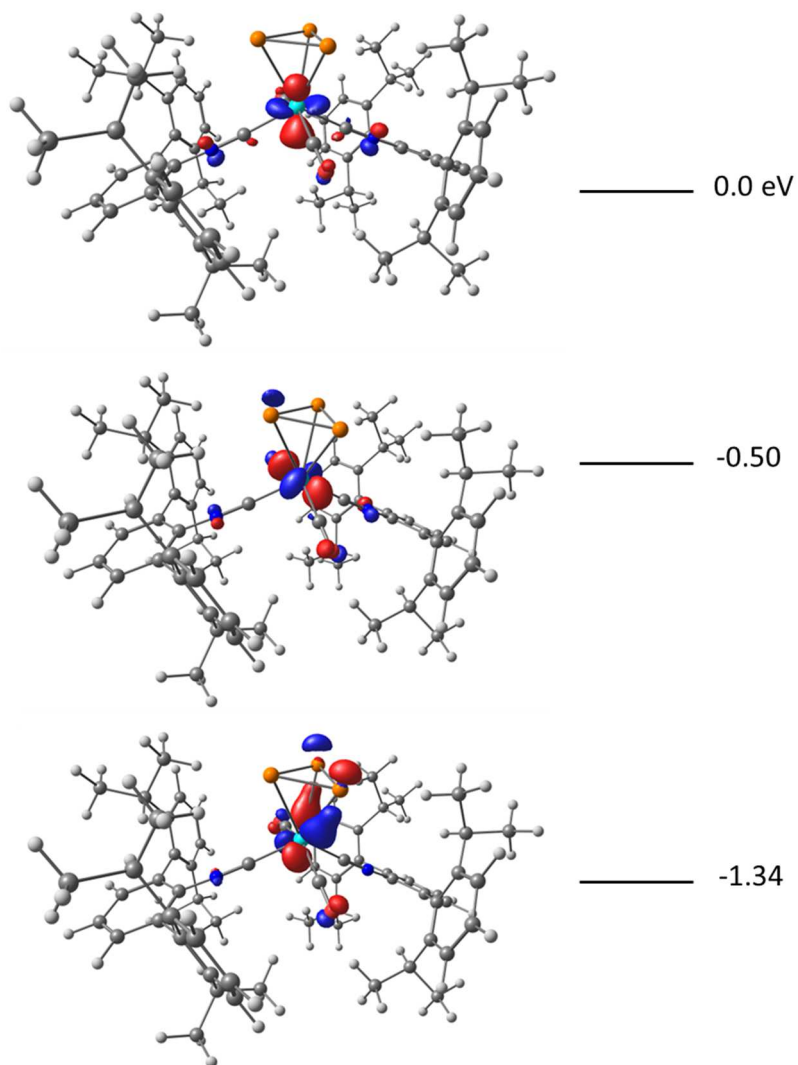


**Figure 6.11.** Occupied metal-based orbitals of the anionic *cyclo*-P<sub>3</sub> complex [7-P<sub>3</sub>]<sup>-</sup>.

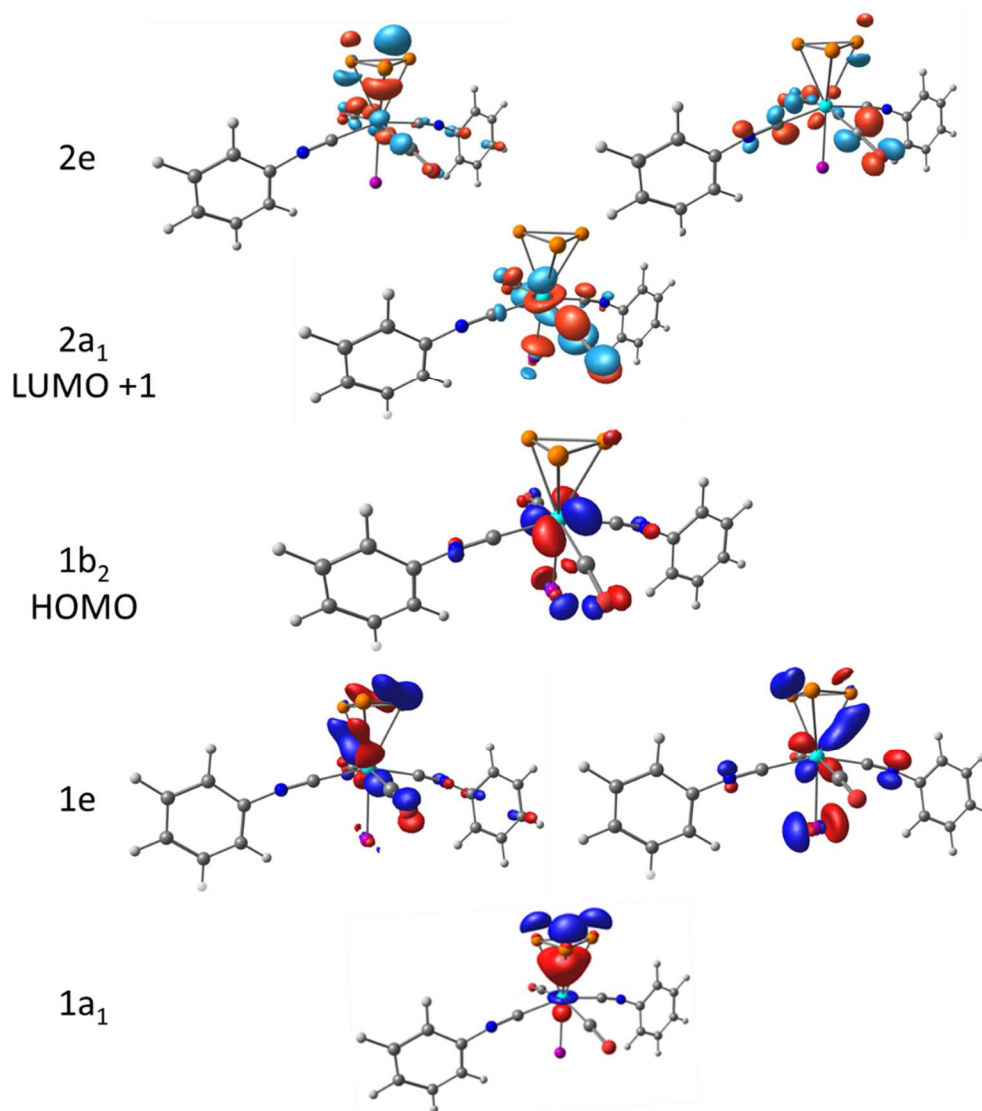


**Figure 6.12.** Selected molecular orbitals. Mulliken designations are based on simplified  $C_{4v}$  symmetric geometry.

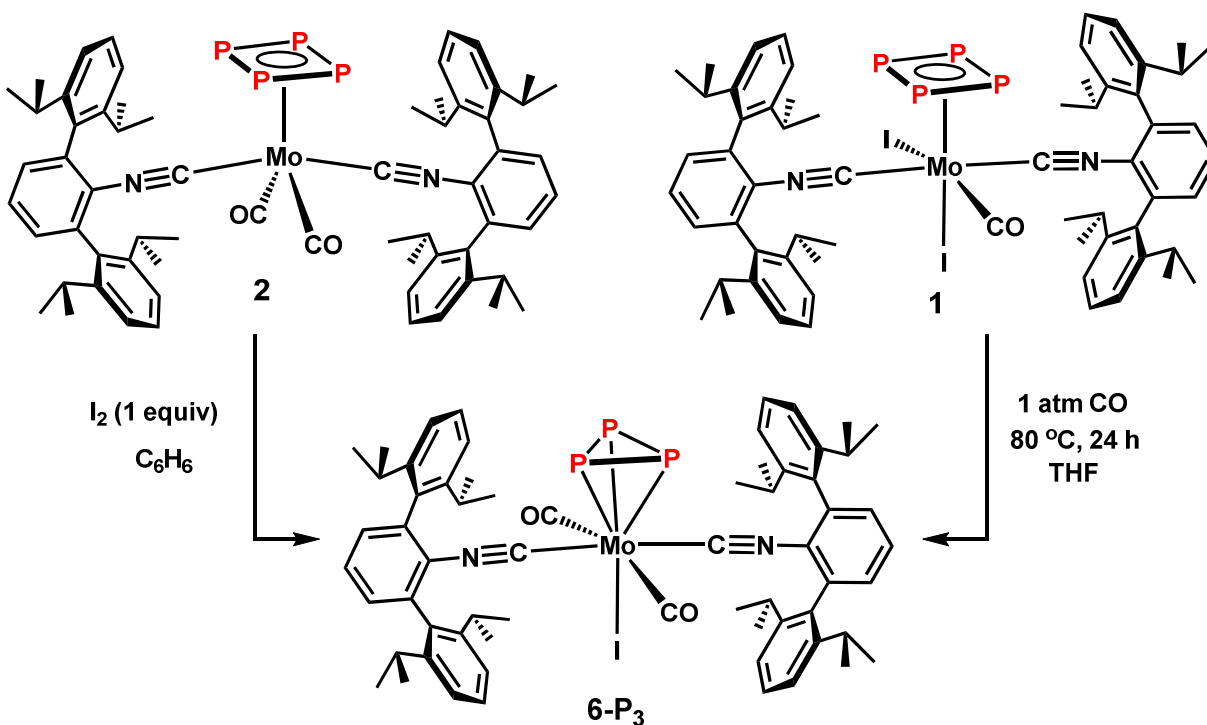
Although the designation of *cyclo*- $P_3$  as a  $3e^-$ , monoanionic ligand is clearly a suitable description of that moiety in **6-P<sub>3</sub>**, we do acknowledge that the extent of electron localization at phosphorus will depend on both the identity of the metal and the ability of the other ligands to stabilize low-valency at the metal-center. Accordingly, the wide range of  $^{31}P$  NMR chemical shifts observed in  $^{31}P$  NMR seems to imply that a continuum exists. For example, the chemical shifts of formally divalent complexes **6-P<sub>3</sub>** and  $CpMo(\eta^3-P_3)(CO)_2$ <sup>30</sup> are -341 ppm and -352 ppm by  $^{31}P$

NMR, while those of the aforementioned high-valent Mo and V complexes are found at -85 ppm and 185 ppm. Interestingly downfield  $^{31}\text{P}$  chemical shifts of  $(\eta^3\text{-P}_3)\text{Mo}(\text{N}[\text{iPr}]\text{Ar}')_3$  and  $(\text{nacnac})\text{V}(\eta^3\text{-P}_3)(\text{NtolyI}_2)$ , were determined to result from a strongly deshielding interaction which arises by coupling of a filled e-set with vacant  $a_1$ -orbitals.<sup>16,33</sup> The shift of **6-P<sub>3</sub>** to higher fields can thus be attributed to stabilization of filled d-orbitals in **6-P<sub>3</sub>** to give comparatively large energy difference between filled and unfilled orbitals, thereby decreasing the deshielding interactions. Accordingly, the  $1e \rightarrow 2a_1$  transition in **6-P<sub>3</sub>** (Figure 6.12) shows  $\Delta E_{1e \rightarrow 2a_1} = 3.6$  eV, while the similar  $e \rightarrow a_1$  deshielding transition of the three-fold symmetric, high-valent Mo and V species give  $\Delta E_{e \rightarrow a_1}$  values of only 2.3 and 1.4, respectively.<sup>16</sup> It is important to note that the higher lying vacant M-based d-orbitals of these high-valent species are not invoked in deshielding interactions, thus preventing the use of  $^{31}\text{P}$  NMR from providing direct indication of the metal-center's oxidation state. Notwithstanding, however, the trend showing low-valent metal-centers to be substantially upfield is likely to be useful for initial assessment of electron distribution in  $\text{P}_3\text{-M}$  coordination complexes by  $^{31}\text{P}$  NMR.

### 6.2.6 P-Atom Extrusion from *cyclo-P<sub>4</sub>* via Iodophosphinidene (P-I) Intermediate

Typically, *cyclo-P<sub>3</sub>* complexes are prepared as fortuitous  $\text{P}_4$ -degradation products in low-to-moderate yields from the reaction between white phosphorus and a reactive metal fragment.<sup>16,34–36</sup> Limiting the utility of *cyclo-P<sub>3</sub>* functionalities, therefore, is a lack of high yielding syntheses based on rational methodologies. The direct P-atom extrusion from *cyclo-P<sub>4</sub>* described in this work may thus serve as a convenient method for the efficient preparation of *cyclo-P<sub>3</sub>* under mild conditions. Interestingly, the mechanism of  $\text{P}_3$  formation in this system appears to diverge from that of known examples. Recent mechanistic studies have posited two mechanisms by which *cyclo-P<sub>3</sub>* is generated – transfer of  $\text{P}_2$  to a monometallic phosphide complex,<sup>37</sup> and bimolecular P-

atom removal via a bimetallic, P<sub>4</sub>-bridging intermediate.<sup>33</sup> Clearly, in the absence of a thermodynamic driving force for generation of terminal phosphide, the former may be excluded from consideration in the formation of **6-P<sub>3</sub>**. Furthermore, the latter mechanistic proposal is also unlikely in the present work due to the absence of metals bearing open coordination sites (and the mild reaction conditions preventing the formation of such species). The feasibility of this pathway is further restricted by the sterically encumbering nature of CNAr<sup>Dipp<sub>2</sub></sup> ligands—to date, the tetranuclear compound **5** remains the sole example of bimetallic reactivity among complexes bearing ≥2 CNAr<sup>Dipp<sub>2</sub></sup> ligands. Notwithstanding, the formation of **6-P<sub>3</sub>** from **2** does resemble the synthesis of (triphos)Rh(η<sup>3</sup>-P<sub>3</sub>) from the mixture of [Rh(C<sub>2</sub>H<sub>2</sub>)<sub>2</sub>(Cl)]<sub>2</sub>, triphos, and P<sub>4</sub>.<sup>36</sup> In that system, formal loss of [P-Cl]<sup>38</sup> from the dinuclear precursor can more easily be considered as proceeding by bimolecular extrusion of the more thermodynamically favorable dimer, P<sub>2</sub>Cl<sub>2</sub>.



**Scheme 6.2.** P-atom extrusion pathways for synthesis of **6-P<sub>3</sub>** from di- and tetravalent *cyclo*-P<sub>4</sub> complexes, **1** and **2**, respectively.

Noting that the steric encumbering ligand environment rendered binuclear extrusion of  $P_2I_2$  unlikely in the synthesis of **6-P<sub>3</sub>**, we were intrigued by the possibility that iodophosphinidine (P-I) was generated as a fleeting intermediate. Although phosphorus monohalides<sup>39-42</sup> and the related arsenic species<sup>43,44</sup> have long been known known to spectroscopists, the participation of these intermediates in chemical synthesis has only rarely been invoked.<sup>45,46</sup> The general absence of phosphorus monohalides from the literature is surprising when considering the potential application of P-X in synthesis of coordinatively unsaturated phosphorus derivatives.

As a starting point toward establishing the intermediacy of P-X in the formation of **6-P<sub>3</sub>**, we sought to establish the 1:1 ratio of P:I atoms in the leaving group. Importantly, formation of common  $P_xI_y$  allotropes (e.g.  $PI_3$ ,  $P_2I_4$ ) in the reaction between **2** and  $I_2$  (1 equiv) was ruled out by the absence of observable side-products by  $^{31}P$  NMR. To further ensure a single iodine atom was involved in the P-atom abstraction, we considered an alternative pathway utilizing the tetravalent complex **1**. Satisfyingly, thermolysis of a THF solution of **2** at 80 °C under 1 atm CO showed complete conversion of **1** to the desired *cyclo*- $P_3$  product **6-P<sub>3</sub>** by  $^{31}P$  and  $^1H$  NMR. Importantly, the intramolecular elimination from **1** confirms that PI is a competent leaving group in the formation of **6-P<sub>3</sub>**.

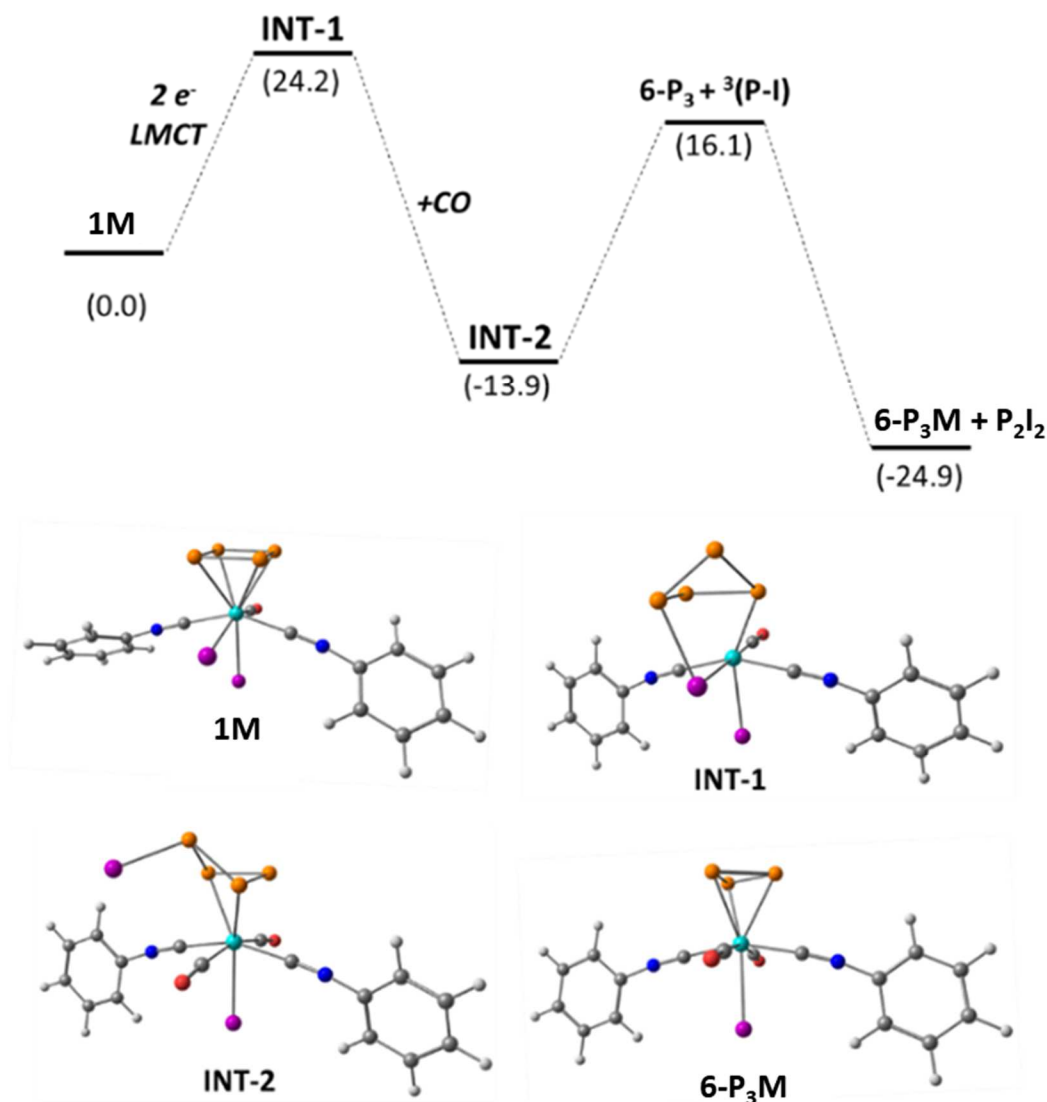


**Figure 6.13.** Geometry optimization of plausible intermediates in the elimination of PI from tetravalent *cyclo*-P<sub>4</sub> model complex ( $\eta^4$ -P<sub>4</sub>)MoI<sub>2</sub>(CO)(CNPh)<sub>2</sub> (**1M**).

Previously, it was shown that low-lying d-orbitals in the tetravalent *cyclo*-P<sub>4</sub> complex provided low-lying excited states by which reductive elimination of white phosphorus was achieved. Accordingly, we propose that accessibility of the low-lying d-orbital manifold in **1** could facilitate reductive elimination of PI upon coordination of a CO ligand. To further explore mechanistic aspects of the P-atom extrusion process from **1**, a series of potential intermediates were identified by DFT (Figure 6.13). Interestingly, breaking planarity of the *cyclo*-P<sub>4</sub> motif in



**1M** resulted in optimization of the structure **INT-1** wherein P<sub>4</sub> is bridged in butterfly conformation between iodine and Mo. Importantly, orbital analysis revealed the metal-center of **INT-1** showed two filled d-orbitals, thus indicating the transition of **1** to **INT-1** occurs with a reductive of insertion of I with P<sub>4</sub>, resulting in Mo(IV) → Mo(II). Coordination of CO displaces bridging iodine to give **INT-2** while retaining the Mo(II) oxidation state. Important to note, the formation of the high energy intermediate INT-1 is consistent with the elevated temperatures required to access 6-P3 from **1** compared to **2**, which could more easily access INT-T upon addition of I<sub>2</sub>. In the next step, release of PI, which has a triplet ground-state, is not a thermodynamically feasible endpoint. We thus predict that PI exists only as a fleeting intermediate which rapidly associates with additional equivalents of PI to provide a significant thermodynamic driving force in the resulting oligomeric species P<sub>x</sub>I<sub>y</sub>. Consistent with this notion, formation of the dimeric species (P<sub>2</sub>I<sub>2</sub>) was found to reduce the overall enthalpy of reaction to -26 kcal/mol.

With confirmation that release of monovalent phosphorus was thermodynamically feasible by DFT, we were intrigued by the possibility that **2** could be used as a mild source of P<sup>(I)</sup>. In recent years, there has been increasing interest in the “transition-metal-like”<sup>47–51</sup> coordination chemistry of main-group molecules. Interestingly, treatment of the reaction mixture generated by addition of I<sub>2</sub> and **2** with 1/4 equiv CNAr<sup>Dipp</sup><sub>2</sub> results in an AA'BB' coupling pattern by <sup>31</sup>P NMR (Figure 6.14) consistent with insertion of an isocyanide into a tetrameric PI ring as is shown in the proposed intermediate as shown in (Figure 6.14, Scheme 6.3).<sup>52</sup> Unfortunately, further characterization of this species was hindered by rapid decomposition leading to complete disappearance of the species within 10 minutes at 22 °C. Motivated by the apparent reactivity of σ-donating isocyanide ligands toward the extruded phosphorus iodide products, we turned our attention to chelating phosphines since they would be expected to provide enhanced stabilization monovalent phosphorus.<sup>45,46</sup>

Interestingly, treatment of the reaction mixture generated by addition of I<sub>2</sub> and **2** with 1 equiv dppe resulted in formation of the triphosphazolium salt (**7**),<sup>45,46</sup> which precipitated from the C<sub>6</sub>D<sub>6</sub> reaction mixture to give **7** in 85% yield (Scheme 6.3).

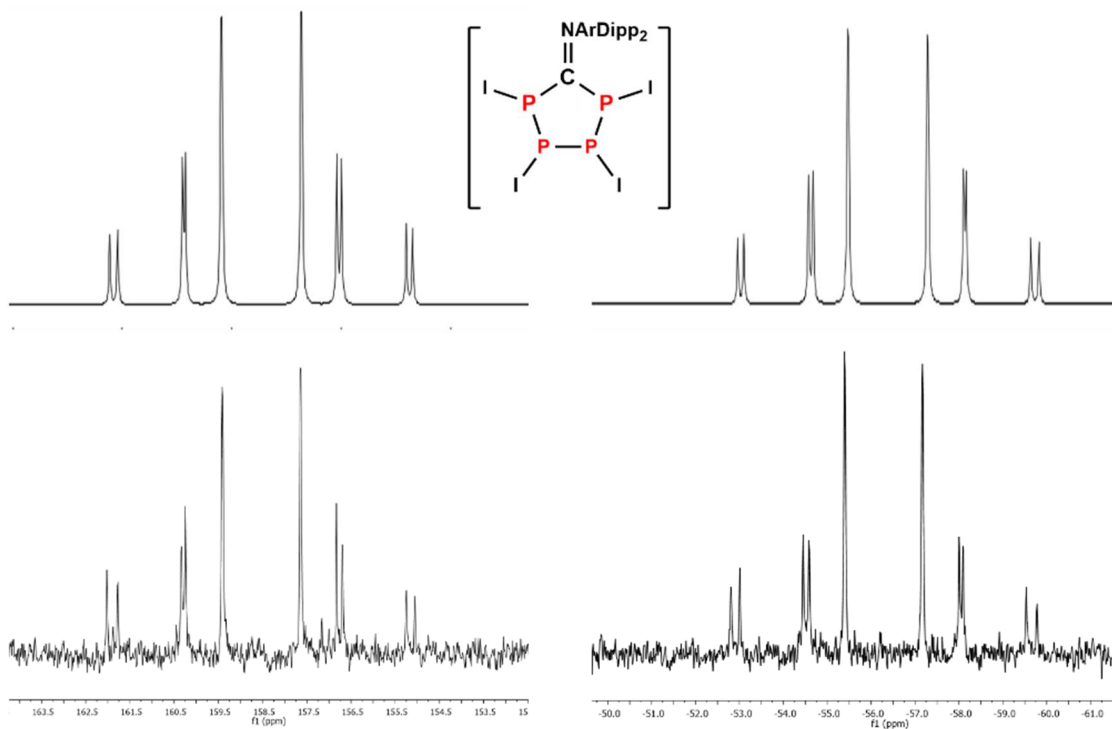
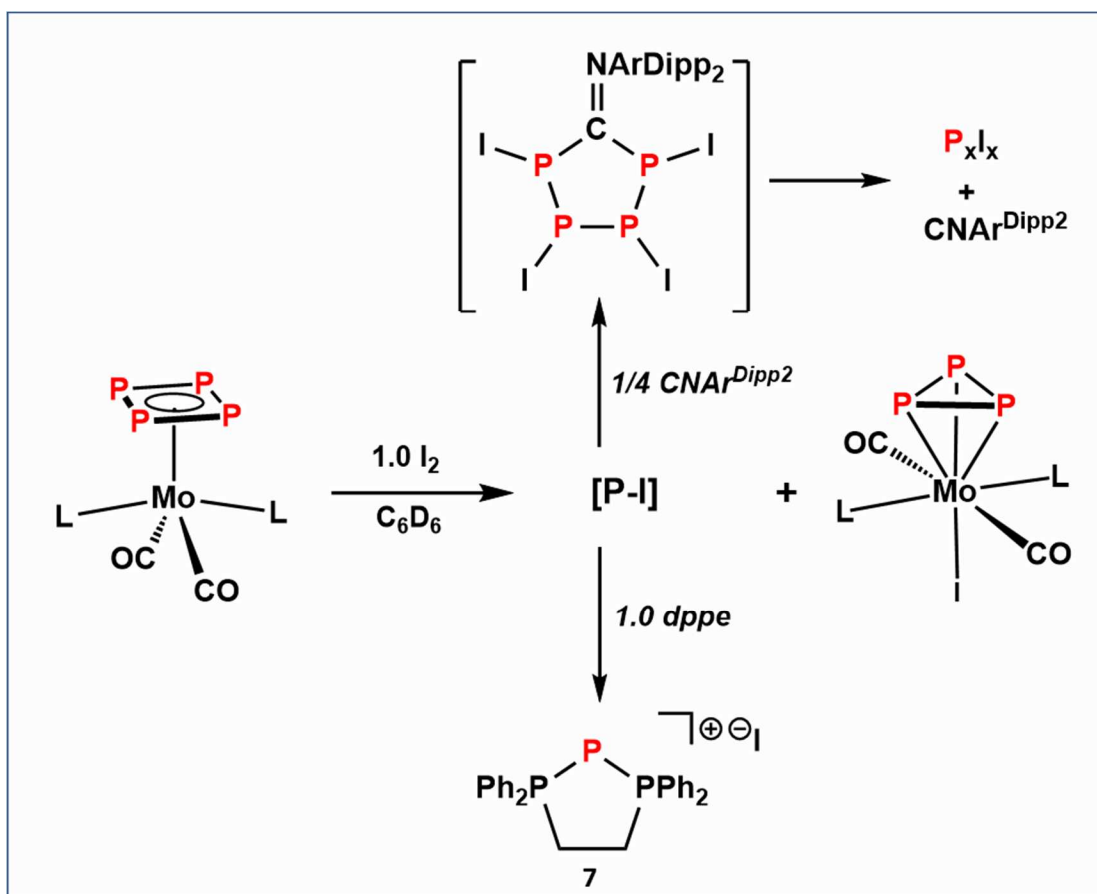


**Figure 6.14.** Proposed intermediate (in brackets), <sup>31</sup>P NMR (bottom), and WinDNMR simulated spectrum (top) of phosphorus species trapped by CNAr<sup>Dipp</sup><sub>2</sub>. Coupling constants: JAA' = -15 Hz, JBB'=193 Hz, JAB = 403 Hz, JAB' = -184 Hz.

The rate of **6-P**<sub>3</sub> formation was not enhanced in the presence of dppe, with a 0.5 M solution of **2** reaching complete conversion in about 15 min at r.t. This suggests that the activation energy is not significantly affected by the presence of dppe. It seems likely therefore, that release of PI proceeds by solvent assisted pathways – ultimately leading to P<sub>x</sub>I<sub>x</sub> oligomers. The initial formation of these oligomers is supported both by the suprathermochemical of PI with CNAr<sup>Dipp</sup><sub>2</sub>, and the presence of a broad peak at +40 ppm by <sup>31</sup>P NMR which we attribute to low-molecular-weight P<sub>x</sub>I<sub>x</sub> oligomers. Importantly, while this intermediate species disappears within 1 h under standard

conditions due to further oligomerization, the rate of disappearance for this peak was found to be correlated to the growth of phosphazolium **7**. This suggests that the intermediate oligomeric species are suitable sources of P-I in the formation of **7**. Importantly, these findings indicate that **2** is indeed a suitable source of P-I. Furthermore, the high stability of the 18-e- *cyclo*-P<sub>3</sub> complex **2** is an important feature of this method, as this “leaving group” is unlikely to interfere in reactions where P-I is desired.



**Scheme 6.3.** [P-I] group transfer with CNAr<sup>Dipp</sup><sub>2</sub> and dppe.

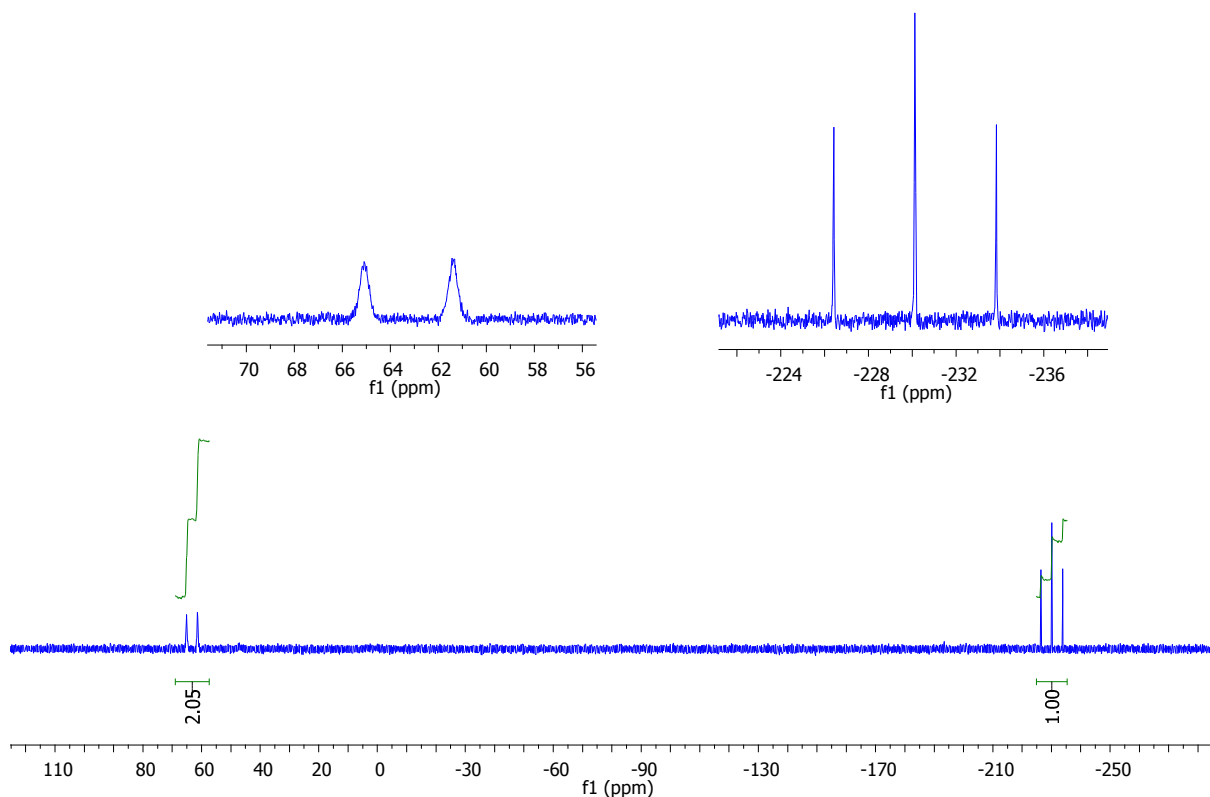


**Figure 6.15.**  $^{31}\text{P}$  NMR (121.5 MHz,  $\text{CDCl}_3$ ) of triphosphazole salt **7**,  $^1J_{PP} = 452$  Hz.

### 6.3 Conclusions

The reactivity of the  $(\eta^4\text{-Mo}(\text{CO})_2(\text{CNAr}^{\text{Dipp}2})_2)$  (**2**) has been investigated with nucleophiles and electrophiles. **2** was found to undergo nucleophilic attack with  $^-\text{[OH]}$  and  $^-\text{[TEMPO]}$  at *cyclo*- $\text{P}_4$  to give unusual cyclophosphaallene complexes. Also described herein is a new, well-defined synthetic method for the synthesis of a *cyclo*- $\text{P}_3$  complex (**6-P<sub>3</sub>**) by site-directed oxidation of the *cyclo*- $\text{P}_4$  unit of complex **2** with diiodide reagent. Interestingly, **6-P<sub>3</sub>** is similarly accessible from the tetravalent *cyclo*- $\text{P}_4$  complex **2** under thermolytic conditions in the presence of 1 atm CO. In

that process, reconfiguration of *cyclo*-P<sub>4</sub> results in ligand-to-metal-charge transfer, which is followed by release of PI – this process can thus be regarded as a two-step reductive elimination of PI. Furthermore, the reaction between I<sub>2</sub> and **2** was shown to be a suitable source of PI in reactions with neutral electron donating ligands CNAr<sup>Dipp</sup><sub>2</sub> and dppe.

## 6.4 Synthetic procedures, characterization data, and calculations

**General considerations.** All manipulations were carried out under an atmosphere of purified dinitrogen using standard Schlenk and glovebox techniques. Unless otherwise stated, reagent-grade starting materials were purchased from commercial sources and either used as received or purified by standard procedures.<sup>53</sup> Solvents were dried and deoxygenated according to standard procedures.<sup>54</sup> Benzene-d<sub>6</sub> (Cambridge Isotope Laboratories) was distilled from NaK alloy/benzophenone ketyl and stored over 4 Å molecular sieves under N<sub>2</sub> for at least 24 h prior to use. Celite 405 (Fisher Scientific) was dried under vacuum (24 h) at a temperature above 250 °C and stored in the glovebox prior to use. KBr (FTIR grade from Aldrich) was stirred overnight in anhydrous THF, filtered and dried under vacuum at a temperature above 250 °C prior to use. The *m*-terphenyl isocyanide CNAr<sup>Dipp</sup><sub>2</sub> was prepared as previously reported.<sup>55</sup>

Solution <sup>1</sup>H, <sup>13</sup>C{<sup>1</sup>H}, <sup>31</sup>P NMR spectra were recorded on a Bruker Avance 300, a Jeol ECA 500, or a Varian X-SENS 500 spectrometer. <sup>1</sup>H and <sup>13</sup>C{<sup>1</sup>H} chemical shifts are reported in ppm relative to SiMe<sub>4</sub> (<sup>1</sup>H and <sup>13</sup>C δ = 0.0 ppm) with reference to residual solvent resonances of 7.16 ppm (<sup>1</sup>H) and 128.06 ppm (<sup>13</sup>C) for C<sub>6</sub>D<sub>6</sub>, 7.26 ppm (<sup>1</sup>H). FTIR spectra were recorded on a Thermo-Nicolet iS10 FTIR spectrometer. FTIR samples were prepared as C<sub>6</sub>D<sub>6</sub> or THF solutions injected into a ThermoFisher solution cell equipped with KBr windows. Solvent peaks were digitally subtracted from all spectra by comparison with an authentic spectrum obtained

immediately prior to that of the sample. The following abbreviations were used for the intensities and characteristics of important IR absorption bands: vs = very strong, s = strong, m = medium, w = weak, vw = very weak; br = broad, sh = shoulder. Combustion analyses were performed by Midwest Laboratories of Indianapolis, IN (USA) or or Robertson Microlit Laboratories of Madison, NJ (USA).

**Synthesis of  $(\eta^3\text{-P}_3)\text{MoI}(\text{CO})_2(\text{CNAr}^{\text{Dipp}2})_2$  (**6-P<sub>3</sub>**).** To a toluene solution of  $(\eta^4\text{-P}_4)\text{Mo}(\text{CO})_2(\text{CNAr}^{\text{Dipp}2})_2$  (**3-P<sub>4</sub>**, 50 mg, 44.5  $\mu\text{mol}$ , 1 equiv, 5 mL) was added a toluene solution of  $\text{I}_2$  (11.3 mg, 44.5  $\mu\text{mol}$ , 1 equiv). After 30 min stirring at r.t., the reaction mixture was concentrated, and taken up in a 2:1  $\text{Et}_2\text{O}$ /pentane solution (10 mL). Suspended solids were removed by filtration, and the volume was reduced to ca. 0.5 mL. Storage at  $-40\text{ }^\circ\text{C}$  overnight afforded **4-P<sub>3</sub>** as greenish-yellow suitable for X-ray crystallography. Yield: 33 mg, 27.6  $\mu\text{mol}$ , 62%.  $^1\text{H}$  NMR (300 MHz,  $\text{C}_6\text{D}_6$ )  $\delta$  7.39 (dd,  $J = 13.9, 6.2$  Hz, 1H), 7.22 (d,  $J = 7.7$  Hz, 2H), 6.89 (dd,  $J = 16.3, 14.2$  Hz, 1H), 6.79 (dd,  $J = 8.8, 6.0$  Hz, 1H), 2.63 (sept,  $J = 6.8$  Hz, 8H), 1.42 (d,  $J = 6.8$  Hz, 5H), 1.02 (d,  $J = 6.8$  Hz, 5H) ppm;  $^{13}\text{C}$  NMR (126 MHz,  $\text{C}_6\text{D}_6$ )  $\delta$  204.9 (CO), 161.5 (CNAr), 146.5, 139.6, 134.9, 130.5, 130.0, 124.1, 31.5, 24.8, 24.6. ppm;  $^{31}\text{P}\{^1\text{H}\}$  NMR (121 MHz,  $\text{C}_6\text{D}_6$ )  $\delta$  ppm -341.2 (s) ppm. FTIR (KBr windows,  $\text{C}_6\text{D}_6$ ,  $25\text{ }^\circ\text{C}$ ):  $\nu(\text{C}\equiv\text{N}) = 2163$  (m), 2098 (vs),  $\nu(\text{C}\equiv\text{O}) = 1983$ , other: 2962 (s), 2928 (m), 2870 (w), 1470 (w), 1416 (w), 1362 (w), 1254 (w), 1056 (m), 756 (m)  $\text{cm}^{-1}$ .

**Synthesis of  $[(\eta^3\text{-P}_3)\text{Mo}(\text{CO})_2(\text{CNAr}^{\text{Dipp}2})_2][\text{K}]$  (**7-P<sub>3</sub><sup>-</sup>**).** To a thawing THF solution of  $(\eta^3\text{-P}_3)\text{MoI}(\text{CO})_2(\text{CNAr}^{\text{Dipp}2})_2$  (0.040 g, 31.9  $\mu\text{mol}$ , 1.0 equiv, 3 mL) was added THF suspension of  $\text{KC}_8$  (0.015 g, 0.11 mmol, 3.4 equiv, 2 mL). The reaction mixture was shaken rigorously for 4 min, filtered through Celite, then reduced *in vacuo*. **7-P<sub>3</sub><sup>-</sup>** was the sole reaction product by  $^1\text{H}$  and  $^{31}\text{P}\{^1\text{H}\}$  NMR. X-ray quality crystals were obtained by crystallization from 0.3 mL  $\text{Et}_2\text{O}$  (0.019

g, 0.018  $\mu\text{mol}$ , 53%).  $^1\text{H}$  NMR (500 MHz,  $\text{C}_6\text{D}_6$ )  $\delta$  7.53 (t,  $J = 7.7$  Hz, 4H), 7.39 (d,  $J = 7.8$  Hz, 8H), 6.93 (d,  $J = 7.6$  Hz, 4H), 6.87 – 6.83 (sept,  $J = 6.8$  Hz, 2H), 2.88 – 2.80 (sept,  $J = 6.8$  Hz, 8H), 1.50 (d,  $J = 6.8$  Hz, 24H), 1.19 (d,  $J = 6.8$  Hz, 24H) ppm;  $^{13}\text{C}$  NMR (126 MHz,  $\text{C}_6\text{D}_6$ )  $\delta$  241.6 (CO, m), 195.7 (CNAr), 147.1, 137.0, 136.2, 130.2, 129.7, 129.4, 126.1, 123.7, 31.5, 24.9, 24.7 ppm;  $^{31}\text{P}$  NMR (162 MHz,  $\text{C}_6\text{D}_6$ )  $\delta$  -396.4 (s) ppm. FTIR (KBr windows,  $\text{C}_6\text{D}_6$ , 25  $^\circ\text{C}$ ):  $\nu(\text{C}\equiv\text{N}) = 2080$  (s), 1986 (vs), 1933(s),  $\nu(\text{C}\equiv\text{O}) = 1846$  (s), 1705 (m), other: 2962 (s), 2928 (m), 2867 (w), 1575 (m), 1467 (m), 1413(m), 1250 (w), 1103 (w), 1058 (m), 757 (m).

**Synthesis of phosphallyl [3]<sup>-</sup>.** To a thawing THF solution of 2 (0.100 g, 89  $\mu\text{mol}$ , 1.0 equiv, 1 mL) was added a THF solution of  $[\text{Na}][\text{CPh}_3]$  (0.032 g, 135  $\mu\text{mol}$ , 1.5 equiv, 1 mL). The reaction was stirred 1 min at rt then treated with  $\text{H}_2\text{O}$  (2.5  $\mu\text{l}$ , 135  $\mu\text{mol}$ , 1.5 equiv). The reaction was stirred overnight, then concentrated, dissolved in  $\text{Et}_2\text{O}$ , filtered, and crystallized overnight at -40  $^\circ\text{C}$  to give 3 as a yellow crystalline solid (0.037 g, 32  $\mu\text{mol}$ , 36%).  $^1\text{H}$  NMR (500 MHz,  $\text{C}_6\text{D}_6$ )  $\delta$  7.67 (t,  $J = 7.7$  Hz, 4H), 7.49 (d,  $J = 7.8$  Hz, 8H), 6.99 (d,  $J = 7.6$  Hz, 4H), 6.91 – 6.87 (m, 2H), 2.86 (sept,  $J = 6.8$  Hz, 8H), 1.46 (d,  $J = 6.8$  Hz, 24H), 1.21 (d,  $J = 6.8$  Hz, 24H) ppm;  $^{13}\text{C}\{^1\text{H}\}$  NMR (126 MHz,  $\text{C}_6\text{D}_6$ )  $\delta$  227.7 (m,  $\text{C}\equiv\text{O}$ ), 184.0 (d,  $^2J_{\text{C,P}} = 13.7$  Hz,  $\text{C}\equiv\text{NAr}$ ), 146.8, 138.1, 135.8, 130.4, 129.9, 129.1, 127.6, 123.9, 31.6, 24.9, 24.8 ppm;  $^{31}\text{P}$  NMR (161.9 MHz,  $\text{C}_6\text{D}_6$ )  $\delta$  38.8, (dtd,  $^1J_{\text{PH}} = 411$  Hz,  $^1J_{\text{PP}} = 238$  Hz,  $^2J_{\text{PP}} = 26$  Hz, 1P)  $^2J_{\text{PP}} = 26$  Hz, 1.06 (t,  $^1J_{\text{PP}} = 238$ , 2P), -14.2 (td,  $^1J_{\text{PP}} = 238$ ,  $^2J_{\text{PP}} = 26$  Hz, 1P), see main text for  $^{31}\text{P}\{^1\text{H}\}$  NMR. FTIR (KBr windows,  $\text{C}_6\text{D}_6$ , 25  $^\circ\text{C}$ ):  $\nu(\text{C}\equiv\text{N}) = 2095$  (m), 2045 (vs),  $\nu(\text{C}\equiv\text{N}) = 1962$  (w), 1899 (m),  $\nu(\text{P}=\text{O}) = 1119$  (vs), 1073(s), other: 2975 (vs), 2930 (m), 2868 (s), 1380 (w), 755 (w).

## 6.5 Details of DFT computational studies

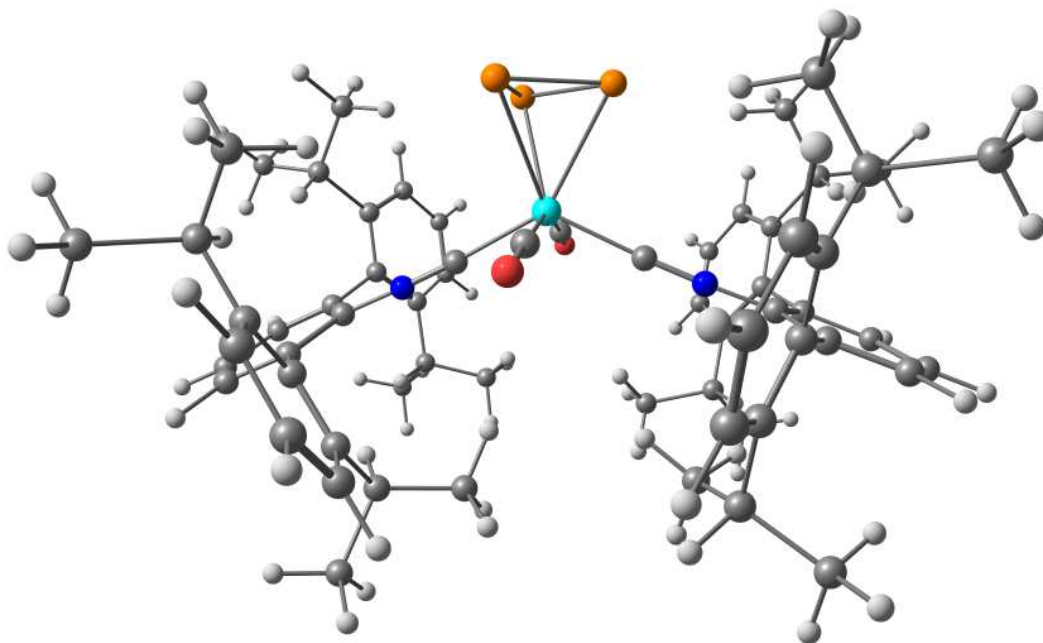


**Figure 6.16.** Optimized geometry of *cis,trans*-Mo(CO)<sub>2</sub>(CNAr<sup>Dipp2</sup>)<sub>2</sub>(η<sup>3</sup>-P<sub>3</sub>) ([7-P<sub>3</sub>]<sup>-</sup>).

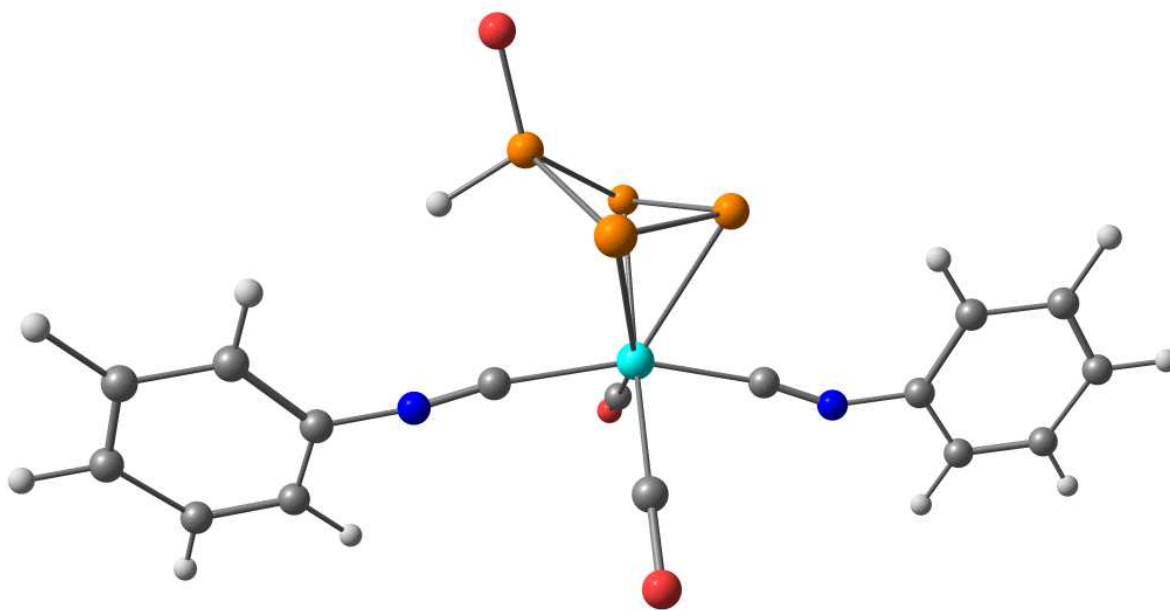


**Figure 6.17.** Optimized coordinates of [3M]<sup>-</sup>



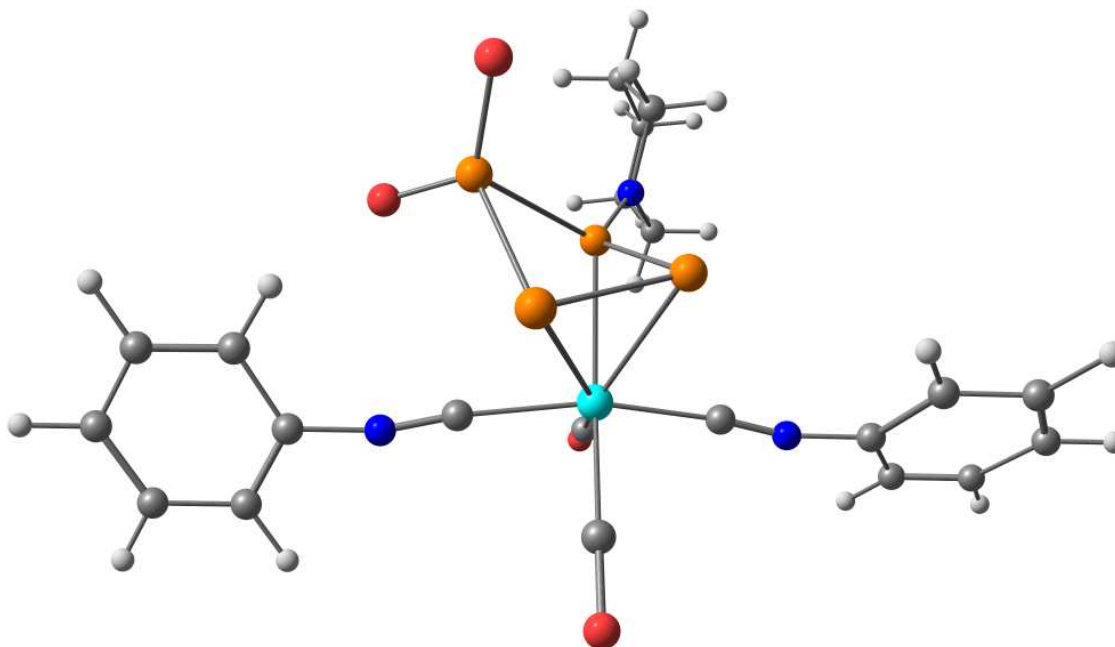


**Figure 6.18.** Optimized coordinates of  $[4M]^-$

### 6.5.1 Geometry optimized coordinates

#### *cis,trans*- $\text{Mo}(\text{CO})_2(\text{CNAr}^{\text{Dipp}2})_2(\eta^3\text{-P}_3)\text{]}^-$ ( $[\text{7-P}_3\text{M}]^-$ )

Mo	4.56974327017032	17.02047903146969	12.19453191109670
P	2.99060850010274	14.98251338238897	12.08274531150489
N	5.71142807657383	17.00146188709827	9.16385627001922
O	7.67851822386223	17.13261197224541	12.92906636907235
C	5.29702245573965	17.04854644655516	10.29538199254060
C	6.54070900812159	17.06489566377221	12.69635467119835
P	3.53653371924864	15.59570705187885	14.10714284022761
P	4.96986040398924	14.55214192750080	12.82403386823038
N	4.34299077424741	19.50718811307217	14.24223442108073
O	2.03197655458236	18.26651564041313	10.70719339877307
C	4.43270963474732	18.60387024964417	13.45098438667282
C	2.92076116058939	17.78842799427986	11.28840173154905
C	4.21159215990743	20.49024551367113	15.16855424638739
C	2.98714022415412	21.22215818859383	15.26156842038283
C	5.29732100479553	20.80225203602285	16.04695432649751
C	2.88650272065008	22.24870082121930	16.20598249611286
C	5.12822275053156	21.82853830451679	16.98117814061646
C	3.94224943890578	22.56281116183844	17.06486005668908
H	1.94858396020651	22.80512373407405	16.26506447104732
H	5.95291443579782	22.04483619377904	17.66330870700117
H	3.83807040023513	23.36288214990324	17.79961138462716
C	6.20295576969024	16.90269835402202	7.90199319015762
C	7.61460243113053	16.92941839915984	7.67802038331445
C	5.31229497536288	16.76735849248895	6.79121143741913
C	8.09232576251599	16.83227625870956	6.36724135764814
C	5.85021680814117	16.67640644778946	5.50376310386772

C	7.22813269527180	16.70787904377755	5.27736606768754
H	9.17285701672503	16.86038922084234	6.20924657501472
H	5.16054181741555	16.57470171504379	4.66325793160194
H	7.62396760844228	16.63616046188025	4.26308479022528
C	3.82392233783699	16.70287024308309	6.96119092438623
C	3.04526084538147	17.87653236622762	6.81928088697118
C	3.19794711399008	15.45299234388736	7.19219018220238
C	1.64944706550404	17.77773313983996	6.90050293835212
C	1.79983334631010	15.40181233120941	7.26880472861929
C	1.02804892956137	16.55231290219965	7.12312188552537
H	1.04100116445064	18.67892651345579	6.80326285781199
H	1.30737203147608	14.44610134565036	7.45643998223750
H	-0.06014626272562	16.49470848090204	7.19842246863647
C	8.60398296628999	17.07310464489947	8.79558063572272
C	9.01811470452699	18.36366019993425	9.20378803577266
C	9.17813054539163	15.91982613430058	9.38285257731545
C	10.02105258365336	18.47716818744124	10.17554667636540
C	10.18035002714040	16.08120200609435	10.34883776161316
C	10.60458223093127	17.34748166129954	10.74194637903766
H	10.34385787384000	19.46856346786948	10.50208542612863
H	10.62516310578401	15.19917153325073	10.81316721130014
H	11.37673550002919	17.45435129725965	11.50658584519693
C	6.57765813612107	20.01798671506390	16.04944502736780
C	7.73703856641502	20.47071491243267	15.36644291987987
C	6.62993804175677	18.82902077242804	16.82408845093820
C	8.91604950931318	19.71776958413476	15.48279242011198
C	7.83384077363646	18.11742232836239	16.90829589847213
C	8.97398352087068	18.55478072455933	16.24328451730956
H	9.80529948495541	20.05378776158797	14.94435539322246
H	7.87356887074677	17.19891545713767	17.49643784911136
H	9.90109557606778	17.98107468722817	16.30090653014373
C	1.80362613801128	20.90778614510916	14.39455703617408
C	1.64598066642038	21.55582900772954	13.14518308111505
C	0.81387438112705	20.00791968843410	14.86246090633402
C	0.49528030445733	21.29691521466058	12.38836619526320
C	-0.32100896527096	19.78150777152538	14.07212347732725
C	-0.48332006263923	20.41843028389765	12.84456616783424
H	0.36741874923122	21.78170263221282	11.41845159440761
H	-1.08627203793948	19.08347357160509	14.41808837135794
H	-1.36631026449887	20.21764106133965	12.23435416961114
C	8.74455715053983	14.51348815740478	8.98259569021958
H	7.85844201220073	14.61528087957649	8.33785624091335
C	8.33516803466905	13.66000058581167	10.19471488486600
C	9.83462853581161	13.80660869037311	8.15468769506933
H	10.09059100139095	14.38085342312191	7.25221336325865
H	10.75547053812807	13.68039008335744	8.74489967026189
H	9.49555975024929	12.80773490342091	7.83973671862043
H	9.18811132433360	13.46799982186668	10.86394392436826
H	7.95350511736603	12.68326645372444	9.86073456960859
H	7.54845268552386	14.15087783693042	10.78413080073225
C	8.40225085742219	19.62820310701349	8.615498291707875
H	7.63822303903055	19.31617092264932	7.88806175779530
C	9.44209657143945	20.46646253146289	7.85067635503782
C	7.69767008011036	20.46987217508692	9.69272788238391
H	6.94429546870390	19.87832272662961	10.23133721106884
H	8.41632286184678	20.85288251577773	10.43296093566802

H	7.19405091926589	21.33639507528250	9.23702041040024
H	10.23274303138721	20.83214489802230	8.52389363494086
H	8.96640307829908	21.34455108854235	7.38679148391653
H	9.92311525748131	19.87818579747894	7.05539885885633
C	4.00713077652959	14.16494164320985	7.30654741015172
H	5.05185876080158	14.44953986881900	7.50117327132678
C	3.98283560745528	13.38912208600616	5.97460162229077
C	3.55411652165968	13.26599364165789	8.46711316055632
H	3.54130632261150	13.81057269060562	9.42181011851055
H	2.54556573986195	12.85762385486669	8.29881568152606
H	4.23840818133340	12.41102652436165	8.57240063055074
H	2.95320402092391	13.09773952229981	5.71497321146927
H	4.58859812378843	12.47261494775668	6.04758317213586
H	4.38088352637760	13.99658749956218	5.14883926596800
C	3.68392679756217	19.23799488264158	6.56672050536994
H	4.77227120378622	19.11367858175509	6.67346961382866
C	3.2352652969198	20.29340990481946	7.59118539222858
C	3.41738328924744	19.72305049844775	5.12968019814386
H	3.78729256830958	19.00183253989342	4.38720980374921
H	2.33863558846606	19.86036676786268	4.95623488779512
H	3.91386432603783	20.68877847039227	4.94606316627093
H	2.16238753702922	20.51892613522337	7.49585226010119
H	3.78811694480318	21.23294957376704	7.43751626796062
H	3.41206147859221	19.95319050502653	8.61981902982208
C	0.93527019663799	19.30644691884402	16.21165852039271
H	1.96212065220234	19.46362356278123	16.57378725795774
C	0.70954374478396	17.78942332925293	16.11506563321181
C	-0.01755430301990	19.93718859102730	17.24481861239229
H	0.17843650235018	21.01232905471966	17.36837746857779
H	-1.06759737961061	19.82063669805935	16.93156509431778
H	0.09769682333094	19.45268488947728	18.22684401125918
H	-0.32179873772667	17.54972443499988	15.81373144128117
H	0.88110544410235	17.31604445163358	17.09392298724951
H	1.39106794807813	17.32366842919188	15.39001494161380
C	2.68341475096500	22.53982029573691	12.61628311807181
H	3.53800913870961	22.51919568326400	13.30926307866515
C	2.13530003535908	23.97916819254132	12.61123463878359
C	3.21093168306531	22.14672789617573	11.22735674323073
H	3.62206795184760	21.12860956343556	11.23148782900724
H	2.41698882653908	22.18504740709298	10.46596570791731
H	4.00739922533632	22.83834111769197	10.91212381281128
H	1.27685201409869	24.07135081857470	11.92743865798958
H	2.90965165060590	24.68837430493790	12.27921896839990
H	1.79976430714416	24.28290414928736	13.61348112894632
C	5.42507315058438	18.33335210073471	17.61900992121498
H	4.53061938982595	18.83071084230930	17.21564363519419
C	5.54793600724224	18.74864476966542	19.09838738753378
C	5.19790977631802	16.81960034235313	17.49240997776397
H	5.12019392789778	16.51123272557171	16.44064952096479
H	6.00622627584635	16.23797454417209	17.96207630425715
H	4.26040055681712	16.53604680618926	17.99405626415147
H	6.44731558438211	18.30631469150535	19.55477683827899
H	4.67251470642406	18.40621407183859	19.67227167049595
H	5.61840740134839	19.84136179101795	19.20181518195840
C	7.84149225887023	21.74115937751214	14.51548534231987
H	8.79322969334685	21.62335339064203	13.96916335818694

C	7.99191472634124	23.01589657750725	15.36904251274957
C	6.75619804228577	21.92229908775540	13.44418323462497
H	6.59966445945108	21.00166271228294	12.86668391796621
H	5.79558523049445	22.21956762523969	13.88262528351306
H	7.05851438216034	22.71669449969972	12.74453048587312
H	7.06285461359739	23.24621850663265	15.90777984208866
H	8.22672796611259	23.87707813269931	14.72343359633446
H	8.80097672277731	22.91016129653220	16.10714901419071

### Model Complex 3M

Mo	12.84938880311212	13.82110804168593	15.20749212940757
P	12.14753165028659	15.03126277344692	17.33390889265780
P	14.30330284097314	14.64371741877661	17.28632941595569
P	11.65078306242400	12.88686937901048	17.42722881577668
P	13.68405875442249	12.75541878858773	18.29154505265953
N	10.74173428597284	16.05241443265978	14.19300788764459
N	15.08873121960924	11.47821071038000	14.80440383028241
O	14.65818359979398	15.32217371760130	13.09247018478326
O	11.09566091868264	11.93657325681907	13.36788152866471
C	16.04769743361683	10.51384363323516	14.68560699666557
C	9.59558614972080	17.69303679778771	15.55833739807875
C	17.80072575882966	9.15963696350550	15.67041134112374
H	18.39758288940841	8.88028466987031	16.54060447368769
C	16.82871637460080	10.14796794667465	15.80220221212367
C	11.50183355458335	15.24641073733311	14.67622287487262
C	9.27997984657658	17.65082975849007	13.14469415819369
C	14.27139480274406	12.31097853640111	15.05697989180588
C	16.26164852436740	9.87701704389202	13.44600530916967
C	9.88374494963361	17.11913498640334	14.30113930198231
C	17.24026482851107	8.89220569268290	13.33355242850713
H	17.39924956700172	8.40420239498293	12.37014316938368
C	18.01477829613492	8.52690977578834	14.44025072414149
H	18.77889792193080	7.75364579221924	14.34499731137222
C	8.40872657746338	18.73399773296192	13.24569325622682
H	7.94895248510885	19.13830683862652	12.34175163263147
C	13.99173878852934	14.75834408071330	13.87006419631106
C	8.72131719001201	18.77353364649071	15.64167994204280
H	8.50590714407655	19.21040764291158	16.61891332512885
C	8.12323024260195	19.30290063968019	14.49144328461725
H	7.44194641020623	20.15224404806048	14.56661097401370
C	11.74638103239372	12.64425085046218	14.02988650019209
H	10.07093543170384	17.27421144409856	16.44686877293950
H	9.51011841854908	17.19933678603104	12.17918281967552
H	16.65079877013793	10.64490844752812	16.75602089808358
H	15.65152524040437	10.16872711284868	12.59122972106907
O	13.87424039692370	12.61734421446891	19.78201178222189
H	14.35914483895198	11.66478726688358	17.63155656590606

### Model Complex 4M

Mo	-0.22469515423580	8.40436080701322	10.25837516682995
P	-0.65607525677822	6.19362809421945	8.89129702114970
P	0.84994032476137	7.62416091415906	8.08968041591302
P	0.82119435825700	5.93846194015934	10.41523350358481
P	2.51105789495934	6.25302473262295	8.83729758094649
N	2.54264768074094	9.00011428654289	11.90103557655259
O	-0.18787397224002	11.55141607666578	9.94300727841691
N	-3.27461720397701	8.78471440152856	9.22736192517969
N	0.79677287793303	8.18962978028137	6.48806559654400
O	2.65985787802567	5.02971269169285	7.97518800109194
O	-1.56579989701650	8.15833222885190	13.10615861357225
O	3.69896200273533	7.02384615813779	9.35299114902948
C	1.58015420839296	8.72132743818283	11.26254348843632
C	-2.13681410039854	8.57973227623457	9.55674149271747
C	0.23121855109816	9.47981820188893	6.10045227483213
C	1.04573929511017	7.26858980826350	5.37460816426427
C	1.13167659985195	10.18401764234037	5.07602904930347
H	2.08295248660484	10.45101972605692	5.56578535992297
H	0.65485453710837	11.12354325140526	4.75151900155773
C	1.96572675453934	7.91627966069165	4.33211751546034
H	2.96224476367292	8.05571212276925	4.78232152842427
H	2.08712108004367	7.23453617215608	3.47437731116418
C	-0.21177670218682	10.39209935288923	10.08276035235974
C	1.40810425746809	9.27084276185432	3.87333463464938
H	2.10332500325767	9.75816420641115	3.16998402345406
H	0.46464002044105	9.10629329145029	3.31989154749449
C	-1.06561168092406	8.25768989604986	12.05481978623884
C	3.79742577135266	9.15037386000935	12.44045943873160
C	3.97285173632660	9.94224003259086	13.58998196664092
C	4.89571225130931	8.50829908610658	11.83600577874688
C	5.24817509025109	10.09222072512980	14.13316201915377
C	6.16110821358495	8.67530076238133	12.39662803438642
C	6.34655518331416	9.46141568122438	13.54015447412127
H	3.10546584965378	10.42530018274441	14.04037948732483
H	4.71506039042190	7.90056615092738	10.94239197053555
H	5.38292948776431	10.70294066293856	15.02798420813563
H	7.01532676575452	8.18086049827772	11.93028674129931
H	7.34338215476125	9.58130188672387	13.96875154992753
C	-4.52539908394898	8.55363470997526	8.72591190784499
C	-4.86572186028408	7.28450858007099	8.20782285550091
C	-5.48683495347538	9.58450413669329	8.71875819755443
C	-6.14217820048374	7.06586406975653	7.69642710265618
C	-6.75924990150557	9.34689525613729	8.20305533633112
C	-7.09674505519970	8.09022092227683	7.68861850062692
H	-4.11358620965539	6.49443991318814	8.21878796047947
H	-5.21478405421083	10.55979153893355	9.12305263791416
H	-6.39417821496834	6.08178348641890	7.29642395579271
H	-7.49583899975742	10.15320837354419	8.20320207859696
H	-8.09393985043953	7.91041749553674	7.28428357288419
H	1.49176029873763	6.34884143663527	5.77852848681249
H	-0.77789974080088	9.33503117034187	5.65753120617366
H	0.10606412737924	10.08839631939020	7.00630078144954
H	0.08237148787324	6.99079766952704	4.89404651228805

## 6.6 Crystallographic determination of molecular structures

**Table 6.1.** Crystallographic Data Collection and Refinement Information

	$[(\eta^3\text{-P}_3\text{P}(\text{O})\text{H})\text{MoI}(\text{CO})_2(\text{CNAr}^{\text{Dipp}2})_2]\text{Na}$ $([\mathbf{3}][\text{Na}]\cdot\text{THF}_4)$ $\text{C}_{79}\text{H}_{83}\text{IMoN}_2\text{NaO}_7\text{P}$	$[(\eta^3\text{-P}_2\text{P}(\text{TEMP})\text{P}(\text{O})_2)\text{Mo}(\text{CO})_2(\text{CNAr}^{\text{Dipp}2})_2]\text{Na}$ $([\mathbf{4}][\text{Na}]\cdot\text{THF}_4)$ $\text{C}_{81}\text{H}_{107.2}\text{NaMoN}_3\text{O}_6\text{P}_4$	$[\text{Mo}(\text{CO})_2(\text{CNAr}^{\text{Dipp}2})_2(\eta^4\text{-P}_4)(\text{Mo}(\text{CO})_4)]_2$ $(\mathbf{5})$ $\text{C}_{144}\text{H}_{168}\text{Mo}_4\text{N}_4\text{O}_{14}\text{P}_8$
Formula	4	$\text{C}_{81}\text{H}_{107.2}\text{NaMoN}_3\text{O}_6\text{P}_4$	$\text{C}_{144}\text{H}_{168}\text{Mo}_4\text{N}_4\text{O}_{14}\text{P}_8$
Crystal System	Orthorhombic	Orthorhombic	Triclinic
Space Group	$P2_12_12$	$P2_1/n$	P-1
$a$ , Å	25.3202(7)	15.9654(6)	18.2414(12)
$b$ , Å	17.0054(5)	18.4748(7)	19.7613(11)
$c$ , Å	18.1485(5)	28.6542(12)	22.4290(15)
$\alpha$ , deg	90	90	70.283(3)
$\beta$ , deg	90	93.037(2)	81.394(4)
$\gamma$ , deg	90	90	70.065(3)
$V$ , Å <sup>3</sup>	7814.4(5)	8439.9(6)	7149.5(8)
$Z$	4	4	4
Radiation ( $\lambda$ , Å)	Mo-K $\alpha$ , 0.71073	Mo-K $\alpha$ , 0.71073	CuK $\alpha$ , 1.54178
$\rho$ (calcd.), g/cm <sup>3</sup>	1.224	1.399	1.305
Temp, K	100	100	100
$\theta$ max, deg	51.48	41.656	117.966
data/parameter	14896/943	8839/862	20062/1772
$R_1$	0.1134	0.0684	0.0515
w $R_2$	0.2721	0.1479	0.0940
GooF	1.267	1.003	1.079

**Table 6.1 cont.** Crystallographic Data Collection and Refinement Information

	$(\eta^3\text{-P}_3)\text{MoI}(\text{CO})_2$ $(\text{CNAr}^{\text{Dipp}^2})_2$ <b>(6-P<sub>3</sub>)</b>	$[(\eta^3\text{-P}_3)\text{Mo}(\text{CO})_2$ $(\text{CNAr}^{\text{Dipp}^2})_2]\text{K}$ <b>(7-P<sub>3</sub>)</b>
Formula	$\text{C}_{64}\text{H}_{74}\text{IMoN}_2\text{O}_2\text{P}_3$	$\text{C}_{64}\text{H}_{74}\text{KMoN}_2\text{O}_2\text{P}_3$
Crystal System	Monoclinic	Trigonal
Space Group	$P2_1/c$	$P\bar{3} 1 c$
$a$ , Å	19.335(4)	27.0613(19)
$b$ , Å	16.924(2)	27.0613(10)
$c$ , Å	20.740(5)	15.4721(13)
$\alpha$ , deg	90	90
$\beta$ , deg	114.262(7)	90
$\gamma$ , deg	90	120
$V$ , Å <sup>3</sup>	6187(2)	9812.4(13)
$Z$	4	6
Radiation ( $\lambda$ , Å)	Mo-K $\alpha$ , 0.71073	Mo-K $\alpha$ , 0.71073
$\rho$ (calcd.), g/cm <sup>3</sup>	1.310	1.149
Temp, K	100	100
$\theta$ max, deg	25.747	23.286
data/parameters	11789/729	4742/353
$R_1$	0.0491	0.0915
w $R_2$	0.1246	0.2154
GooF	1.030	1.189

## 6.7 Acknowledgements

Chapter 6 is adapted from Kyle A. Mandla, Curtis E. Moore, Milan Gembicky, Arnold L. Rheingold, and Joshua S. Figueroa, “*cyclo-P<sub>4</sub>* as a Stoichiometrically Precise Source of P-I.” Manuscript in Progress. The dissertation author is the first author of this paper.

## 6.8 References

- (1) Caporali, M.; Gonsalvi, L.; Rossin, A.; Peruzzini, M. *Chem. Rev.* **2010**, *110* (7), 4178–4235.
- (2) Cossairt, B. M.; Piro, N. A.; Cummins, C. C. **2010**, 4164–4177.
- (3) Scherer, O. J.; Vondung, J.; Wolmersh?user, G. *Angew. Chemie Int. Ed. English* **1989**, *28* (10), 1355–1357.
- (4) Herberhold, M.; Frohmader, G.; Milius, W. *J. Organomet. Chem.* **1996**, *522*, 185–196.
- (5) Dielmann, F.; Timoshkin, A.; Piesch, M.; Scheer, M.; Bal?zs, G.; Scheer, M. *Angew. Chemie Int. Ed.* **2017**, *56* (6), 1671–1675.
- (6) Cavaillé, A.; Saffon-Merceron, N.; Nebra, N.; Fustier-Boutignon, M.; Mézailles, N. *Angew. Chemie Int. Ed.* **2018**, *57*, 1874–1878.
- (7) Criegee, R.; Förg, F.; Brune, H.-A.; Schönleber, D. *Chem. Ber.* **1964**, *97* (12), 3461–3468.
- (8) Criegee, R.; Ludwig, P. *Chem. Ber.* **1961**, *94* (8), 2038–2043.
- (9) Maitlis, P. *Adv. Organomet. Chem.* **1966**, *4*, 95–143.
- (10) Dielmann, F.; Peresyphkina, E. V.; Krämer, B.; Hastreiter, F.; Johnson, B. P.; Zabel, M.; Heindl, C.; Scheer, M. *Angew. Chemie Int. Ed.* **2016**, *55* (47), 14833–14837.
- (11) Mädl, E.; Balázs, G.; Peresyphkina, E. V.; Scheer, M. *Angew. Chemie Int. Ed.* **2016**, *55* (27), 7702–7707.
- (12) Mirabello, V.; Caporali, M.; Gonsalvi, L.; Manca, G.; Ienco, A.; Peruzzini, M. *Chem. - An Asian J.* **2013**, *8* (12), 3177–3184.
- (13) Scheer, M.; Herrmann, E.; Sieler, J.; Oehme, M. *Angew. Chemie Int. Ed. English* **1991**, *30* (8), 969–971.
- (14) Wang, L.-P.; Tofan, D.; Chen, J.; Voorhis, T. Van; Cummins, C. C. *RSC Adv.* **2013**, *3*, 23166–23171.
- (15) Cossairt, B. M.; Diawara, M.; Cummins, C. C. *Science (80-. )*. **2009**, *323*, 602.



- (16) Pinter, B.; Smith, K. T.; Kamitani, M.; Zolnhofer, E. M.; Tran, B. L.; Fortier, S.; Pink, M.; Wu, G.; Manor, B. C.; Meyer, K.; et al. *J. Am. Chem. Soc.* **2015**, *137* (48), 15247–15261.
- (17) Atwood, J. L.; Stone, K. E.; Alt, H. G.; Hrcir, D. C.; Rausch, M. D. *J. Organomet. Chem.* **1977**, *132* (3), 367–375.
- (18) Seitz, A. E.; Vogel, U.; Eberl, M.; Eckhardt, M.; Balázs, G.; Peresykina, E. V.; Bodensteiner, M.; Zabel, M.; Scheer, M. *Chem. - A Eur. J.* **2017**, *23* (43), 10319–10327.
- (19) Sikora, D. J.; Rausch, M. D.; Rogers, R. D.; Atwood, J. L. *J. Am. Chem. Soc.* **1981**, *103* (5), 1265–1267.
- (20) Shen, H.; Jordan, R. F. *Organometallics* **2003**, *22* (10), 2080–2086.
- (21) Choukroun, R.; Lorber, C.; Lepetit, C.; Donnadieu, B. **2003**.
- (22) Ditri, T. B.; Moore, C. E.; Rheingold, A. L.; Figueroa, J. S.; Ditri, B.; Moore, C. E.; Rheingold, A. L.; Figueroa, J. S. *Inorg. Chem.* **2011**, *50* (20), 10448–10459.
- (23) Ellis, J. E. *Organometallics* **2003**, *22* (17), 3322–3338.
- (24) Willner, H.; Aubke, F. *Organometallics*. 2003, pp 3612–3633.
- (25) Lupinetti, A. J.; Fau, S.; Frenking, G.; Strauss, S. H. *J. Phys. Chem. A* **1997**, *101* (49), 9551–9559.
- (26) Bistoni, G.; Rampino, S.; Scafuri, N.; Ciancaleoni, G.; Zuccaccia, D.; Belpassi, L.; Tarantelli, F. *Chem. Sci.* **2016**, *7* (2), 1174–1184.
- (27) Wolczanski, P. T. *Organometallics* **2017**, *36* (3), 622–631.
- (28) Di Vaira, M.; Sacconi, L.; Stoppioni, P. *J. Organomet. Chem.* **1983**, *250* (1), 183–195.
- (29) Mealli, C.; Midollini, S.; Moneti, S.; Albright, T. A. *Helv. Chim. Acta* **1983**, *66* (2), 557–569.
- (30) Scherer, O. J.; Sitzmann, H.; Wolmershäuser, G. *J. Organomet. Chem.* **1984**, *268* (1), C9–C12.
- (31) Scherer, O. J.; Sitzmann, H.; Wolmershäuser, G.; IUCr. *Acta Crystallogr. Sect. C Cryst. Struct. Commun.* **1985**, *41* (12), 1761–1763.
- (32) Hughes, R. P.; Reisch, J. W.; Rheingold, A. L. *Organometallics* **1985**, *4* (10), 1754–1761.
- (33) Stephens, F. H.; Johnson, M. J. A.; Cummins, C. C.; Kryatova, O. P.; Kryatov, S. V.; Rybak-Akimova, E. V.; McDonough, J. E.; Hoff, C. D.; Uni, V.; V, M. D.; et al. *J. Am. Chem. Soc.*

- 2005**, *127*, 15191–15200.
- (34) Breunig, J. M.; Tofan, D.; Cummins, C. C. *Eur. J. Inorg. Chem.* **2014**, 1605–1609.
- (35) Vaira, M. Di; Midollini, S.; Saccon, L. *J. Am. Chem. Soc.* **1979**, *101* (7), 1757–1763.
- (36) Bianchini, C.; Mealli, C.; Meli, A.; Sacconi, L. *Inorganica Chim. Acta* **1979**, *37*, L543–L544.
- (37) Piro, N. A.; Cummins, C. C. *J. Am. Chem. Soc.* **2008**, *130*, 9524–9535.
- (38) Majoral, J.-P., Ed.; *Topics in Current Chemistry*; Springer Berlin Heidelberg: Berlin, Heidelberg, 2002; Vol. 220.
- (39) Basco, N.; Yee, K. K. *Chem. Commun.* **1967**, *21*, 1146–1147.
- (40) Colin, R.; Devillers, J.; Prevot, F. 1972; Vol. 44.
- (41) Colin, R. *Can. J. Phys.* **1979**, *57*, 1051–1058.
- (42) Colin, R.; Herman, M.; Prevot, F. *Chem. Phys. Lett.* **1996**, *91* (3), 213–216.
- (43) Beutel, M.; Setzer, K. D.; Fink, E. H. *J. Mol. Spectrosc.* **1999**, *194*, 250–255.
- (44) Liuand, D. S.; Jones, W. E. *Can. J. Phys.* **1972**, *50* (12), 1230–1251.
- (45) Ellis, B. D.; Macdonald, C. L. B. *Inorg. Chem.* **2006**, *45* (17), 6864–6874.
- (46) Ellis, B. D.; Carlesimo, M.; Macdonald, C. L. B. *Chem. Commun.* **2003**, No. 15, 1946.
- (47) Hansmann, M. M.; Bertrand, G. *J. Am. Chem. Soc.* **2016**, *138*, 15885–15888.
- (48) Braunschweig, H.; Krummenacher, I.; Andrélé, M.-A.; Andrélégaré, A.; Matler, A.; Radacki, K.; Ye, Q. **2017**.
- (49) Liu, L.; Ruiz, D. A.; Munz, D.; Bertrand, G. **2016**.
- (50) Hansmann, M. M.; Jazzar, R.; Bertrand, G. *J. Am. Chem. Soc.* **2016**, *138*, 8356–8359.
- (51) Mathey, F. *Angew. Chemie Int. Ed. English* **1987**, *26* (4), 275–286.
- (52) Bashforth, R.; Boyall, A. J.; Coffey, P. K.; Dillon, K. B.; Goeta, A. E.; Howard, J. A. K.; Kenwright, A. M.; Probert, M. R.; Shepherd, H. J.; Thompson, A. L. **2012**, *41*, 1165–1172.
- (53) Armarego, W. L. F.; Chai, C. L. L. 5th ed.; Elsevier, 2003.

- (54) Pangborn, A. B.; Giardello, M. A.; Grubbs, R. H.; Rosen, R. K.; Timmers, F. J. *Organometallics* **1996**, *15* (5), 1518–1520.
- (55) Fox, B. J.; Sun, Q. Y.; DiPasquale, A. G.; Fox, A. R.; Rheingold, A. L.; Figueroa, J. S. *Inorg. Chem.* **2008**, *47* (19), 9010–9020.